UNIVERSIDAD DE CANTABRIA

ESCUELA TÉCNICA SUPERIOR DE INGENIEROS INDUSTRIALES Y DE TELECOMUNICACIÓN

DEPARTAMENTO DE INGENIERÍA QUÍMICA Y QUÍMICA INORGÁNICA

Membrane technologies for hydrogen and carbon monoxide recovery from residual gas streams

(Tecnologías de membranas para la recuperación de hidrógeno y monóxido de carbono de gases residuales)

Memoria de Tesis Doctoral presentada para optar al título de Doctora por la Universidad de Cantabria.

Programa de Doctorado en Ingeniería Química y de Procesos

Directores de Tesis:

Dra. Ane Miren Urtiaga Mendia

Dr. Eugenio Daniel Gorri Cirella

Oana Cristina David

Santander, Mayo 2012

Agradecimientos

Me gustaría expresar mi gratitud a mis directores de tesis, la Dra. Ane Miren Urtiaga y el Dr. Daniel Gorri, por la confianza el esfuerzo y tiempo dedicados para que este trabajo saliera adelante. Gracias por haberme dado la oportunidad de trabajar en el fascinante mundo de la investigación. También me gustaría agradecer a la responsable del grupo de investigación "Procesos avanzados de separación", dentro de cual este trabajo ha sido llevado a cabo, a la Dra. Inmaculada Ortiz por su exigencia y profesionalidad que determinó la calidad de este trabajo.

Gracias a la Dra. Kitty Nijmeijer por la oportunidad de trabajar en el grupo de investigación "Membrane Science and Technology Group", University of Twente y a todo el personal de dicho departamento por la calurosa acogida y por dedicarme una buena parte de su tiempo en transferir sus conocimientos y experiencia en el campo de las membranas. "I want to express my acknowledgments to Prof. Dr. Kitty Nijmeijer for giving me the opportunity to work in Membrane Science and Technology Group, University of Twente. I am also grateful to the people from this group for dedicating important part of their time in sharing their knowledge and experience in the membrane field"

Gracias a la Dra. Nazely Diban por animarme en los momentos difíciles y por ser un ejemplo a seguir de dedicación y trabajo. Gracias a Dra. Clara Casado por ayudarme en los primeros pasos en el campo de las membranas y de las instalaciones de gases. También quiero agradecer a todos los compañeros de trabajo, entre ellos a Alfredo, Marcos, Gabriel, Mariana, Marisol, Sonia, Hala, Vanesa, Elia, Karima, Bea, Esther, Antía el que hayan compartido estos años conmigo y haber recibido su atención.

También quiero agradecer al personal de mantenimiento, Felix, Elena y Rafa y al personal administrativo, Inmaculada y Pilar.

Quiero expresar mis agradecimientos a mis padres, mi hermana y mis abuelas por apoyarme incondicionalmente en todas las decisiones tomadas durante mi vida y por soportar estar tan lejos de mí. "Vreau să mulţumesc părinţilor, surorii şi bunicilor pentru sprijinul necondiţionat ce mi l-au acordat în toate deciziile luate pe parcursul vieţii şi pentru faptul că au suportat sa fie atât de departe de mine"

Por último agradezco al Ministerio de Educación Cultura y Deporte la concesión de la beca FPU que ha permitido la elaboración de este trabajo de Tesis Doctoral.

Reconocimiento

*Nuestro agradecimiento a **Huntsman Corporation** por la autorización para la reproducción del documento* **Matrimid®** 5218**/ Matrimid®** 9725

SUMMARY (RESUMEN)

SUMMARY

This PhD thesis work is aimed to the separation and recovery of valuable gases, hydrogen and carbon monoxide, from industrial residual gas streams by means of membrane technology. The work has been developed within the Research Group Advanced Separation Processes of the Department of Chemical Engineering of the University of Cantabria (Spain) under the frame of the projects: ENE 2010-15585, CTQ 2008-00690/PPQ and CTM 2006-00317 supported by the Ministry of Science and Innovation of Spain. Also, the PhD candidate has been granted with a FPU postgraduate research fellowship with the reference AP2008-04646 from the Ministry of Education, Culture and Sport (Spain). The training period has been completed by a short stage period in the Membrane Science & Technology Group, University of Twente, The Netherlands under, the supervision of Dr. Kitty Nijmeijer.

Sustainable industrial growth is based on the development of new industrial processes able to solve global important problems like greenhouse gas emissions, energy efficiency and toxic waste. Many academic and industrial efforts are being made in order to reach the zero discharge goal.

The separation and valorization of industrial flue gases with complex composition allows approaching sustainability by means of different routes. The production of streams concentrated in valuable components can include (i) a reuse in the same industrial process to increase the energy efficiency of the overall process or (ii) the further use as reactants in the synthesis of various chemicals.

In this thesis, a case of study is defined as the tail gas generated in the manufacturing of carbon black, a commodity whose global production reaches 80 million tons, in medium - high sized installations. The tail gas is formed, in a dry basis, by the following gas mixture, in vol %: 60.5% N_2, 17.9 % CO, 16.4 % H_2 and 5.3 % CO_2. Hydrogen and carbon monoxide are identified as major valuable components. It is envisaged that membrane technology will allow to obtain H_2 enriched permeate stream when polymeric membranes are used and CO can be obtained as permeate gas stream when facilitated transport - supported liquid membranes are used.

Chapter I of this thesis gives a brief introduction over different gas separation methods and shows the industrial sources and importance of H_2 and CO. The first part of chapter I focuses on more detailed aspects of polymeric membrane-based H_2 separation, including the transport mechanism, the selection of the polymeric material for the manufacturing of membranes, and the mixed gas permeation through polymeric membranes. Also, a description of the production process of carbon black is included. In the second part the CO separation by means of π - complexation is exposed showing the particular aspects involved when facilitated transport - supported liquid membranes are used. Also, an overlook on room temperature ionic

liquids is given with the principal focus on their potential use as liquid phase in facilitated transport - supported ionic liquid membranes.

Chapter II and III of this thesis deal with the study of polymeric membrane based separation of hydrogen from mixed gas streams composed of H_2, CO, N_2 and CO_2 at different operation conditions, using membranes prepared with a commercial glassy polymer, Matrimid. The methodologies used to prepare both planar and asymmetric hollow fiber membranes are described in detail. In chapter II the use of a planar Matrimid membrane allowed to describe H_2 and CO_2 permeation behavior of pure, binary, ternary and quaternary mixtures using the "dual-mode sorption, partial immobilization" model. Non-ideal effects, such as competitive sorption between permeants, have been characterized, providing the mass transfer parameters for the systems. These results provide useful knowledge related to the intrinsic material properties. In chapter III the use of a asymmetric hollow fiber membrane made of the same polymeric material allowed to determine the major differences between the gas permeation (pure and mixed) through an dense isotropic structure (planar membrane) and an asymmetric structure (hollow fiber). Also, a comparative permeation performance with another asymmetric hollow fiber made from a much more permeable glassy polymer, polyphenylene oxide, was made.

Chapter IV is focused on the design of a liquid phase system to be used in facilitated transport-supported ionic liquid membranes for the recovery of carbon monoxide. A comprehensive look at the reaction mechanism and the equilibrium parameters obtained from the experimental characterization of the physical and chemical solubility of carbon monoxide in pure ionic liquid 1-Hexyl-3-methylimidazolium chloride ([hmim][Cl]) and 1-Hexyl-3-methylimidazolium chlorocuprate obtained by mixing copper chloride with [hmim][Cl] is presented. The latter one presented excellent solubility selectivity properties for the separation of the mixture CO/N_2.

Finally, in Chapter V overall conclusions of the entire work are made. Also prospects for further research are included.

RESUMEN

Esta tesis doctoral está enfocada hacia la separación y recuperación de hidrogeno y monóxido de carbono de efluentes gaseosos residuales procedentes de procesos industriales de combustión mediante la tecnología de membranas. El presente trabajo ha sido llevado a cabo en el grupo de investigación Procesos Avanzados de Separación del Departamento de Ingeniería Química y Química Inorgánica de la Universidad de Cantabria (España), en el marco de los proyectos ENE 2010-15585, CTQ 2008-00690/PPQ y CTM 2006-00317 financiados por el Ministerio de Ciencia e Innovación de España. Asimismo, la candidata a doctora Oana C. David disfruto de una Beca del Programa de Formación de Profesorado Universitario (FPU) con la referencia AP2008-04646, financiada por el Ministerio de Educación, Cultura y Deporte de España. La formación ha sido completada mediante una estancia de 4 meses en el grupo de investigación Membrane Science & Technology de la University of Twente (Países Bajos) bajo la supervisión de la Dra. Kitty Nijmeijer.

El crecimiento industrial sostenible está basado en el desarrollo de nuevos procesos industriales capaces de resolver problemas globales como la emisión de gases residuales, la eficiencia energética y la generación de residuos tóxicos. En la actualidad, se realizan muchos esfuerzos académicos e industriales para conseguir el objetivo de vertido cero.

La separación y valorización de gases residuales de la industria con composición compleja permite acercarse al objetivo de sostenibilidad mediante varias aproximaciones. Las corrientes gaseosas concentradas en componentes con valor añadido se pueden reusar mediante combustión en el mismo proceso industrial para aumentar la eficiencia energética global, o bien posteriormente como reactivos en la síntesis de compuestos químicos múltiples.

En el presente trabajo se ha definido como caso de estudio la corriente de gases generada en la fabricación de negro de carbono, un *commodity* cuya producción mundial alcanza los 80 millones de toneladas anuales, en plantas de tamaño medio - grande. Esta corriente residual está formada por la siguiente mezcla gaseosa, cuya composición en porcentajes de volumen es: 60.5 % N_2, 17.9 % CO, 16.4 % H_2 and 5.3 % CO_2, de la cual el hidrógeno y el monóxido de carbono son los más valiosos. Se espera que el uso de tecnologías de separación con membranas permita obtener en el lado del permeado de la membrana una corriente enriquecida en hidrógeno al emplear una membrana polimérica y una corriente enriquecida en monóxido de carbono mediante el transporte facilitado a través de una membrana líquida soportada.

El Capítulo I de la tesis contiene una introducción sobre los distintos métodos de separación de gases y presenta las fuentes e importancia industrial de H_2 y CO. La primera parte del capítulo I enfoca aspectos detallados relacionados con la

separación de H_2 basada en la tecnología de membranas, así como el mecanismo de transporte, la selección del material polimérico empleado en la fabricación de las membranas y la permeación de mezclas gaseosas a través de membranas poliméricas. Además, se incluye una descripción del proceso productivo del negro de carbono. En la segunda parte del capítulo I se expone la separación del CO mediante la complejación - π indicando los aspectos particulares que aparecen en procesos de transporte facilitado a través de membranas líquidas soportadas.

Los capítulos II y III de la tesis abarcan el estudio de la separación selectiva de hidrógeno a partir de corrientes gaseosas compuestas por mezclas de H_2, CO, N_2 y CO_2 utilizando membranas preparadas a partir de un polímero comercial de tipo vítreo, denominado Matrimid. Se describen en detalle las distintas metodologías empleadas en la elaboración de membranas con morfología bien de película plana densa o bien en configuración de fibra hueca. En el capítulo II el uso de una membrana plana de Matrimid permitió la descripción de las propiedades de permeación del H_2 y CO_2 puros y en mezclas binarias, ternarias y cuaternarias mediante el uso del modelo matemático "modo dual de adsorción, inmovilización parcial" *("dual-mode sorption, partial immobilization")*. Se caracterizaron efectos no-ideales como son la adsorción competitiva, que permitieron determinar los parámetros de transferencia de materia implicados en los sistemas bajo estudio. En el capítulo III el uso de una membrana con una morfología de fibra hueca asimétrica preparada del mismo material polimérico permitió establecer las principales diferencias en la permeación de gases puros o mezclas de gases que aparecen al utilizar una estructura asimétrica (fibra hueca) frente al caso de aplicar una estructura isotrópica densa (membrana plana). Además, se realizó un estudio comparativo entre las propiedades de permeación de gases de la fibra hueca de Matrimid con los de otra fibra hueca asimétrica basada en un polímero mucho más permeable (PPO).

El capítulo IV está enfocado al diseño de un sistema líquido para ser usado en el transporte facilitado a través de membranas líquidas soportadas para la recuperación del CO. Se realizó un análisis exhaustivo sobre el mecanismo de reacción y los parámetros de equilibrio obtenidos mediante la caracterización experimental de la solubilidad física y química del monóxido de carbono en el líquido iónico puro 1-Hexil-3-metilimidazolio cloruro ([hmim][Cl]) y en 1-Hexil-3-metilimidazolio clorocuprato obtenido mediante la mezcla de cloruro de cobre (I) con [hmim][Cl]. Esta última mezcla presenta unas propiedades de selectividad de la solubilidad excelentes para la separación CO/N_2.

Finalmente, el capítulo V presenta las conclusiones globales del trabajo de tesis doctoral. Además, se incluyen perspectivas para la investigación futura.

Table of contents

Chapter IV

Chapter V

Chapter I

INTRODUCTION

1.1. GAS SEPARATION

The major, industrially applied gas separation technologies like pressure swing adsorption (PSA), temperature swing adsorption (TSA), liquid absorption and stripping, cryogenic distillation and membrane separation play today a critical role in a number of large chemical processes as summarized in Table I - 1.

Table I - 1. Gas separation technologies and their applications

Technology	Separation	Process	Ref
PSA and TSA	O_2/N_2	Air separation	[1]
	CO, CO_2, CH_4, N_2/H_2	Hydrogen purification	
	H_2O/EtOH, air	Ethanol and air drying	
	CO_2/C_2H_4, CH_4	Enrichment of natural gas	
Cryogenic distillation	O_2/N_2	Air separation	[2]
	olefin/paraffin	Ethylene plant	
Absorption and stripping	SO_3	Concentration of sulfuric acid	[2]
	CO_2/H_2S	CO_2 Recovery from flue gases	
	NH_3	Phosam process	
	CO_2	The production of sodium carbonate	
	olefin/paraffin	Ethylene plant	
Membrane separation	O_2/N_2	N_2 or O_2 enrichment of air	[3]
	CO_2, H_2S, H_2O/CH_4	Enrichment of natural gas	
	CO, CO_2, CH_4, N_2/H_2	Hydrogen purification	
	Ethylene, propylene/N_2	Polyolefin plant resin degassing	
	H_2O/Air, H_2O/CH_4	Air drying, natural gas drying	

As listed in Table I - 1 gas separation technologies are in most cases competing for the same application. For high product purity requirements, a combination of technologies is preferred. For example, in the production of high purity N_2, O_2 and Ar from air, a PSA unit is used to remove CO_2 and H_2O prior to the cryogenic distillation in order to avoid the deposition of frozen CO_2 and H_2O within the process equipment [4].

The selection of a separation process must take into account first the recovery and purity specifications of the product, then the difference between the properties of the components to be separated and finally the scale of operation [3, 5, 6]. The specific advantages and disadvantages of each technology are reported in Table I - 2.

Table I - 2. Pros and cons of existing gas separation technologies

Technology and property differences	Advantages	Disadvantages
PSA and TSA Surface sorption	High purity product Suitable at small-scale for air separation	High power usage and costs Slow heating and cooling steps for TSA Low adsorbate concentrations in the feed (less than 3 wt. %)
Cryogenic distillation - Gas boiling temperatures	The most economic for large scale separation of air	It is not practical for high purity High energy requirements Difficulty in separating gases of similar volatility [7]
Absorption and stripping Physical or/and chemical absorption	Excellent for acid gas (H_2S, COS) removal before PSA	Limited loadings High energy requirements. Solvent corrosion and degradation.
Membrane separation Diffusivity and solubility	Low power usage and costs, Simplicity in operation [8], Compactness and portability Small scale separations Scalability to small sizes	Modest operating temperature Limited gas purity Structural damage with plasticizing gases Productivity/selectivity trade – off Low pressure product (H_2)
Supported liquid membranes Diffusivity and reaction equilibrium	High gas selectivity and permeability values The possibility to use expensive carriers (low quantity used)	Carrier chemical degradation Loss of solvent (volatilization) Membrane instability It is not yet industrialized [9]

Table I - 2 stresses the economics and operational advantages that membrane technology presents over the other gas separation alternatives, making it the preferred technology for modest product purity requirements and for small scale separation. In recent years much progress has been made in the field of gas separation by supported liquid membrane technology, but the implantation of this technology at industrial scale is expected to be on the midterm since developments are still needed [9]. Since 1980 when the first large industrial application of membrane technology was launched by Permea, membrane – based operations, substituting or integrated with the traditional ones, have experienced a rapid growth,

with many companies, such as Cynara –Natco, Separex – UOP, GMS, Generon, Praxair, AirProducts, UBE. A list of the main industrial applications of membrane technology in gas separation along with the membrane materials used and the status of the membrane technology is given in Table I -3. Also, a comparison of membrane with other gas separation technologies is made in references [10, 11].

Table I – 3. Main applications of membrane technology for gas separation [12].

Separation	Process	Traditional technology	Membrane material	Status of membrane technology application
H_2/N_2	Ammonia purge gas	PSA	Pd-based Polysulfone	Lab scale Plant installed (Prism by Permea)
H_2/CO	Adjustment of H_2/CO ratio in syngas plant	PSA	Pd-based Silicon rubber Polyimide	Lab scale Lab scale Plant installed (Separex)
H_2/ hydrocarbons	H_2 recovery in refineries	PSA	Pd-based Silicon rubber	Lab scale Plant installed (Sinopec Zhenhai, China);
			Polyimide	Prism by Permea (Du Pont)
			Cellulose acetate	Separex – UOP (Petronor, Spain)
H_2/light hydrocarbons	Ethylene cracker	Cryogenic distillation	Pd-based PTMS, PMP	Lab scale Pilot plant
O_2/N_2	Air separation	Cryogenic distillation	Silicon rubber	Plant installed: (Cynara; Separex; GMS; Air Products)
			Polysulfone	Plant installed (Permea)
			Polyimide	Plant installed (Medal; Dow-Generan; UBE)
			Polyphenylene	Plant installed (Aquilo)
			Ethyl Cellulose	Plant installed (Air Liquide)
			Ion transport	Lab scale
N_2/CH_4	Nitrogen removal	Cryogenic distillation	Silicon rubber PMP Parel PEBAX	Pilot plant Lab scale

Table I – 3. (continued)

Separation	Process	Traditional technology	Membrane material	Status of membrane technology application
H_2O/CH_4	Dehydration	Glycol absorption	Cellulose acetate Polyimide Polyaramide	Plant installed
CO_2/CH_4	Sweetening of natural gas	Amine absorption	Cellulose acetate	Offshore platforms in Thailand gulf (Cynara – NATCO; Grace – Separex)
			Polyaramide	Plant installed (Medal)
			Polyimide	Plant installed (Medal)
			Perfluoro - polymers	Plant installed (MTR)
CO_2/ Hydrocarbons	Natural gas liquid removal	Glycol absorption and cooling in a propane refrigeration plant (-20^{o}C)	Cellulose acetate Polyaramide Polyimide	Early commercial stage. A demonstration system installed
CO_2/N_2	CO_2 capture from flue gases streams	Amine absorption	Polyimide FSC, PEEKWC, Zeolite, silica based carbon.	Pilot plant Lab scale
VOCs/gas	Polyolefin plant resin degassing; Ethylene recovery	Adsorption, Refrigeration and turbo expander plants	Silicone rubber, PTMS	Plant installed (MTR; OPW Vaporsaver™)

1.2. CARBON BLACK MANUFACTURE

Carbon black is a generic term for an important family of products used widely to modify the mechanical, electrical, and other physical properties of the medium in which it is dispersed. It is the most widely used nano - material, with particle dimensions ranging from tens of nanometers to a few hundred nanometers. It plays a major role in elastomers, plastics, paints and inks as a reinforcing agent, a black pigment, and an electrically conductive material [13].

There are two main types of carbon black: rubber grade, and special grade. The rubber grades are primarily used as a reinforcing agent in tyres and other rubber products to improve their mechanical properties. Most of the special grades are manufactured to meet product specifications for imparting certain properties required by the end - use products, such as dispersion, pigmentation, and electrical conductivity.

There are several alternatives for the manufacture of carbon black, including oil-furnace black process, thermal black process, acetylene black process, lampblack process, and impingement black process. The oil-furnace black process is predominant. In this process carbon black is produced by injecting a hydrocarbon raw material into a flow of reducing hot gas wherein the feedstock is pyrolyzed and converted into a smoke before being quenched by a water spray. The carbon black formation can be described in terms of nucleation, growth and structure development and occurs by condensation and dehydrogenation reaction as described by Equation I – 1. [14].

$$C_nH_{2n+2} \rightarrow n \cdot C + (n+1) \cdot H_2 \qquad \text{(I - 1)}$$

The carbon black production process scheme using an axial flow reactor developed by Columbian Black Company [15] is shown in Figure I – 1.

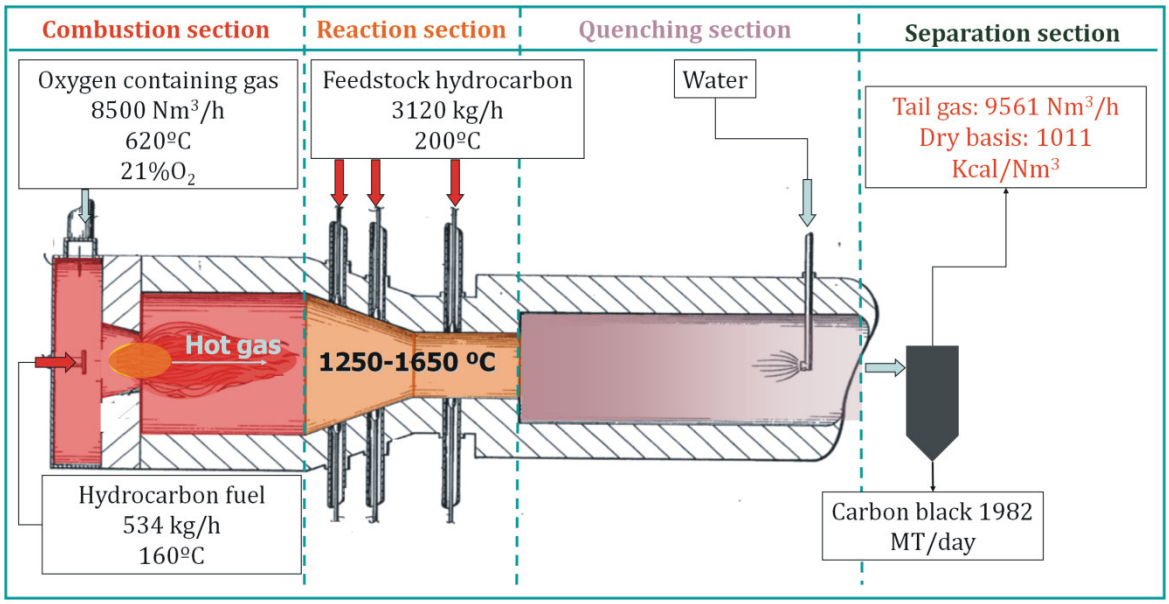

Figure I – 1. Carbon black manufacturing process scheme

The hot gas is produced by burning fuel into a combustion chamber. The hot gas flows from the combustion chamber into a reaction chamber which is in open communication with the combustion chamber. The hydrocarbon raw material is introduced into the hot gas as the hot gas flows through the reaction chamber, thereby forming a reaction mixture comprising particles of forming carbon black. The reaction mixture flows from the reaction chamber into an exit chamber which is in open communication with reaction chamber. At some location in the exit chamber a quench spray is introduced into the flowing reaction mixture, thereby lowering the temperature of the reaction mixture below the temperature necessary for carbon black production and halting the carbon black formation reaction. The carbon black particles are then separated from the flow of gas. The carbon black formation occurs in the temperature range of 1250 to 1650 ^{o}C.

After collecting carbon black in bag filters a tail gas stream is generated that can contain as much as 40 to 55 mol% of water vapor due to the process water used to control the reaction effluent. Even diluted with water the tail gas stream possesses sufficient heating value in order to be used as flue gas under dryers, boilers, and in incinerators. On dry basis the heating value of the tail gas is of 1011 kcal/m^3 (STP) [16]. This combustion step to recover heat has the added benefit of cleaning up the effluent gas from carbon black particulate. It ultimately contains gaseous components in an oxidized state: CO_2, SO_2, NO_x with small amount of CO and it is discharged to the atmosphere or given further treatment (stack gas scrubbing).

Typical hydrocarbon feedstock for the oil-furnace process include: cat cracker decant oil, ethylene plant residuum from naphtha cracking, ethylene plant residuum from gas oil cracking, extract from solvent refining of cat cracker cyclic oils and coal tar distillate.

A comprehensive review of the technical and commercial aspects of carbon black usage along with the history of carbon black, its microstructure, chemical composition, morphology, surface activity, and characterization are discussed in reference [13].

1.3. HYDROGEN

Hydrogen (H_2) in the lithosphere is, with few exceptions, bound to other elements (e.g., as in water) and must be separated by using other sources of energy to produce molecular hydrogen. Properly considered, hydrogen fuel is not a primary energy source in the context of a hydrogen economy [17]. The increased awareness of the finite nature of our fossil fuel sources and their uneven distribution favor today a transition to a new energy system based on hydrogen, a clean energy vector.

Hydrogen can be produced by various means:

- steam reforming, partial oxidation, autothermal reforming, combined two step reforming of light hydrocarbons (mainly methane),
- gasification of coal, petroleum, petcoke, biomass,
- petroleum refining,
- from coke oven gas,
- supercritical water gasification (dissolution of organic compounds and lignocellulosic materials as solid biomass in supercritical water at elevated temperature)
- electrolysis of water by wind, solar or grid energy,
- thermal splitting of water by nuclear energy.

Today, the most widely used method (80 %) for H_2 production is the steam reforming of light hydrocarbons [18, 19]. The production of H_2 from the gasification of coal is expected to present a significant increase in the future due to the great research effort dedicated to the technological improvement to make the process economic. The gasifier feed stocks (coal, biomass and petroleum coke) are all significantly lower cost than oil or natural gas, but gasification and downstream processing of syngas to make electricity are expensive [20]. In the low oxygen environment of the gasifier secondary compounds like hydrogen sulfide (H_2S), carbonil sulfide (COS), ammonia (NH_3), hydrogen cyanide (HCN), hydrogen chloride (HCl) together with trace elements like mercury, arsenic and other heavy metals are formed and must be removed. Technologies such as the co-production of H_2 and power from the coal generated syngas in an Integrated Gasification Combined Cycle (IGCC) are contemplated [21]. Both methods generate in the first stage syngas that is followed by the high or low – temperature, water-gas shift (WGS) reaction for further hydrogen conversion:

$$CO + H_2O \rightleftharpoons CO_2 + H_2 \qquad \text{(I - 2)}$$

The separation of CO_2 from shifted syngas is done currently by amine absorption, but may also be done by the absorption of CO_2 in chilled methanol or ethylene glycol (the Rectisol® or Selexol® process, respectively) or by means of membrane technology. Membrane-based technology approaches may reduce the cost of amine based process estimated in \$40-100/ton CO_2 [22]. Other sources of hydrogen include the tail gas stream from petroleum refining, ammonia purge gas, coke oven gas and the flue gases from carbon black manufacturing. The typical composition of these major sources of H_2 is listed in Table I - 4.

Table I – 4. Typical compositions found in common hydrogen sources.

Hydrogen source	Composition (mol %)							T (°C)	P (bar)	Ref
	H_2	N_2	CO_2	CO	CH_4	H_2S	Other			
Syngas from autothermal reforming of natural gas	56.8	0.2	2.9	29	1.0	-	10.1 H_2O	1063		[23]
Syngas from gasification of coal with oxygen and steam	25 - 30	0.5 - 4	5-15	30-60	0-5	0.2-1	2-30 H_2O	1315		[24]
Dry shifted syngas	56.5	0.7	40.6	0.8	1.8	0.5	-	200		[20]
Hot shifted syngas	50.9	0.7	36.8	1.1		0.5	10 H_2O	200		
Petroleum refining										[25]
Naptha hydrotreater	90	-	-	-	5.2	-	4.8 C_{2+}	35	40	
Light naptha isomerization	85	-	-	-	5.2	-	9.8 C_{2+}	30	19	
Mild hydrocracking	32	-	-	-	23.1	-	38.9 C_{2+}	40	12	
Ammonia purge gas	60	20	-	-	13	-	2 NH_3, 4.5 Ar		131	[26]
Dry coke oven gas	56.4	5.5	3.1	8.4	26.6	-	-			[27]
Carbon black manufacturing tail gases	16.3	60.7	5.3	17.8	0.7	-	-	200		[16]

1.3.1. Hydrogen separation by polymeric membranes

Today, membrane technology is successfully applied at industrial level for hydrogen recovery from ammonia purge streams, syngas ratio adjustment and hydrogen recovery in refineries. These three applications involve easy task separations since the extraordinary small molecular size of H_2 makes it extremely permeable and easily collected as permeant compared to the other slower permeating components: N_2, CO and CH_4. Surprisingly, it is difficult to separate H_2 from CO_2 [28].

Broadly, hydrogen selective membranes (based on the materials used) can be categorized into two types: organic (polymer) and inorganic (metallic, carbon, and ceramic). High-purity hydrogen (up to 99.99%) could be available through dense metallic membranes and especially through Pd and its alloys, but the commercial application of metallic membranes faces today important limitations due to drawbacks like: (i) poisoning effect that hydrogen sulfide (H_2S) and other feedstocks have on the hydrogen transport mechanism, (ii) high cost for the preparation of Pd membranes and (iii) mechanical stability [7]. The key advantages of polymer membranes are the ability to cope with high pressure drops and low cost. Therefore, the separation of H_2 by polymeric membranes has become an attractive existing technology.

Generally, gas transport in non-porous (dense) membranes occurs via the solution-diffusion mechanism, comprised of three main steps:

1. Sorption of the gaseous penetrants at the upstream side of the membrane,
2. Diffusion of the penetrants across the membrane,
3. Desorption of the penetrants at the downstream side of the membrane [29].

The solution diffusion mechanism is driven by a difference in the thermodynamic activities existing at the upstream and downstream faces of the membrane as well as the interacting force working between the molecules that constitute the membrane material and the permeate molecules. The activity difference causes a concentration difference that leads to diffusion in the direction of decreasing activity. Fick's law is the simplest description of gas diffusion through a nonporous structure [30], i.e.

$$J_i = -D_i \frac{dC_i}{dx} \qquad (\mathrm{I}-3)$$

where J_i is the permeation flux through the membrane of a component i, D_i is the diffusion coefficient and the driving force dC_i/dx is the concentration gradient across

the membrane. Under steady-state conditions this equation can be integrated to give:

$$J_i = D_i \frac{(C_{2,i} - C_{1,i})}{\delta} \qquad (\mathrm{I}-4)$$

where $C_{2,i}$ and $C_{1,i}$ are the concentration at the upstream and downstream side of the membrane, respectively and δ is the thickness of the membrane.

In ideal systems, the concentrations are related to the partial pressures by Henry's law which states that a linear relationship exists between the concentration inside the membrane (C_i) and the (partial) pressure of gas outside the membrane (p_i), i-e.

$$C_i = S_i \cdot p_i \qquad (\mathrm{I}-5)$$

where S_i (cm^3(STP) cm^{-3} bar^{-1}) is the solubility coefficient of component i in the membrane. Henry's law is mainly applicable to amorphous elastomeric polymers because solubility behavior is often more complex below the glass transition temperature, as described in chapter II by the "dual sorption partial immobilization model".

Combining Equation I - 4 with Equation I - 5 gives:

$$J_i = D_i \cdot S_i \frac{(p_{2,i} - p_{1,i})}{\delta} \qquad (\mathrm{I}-6)$$

an equation which is generally used for the description of gas permeation through membranes. The product of the diffusion coefficient and solubility coefficient is called the permeability coefficient P_i, i.e.

$$P_i = D_i \cdot S_i \qquad (\mathrm{I}-7)$$

The diffusion coefficient is a kinetic parameter that measures the mobility of the penetrant molecules in the membrane and is mainly dependent by the gas kinetic diameter. The kinetic diameter of a gas is defined as the intermolecular distance of closest approach for two molecules colliding with zero initial kinetic

energy [31]. This is dependent on the molecular size, shape, as well as dipole-dipole interactions. In polymer materials, diffusion coefficients decrease as the molecular size increases, because large molecules interact with more segments of the polymer chain than small molecules do.

The solubility coefficient is a thermodynamic parameter expressed by the ratio of the dissolved penetrant concentration in the polymer to the pressure of the continuous gas phase and it is a measure of the energy required by the gas to be sorbed by the polymer [32]. The value of the solubility coefficient increases with increasing gas condensability. A measure of the gas condensability is given by the gas critical temperature [33].

In general, gases with large diffusivity values present low solubility values and the opposite. Table I - 5 lists the values of the kinetic diameter and the critical temperature of a range of species found in H_2 recovery.

Table I – 5. Kinetic diameter [31] and critical temperature [34] of various molecules found in H_2 recovery.

Gas	Kinetic diameter (Å)	Critical temperature (K)
H_2O	2.65	647.3
H_2	2.89	33.2
CO_2	3.3	304.2
O_2	3.46	154.6
H_2S	3.6	373.2
N_2	3.64	126.2
CO	3.76	132.9
CH_4	3.8	190.6
C_3H_8	4.3	369.8

Below the glass-transition temperature, the polymer chains are essentially fixed; the polymer is a rigid, tough, glassy material and the effect of differences in size of the permeating gases on their relative mobility is large. If the polymer is above its glass transition temperature, motion of the polymer chains is possible. The polymer is then rubbery and elastic and the effect of molecular size of the permeating gases on relative mobility is reduced. Therefore, glassy polymers discriminate gas species transport according to gas diffusivity and elastic polymer according to gas solubility. Consequently, the order of gas permeability in glassy

polymers is therefore determined by the gas kinetic diameter, whereas in rubbery polymers the order is determined by gas condensability [32]. In Figure I – 2 the values of the kinetic diameter and gas critical temperature are listed in an increasing order to show the difference in the order of gas permeability for glassy and for rubbery polymeric membranes.

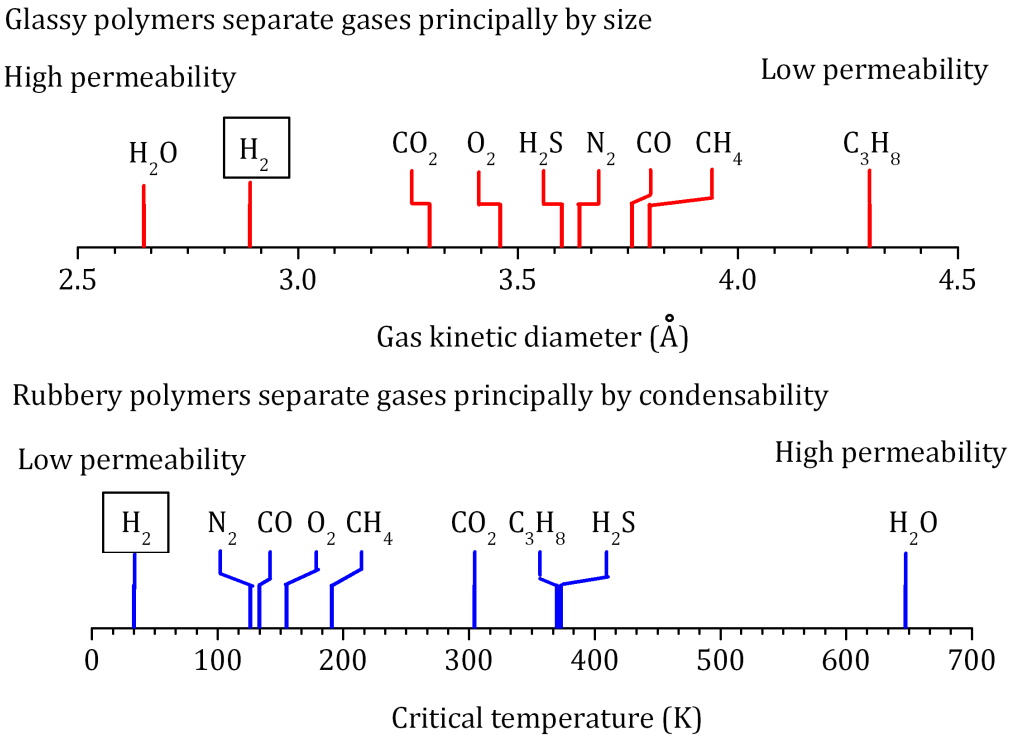

Figure I - 2. Depiction showing the relative size (kinetic diameter) and condensability (boiling point) of various gases. Glassy membranes generally separate using differences in size; rubbery membranes separate using differences in condensability.

The separation factor (ideal selectivity) characterizes membranes in terms of separation and is defined, in the case of negligible downstream pressure, as the ratio of permeabilities

$$\alpha_{i/j} = \frac{P_i}{P_j} \qquad (I-8)$$

In the case of gas mixture the gas selectivity is calculated according to equation I – 9:

$$\alpha_{i/j}^{mixture} = \frac{C_i^P / C_j^P}{C_i^F / C_j^F} \qquad (I-9)$$

where C is the gas concentration (vol %) and P refers to the permeate and F to the feed side of the membrane

Membranes based on rubbery polymers minimize size selectivity and maximize sorption selectivity, and, therefore are used for the separation of highly condensable gases like propane and other hydrocarbons from methane. Membranes based on glassy polymers are best used for the separation of highly mobile gases like hydrogen, i.e. H_2/CO and H_2/N_2 separations.

Although H_2 has a high diffusivity, because of its low condensability, it has a very low solubility in membranes. A more soluble, lower diffusivity gas such as CO_2 may have a steady state permeability comparable to that of H_2 [28]. Therefore, for H_2/CO_2 separation both glassy and rubbery polymers can be used with H_2 or CO_2 respectively as the permeating specie, but the application of polymeric membranes for separation H_2 and CO_2 is restrained.

Gas separation membranes need to be highly permeable to one of the mixture components while significantly rejecting the other components. The vast amounts of polymers that have been investigated, however, show the general trend that highly permeable polymers possess low selectivities. This effect is referred as the permeability/ selectivity trade off relationship and Robeson [35] has suggested that possesses an upper limit which needs to be exceeded in order to obtain progress in the application of polymeric membranes for gas separation. This upper limit, also referred to as upper bound, was determined by plotting the ideal separation factor versus permeability values of multiple gas pairs of interest. This limit is given by the latest gas separation data available in the literature and belongs to high performance polymers unavailable at commercial scale. The last available upper bound correlations were reported in 2008 and are shown in Figure I - 3 for H_2/N_2 and H_2/CO_2 gas pairs of interest in this work. Figure I – 3 also includes the prior upper bound reported in 1991 [36]. In the case of H_2/N_2 correlation, although a large amount of data has been generated since 1991, a very minor shift in the upper bound relationship is noted. In the case of H_2/CO_2 a limited shift in the upper bound relationship is noted, primarily a slight slope change resulting from a number of data points at the higher permeability end of the relationship. The limited number of data points at the lower permeability area of the dataset may have skewed the slope versus the original correlation.

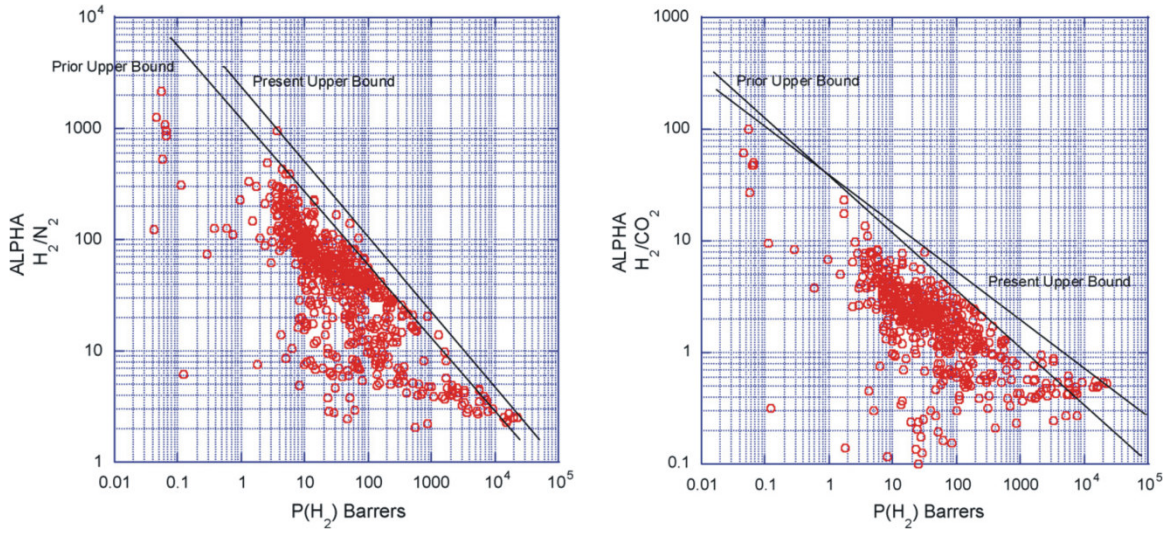

Figure I – 3. The upper bound correlations for H_2/N_2 and H_2/CO_2 separation [35].

A further limitation for H_2 recovery is given by streams like the shifted syngas and refinery purges that contain components that strongly affect the membrane performance and durability (CO_2 and light hydrocarbons) [12].

Different ways to overcome this problems include today the development of new membrane materials like polymers with high inner porosity [37-40], hiperbranched polyimides [41, 42], perfluorinated copolymers [43, 44] or the incorporation of inorganic nano – particles of high porosity and permeability into the polymer matrix (Mixed Matrix Membranes - MMM_s) [45-47].

1.3.2. Polymer selection

In order to choose the best performance material for H_2 recovery from the carbon black manufacturing tail gas stream first of all it must be determined if a glassy or rubbery polymer will be used. As explained in section 1.3.1 the separation of H_2 from N_2 is best done by membranes based on glassy polymers meanwhile for H_2/CO_2 separation both glassy and rubbery polymers can be used. Therefore, considering the high concentration of N_2 in the carbon black manufacturing tail gas (see Table I – 4) it was determined that a H_2 permeable polymer (a glassy polymer) must be used. Also, due to the low concentration of H_2 in the gas mixture of case studied in this work, a polymer with high selectivity towards H_2 and reasonable permeability is needed.

At this point, an analysis of gas permeation properties of various commercial polymers was made (data listed in Table I – 6) by plotting H_2/N_2 and H_2/CO_2 selectivity values versus H_2 permeability in Robeson-type plots (see Figure I - 4)

where the Robesson upper - bound limit was included. Little or no available data was found for CO, but it is known that CO transport behavior is similar to that of N_2 and therefore it can be assumed that an optimum polymer choice for H_2/N_2 will also apply for H_2/CO separation.

Table I - 6. Glass transition temperature (Tg), density and permeation properties of commercial available polymers used in membrane based gas separation

Commercial Polymers	Tg (K)	Density (g/cm^3)	P_{H2} (Barrer)	Ideal selectivity		Exp. Cond.
				H_2/N_2	H_2/CO_2	
Poly (vinylidene floride), PVDF	238[a]	1.75[a]	2.4[b]	3.42[b]	2[b]	30°C, 1.4 bar
Poly (methyl methacrilate), PMMA	379[a]	1.17[a]	2.4[b]	2[b]	4[b]	30°C, 1.4 bar
Cellulose acetate, CA	243-473[a]	1.3[a]	2.63[c]	12.52[c]	0.4[c]	30°C
Polyetersulfone, PES	498[a]	1.37[a]	8.96[d]	69.5[d]	2.7[d]	35°C, 3.5 bar
Polyetherimide, Ultem	209[e]	1.27[e]	11[f]	50[f]	5.9[c]	30°C
Bisphenol-A polycarbonate	423[a]	1.2[e]	11.5[g]	42.6[g]	2.1[g]	25°C, 3.7bar
Bisphenol – A Polysulfone	459[a]	1.24[e]	14[c]	56[c]	2.5[c]	30°C
Poly (ethylene) low density, LDPE	148[a]	0.92[a]	17.3[b]	4.1[b]	1[b]	30°C, 1.4 bar
Polystyrene, PS	373[a]	1.04[a]	23.8[b]	28.8[b]	2.3[b]	30°C, 1.4 bar
Polyimide , Matrimid	502[d]	1.24[e]	27.16[h]	97[h]	3.9[h]	35°C, 3.5 bar
Polyimide, PBI	691[i]	1.331[i]	0.6[i]	125[i]	3.75[i]	35°C, 20 bar
Ethyl cellulose,	316[a]	1.14[a]	87[c]	27.2[c]	3.3[c]	30°C
Polyphenyleneoxide, PPO	483[a]	1.06[e]	113[c]	29.7[c]	1.5[c]	30°C
Poly (4-methyl pentene-1)	323[a]	0.814[a]	125[c]	18.7[c]	1.5[c]	30°C
Poly (dimethylsiloxane), PDMS	150[a]	0.97[a]	550[c]	2.2[c]	0.2[c]	30°C

[a]: [48], [b]: [49], [c]: [50], [d]: [51], [e]: [29], [f]: [52], [g]: [53], [h]: [54]. [i]:[55]

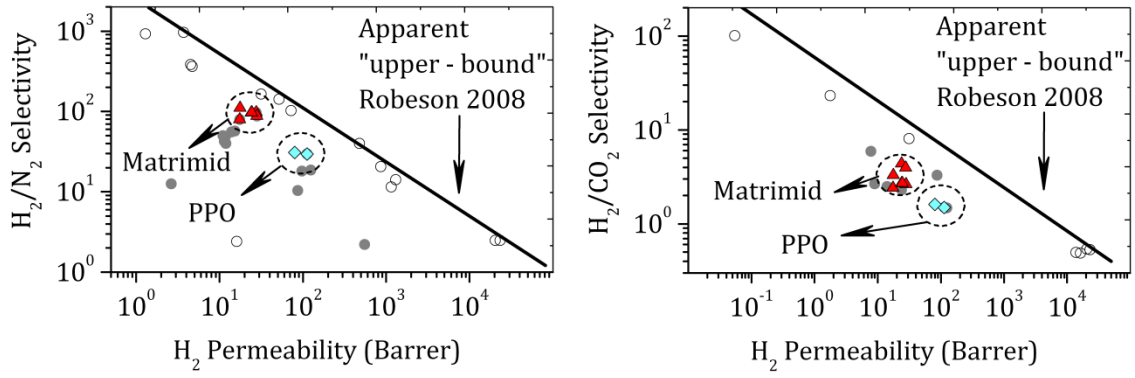

Figure I - 4. H_2/N_2 and H_2/CO_2 upper limit selectivity/permeability trade - off.
(○) New Robeson data 2008, (●) Comercial polymers data (see Table I - 6)

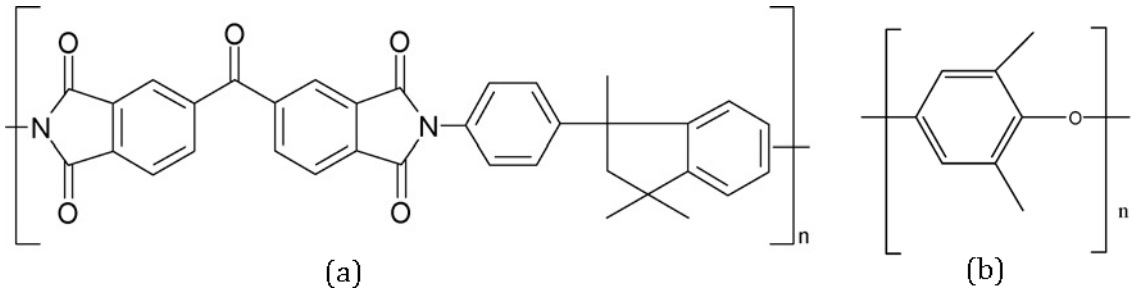

Figure I – 5. The chemical structure of (a) Matrimid® 5218 and (b) PPO monomer unit

It was decided that the commercial Matrimid® 5218, an aromatic polyimide of 3,3',4,4'-benzophenone tetracarboxylic dianhydride and diaminophenylidane, presents a good tradeoff between H_2 permeability and both H_2/N_2 and H_2/CO_2 selectivities and it was considered to be the optimum polymer for H_2 recovery.

Also, it was decided to study a more permeable material. PPO, poly(2,6-dimethyl-1,4-phenyelene oxide), is a polymer that, because it posses high fractional free volume, it exhibits unexpectedly high values of gas permeabilities for a glassy polymer. The gas selectivity of this material is relatively low but still higher when compared with rubbery polymers. This opposite gas performance properties are reflected in Figure I – 4 and the chemical structure of these polymers is shown in Figure I - 5.

Aromatic polyimides are one of the most important classes of high performance polymers. They are highly thermally stable, have high glass transition temperatures and relatively low dielectric constants. The various polyimides have become important in many applications, such as semiconductor devices, high temperature adhesives, and high performance composite materials [56]. Matrimid attracted a lot of attention for gas separation membranes due to the combination of

relatively high gas permeability coefficients and separation factors coupled with excellent mechanical properties solubility in non-hazard organic solvents and commercial availability [57]. It has a high glass transition temperature (see Table I – 6). Detailed polymer data are found in the Polymer Data Sheet provided by the manufacturer (see Appendix I).

As means of improving membrane performance towards the permeation of gas mixtures of H_2 that contain CO_2 and suppress CO_2 induced plasticization, polymer blending method has been recently approached [58, 59]. New asymmetric hollow fiber membranes were fabricated from polymer blends of Matrimid and another polyimide, poly(2,2'-(1,3- phenylene)-5,5'-bibenzimidazole), (PBI) [60].

PBI is a high performance polymer with a relatively high glass transition temperature (~418 ◦C), outstanding thermal and chemical stabilities [60], high H_2/N_2 and H_2/CO_2 gas selectivity but extremely low gas permeability due to a high packing density of the polymer matrix (see Table I – 6).

Severe brittleness of PBI material has been a major limitation for its applications in membrane processes and in literature a blend of Matrimid with PBI was already employed to synergize the advantages of each material to create a superior membrane for pervaporation and gas separation [60-62].

The nature of miscibility of Matrimid/PBI in all polymer compositions is believed to be the intense hydrogen bonding between N-H group of PBI and C=O group of Matrimid which provides a specific interaction for intermolecular compatibility [63] as expressed in Figure I - 6.

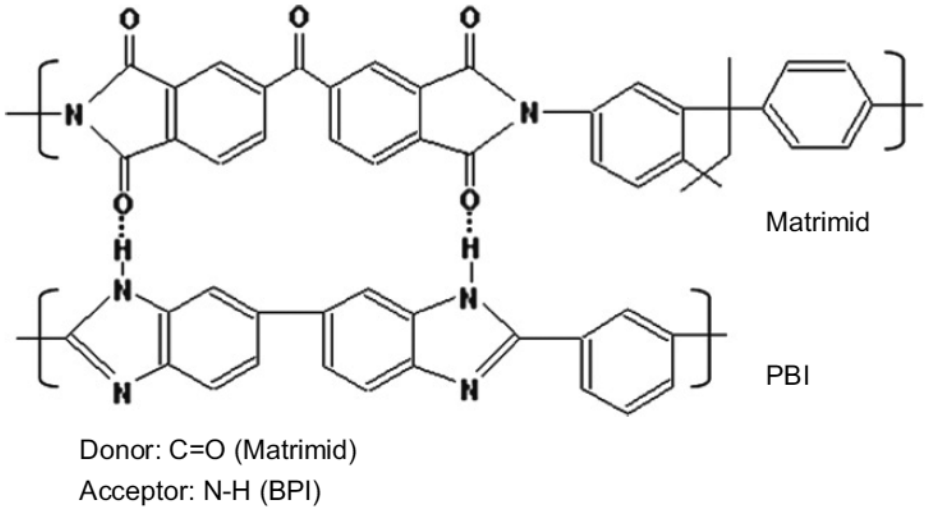

Figure I – 6. Chemical structures of PBI and Matrimid. The dotted line between the polymers represent hydrogen bonding interaction between functional groups of polymers.

A literature survey shows that a blend of 50 wt % of each polymer was revealed to be the best for H_2 separation with a value of H_2 permeability of 13 Barrer and H_2/CO_2 and H_2/N_2 selectivity of 6.05 and 181.38 respectively [54]. Therefore, asymmetric hollow fiber membranes based 50 wt % of each polymer where fabricated in this work.

1.3.3. Mixed gas permeation in polymeric membranes

Generally, the permeation behavior of a pure gas through a membrane depends mainly on the properties of the gas and membrane as well as the operation conditions.

As for gas mixtures the transport behavior of one component through the membrane is affected by the presence of other penetrants so that it deviates from that of the pure gas. Therefore, using the permeation data of pure gases to estimate the separation properties of gas mixtures may lead to wrong results [64, 65]. The deviations are in general attributed to different factors, from which the solubility coupling by competitive sorption effects, membrane plasticization and the concentration polarization phenomena are more prevalent.

The solubility coupling occurs between the penetrants and the polymer matrix, and in the case of glassy polymers is a negative effect which means that induces a decrease in the gas permeability. In the polymer matrix a fixed amount of sorption sites are present, which get saturated at a certain pressure, thereby leading to a decrease in solubility coefficient at higher penetrant pressures [66]. This may be explained in terms of the simple dual-mode sorption, partial immobilization model: penetrants compete for sorption sites which are associated with the non-equilibrium free volume in glassy polymers [67].

On the other hand, some penetrants sorb into polymers to such a degree that they plasticize the polymer. Plasticization effectively increases the chain spacing in the polymer and increases the chain mobility so that the diffusion and permeation coefficients increase with increasing penetrant pressure. Finally, the concentration polarization phenomenon is a consequence of the depletion of fast permeating molecules at the membrane surface due to the accumulation of slow permeating molecules in the gas phase adjacent to the membrane.

1.4. CARBON MONOXIDE

Carbon monoxide is a key raw material in the synthetic routes for a variety of major chemical products including methanol, formaldehyde, acetic acid, isocyanates, aldehydes, formic acid, pesticides, and herbicides. It has an increased importance as raw material for liquid hydrocarbon fuels in the Fischer-Tropsch process where CO molecules are coupled to C-C bond formation [68].

All sources of carbon monoxide are essentially gas mixtures, most common being the synthesis gas and coke-oven gas [69] with typical composition listed in Table I - 4.

Today, chemicals and liquid transportation fuels obtained from synthesis gas represent the leading products with 45% and 38%, respectively, of the world gasification capacity for operating plants identified in the 2010 database compiled by the U.S. Department of Energy - National Energy Technology Laboratory [70]. The other products are electric power and gaseous fuels (40 - 60 vol % H_2 purity requirement).

The recovery of CO from synthesis gas and coke – oven gas would represent an abundant and relatively inexpensive source of CO that would greatly enhance further growth of CO as a raw material for the chemical industry. Such growth could result in the CO-based chemical industries approaching the same level of importance as the ethylene-based chemical industries [71]. The recovery of CO from the flue gases would also contribute to the reduction in the process emissions approaching the zero discharge goal.

1.4.1. Carbon monoxide separation

Pure carbon monoxide is obtained either by reversible complexation or cryogenic separation, using technologies like CO absorption in ammoniacal cuprous chloride, aromatic $CuAlCl_4$ solution (COSORB), cryogenic fractionation and pressure swing adsorption (PSA) [72-74].

Chemical complexation

The separation of CO by reversible complexation is based on its ability along with that of olefins, aromatic and thiophenic compounds to form a π complexation bound with *d*- block transition metals and their ions [75]. As shown in Figure I – 7 the bound is constituted of two contributions: the usual σ bound formed by the

overlapping of the bounding π electrons of the gas to the unoccupied outermost *s* orbital of the metal and the additional back-donation from the metal *d* orbital to the empty antibonding π orbital of the gas [76-79]. Also a possible redistribution between *d* orbitals is shown.

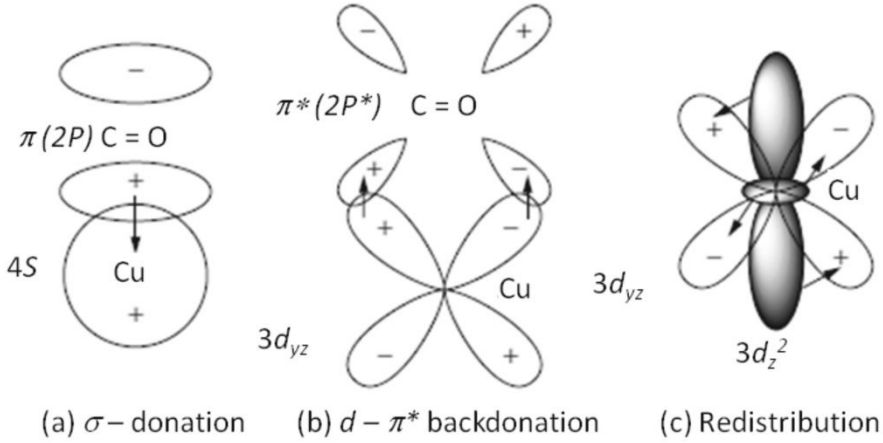

Figure I – 7. Scheme of the CO-Cu interactions by π-complexation, showing (a) donation of π-electrons of carbon monoxide to the 4*s* orbital of Cu, (b) backdonation of electrons from the 3d_{yz} orbitals of Cu to the antibonding π^* orbitals of carbon monoxide, and (c) electron redistribution. (c) depicts the possible electron redistribution from the 3d_z^2 orbitals to the 3d_{yz} orbitals

Calculations based on the molecular orbital theory estimate that the bounding strength follows the order [76]:

$Cu^+ > Ag^+$ and $CO > C_2H_4$

The π-complexation bonds are stronger than those formed by van der Waals interactions, but they are also weak enough to be broken by traditional engineering means such as increasing temperature and/or decreasing pressure [80]. Therefore the chemical complexation reaction is reversible and thus industrially applicable. In addition, like all chemical reactions, the complexation reactions are highly selective.

In order for the reaction to be reversible in an economically attractive process it must have appropriate bond energy. Figure I – 8 shows the typical bond energy involved in some chemical reactions. Complexation reactions with bond energies

less than 10 kJ mol^{-1} are similar to ordinary associations by van der Waals forces in the condensed state, and reactions with bound energies above 50 kJ mol^{-1} tend to be difficult to reverse without undue expense.

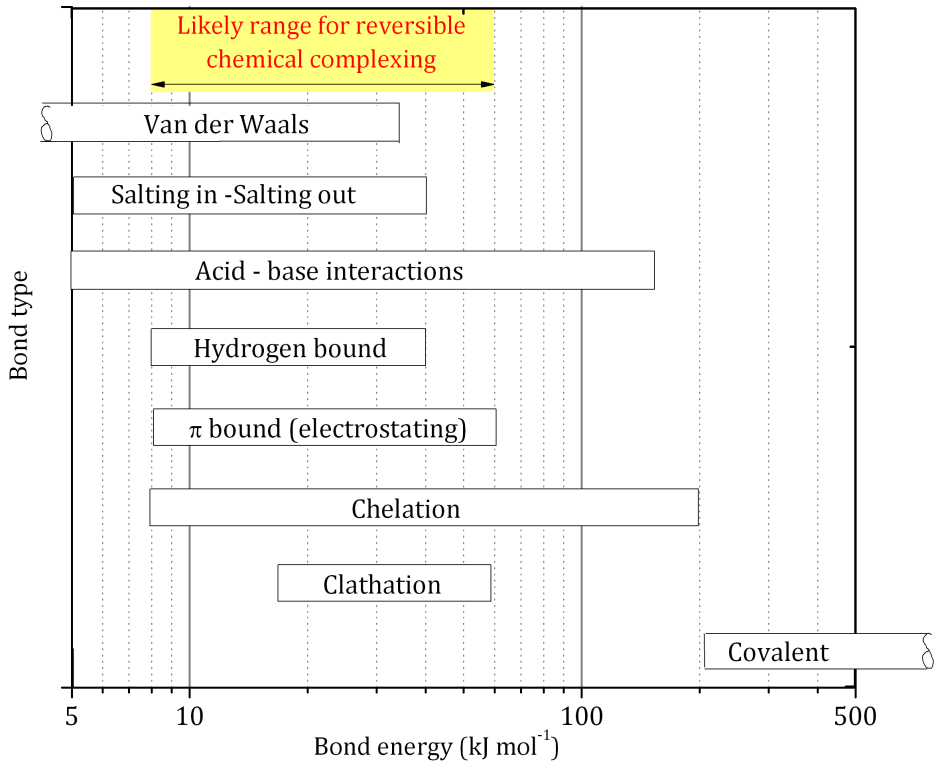

Figure I – 8. Bound energy most suited for reversible chemical complexation separation processes [80].

Copper (I) salt solutions are able to absorb carbon monoxide to form carbonyl complexes. This property is used in two industrial processes to selectively separate carbon monoxide from a mixture of gases [74]. The copper – ammonium salt wash developed by BASF uses aqueous ammonia solutions of copper carbonate, formate, acetate, lactate, or a mixture thereof. The absorption – desorption reaction is thought to be an equilibrium between free and coordinated carbon monoxide that is highly dependent on the temperature, pressure, and acidity of the medium (see Equation I – 10)

$$[Cu(NH_3)_2]^+ + CO + NH_3(aq) \rightleftharpoons [Cu(NH_3)_3(CO)]^+ \qquad \text{(I - 10)}$$

The regeneration of CO is done by heating the rich solution to 350 K, usually at atmospheric pressure. The vapor pressure of ammonia at this temperature is significant and a scrubber can be used to wash the off-gas.

The Cosorb process, developed in the early 1970s by Tenneco Chemicals, is based on a similar principle. It uses a copper (I) organometallic complexes in organic solvents (preferably $CuAlCl_4$ in toluene). First a complex is formed with one molecule of $CuAlCl_4$ and one or two molecules of toluene. The chemical complexation between CO and this complex was proposed to follow the reaction described by Equation I – 11.

$$CO + CuAlCl_4 toluene_2 \rightleftarrows CuAlCl_4 toluene CO + toluene \qquad \text{(I - 11)}$$

This process provides several advantages such as lower corrosion, higher complex stability, and higher purity of the gas produced. Nevertheless, several impurities such as water or sulfur compounds (SO_2, H_2S, COS, etc.) destroy the copper complex. A very careful purification of the feed gas is therefore required. Also, the availability of Cu^+ is lowered due to the mixture of CuCl with $AlCl_3$

Generally, conventional absorption processes present the drawback of high energy consumption and operating cost and in particular for CO the main problem is the low solubility in liquid media and the instability of Cu^+ ion which in a disproportionation reaction gives Cu^0 and Cu^{2+}.

Cryogenic separation and PSA

Processes for the cryogenic separation of pure carbon monoxide from a mixture of gases have been developed by, among others, Air Liquide and Linde.

The CO/H_2 separation is made by a low-temperature partial-condensation process where the mixture of gases is cooled to a temperature of approximately 70 K. The CO/N_2 separation is difficult owing to the similar boiling point. Cryogenic distillation is also an energy intensive and expensive separation method.

Two commercial PSA plants have been in operation in Japan since 1989 for the recovery of CO from converter gases of steel plants. Depending on the use of the syngas the desired composition ranges from 100% hydrogen (for the production of hydrogen or ammonia) to 100% CO for carbon monoxide or acetic acid production.

1.4.2. Facilitated transport supported liquid membranes

The principle of the transport of CO through facilitated transport supported liquid membrane is described in Figure I – 9.

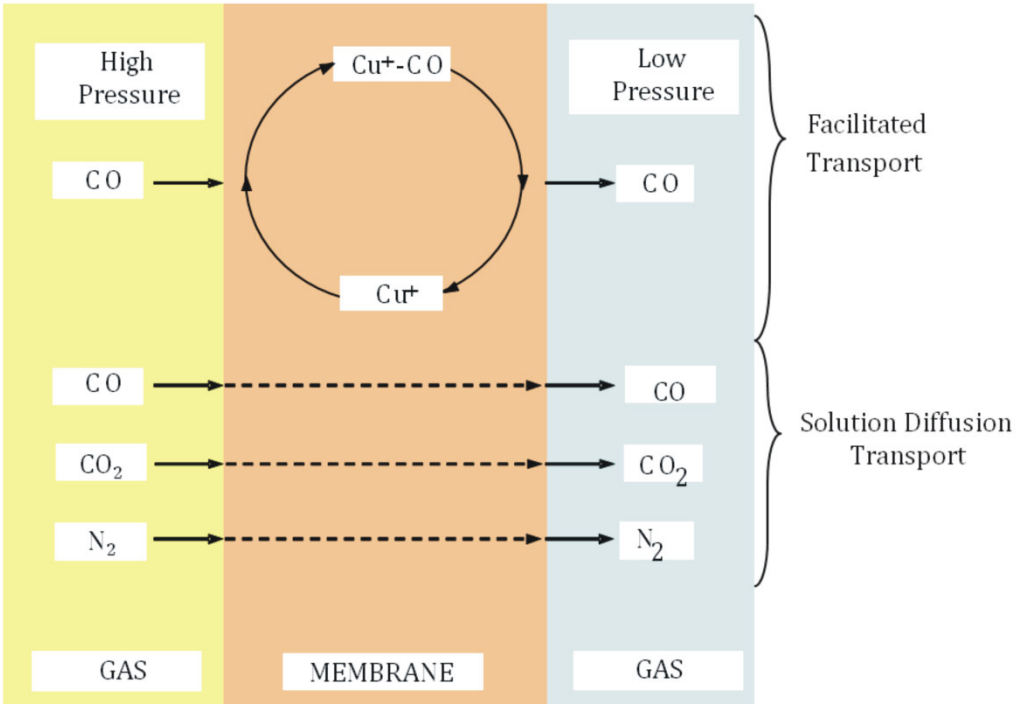

Figure I – 9. The principle of the transport of CO through facilitated transport supported liquid membrane

In an SLM system an organic solvent is immobilized into the pores of a porous polymer or inorganic support material by capillary forces [9]. Solution – diffusion is the typical solute transport mechanism in a dense, non – porous polymer or liquid phase [81].

Facilitated transport membranes operate based on solute partitioning (solubility) and diffusion but also include a reversible complexation as a component of the membranes separation. The complexation reaction in the membrane creates an additional transport that is synergetic with the solution – diffusion mechanism. Facilitated transport is analogous to a chemical absorption process on the feed (high – partial pressure) side and a stripping process on the permeate side of the membrane (low partial pressure side) [82].

At the feed side of the membrane CO first dissolves in the membrane, and then it can diffuse or react with the complexing agent. CO diffusion across the facilitated transport membrane can take place by two mechanisms: (a) diffusion of the uncomplexed species or (b) diffusion of the carrier – solute complex. The selectivity and reversibility is critical for the separation performance of facilitated transport membranes.

Therefore, the key issue in developing a separation process based on reversible complexation is the ability of a carrier to bind selectively to the permeant with appropriate bond energy equilibrium and rate constants (K_{eq}). For a system to be efficient enough recommended values of the equilibrium parameters by Noble et al [68] are between 2 x 10^2 M^{-1} and 2 x 10^4 M^{-1} for facilitated transport of gases in liquid membranes at solubilities around 5 x 10^{-3} M and partial pressures from 1.01 x 10^4 Pa to 1.01 x 10^5 Pa. Table I - 7 shows the values of the equilibrium constants (K_{eq}) reported in the literature for CO complexation with transition metals and their ions. The literature data listed in Table I – 7 are in general previous to 1995; little research effort is dedicated at the present to the facilitated transport of CO through supported liquid membranes.

Facilitated transport membranes have several general characteristics:

1. They can be highly selective, especially at low driving forces where other separation methods are not.
2. Very high permeability compared to conventional membranes can be obtained for the solute of interest at very low concentration driving forces.
3. A minimum permeability is reached at high concentration driving forces due to saturation of the reactive transport pathway.
4. The amount of solvent used is very small in comparison with conventional solvent extraction separation approaches for liquid membranes.
5. The quantity of complexing agent used is also very small.
6. Membrane technology allows for continuous separation.
7. Membrane technology is easily scaled for various applications.
8. The use of chemical reaction provides enhanced solute flux as well as selectivity.
9. They are often unstable in the immobilized liquid membrane configuration due to evaporation and/or solvent displacement.

Three methods to address the stability problems with facilitated transport membranes are the use of fixed – site carrier membranes, hollow-fiber-contained liquid membranes and the use of molten salts with negligible vapor pressure as solvents [83, 84]. Ionic liquids can also be excellent solvents for the carrier agent.

Table I – 7 Equilibrium constants (K_{eq}) for CO complexation with transition metal derivatives using facilitated transport liquid membrane systems

Element	Coordination complex	Experimental conditions	K_{eq} (kg mol^{-1})	Ref
Cu^{+}	$CuCl_3^{2-}$	0.2 M CuCl, 1.0 M KCl, 0.1 M HCl in water	1000	[69, 85]
		0.1 M CuCl, 1.0 M KCl, 0.2 M HCl in water		[86]
	$CuAlCl_4tol_2$	p_{CO} max = 1 bar, 0.15 -1.7 M in toluene	447[e]	[87]
	CuI/NMIm[a]	2 x10^{-5}M in Dimethyl sulfoxide	1700	[88]
	CuSCN/NMIm		570	
	$L^{b}CuB(C_6F_5)_4$	Tetrahydrofuran solvent	660-56000	[89]
Fe^{2+}	$Fe(TIM^{c})(C_6H_5CN)_2Cl_2$	0.015 M in Benzonitrile	420[e]	[68]
	$Fe(Me_4TIM)(C_6H_5CN)_2Cl_2$	0.046 M in Benzonitrile	180[e]	
	$Fe(Me_2Ph_2TIM)(C_6H_5CN)_2Cl_2$	0.050 M in Benzonitrile	130[e]	
	$Fe(Ph_4TIM)(C_6H_5CN)_2Cl_2$	0-0.064 M/Nitrobenzene	190.1[e]	[90]
Pd^{0}	$Pd_2(dpm^{d})_2NCO_2$	Dimethylacetamide	370000	[91]
	$Pd_2(dpm)_2Cl_2$		240000	
	$Pd_2(dpm)_2Br_2$		35000	
	$Pd_2(dpm)_2I_2$		1300	

[a] N-methylimidazole ligand, [b] Ligand-Cu(I) complexes based on pyridylalkylamine compounds, [c] Tetraimine macrocyclic ligand (2,3,9,10-tetrametbyl-l,3,8,11-tetraazacyclotetradeca-1,3,8,10 tetraene), [d] $Ph_2PCH_2PPh_2$ ligand, [e] the presented values belong to the reduced equilibrium constant (M^{-1}) defined as the ratio between the equilibrium constant (-) and the constant concentration (M) of touene, benzonitrile and nitrobenzene respectively.

1.4.3. Ionic liquids

The common definition of ionic liquids (ILs) is that they are liquids that are composed entirely of ions and are fluid below 100 ^{o}C [92]. Often, this melting point is even lower than room temperature; therefore ionic liquids are free flowing at room temperature, hence the generic term, room temperature ionic liquids (RTILs). The term ionic liquid covers inorganic as well as organic molten salts. However, the recent literature deals with RTILs made of a bulky nitrogen or phosphorous-containing dissymmetrical and diffusely charged organic cation and a variety of organic or inorganic anions [93], leading to a disturbed molecular packaging with high cohesive energy density given by Coulombic interactions between the constituents [94, 95]. Figure I – 10 shows the chemical structure of typical anions and cations of commonly found in ionic liquids.

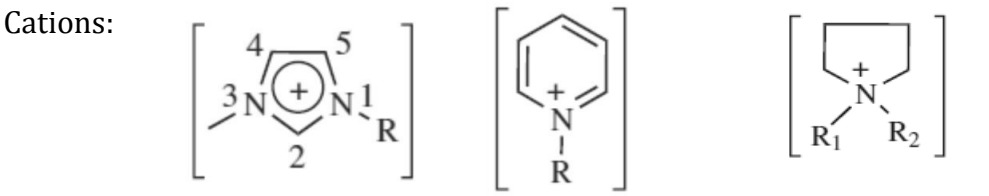

Figure I – 10. Some commonly used ionic liquids [96].
[a] trifluoromethanesulfanate: $[CF_3SO_3]^-$,
[b]bis(trifluoromethylsulfonyl)imide: $[(CF_3SO_2)_2N]^-$

There are a large number of organic cations and anions that can be combined to form different ionic liquids. Overall, the number of possible ionic liquids is estimated around 10^{18}, whereas the number of traditional solvents widely used in industry accounts for a few hundred [97].

In addition, their miscibility with water or organic solvents can be tuned through side chain lengths on the cation and choice of the anion. Furthermore, they can be functionalized to act as acids, bases or ligands [98]. Therefore, the possibility arises to optimize the ionic liquid for a specific application by stepwise tuning the relevant solvent properties. For this reason ionic liquids have been referred to as "designer solvents" [99].

The main advantage of ionic liquids is that they are a new class of solvents by their non-molecular nature. The ionic liquid environment is very different of that of all molecular polar or non-polar organic solvents giving them the following main physical properties:

- non-measurable vapor pressure which makes them very easy to contain, manipulate, transfer, and allows their use under high vacuum or heating conditions; thus they are considered "environment friendly" alternatives to VOCs,
- intrinsic conductivity (Coulombic fluids) and wide electrochemical stability window
- non-flammability associated with the low vapor pressure,
- thermal stability (some of them can be heated up to 400 ◦C without degradation which is much greater than most classical organic solvents),
- wide liquid range (ranging from 75 to 300 °C, which allows a better kinetic control on reactions [92]),
- solvating properties for a wide range of organic, inorganic, and organo-metallic compounds [100].
- high heat capacity

Based on their unique properties ionic liquids have been extensively studied over the last 10 years and more than 16000 publications contain the phrase "ionic liquid(s)" in the title. There have been many reviews on ionic liquids focused on particular applications, e.g., analysis [101-105], synthesis and (bio)catalysis [95, 106], electrochemical devices [107, 108], engineering fluids [109-111], separation and purification technology [112-116]. The first international congress dedicated to the use of ionic liquids in separation and purification technology (ILSEPT) took place last year (2011) in Sitgets, Spain. A brief overview on the applications of ionic liquids is given in Table I – 8.

Table I - 8. Current status of ionic liquids applications at R&D, pilot and commercial level.

Application	Status R&D	Pilot	Commercialized
Separation and purification technology	Deep desulfuration Gas separation	Liquid-liquid-extraction	Entrainer in extractive distillation (Basil process – BASF [120])
Functional fluids		Hydraulic oils, storage media for gases, lubricants, surfactants	
Synthesis and Catalysis	Enzymatic reaction	Immobilization of catalysis	Nano-particule-synthesis Solvents for organic reactions
Analytics	Electrophoresis Solvents for GC head-space	matrix-materials for MALDI-TOF-MS	Solvents for Karl-Fischer titration Solvents for protein crystallization Materials for GC columns
Electro-chemical applications	Fuel cells and batteries Metal deposition and Metal finishing,	Dye sensitized solar cells	Sensors Supercapacitors
Thermo-dynamic applications	Thermal fluids (storage and transfer) Phase changing materials	Sorption cooling media	

The use of ionic liquids also has some disadvantages: the physical properties are not always known, their viscosity is usually higher than that of common solvents. Also, the green credentials of ionic liquids are being increasingly questioned due to the growing evidence of their toxicity to aquatic ecosystems, although the mechanisms of toxicity are unknown [117-119].

Ionic liquids have found much interest in gas separation by supported liquid membranes (SILMs) as efficient means to suppress the drawbacks associated to this technology (see Table I - 2). The use of these new solvents as a liquid membrane phase results in the stabilization of the SLMs due to their negligible vapor pressure, and their high viscosity (up to 500 cP) which could slow down the displacement of the liquids from the micropores under pressure [112].

1.5. THESIS SCOPE AND OUTLINE

The separation and valorization of industrial flue gases with complex composition such as the tail gas generated in the manufacturing of carbon black needs a complex approach. First, membrane technology was selected as the best technology because presents over the other gas separation alternatives economics and operational advantages. Then, the low concentration in valuable components, i. e. H_2 and CO, with N_2 as the major impurity and the permeation order through membranes ($H_2 \gg CO \cong N_2$) determines the need for a dual approach: (I) the separation and recovery of H_2 using H_2 permeable polymers and (II) the separation and recovery of CO by means of chemical complexation using facilitated transport membranes.

Therefore the present thesis has the following objectives:

1. The study of polymeric based membrane permeation for pure gases, binary, ternary and quaternary mixtures of H_2, CO, N_2 and CO_2 at different operation conditions using dense polymeric films.

2. The description of H_2 and CO_2 permeation behavior of pure, binary, ternary and quaternary mixtures using an appropriate mathematical model.

3. The study of permeation behavior of pure gases, binary, ternary and quaternary mixtures of H_2, CO, N_2 and CO_2 through hollow fiber membranes in order to determine the major differences between the gas permeation through a dense isotropic structure (dense-thick film) and an asymmetric structure (hollow fiber, dense thin film supported on a porous sublayer).

4. The design and experimental characterization of a liquid phase system to be used in facilitated transport-supported ionic liquid membranes (SILMs) for the recovery of carbon monoxide.

5. General prospects for further research and industrial implementation.

References

1. S. Sircar, Basic research needs for design of adsorptive gas separation processes, Ind. Eng. Chem. Res. 45 (2006) 5435-5448.

2. R.W. Rousseau, Handbook of Separation Process Technology, John Wiley & Sons, New York, 1987.

3. P. Bernardo, E. Drioli, G. Golemme, Membrane gas separation: A review/state of the art, Ind. Eng. Chem. Res. 48 (2009) 4638-4663.

4. Universal Industrial Gases Inc., Overview of cryogenic air separation and liquefier systems, http://www.uigi.com/cryodist.html (2011).

5. H.R. Null, Selection of Separation Process, in: R.W. Rousseau (Ed.), Handbook of Separation Process Technology, John Wiley & Sons, New York, 1987, pp. 982.

6. E. Drioli, A.I. Stankiewicz, F. Macedonio, Membrane engineering in process intensification-An overview, J. Membr. Sci. 380 (2011) 1-8.

7. S. Adhikari, S. Fernando, Hydrogen membrane separation techniques, Ind. Eng. Chem. Res. 45 (2006) 875-881.

8. L. Shao, B.T. Low, T.-S. Chung, A.R. Greenberg, Polymeric membranes for the hydrogen economy: Contemporary approaches and prospects for the future, J. Membr. Sci. 327 (2009) 18-31.

9. V.S. Kislik, Liquid membranes: principles and applications in chemical separations and wastewater treatment, Elsevier, Amsterdam, 2010.

10. R. Prasad, R.L. Shaner, K.J. Doshi, Comparision of membranes and other gas separation technologies, in: D.R. Paul, P.Y. Yampolskii (Eds.), Polymeric Gas Separation Membranes, CRC Press, Boca Raton, 1994, pp. 531.

11. W.J. Koros, G.K. Fleming, Membrane-based gas separation, J. Membr. Sci. 83 (1993) 1-80.

12. A. Brunetti, P. Bernardo, E. Drioli, G. Barbieri, Membrane Engineering: Progress and Potentialities in Gas Separation, in: Y. Yampolskii, B. Freeman (Eds.), Membrane Gas Separation, John Wiley and Sons Ltd, Chichester, 2010, pp. 281.

13. M. -J. Wang, C.A. Gray, S.R. Reznek, K. Mahmud, Y. Kutsovsky, Carbon Black, in: J. Kroschwitz (Ed.), Encyclopedia of Polymer Science and Technology, John Wiley & Sons, Inc., New York, 2002.

14. G. Kuhner, M. Voll, Manufacture of carbon black, in: D. Jean-Baptiste, R.C. Bansal, M.-J. Wang (Eds.), Carbon black: science and technology, CRC Press, Boca Raton, 1993.

15. W.R. Jones, Reactor and method for production of carbon black with broad particle size distrtibution EP0384080A2 (1989).

16. Columbian Carbon (Spain) personal communication.

17. Committee on Alternatives and Strategies for Future Hydrogen Production and Use, National Research Council, The Hydrogen Economy: Opportunities, Costs, Barriers, and R&D Needs, National Academies Press, 2004.

18. N.W. Ockwig, T.M. Nenoff, Membranes for hydrogen separation, Chem. Rev. 107 (2007) 4078-4110.

19. W.J. Koros, D.G. Woods, Elevated temperature application of polymer hollow-fiber membranes, J. Membr. Sci. 181 (2001) 157-166.

20. T.C. Merkel, M. Zhou, R.W. Baker, Carbon dioxide capture with membranes at an IGCC power plant, J. Membr. Sci. 389 (2012) 441-450.

21. The National Energy Technology Laboratory, U.S. Department of Energy, Hydrogen from Coal Program Central Production RD&D, http://www.netl.doe.gov/technologies/hydrogen_clean_fuels/central.html (2012).

22. M. Ramezan, T.J. Skone, N. Nsakala, G.N. Liljedahl, Carbon Dioxide Capture from Existing Coal-Fired Power Plants DOE/NETL-401/110907 (2007).

23. J.R. Rostrup-Nielsen, Syngas in perspective, Catal. Today 71 (2002) 243-247.

24. National Energy Technology Laboratory, U.S. Department of Energy, Gasification encyclopedia,
http://www.netl.doe.gov/technologies/coalpower/gasification/gasifipedia/4-gasifiers/index.html (2012).

25. S.P. Kaldis, G.C. Kapantaidakis, G.P. Sakellaropoulos, Simulation of multicomponent gas separation in a hollow fiber membrane by orthogonal collocation - Hydrogen recovery from refinery gases, J. Membr. Sci. 173 (2000) 61-71.

26. D.L. Maclean, R. Krishnamurthy, S.L. Lerner, Argon recovery from hydrogen depleted ammonia plant purge gas utilizing a combination of cryogenic and non-cryogenic separation means Patent US4687498 (1987).

27. J. Yang, C.-H. Lee, Adsorption dynamics of a layered bed PSA for H2 recovery from coke oven gas, AIChE J. 44 (1998) 1325-1334.

28. W.J. Koros, R.T. Chern, Separation of Gaseous Mixtures Using polymer Membranes, in: R.W. Rousseau (Ed.), Handbook of Separation Process Technology, John Wiley & Sons, New York, 1987, pp. 862.

29. P. Pandey, R.S. Chauhan, Membranes for gas separation, Progr. Polym. Sci. 26 (2001) 853-893.

30. M. Mulder, Basic Principles of Membrane Technology, Kluwer Academic Publishers, Dordrecht, 1996.

31. D.W. Breck, Zeolite Molecular Sieves: Structure, Chemistry, and Use, John Wiley & Sons, New York, 1974.

32. R.W. Baker, K. Lokhandwala, Natural gas processing with membranes: An overview, Ind. Eng. Chem. Res. 47 (2008) 2109-2121.

33. C.A. Scholes, S.E. Kentish, G.W. Stevens, Effects of minor components in carbon dioxide capture using polymeric gas separation membranes, Sep. Purif. Rev. 38 (2009) 1-44.

34. J.A. Dean, Lange's Handbook of Chemistry, 15th ed., McGraw-Hill, New York, 1999.

35. L.M. Robeson, The upper bound revisited, J. Membr. Sci. 320 (2008) 390-400.

36. L.M. Robeson, Correlation of separation factor versus permeability for polymeric membranes, J. Membr. Sci. 62 (1991) 165-185.

37. N. Du, G.P. Robertson, J. Song, I. Pinnau, M.D. Guiver, High-performance carboxylated polymers of intrinsic microporosity (PIMs) with tunable gas transport properties, Macromolecules 42 (2009) 6038-6043.

38. W. Fang, L. Zhang, J. Jiang, Gas permeation and separation in functionalized polymers of intrinsic microporosity: A combination of molecular simulations and ab initio calculations, J. Phys. Chem. C 115 (2011) 14123-14130.

39. B.S. Ghanem, N.B. McKeown, P.M. Budd, N.M. Al-Harbi, D. Fritsch, K. Heinrich, L. Starannikova, A. Tokarev, Y. Yampolskii, Synthesis, characterization, and gas permeation properties of a novel group of polymers with intrinsic microporosity: PIM-polyimides, Macromolecules 42 (2009) 7881-7888.

40. I. Pinnau, S. Thomas, M.D. Guiver, N. Du, J. Song, Gas transport properties of intrinsically microporous polymers, ACS National Meeting Book of Abstracts (2009).

41. J. Peter, A. Khalyavina, J. Kříž, M. Bleha, Synthesis and gas transport properties of ODPA-TAP-ODA hyperbranched polyimides with various comonomer ratios, Eur. Polym. J. 45 (2009) 1716-1727.

42. D.M. Sterescu, D.F. Stamatialis, M. Wessling, Boltorn-modified polyimide gas separation membranes, J. Membr. Sci. 310 (2008) 512-521.

43. V. Arcella, A. Ghielmi, G. Tommasi, High performance perfluoropolymer films and membranes, Ann. N. Y. Acad. Sci. 984 (2003) 226-244.

44. N.A. Belov, A.A. Zharov, A.V. Shashkin, M.Q. Shaikh, K. Raetzke, Y. Yampolskii, Gas transport and free volume in hexafluoropropylene polymers, J. Membr. Sci. 383 (2011) 70-77.

45. P. Gorgojo, S. Uriel, C. Téllez, J. Coronas, Development of mixed matrix membranes based on zeolite Nu-6(2) for gas separation, Micropor. Mesopor. Mat. 115 (2008) 85-92.

46. M. Askari, Y. Xiao, P. Li, T.-. Chung, Natural gas purification and olefin/paraffin separation using cross-linkable 6FDA-Durene/DABA co-polyimides grafted with α, β, and γ-cyclodextrin, J. Membr. Sci. 390-391 (2012) 141-151.

47. M.G. García, J. Marchese, N.A. Ochoa, High activated carbon loading mixed matrix membranes for gas separations, J. Mater. Sci. (2011) 1-12.

48. J.E. Mark, Polymer Data Handbook, 2nd ed., Oxford University Press, Oxford, 2009.

49. C.J. Orme, M.L. Stone, M.T. Benson, E.S. Peterson, Testing of polymer membranes for the selective permeability of hydrogen, Sep. Sci. Technol. 38 (2003) 3225-3238.

50. V. Abetz, T. Brinkmann, M. Dijkstra, K. Ebert, D. Fritsch, K. Ohlrogge, D. Paul, K.-. Peinemann, S.P. Nunes, N. Scharnagl, M. Schossig, Developments in membrane research: From material via process design to industrial application, Adv. Eng. Mater. 8 (2006) 328-358.

51. Y. Li, T.-S. Chung, Highly selective sulfonated polyethersulfone (SPES)-based membranes with transition metal counterions for hydrogen recovery and natural gas separation, J. Membr. Sci. 308 (2008) 128-135.

52. D. Wang, W.K. Teo, K. Li, Permeation of H2, N2, CH4, C2H6, and C3H8 through asymmetric polyetherimide hollow-fiber membranes, J. Appl. Polym. Sci. 86 (2002) 698-702.

53. P. Hacarlioglu, L. Toppare, L. Yilmaz, Polycarbonate-polypyrrole mixed matrix gas separation membranes, J. Membr. Sci. 225 (2003) 51-62.

54. S.S. Hosseini, M.M. Teoh, T.-S. Chung, Hydrogen separation and purification in membranes of miscible polymer blends with interpenetration networks, Polymer 49 (2008) 1594-1603.

55. S.C. Kumbharkar, P.B. Karadkar, U.K. Kharul, Enhancement of gas permeation properties of polybenzimidazoles by systematic structure architecture, J. Membr. Sci. 286 (2006) 161-169.

56. H. Kawakami, M. Mikawa, S. Nagaoka, Gas permeability and selectivity through asymmetric polyimide membranes, J. Appl. Polym. Sci. 62 (1996) 965-971.

57. S. Shishatskiy, C. Nistor, M. Popa, S.P. Nunes, K.V. Peinemann, Polyimide asymmetric membranes for hydrogen separation: Influence of formation conditions on gas transport properties, Adv. Eng. Mater. 8 (2006) 390-397.

58. B.T. Low, T.-S. Chung, H. Chen, Y.-. Jean, K.P. Pramoda, Tuning the free volume cavities of polyimide membranes via the construction of pseudo-interpenetrating networks for enhanced gas separation performance, Macromolecules 42 (2009) 7042-7054.

59. B.T. Low, Y. Xiao, T.-S. Chung, Amplifying the molecular sieving capability of polyimide membranes via coupling of diamine networking and molecular architecture, Polymer 50 (2009) 3250-3258.

60. S.S. Hosseini, N. Peng, T.-S. Chung, Gas separation membranes developed through integration of polymer blending and dual-layer hollow fiber spinning process for hydrogen and natural gas enrichments, J. Membr. Sci. 349 (2010) 156-166.

61. G. Kung, L.Y. Jiang, Y. Wang, T.-S. Chung, Asymmetric hollow fibers by polyimide and polybenzimidazole blends for toluene/iso-octane separation, J. Membr. Sci. 360 (2010) 303-314.

62. S.S. Hosseini, T.-S. Chung, Carbon membranes from blends of PBI and polyimides for N2/CH4 and CO2/CH4 separation and hydrogen purification, J. Membr. Sci. 328 (2009) 174-185.

63. E. Földes, E. Fekete, F.E. Karasz, B. Pukánszky, Interaction, miscibility and phase inversion in PBI/PI blends, Polymer 41 (2000) 975-983.

64. F. Wu, L. Li, Z. Xu, S. Tan, Z. Zhang, Transport study of pure and mixed gases through PDMS membrane, Chem. Eng. J. 117 (2006) 51-59.

65. T.-S. Chung, L. Shao, P.S. Tin, Surface modification of polyimide membranes by diamines for H2 and CO2 separation, Macromol. Rapid Comm. 27 (2006) 998-1003.

66. S.S. Dhingra, E. Marand, Mixed gas transport study through polymeric membranes, J. Membr. Sci. 141 (1998) 45-63.

67. W.J. Koros, R.T. Chern, V. Stannett, H.B. Hopfenberg, Model for permeation of mixed gases and vapors in glassy polymers., J. Polym. Sci. , Part A-2: Polym. Phys. 19 (1981) 1513-1530.

68. C.A. Koval, R.D. Noble, J.D. Way, B. Louie, Z.E. Reyes, B.R. Bateman, G.M. Horn, D.L. Reed, Selective transport of gaseous CO through liquid membranes using an iron(II) macrocyclic complex, Inorg. Chem. 24 (1985) 1147-1152.

69. G.S. Patil, S. Baruah, N.N. Dutta, Facilitated transport of carbon monoxide: A review, Gas Sep. Purif. 5 (1991) 2-8.

70. National Energy Technology Laboratory (NETL), U.S. Department of Energy, 2010 Worldwide gasification database, http://www.netl.doe.gov/technologies/coalpower/gasification/worlddatabase/index.html. (2012)

71. J.L. Anthony, J.L. Anderson, E.J. Maginn, J.F. Brennecke, Anion effects on gas solubility in ionic liquids, J. Phys. Chem. B 109 (2005) 6366-6374.

72. J. Kumełan, A.P.S. Kamps, D. Tuma, G. Maurer, Solubility of CO in the ionic liquid [bmim][PF6], Fluid Phase Equilib. 228-229 (2005) 207-211.

73. C.A. Ohlin, P.J. Dyson, G. Laurenczy, Carbon monoxide solubility in ionic liquids: Determination, prediction and relevance to hydroformylation, Chem. Comun. 10 (2004) 1070-1071.

74. J. Bierhals, Carbon Monoxide , in: Ullmann's Encyclopedia of Industrial Chemistry, Wiley-VCH, Weinheim, 2001.

75. A.J. Hernández-Maldonado, R.T. Yang, Desulfurization of transportation fuels by adsorption, Catal. Rev. Sci. Eng. 46 (2004) 111-150.

76. R.T. Yang, π-Complexation sorbents and applications, in: Adsorbents: Fundamentals and Applications, John Wiley & Sons, Inc., Hoboken, New Jersey, 2003, pp. 191.

77. D.J. Safarik, R.B. Eldridge, Olefin/paraffin separations by reactive absorption: a review, Ind. Eng. Chem. Res. 37 (1998) 2571-2581.

78. T.A. Reine, Olefin/paraffin separation by reactive absorption, PhD dissertation, University of Texas at Austin (2004).

79. A. Ortiz, L.M. Galán, D. Gorri, A.B. De Haan, I. Ortiz, Kinetics of reactive absorption of propylene in RTIL-Ag+ media, Sep. Purif. Technol. 73 (2010) 106-113.

80. C.J. King, Separation processes based on reversible chemical complexation, in: R.W. Rousseau (Ed.), Handbook of Separation Process Technology, Wiley - Interscience, New York, 1987, pp. 760.

81. R.D. Noble, C.A. Koval, Review of facilitated transport membranes, in: Y. Yampolskii, I. Pinnau, B.D. Freeman (Eds.), Materials Science of Membranes, Wiley, West Sussex, 2006, pp. 411.

82. R.D. Noble, C.A. Koval, J.J. Pellegrino, Facilitated transport membrane systems, Chem. Eng. Prog. 85 (1989) 58-70.

83. M.F. San Román, E. Bringas, R. Ibañez, I. Ortiz, Liquid membrane technology: Fundamentals and review of its applications, J. Chem. Technol. Biotechnol. 85 (2010) 2-10.

84. P. Luis, L.A. Neves, C.A.M. Afonso, I.M. Coelhoso, J.G. Crespo, A. Garea, A. Irabien, Facilitated transport of CO2 and SO2 through Supported Ionic Liquid Membranes (SILMs), Desalination 245 (2009) 485-493.

85. D.R. Smith, J.A. Quinn, Facilitated transport of carbon monoxide through cupprous chloride solutions., AIChE J. 26 (1980) 112-120.

86. A. Dindi, R.D. Noble, J. Yu, C.A. Koval, Experimental and modeling studies of a parasitic binding mechanism in facilitated membrane transport, J. Membr. Sci. 66 (1992) 55-68.

87. J.A. Hogendoorn, W.P.M. van Swaaij, G.F. Versteeg, The absorption of carbon monoxide in COSORB solutions: absorption rate and capacity, Chem. Eng. J. Biochem. Eng. J. 59 (1995) 243-252.

88. M. Junidi, O. Munchise, K. Osama, New carrier systems for separation of carbon monoxide, Mitsubishi Kasei R&D Review 6, (1) (1992) 96-101.

89. H.C. Fry, H.R. Lucas, A.A.N. Sarjeant, K.D. Karlin, G.J. Meyer, Carbon monoxide coordination and reversible photodissociation in copper(I) pyridylalkylamine compounds, Inorg. Chem. 47 (2008) 241-256.

90. C.S. Sharma, P.K. Goswami, N.N. Dutta, Studies on facilitated transport of carbon monoxide using a novel iron(II) complex, Sep. Sci. Technol. 28 (1993) 1789-1797.

91. S.E. Lyke, M.A. Lliga, R.M. Ozanich, D.A. Nelson, B.R. James, C.-. Lee, Separation of syngas components using a dissolved palladium complex, Ind. Eng. Chem. Prod. Res. Dev. 25 (1986) 517-521.

92. G.W. Meindersma, M. Maase, A.B. De Haan, Ionic Liquids, in: Ullmann's Encyclopedia of Industrial Chemistry, Wiley-VCH Verlag GmbH & Co. KGaA, 2000.

93. P. Wasserscheid, T. Welton, Ionic Liquids in Synthesis, 2nd ed., Wiley, New York, 2007.

94. T. Welton, Room-Temperature Ionic Liquids. Solvents for Synthesis and Catalysis, Chem. Rev. 99 (1999) 2071-2083.

95. J.P. Hallett, T. Welton, Room-temperature ionic liquids: Solvents for synthesis and catalysis. 2, Chem. Rev. 111 (2011) 3508-3576.

96. A. Stark, K.R. Seddon, Ionic Liquids, in: Kirk-Othmer Encyclopedia of Chemical Technology, John Wiley & Sons, Inc., 2000.

97. L.C. Branco, G.V.S.M. Carrera, J. Aires-de-Sousa, I. Lopez Martin, R. Frade, C.A.M. Afonso, Physico-Chemical Properties of Task-Specific Ionic Liquids, in: A. Kokorin (Ed.), Ionic Liquids: Theory, Properties, New Approaches, InTech, 2011, pp. 61.

98. G. Laus, G. Bentivoglio, H. Schottenberger, V. Kahlenberg, H. Kopacka, T. Röder, S. Sixta, Ionic Liquids: Current developments, potential and drawbacks for industrial applications, Lenzinger Berichte 84 (2005) 71-85.

99. M. Freemantle, Designer solvents, Chem. Eng. News 76 (1998) 32-37.

100. R.D. Rogers, K.R. Seddon, Ionic Liquids - Solvents of the Future?, Science 302 (2003) 792-793.

101. S.A. Shamsi, N.D. Danielson, Utility of ionic liquids in analytical separations, J. Sep. Sci. 30 (2007) 1729-1750.

102. D. Bankmann, R. Giernoth, Magnetic resonance spectroscopy in ionic liquids, Prog. Nucl. Magn. Reson. Spectrosc. 51 (2007) 63-90.

103. S. Pandey, Analytical applications of room-temperature ionic liquids: A review of recent efforts, Anal. Chim. Acta 556 (2006) 38-45.

104. M. Koel, Ionic liquids in chemical analysis, Crit. Rev. Anal. Chem. 35 (2005) 177-192.

105. T.D. Ho, A.J. Canestraro, J.L. Anderson, Ionic liquids in solid-phase microextraction: A review, Anal. Chim. Acta 695 (2011) 18-43.

106. F. van Rantwijk, R.A. Sheldon, Biocatalysis in ionic liquids, Chem. Rev. 107 (2007) 2757-2785.

107. R. Hagiwara, J.S. Lee, Ionic liquids for electrochemical devices, Electrochemistry 75 (2007) 23-34.

108. D.S. Silvester, Recent advances in the use of ionic liquids for electrochemical sensing, Analyst 136 (2011) 4871-4882.

109. M.-. Bermúdez, A.-. Jiménez, J. Sanes, F.J. Carrión, Ionic liquids as advanced lubricant fluids, Molecules 14 (2009) 2888-2908.

110. H. Zhao, Innovative applications of ionic liquids as "green" engineering liquids, Chem. Eng. Commun. 193 (2006) 1660-1677.

111. F. Zhou, Y. Liang, W. Liu, Ionic liquid lubricants: Designed chemistry for engineering applications, Chem. Soc. Rev. 38 (2009) 2590-2599.

112. L.J. Lozano, C. Godínez, A.P. de los Ríos, F.J. Hernández-Fernández, S. Sánchez-Segado, F.J. Alguacil, Recent advances in supported ionic liquid membrane technology, J. Membr. Sci. 376 (2011) 1-14.

113. A.B. Pereiro, J.M.M. Araújo, J.M.S.S. Esperana, I.M. Marrucho, L.P.N. Rebelo, Ionic liquids in separations of azeotropic systems - A review, J. Chem. Thermodyn. 46 (2012) 2-28.

114. H. Tadesse, R. Luque, Advances on biomass pretreatment using ionic liquids: An overview, Energy Environ. Sci. 4 (2011) 3913-3929.

115. A. Berthod, M.J. Ruiz-Ángel, S. Carda-Broch, Ionic liquids in separation techniques, J. Chromatogr. A 1184 (2008) 6-18.

116. L. Vidal, M.-. Riekkola, A. Canals, Ionic liquid-modified materials for solid-phase extraction and separation: A review, Anal. Chim. Acta 715 (2012) 19-41.

117. M. Kumar, N. Trivedi, C.R.K. Reddy, B. Jha, Toxic effects of imidazolium ionic liquids on the green seaweed Ulva lactuca: Oxidative stress and DNA damage, Chem. Res. Toxicol. 24 (2011) 1882-1890.

118. M. Alvarez-Guerra, A. Irabien, Design of ionic liquids: An ecotoxicity (Vibrio fischeri) discrimination approach, Green Chem. 13 (2011) 1507-1516.

119. J. Arning, M. Matzke, Toxicity of ionic liquids towards mammalian cell lines, Curr. Org. Chem. 15 (2011) 1905-1917.

120. BASF, BASIL processes, http://www.intermediates.basf.com/chemicals/ionic-liquids/processes (2012).

Chapter II

MIXED GAS SEPARATION STUDY FOR THE HYDROGEN RECOVERY FROM $H_2/CO/N_2/CO_2$ POST COMBUSTION MIXTURES USING A MATRIMID® MEMBRANE

ABSTRACT

In this chapter, the membrane based separation of hydrogen from binary, ternary and quaternary mixtures of H_2, N_2, CO and CO_2 is presented.

Gas permeability values through a polyimide Matrimid 5218 membrane were experimentally obtained using a permeation technique at a constant pressure. Dense films were fabricated by solution casting of polymer solutions in dichloromethane using two methods: casting knife and Petri dishes.

The influence of the feed gas composition, temperature (30 – 100^{o}C), pressure (2 - 6 bar), and sweep gas flow rates on the permeation of gases through the prepared membranes was experimentally analyzed.

As expected, the pure gas permeability of H_2 was only slightly dependant on pressure and had an average value of 24 Barrer at 30 ^{o}C. Hydrogen permeability was not affected by the presence of nitrogen and carbon monoxide, and as a result the mixed gas selectivities for the H_2/N_2/CO mixtures are very close to the ideal selectivities calculated from pure gas permeation data.

On the contrary, a strong dependency of the hydrogen permeability on CO_2 concentration was observed even at low concentrations of CO_2. A reduction of 42 % of the hydrogen permeability coefficient was obtained when a mixture of 10/90 vol % H_2/CO_2 was used as feed gas. Accordingly H_2/CO_2 selectivity decayed from a value of 4.2 calculated from pure gas permeabilities to 2.7 when permeation data were obtained in mixed gas experiments. The preferential sorption of CO_2 on the Langmuir sites of the excess free volume portion of the polymer allowed explaining and quantifying this phenomenon.

The “dual-mode sorption, partial immobilization” model was used to describe H_2 and CO_2 permeation behavior of pure, binary, ternary and quaternary mixtures. The model sorption parameters for N_2 and CO_2 in the polymer Matrimid 5218 were obtained from the literature meanwhile those for H_2 and for CO were unknown and resulted from the fitting of the experimental data to the proposed model. Satisfactory agreement between predicted permeability results and experimental data with a correlation coefficient (R) higher than 0.95 and mean squared relative error (MSRE) lower than 0.01 was attained.

Thus, this chapter reports useful knowledge related to the intrinsic material properties, considering gas mixtures of industrial interest and essential when other membrane configurations like hollow fibers, mixed matrix membranes or polymer blends are proposed.

2.1 THE "DUAL-MODE SORPTION, PARTIAL IMMOBILIZATION" THEORY

Gas sorption and diffusion in glassy polymeric membranes has been described by several established models but the use of the "dual-mode sorption, partial immobilization" theory has been more prevalent [1]. This model originally proposed by Barrer et al. [2] has been extended by Michaels el al. [3], Paul et al. [4], Koros et al. [5] and many others. According to the dual-mode sorption model, gas sorption (C_m) in a polymer occurs in two types of sites, Henry and Langmuir sites respectively. The first type is filled by gas molecules dissolved in the equilibrium free volume portion of the material (concentration C_D) and the second one corresponds to the population dissolved in the excess free volume of the glassy polymer (C_H) [6].

$$C_m = C_D + C_H = k_D \cdot p + \frac{C'_H \cdot b \cdot p}{1 + b \cdot p} \qquad (\text{II} - 1)$$

$$S \equiv \frac{C_m}{p} = k_D \cdot + \frac{C'_H \cdot b}{1 + b \cdot p} \qquad (\text{II} - 2)$$

here, p (bar) is the pressure and k_D (cm^3(STP)/cm^3/bar) represents the Henry law constant. C'_H (cm^3(STP)/cm^3/bar) is the Langmuir capacity constant and characterizes the total sorption capacity of the lower density regions (unrelaxed gaps) in a glassy polymer for a particular penetrant. The parameter b (1/bar) is the Langmuir affinity constant which characterizes the tendency of a given penetrant to sorb in the Langmuir mode. The affinity constants for "non-condensable" penetrants such as helium and hydrogen are small, while more easily condensable polar and polarizable penetrants such as carbon dioxide tend to have significantly larger affinity constants [5].

The dual-mode theory has been extended to multicomponent gas mixtures and is presented in Equation II – 3 [7]:

$$S_i = k_{Di} + \frac{C'_{Hi} \cdot b_i}{1 + \sum_{i=1}^{n} b_i \cdot p_i} \qquad (\text{II} - 3)$$

The primary effect for a mixture is the simple competition by the various penetrants for the excess free volume fraction of the polymer which causes a significant depression in the sorption of all components of the mixture [5].

All the parameters in Equation II - 3 are for pure components. They are obtained from sorption isotherms of pure gases in glassy polymers. Their use for predicting mixture sorption assumes to be negligible the plasticizing effects over k_D, penetrant - penetrant interactions influences on both b_i and c'_H , and bulk flow phenomena.

As a consequence of the existence of two types of adsorption sites in glassy polymeric membranes two diffusion coefficients can be defined. D_D is used for the mobility of the gas population dissolved in the equilibrium free volume of the polymer and D_H for the mobility of the gas population contained in the excess free volume. Then, the Fick's law expression for flux (J) through the membrane has the form:

$$J = -D_D \cdot \frac{dC_D}{dx} - D_H \cdot \frac{dC_H}{dx} \qquad (\text{II} - 4)$$

rearranged to

$$J = -D_D \left(1 + \frac{D_H}{D_D} \cdot \frac{dC_H}{dx}\frac{dx}{dC_D}\right) \cdot \frac{dC_D}{dx} \qquad (\text{II} - 5)$$

The ratio D_H/D_D can be grouped as follows:

$$F = \frac{D_H}{D_D} \qquad (\text{II} - 6)$$

were F can be viewed as the moving fraction of the Langmuir's population.

Then,

$$J = -D_D \left(1 + F \cdot \frac{\partial C_H}{\partial C_D}\right) \cdot \frac{\partial C_D}{\partial x} \qquad (\text{II} - 7)$$

The substitution of Equation II - 1, the ratio dC_H/dC_D gives:

$$\frac{\partial C_H}{\partial C_D} = \frac{\partial \frac{C'_H \cdot b \cdot p}{1 + b \cdot p}}{\partial k_D \cdot p} = \frac{\partial \frac{C'_H \cdot b \cdot p}{1 + b \cdot p}}{k_D \cdot \partial p} = \frac{C'_H \cdot b}{(1 + b \cdot p)^2 \cdot k_D} \qquad (\text{II} - 8)$$

C_H', b and k_D can be grouped as follows:

$$K = \frac{C'_H \cdot b}{k_D} \qquad (\text{II} - 9)$$

where K is a concentration sorption parameter.

The substitution of Equation II – 8 and II – 9 into Equation II – 7 gives:

$$J \cdot dx = -D_D \left(1 + \frac{F \cdot K}{(1 + b \cdot p)^2}\right) \cdot k_D \cdot dp \qquad (\text{II} - 10)$$

the integration from the high pressure side to the low pressure side across the membrane, leads to the expression of permeability expressed by Equation II - 11, which is valid when D_D and D_H are constant and the downstream pressure is negligible [8].

$$\frac{J \cdot \delta}{p} = P = D_D \cdot k_D \cdot \left(1 + \frac{F \cdot K}{1 + b \cdot p}\right) \qquad (\text{II} - 11)$$

For mixed gas permeation expressions analogous to Equation II - 11 can be obtained for any number of additional components in the feed [5]:

$$P_i = D_{Di} \cdot k_{Di} \cdot \left(1 + \frac{F_i \cdot K_i}{1 + \sum_{i=1}^{n} b_i \cdot p_i}\right) \qquad (\text{II} - 12)$$

Alternatively, Equation II - 12 can be expressed in terms of component fugacity rather than partial pressures. The use of penetrant fugacity is clearly preferred as non-ideal gas phase mixture effects can be easily accounted for [9].

$$P_i = D_{Di} \cdot k_{Di} \cdot \left(1 + \frac{F_i \cdot K_i}{1 + \sum_{i=1}^{n} b_i \cdot f_i}\right) \qquad (\text{II} - 13)$$

In Equation II - 13 the solubility parameters c'_H , b, k_D, are those of pure gases and are based on pressure not on pure gas fugacity because the differences are rather small [9]. By fitting Equation II - 13 with mixed gas experimental data of permeability versus fugacity of the gaseous phase, one can obtain diffusivities for the Henry's law and Langmuir mode.

The final expression of the "dual-mode sorption, partial immobilization" model (Equation II – 13) shows this empirical model as an easy to use tool for the estimation of pure and mixed gas permeability data variation with pressure. Other semiempirical approaches have been proposed, using group contribution methods [10], a modified activity coefficient approach [11], or suggestions derived from molecular thermodynamic considerations [12]. Unfortunately, all of them do not allow any reliable predictive evaluation [13].

2.2. THE "NON-EQUILIBRIUM LATTICE FLUID" – NELF MODEL

A reliable tool to estimate the mixed gas solubility in glassy polymers, in the common case in which such data are not experimentally available for the system of interest, has proven to be the NELF model developed by Sarti et al. [13-15]. The NELF model enables to calculate the solubility isotherms in glassy polymers, on the basis of the results on non – equilibrium thermodynamics of glassy polymers. It offers an explicit relationship between penetrant fugacity on one hand, and penetrant solubility in the polymer and the glassy polymer density on the other hand. Thus it accounts for the strong and important relationship existing between the solubility and fractional free volume in the glassy phase.

The NELF model adopts the Lattice Fluid representation of pure substances and their mixtures [16-19]. A two dimensional representation of the Lattice Fluid model description of a hexamer is given in Figure II - 1. There are multiple configurations available to a system of *N* molecules each of which occupies *r* sites (an *r – mer*) and N_0 vacant sites (holes). A random mixing of the *r – mers* which each other and with the vacant sites is assumed.

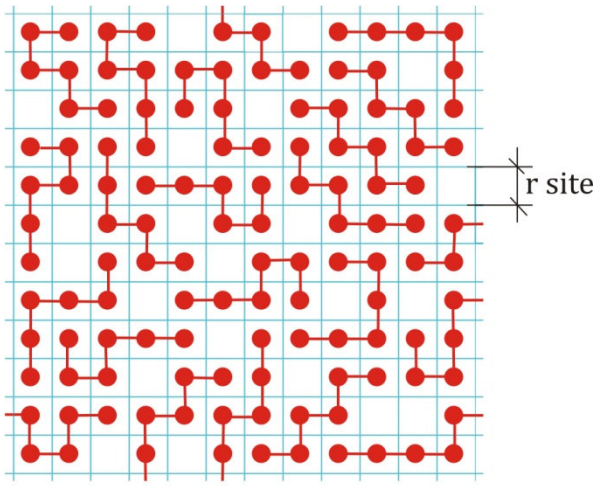

Figure II – 1. A two-dimensional example of a pure lattice fluid. Hexamers are distributed over the lattice, but not all sites are occupied [17].

The NELF model extend the Sanchez – Lacombe equation of state for amorphous phases to the non equilibrium domain typical of glassy polymers, using the same parameters to represent the "pure components" properties and the same mixing rules to calculate the mixture behavior. For all the penetrants, these parameters can be determined using either PVT (pressure- volume – temperature) data or vapor – liquid equilibrium data, while for the polymers they are usually calculated by fitting the PVT data above T_G with the Sanchez – Lacombe equation of state.

2.3. EXPERIMENTHAL METHODOLOGY

2.3.1. Materials

The commercial polymer Matrimid 5218 (polyimide of 3,3´, 4,4´-benzophenone tetracarboxylic dianhydride and diamino-phenylidane) was kindly provided by Huntsman Advanced Polymers in powder form. Dichloromethane (CH_2Cl_2) (Panreac) solvent was used as received for the preparation of the polymer solutions. Gases were purchased from Air Liquide (Spain) with a purity of at least 99.95 %.

2.3.2. Preparation of dense planar Matrimid polymeric membranes

Dense planar polymeric membranes (Figure II – 2) with thickness ranging from 30 to 50 μm were prepared by solution casting according to two procedures, described as follows:

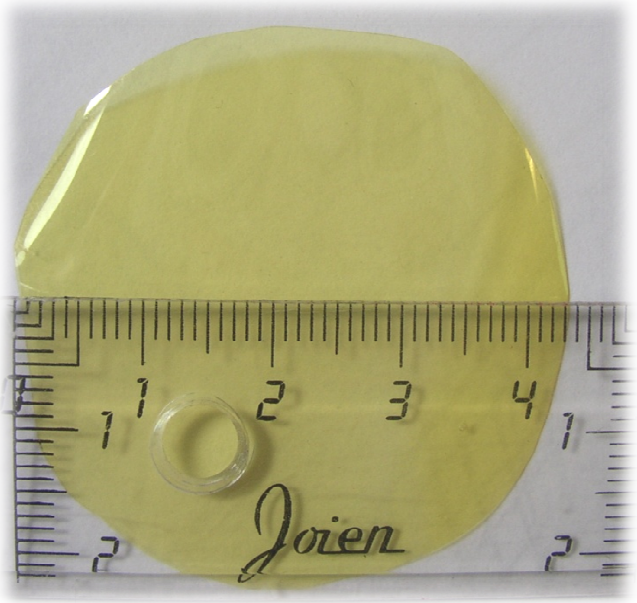

Figure II – 2. Image of a typical Matrimid dense film prepared in this work

(A) <u>Using a casting knife (Elcometer 3580 - see Figure II – 3):</u>

1. Polymer powder drying under complete vacuum at 120°C for at least 12 h (Selecta –vacuum oven).
2. Preparation of polymeric solutions of 20 cm^3 of 15 wt % under continuous stirring of the polymer powder with CH_2Cl_2 as solvent for at least 24 h.
3. Solution casting on a glass plate using a casting knife (Elcometer 3580) of thin wet films. The gap between the blade of the casting knife and the glass plate was from 0.2 to 0.5 mm.
4. Drying of the cast films at room temperature in a covered box for 24 h under a continuous flow of N_2 in order to prevent phase inversion by water absorption from air.
5. Removing of the homogeneous dense films from the glass plate by rinsing with a small amount of water and further drying in a vacuum oven (Selecta Vacioterm-T) at 120 °C for 24 hours and 200 mbar in order to eliminate the remaining solvent.
6. Cutting off the membrane in circular shape with a diameter of 4.45 cm

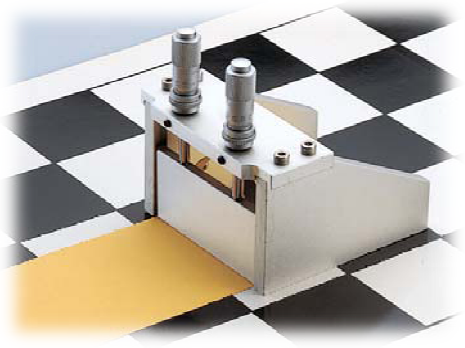

Figure II – 3. The Elcometer casting knife used for the preparation of polymeric dense films

(B) Using a Petri dish

1. Polymer powder drying under vacuum at 120 °C for at least 12 h (Selecta – vacuum oven).
2. Preparation of polymeric solutions concentrations (C_{sol}) of 3 – 5 wt % under continuous mixing of the polymer powder with CH_2Cl_2 as solvent for at least 24 h. The needed solution volume (V_{sol}) for one Petri dish with the diameter d, depends on the thickness desired for the dry film and is estimated according to the following formula:

$$V_{sol} = (\pi d^2/4)\cdot(\delta_{dry}/C_{sol}) \qquad \text{(II - 14)}$$

3. Filtration with a syringe – driven filter unit (Millipore – hydrophobic PTFE 0.2 μm) and concomitant solution casting on a Petri dish (9.5 cm diameter) of thin wet films.
4. Drying of the cast films at room temperature in a covered box for 24 h under a continuous flow of N_2 in order to prevent phase inversion by water absorption from air. The steps 5. and 6. similar to the previous procedure.

The polymer solutions used for solution casting with a casting knife had 15 % wt polymer concentration because sufficiently viscous solution is needed in order to prevent it from running over the central part.

Because of the extra filtration step the films prepared using Petri dishes had in general a better morphology. Polymeric solutions are not entirely homogeneous and even after large periods of mixing they still contain non-solved polymer particles, thus the importance of filtration before casting. The only drawback in using Petri dishes is that polymer solution can adhere to the walls determining a variation in the thickness of the circular shape film, i. e. thinner in the middle and thicker toward the

edge. Membranes with a constant thickness where obtained using large Petri dishes by cutting of the membrane from the middle of the film. In general the optimum membrane thickness was experienced to be around 30 μm and membrane thickness should not exceed 50 μm when Matrimid polyimide is used as membrane material.

CH_2Cl_2 is a good, but highly volatile solvent with a normal boiling point of 40 ^oC. The rapid evaporation of the solvent makes the preparation of homogenous films difficult, i. e. it cools the casting solution, causing gelation of the polymer. The result is a film with a mottled, orange-peel-like surface [6]. When membranes were prepared using the casting knife, smooth films were obtained by covering the cast films with a glass plate raised 1 cm above the film to slow down the evaporation of the solvent. When membranes where prepared using Petri dishes, those were closed with their own cover.A less volatile solvent can be used also. Table II – 1 list the boiling points and hazard information for solvents in which Matrimid has a good solubility at 20 wt % as stated in the data sheet provided by the polymer producer (see Appendix I).

Table II – 1. Matrimid solvents boiling points and hazard information

Solvent	Boling Point (^oC)	Hazards
Dichloromethane	39.6	R40
Ethylene chloride	98.96	R11, R45, R36/37/38,
Chloroform	61.2	R22, R38, R40, R48/20/22
Tetrachloroethane	146.5	possible human carcinogen [20]
Tetrahydrofurane (THF)	66	R11, R19, R39/37
1 , 4 Dioxane	101.1	R11, R19, R36/37, R40, R66
Acetophenone	202	Harmful (Xn)
Cyclohexanone	155.65	R10, R20,
m – Cresol	202.8	R20, R24, R25, R34,
γ – Butyrolactone	204	R22, R36,
Dimethylformamide (DMF)	153	R61, R20/21, R36
Dimethylacetamide (DMAc)	164-166	R61, R20/21
N – methylpirolidone (NMP)	202-204	R36/37/38, R61

R10: Flammable, R11: Highly flammable, R19: May form explosive peroxides, R20: Harmful by inhalation, R22: Harmful if swallowed, R24: Toxic in contact with skin, R25: Toxic if swallowed, R34: Causes burns, R36: Irritating to eyes, Irritating to skin, R40: Limited evidence of a carcinogenic effect , R61: May cause harm to the unborn child, R66: Repeated exposure may cause skin dryness or cracking, R20/21: Harmful by inhalation and in contact with skin, R36/37: Irritating to eyes and respiratory system, R36/37/38: Irritating to eyes, respiratory system and skin, R48/20/22: Harmful: danger of serious damage to health by prolonged exposure through inhalation and if swallowed.

The Risk phrases listed in Table II – 1 are defined in the Appendix III of European Union Directive 67/548/EEC. Taken into account hazard considerations, from all the possible solvents, the more appropriate and already used in literature for Matrimid membrane manufacture are underlined.

When solvents with high boiling points are used, prolonged drying step is needed (up to 2 weeks in vacuum oven at 100 ^{o}C for NMP). Also, in order to obtain a defect free membrane, the mixture of two solvents with high and low boiling points can be done.

2.3.3. **Membrane characterization**

The membrane thickness was measured using a digital micrometer Mitutoyo Digmatic Series 369 (accuracy ± 0.001 mm) (see Figure II - 4). This micrometer is equipped with two plates of 2 mm diameter specially designed to measure thin films. The resulted values of thickness represent an average of five measurements, one in the center of the membrane and four in the borders. Thickness deviations from the average did not exceed 2 μm in any of the membranes used.

Figure II – 4. The digital micrometer used for the measurement of membranes thickness

In order to check the complete evaporation of the solvent, thermogravimetric analysis (25-600 ^{o}C, 10 ^{o}C/min) were performed to film samples before and after vacuum oven drying using a Shimatzu Scientific DTG – 60H equipment. Figure II -5 shows that before vacuum drying the membranes contain some residual solvent having an 8.5 wt % loss at 350 ^{o}C. The vacuum oven treated sample (Figure II – 6) had a 1 wt % mass loss at 350 ^{o}C and 68.4 wt % at 600 ^{o}C. Considering the Matrimid polymer Tg value of 303.3 ^{o}C it can be concluded that no residual solvent was left in the polymer sample and that the membrane manufacturing procedure was correct.

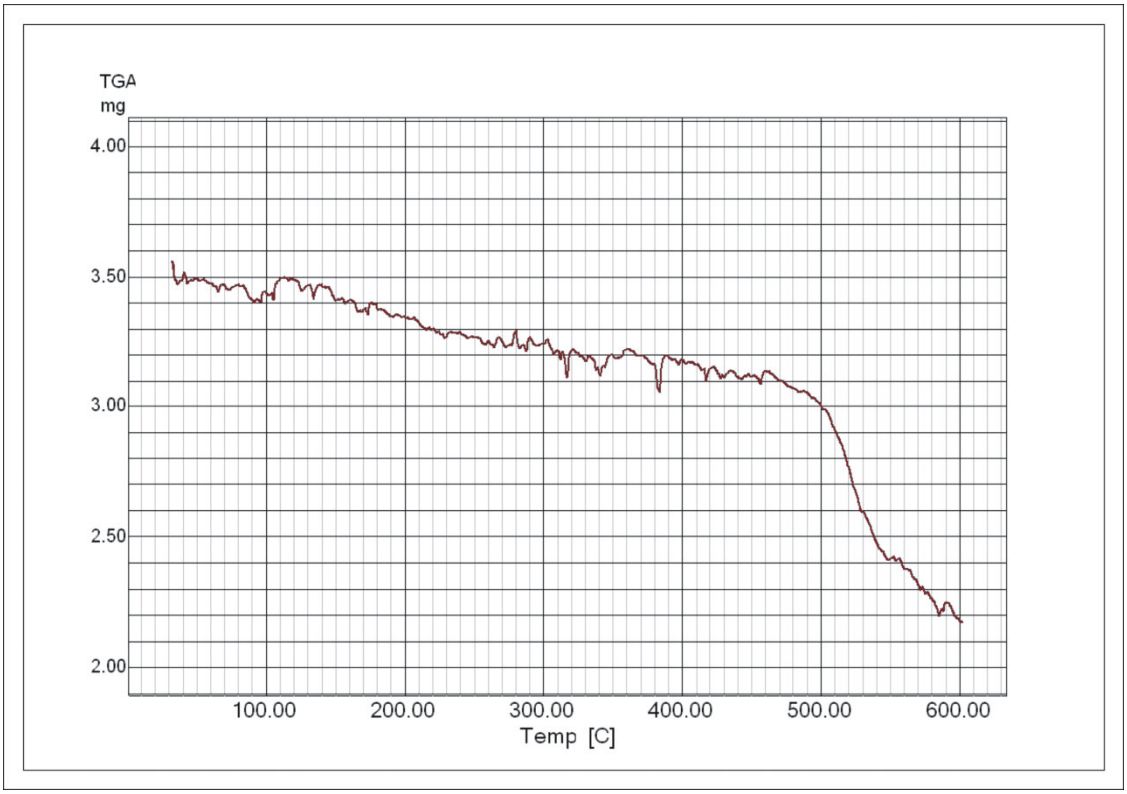

Figure II – 5. Thermal gravimetric analysis report for a Matrimid film sample before vacuum oven drying step

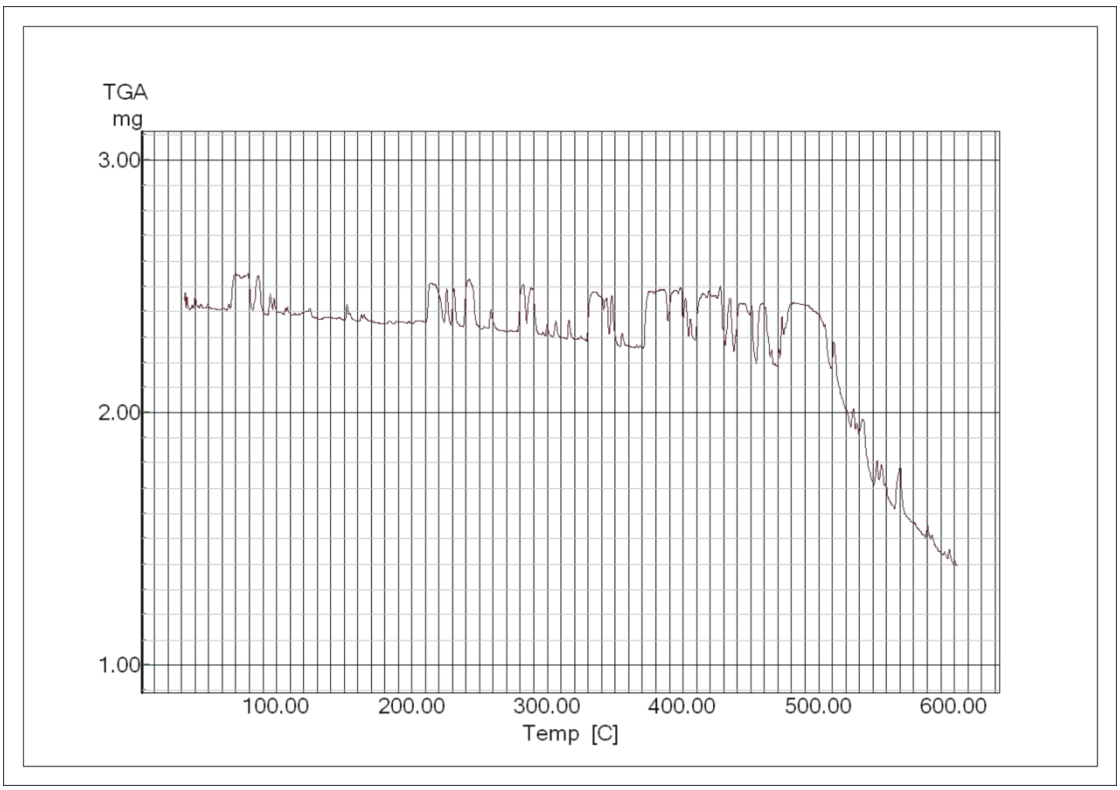

Figure II – 6. Thermal gravimetric analysis report for a Matrimid film sample after vacuum oven drying step

2.3.4. Mixed gas separation set - up

Figure II - 7 shows a schematic diagram of the experimental permeation set-up and Figure II – 8 shows a photographic image taken from the experimental set - up. The design of the feed part of the set-up confers the possibility of performing pure and mixed (binary, tertiary and quaternary) gas permeation experiments, at predetermined gas concentrations and flow rate levels.

The desired concentration of each component of the mixture is obtained by controlling its flow rate by means of mass flow controllers (Brooks 5850S), with a 100 cm^3 (STP) min^{-1} upper limit for the total flow rate. These mass flow controllers present a flow accuracy of 0.9 % at full scale. At 5 % of the full scale the error is 4.7 %. The gas mixture flows over the polymeric membrane film mounted in the membrane test cell and leaves the system via the backpressure regulator (Brooks 5866), which controls the total pressure in the feed side of the membrane.

In the permeate side the total pressure is maintained at atmospheric level. The gas permeates through the membrane material and is removed by an argon sweep gas. The flow rate of the sweep gas was controlled with a mass flow controller (Brooks 5850S), with a 10 cm^3 (STP) min^{-1} full scale and the same characteristic accuracies as the previous ones. The concentration (vol %) of each component in the sweep gas stream leaving the permeate side of the cell is determined via gas chromatography (Agilent Micro GC 3000) equipped with a thermal conductivity detector. The GC is suited with two columns, 1) molecular sieve 5A for H_2, CO and N_2 separation, that employs Ar as carrier gas, and 2) PLOT U for CO_2 separation, that employs He as carrier gas. Ar was used as carrier and sweep gas instead of the cheaper He because He has a similar thermal conductivity with H_2 and therefore H_2 cannot be measured by the chromatograph detector in the presence of He. Due to the differences in concentration at the permeate side of the membrane two chromatographic methods were developed: one for the fast permeating gases i.e. H_2 and CO_2 and the other for the slow permeating gases i.e. N_2 and CO. The only difference between these two methods is the injection time which is 20 times higher in the method used for CO and N_2 analysis; this allows a higher accuracy at low concentrations. Therefore, the error associated to the chromatographic analysis was minimized and the coefficient of variation calculated from peak area deviations of calibration samples was less than 0.4%. A detailed description of the chromatographic methods is found in Appendix II.

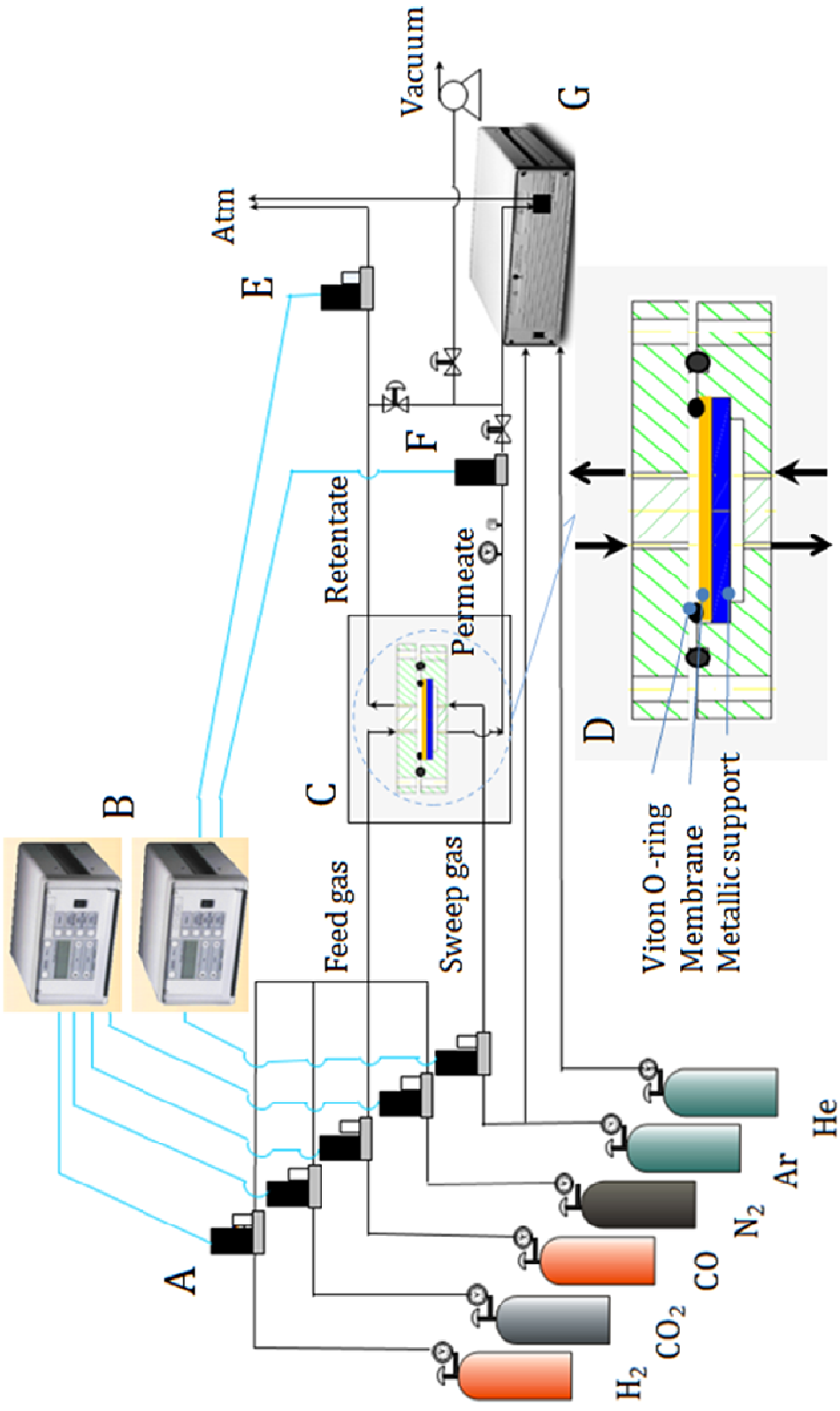

Figure II – 7. The experimental permeation set – up with a detailed view of the permeation cell, (A) Mass flow controller; (B) Control box; (C) Heating oven; (D) Membrane test cell; (E) backpressure regulator; (F) Mass flowmeter, (G) Gas chromatograph

Figure II – 8. The photographic image of the experimental permeation set – up with the heating oven open for a better viewing of the testing cell.

The polymeric film to be characterized is inserted in the permeation test cell (see scale drawings in Appendix III) that includes a porous metallic plate (Mott Corp OD = 1.750", ID =0.125", media grade= 20, material – 316LSS) as support and a filter paper that prevents scratching of the membrane by the metallic support. The membrane test-cell is thermostatized into a heating oven (Memmert Excel). The membrane is cut off from the dried polymeric film in circular shape and after the insertion in the membrane test cell it results an effective membrane area of 12.13 cm^2. The two compartments of the permeation cell are sealed with O-rings (Viton).

Before starting a series of experiments a vacuum pump was used to evacuate the whole test cell from undesired species for at least half an hour. Tests were conducted at specific conditions until constant steady-state values of permeate flux and composition were reached and the permeate, retentate and feed streams remained unchanged for at least 1 h. During this period the concentration of each component was analyzed at least five times.

When a series of experiments were run several times the standard deviation is illustrated in the graphics as bars.

For pure and mixed gas experiments, permeabilities were calculated using Equation II - 15,

$$P_i = \frac{Q_i \cdot \delta}{\mathrm{A} \cdot \Delta p_i} \qquad (\mathrm{II} - 15)$$

where Q_i is the permeate flow rate for the component *i*, δ is the membrane thickness, *A* is the membrane area, Δp_i is the component *i* partial pressure gradient through the membrane. Δp_i is equal to the partial pressure in the feed side considering a null value of the partial pressure in the permeate side. The permeate flow rate value was determined by multiplying the experimental concentration of component *i* (vol %) in the permeate times the Ar sweep gas flow rate. Data were fitted to the model by using fugacities instead of partial pressures (Equation II – 13). Fugacities of the components were calculated using the Peng-Robinson equation [21] for each experimental point at the particular experimental conditions of temperature and total pressure.

2.3.5. Experimental procedure and operation conditions

Pure gas permeation experiments were performed in order to obtain and compare the permeation results with literature data and in this way to assure the reliability of the testing system, and also to have a benchmark for the mixed gas results at 30 ^{o}C and three operational pressures, 2, 4 and 6 bar. The sweep gas flow rate was varied in order to determine the occurrence of concentration polarization phenomena in the permeate side of the membrane and in this way to select the minimum value of this variable that permits to avoid secondary effects when analyzing permeance data. For these experiments, a membrane of 47.8±2 μm thickness was used.

Then, the temperature dependency of the permeability coefficients for H_2, CO_2, CO and N_2 was determined experimentally. Measurements were made for each gas at five or six different temperatures in the range 30–100 ^{o}C, and a feed pressure of 4 bar using the membrane of 47.8±2 μm thickness for H_2 and CO_2 and of 28.9±2 μm thickness for CO and N_2. Steady-state values of permeate flux were obtained overnight and the permeability of gases at the specific temperatures was determined in consecutive days.

Finally, experiments with binary, ternary and quaternary gas mixtures of H_2, N_2, CO and CO_2 were performed at composition and operation experimental conditions listed in Table II – 2 at feed flow rates of 100 cm^3 (STP) min^{-1} and sweep gas flow rates of 6 cm^3 (STP) min^{-1}.

Table II – 2. Gas composition and operation experimental conditions for mixed gas experiments.

Mixture ID	Composition (vol %)	Pressure (bar)	Temperature (°C)	Membrane thickness (μm)
H_2/N_2	2, 3, 4, 5, 10, 30, 50, 75 of H_2 in N_2	4	30	47.8±2
H_2/CO_2	10, 30, 50, 70, 90 of H_2 in CO_2	4, 6	30	47.8±2
H_2/CO	10, 30, 50, 70, 90 of H_2 in CO	4	30	28.9±2
$H_2/CO_2/N_2$	20/60/20, 20/40/40, 20/20/60, 40/40/20, 40/20/40, 60/20/20	4	30	47.8±2
$H_2/CO_2/N_2$/CO	16.3/5.3/60.7/17.8 (M1) 20/**20**/30/30 (M2) 40/**20**/20/20 (M3) 60/**20**/10/10 (M4) 20/30/30/20 (M5)	4	30 - 100	28.9±2

2.4. RESULTS AND DISCUSSION

2.4.1. H_2, N_2, CO_2 and CO pure gas permeation experiments

Table II - 3 lists the average permeability of pure gases as an average of several runs. The permeability coefficients decrease in the following order of average values (Barrer): $P_{H2} = 23.6 > P_{CO2} = 5.7 > P_{CO} = 0.43 > P_{N2} = 0.17$, which is also the order of increasing kinetic diameters of the gas molecules. These results are in agreement with literature data collected in Table II - 3, that present an average H_2 permeability of 23.0 ± 5.1 Barrer, an average CO_2 permeability of 7.9 ± 2.0 Barrer and an average N_2 permeability of 0.26 ± 0.05 Barrer, values obtained in a narrow range of temperatures (30-35 °C) and pressures (2-4 bar). With regard to CO no previous data of its permeability in Matrimid 5218 membranes have been reported, thus the obtained value in this work $P_{CO} = 0.43$ Barrer, constitutes original data for this material.

Table II – 3. Pure gas permeabilities and ideal selectivities values for planar dense Matrimid® 5218 membrane

Permeability (Barrer)				Ideal Selectivity			Exp. Conditions		Ref.
H_2	CO_2	N_2	CO	H_2/N_2	H_2/CO_2	H_2/CO	T (°C)	P (bar)	
24.1	6.4	0.18	0.44	133.9	3.8	54.8	30	2	this
23.7	5.7	0.17	0.43	138.8	4.0	54.9		4	work
23.1	5.2	0.16	0.43	144.4	4.4	53.7		6	
17.5	7.3	0.22	-	79.6	2.4	-	35	4	[22]
27.2	7.0	0.28	-	97.0	3.9	-	35	3.5	[23]
28.1	10.7	0.32	-	87.8	2.6	-	30	3.5	[24]
17.8	5.4	0.16	-	110.9	3.3	-	35	2	[25]
24.0	8.9	0.25	-	96.0	2.7	-	-	-	[26]

1 Barrer = 1 x 10^{10} cm^3(STP) cm cm^{-2} s^{-1} $cmHg^{-1}$

Sweep gas flow rate effect

Figure II - 9 shows that for the highly permeable H_2 the permeability reaches a asymptotic value of 24.1 Barrer when using sweep gas flow rates ≥ 6 cm^3(STP) min^{-1}. At lower Argon flow rates, hydrogen accumulates at the permeate side resulting in a decrease of the effective concentration driving force through the membrane.

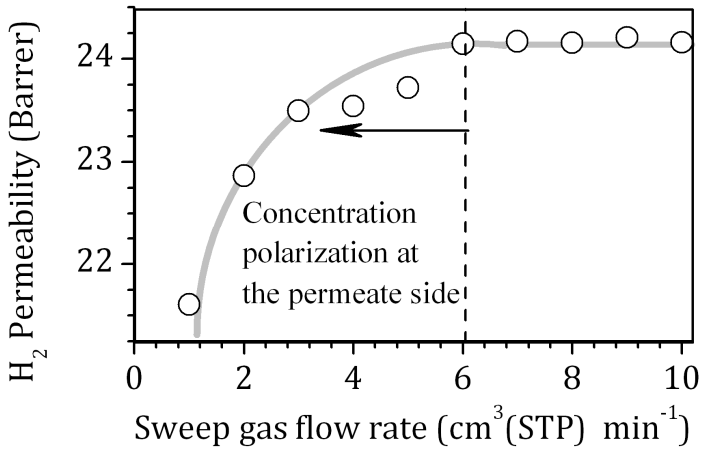

Figure II – 9. Effect of sweep gas flow rate on H_2 permeability, at 30 °C and 4 bar feed pressure**.**

Temperature effect

The temperature dependency of the permeability coefficients for H_2, CO_2, CO and N_2 was determined experimentally and is plotted in Figure II - 10.

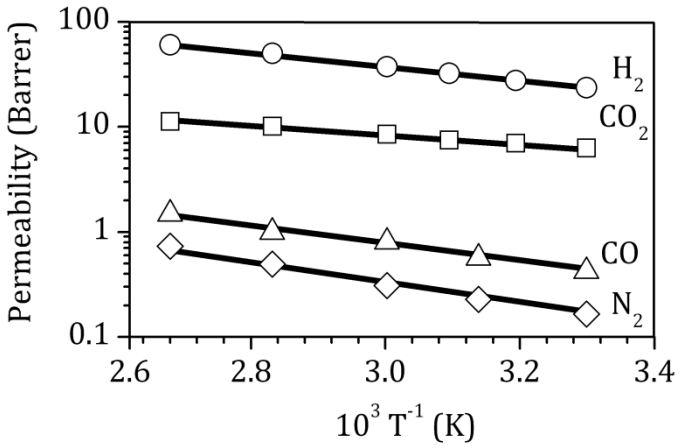

Figure II- 10. The permeability of pure H_2, CO_2, CO and N_2 as a function of temperature at 4 bar feed pressure.

As temperature increased all four gas permeabilities increased. Arrhenius plots are represented in Figure II - 10 showing straight lines with high correlation coefficients ($R^2 > 0.99$) in all cases. Having established the validity of the Arrhenius-type dependence with temperature expressed by Equation II – 16 where R = 8.31 J $mol^{-1}K^{-1}$ is the general gas constant and T is the temperature (K), the specific parameters for permeation of H_2, CO_2, N_2 and CO were calculated (Table II - 4).

$$P = P_0 e^{-\frac{E_{aP}}{RT}} \qquad (II - 16)$$

The permeation activation energy E_{ap} increased in the order $CO_2 < H_2 < CO < N_2$, the same as reported in other glassy polymeric membranes [27, 28] for the case of CO_2, H_2 and N_2.

The very low E_{aP} value of CO_2 compared with those of H_2, CO and N_2, could be attributed primarily to the lower heat consumption for CO_2 diffusion, lowering the amount of energy associated to the permeation phenomenon, as reported for ABS copolymer membranes [29].

Table II – 4. Arrhenius parameters for CO_2, N_2, H_2 and CO permeation through a Matrimid® 5218 dense film

Arrhenius parameters	Gas				Ref.
	N_2	H_2	CO_2	CO	
P_0 (Barrer)	480.7	3789.4	157.3	291.8	this work (pure gas)
	479.6	4964.6	95.8	1908.7	this work (quaternary gas mixture)
E_{aP} (kJ mol^{-1})	20.2	12.8	8.1	16.5	this work (pure gas)
	20.2	13.7	7.0	21.4	this work (quaternary gas mixture)
	13.6	10.5	5.9	-	[26]
	19.7	11.3	9.0	-	[25]

Using the Equation I - 8 (from Chapter I) to calculate ideal gas selectivity values at different temperatures, the relative effects of temperature on the ideal selectivity for H_2/CO_2, H_2/N_2, H_2/CO and CO/N_2 separations through the Matrimid membrane can be determined. Thus, the ideal selectivity $\alpha_{H2/CO2}$ increases with temperature from a value of 4.0 at 30 °C to 5.3 at 100 °C, while the selectivity $\alpha_{H2/N2}$ decreases with temperature from 138.8 at 30 °C to 81.8 at 100 °C, as shown in Figure II - 11.

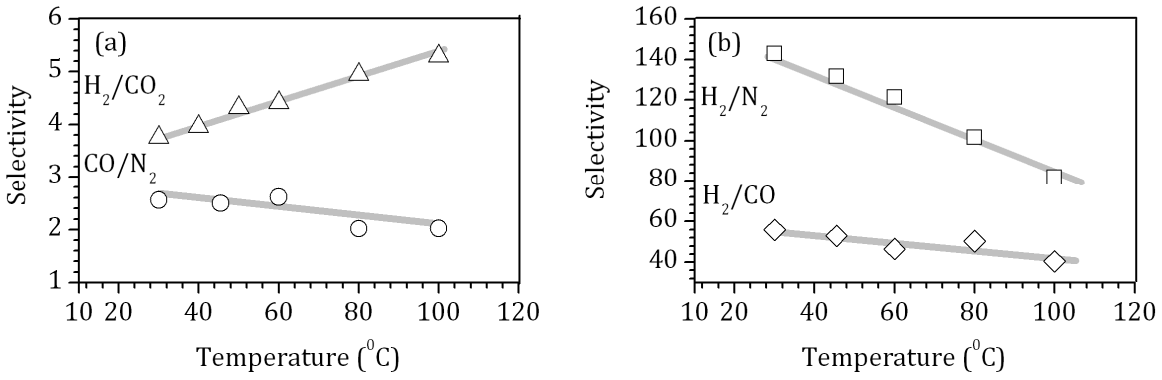

Figure II – 11. Ideal selectivity variation with the temperature for (a) H_2/CO_2, CO/N_2 and (b) H_2/N_2, H_2/CO gas pairs at 4 bar feed pressure

The pairs H_2/CO and CO/N_2 present the same trend of decreasing selectivity with temperature from a value of 55.1 to 40.5 and of 2.5 to 2.0 respectively. In glassy polymers the two parameters determining the permeability, i.e., the diffusion and solubility (Equation I - 7) exhibit also an Arrhenius type dependence with temperature as the permeability parameter. The associated activation energy of diffusion (E_D) is positive meanwhile the enthalpy of sorption (ΔH_s) is negative [1]. Therefore increasing temperature has an opposite effect: the diffusion coefficient increases meanwhile the solubility coefficient decreases. Prior work [26] on the permeability dependence with temperature of dense Matrimid membrane showed that E_D increased in the order $H_2 < CO_2 < N_2$ meanwhile the absolute value of ΔH_s increased in the order $H_2 < N_2 < CO_2$. In all cases E_D is higher than $|\Delta H_s|$ and their sum gives the energy of permeation (E_{aP}) which is always positive and thus their relative contribution determines the increasing rate of permeability with temperature for gases.

In the case of CO_2 at low temperatures, the CO_2 solubility was the major contributing factor to the permeability because of the low diffusivity but as the temperature increased the regime was shifted from diffusion - limited to sorption - limited because of the higher dependence of diffusivity on temperature. Thus, the increasing rate of CO_2 permeability with temperature was lower than the increasing rate of H_2 and therefore the H_2/CO_2 selectivity increased.

Feed pressure effect

Pure gas permeability values obtained at different feed pressures are presented in Table II - 3. For H_2, N_2 and CO there is a slight decrease in permeability with pressure but it does not exceed pure gases deviations of 5% encountered in literature and therefore this variation cannot be attributed to an influence of pressure over permeability in the pressure range under study. In the case of CO_2 the permeability observed a 19 % decrease in the pressure range under study. The behavior of H_2, CO and N_2 is typical for low-sorbing penetrants in glassy polymeric membranes [1], their transport being more diffusion dependent meanwhile the behavior of CO_2 shows higher solubility dependence. When the pressure increases, the solubility coefficient of CO_2 decreases determining a higher decrease in the permeability coefficient for CO_2 than for the more inert H_2, N_2 and CO.

Similar influence of pressure on CO_2 permeability has been previously reported by several studies with other glassy polymers [1, 30] . As shown in Figure II – 12, in glassy polymers CO_2 permeability can decrease with pressure until it reaches a minimum value from which it began to increase again.

The pressure at which permeability presents a minimum is named the plasticization pressure. The decrease in gas permeability is related to competitive solubility effects between the gas and the polymer matrix, the polymer sorption sites becoming saturated with gas molecules and is predicted by the dual mode sorption model. From the plasticization pressure onwards, the polymeric chain packing is disrupted by the penetrant molecules due to the increase in the segmental mobility that expands both the frequency and the average size of transient gaps that enable diffusion, thereby increasing the permeability.

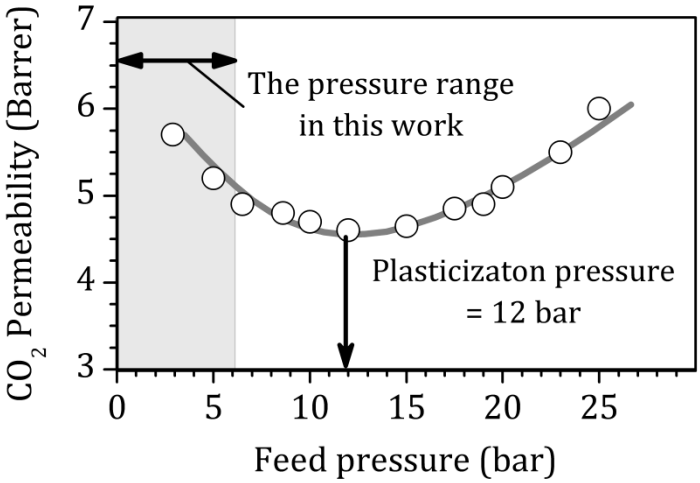

Figure II - 12. Literature results for CO_2 permeability as function of CO_2 pressure for a 30 μm thickness Matrimid dense film at 22 ^{o}C [31].

It has been demonstrated that the plasticization pressure depends on the solvent from where the polymeric films were cast from, on the final membrane thickness and on the experimental temperature, but it corresponds to a constant concentration of CO_2 (cm^3(STP)/cm^3) into the polymer matrix. Table II – 5 list the variation in the CO_2 plasticization pressure.

In the present work the maximum pressure studied was of 6 bar so the plasticization pressure of Matrimid by CO_2 was not reached for the 30 μm film under study. Therefore the experimental results of permeability for CO_2 can be adjusted by the dual sorption partial immobilization model in the entire range of pressure studied.

Table II – 5. Plasticization pressure of Matrimid films cast from different solvents at different temperatures [31].

Solvent	Film thickness (μm)	Temperature (°C)	Plasticization pressure (bar)
$CHCl_3$	16	23	8
	27	25	10
DMAc	14	25	8
	21	24	8
	22	24	10
	33	21	9
	34	27	9
	35	23	8
	23	35	15
NMP	9	21	10
	9	21	9
	29	22	11
	30	**22**	**12**

2.4.2. $H_2/N_2/CO/CO$ binary, ternary and quaternary mixed gas permeation experiments

Analysis of H_2 permeation

H_2 / N_2 mixtures

H_2 /N_2 mixture is formed by a fast permeating gas, i.e. H_2, and a slow permeating gas, i.e. N_2. This type of mixtures might present concentration polarization phenomena at the feed side of the membrane at low concentrations of the fast permeating gas. Figure II - 13 shows that concentration polarization occurs at hydrogen concentrations below 10 vol %. Then, at concentrations higher than 10%, hydrogen permeability leveled off to a constant value, equal to the pure hydrogen permeability, as it is shown in Figure II - 14. This indicates that from this level, H_2 transport is not affected by the presence of N_2 as co-partner in the overall gas transport through the polymer matrix, demonstrating that there is no coupling or competitive sorption between the two species. N_2 permeability presented no variation with its concentration, i.e., its partial pressure.

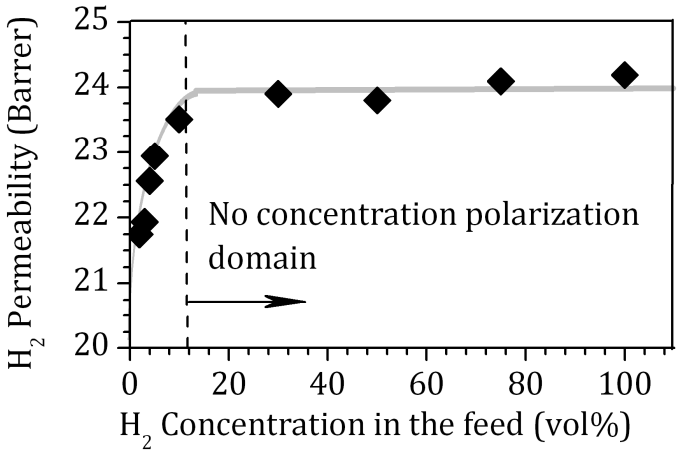

Figure II – 13. H_2 permeability variation with its feed concentration in mixtures with N_2, at 30 °C and 4 bar feed pressure.

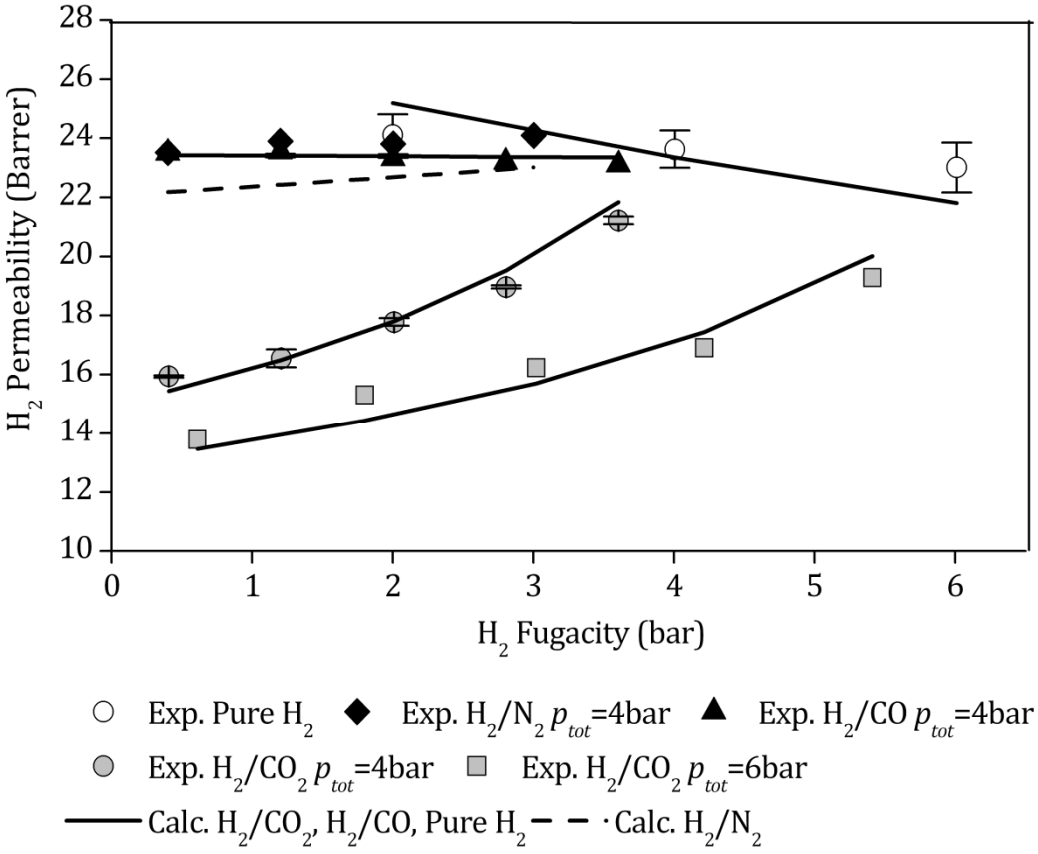

Figure II – 14. H_2 Permeation variation with its fugacity for mixtures: H_2/CO_2 at 4 and 6 bar, H_2/N_2 and H_2/CO at 4 bar total pressure and 30 °C. Data points represent experimental values and lines are model results.

H_2 / CO_2 mixtures

As it can be seen in Figure II - 14, H_2 permeability was strongly affected by the presence of CO_2. For a total pressure of 6 bar, the value of P_{H_2} with a mixture 10/90 (vol %) H_2/CO_2 became 42% lower than the permeability obtained working with pure gas. Furthermore, hydrogen permeability is influenced by the total pressure of the feed gas, that is, at a given hydrogen partial pressure, hydrogen permeability increases at lower CO_2 partial pressure. Then, hydrogen permeability is better plotted as a function of CO_2 fugacity (Figure II - 15) that shows similar H_2 permeabilities at equal CO_2 fugacities, but independent of the presence of other components.

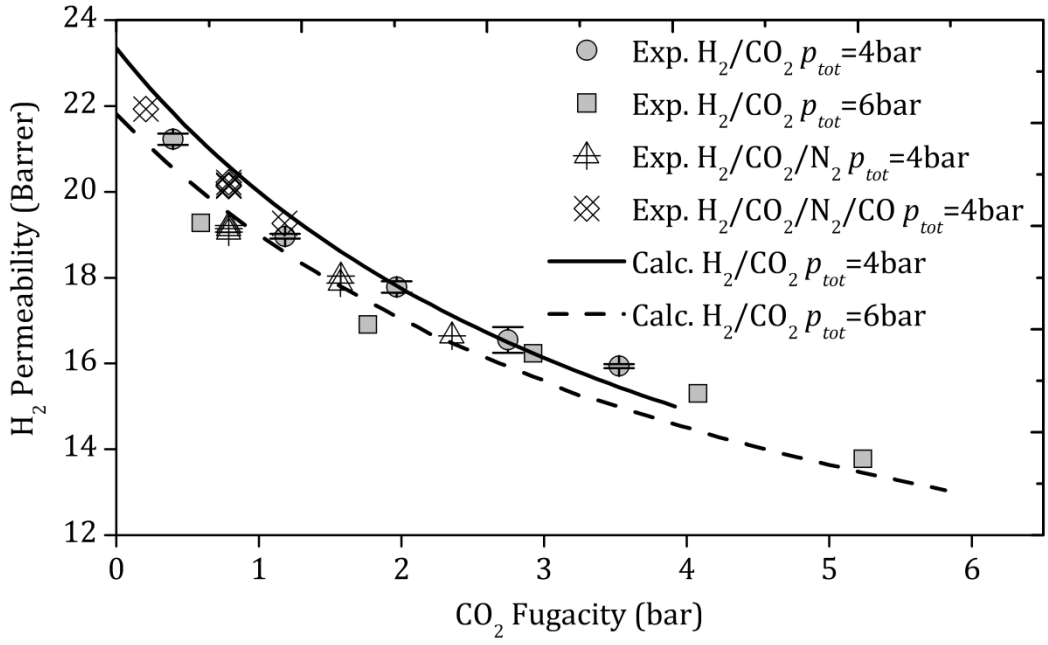

Figure II - 15. H_2 permeability variation with CO_2 fugacity for mixtures: H_2/CO_2 at 4 and 6 bar, $H_2/N_2/CO_2$ and $H_2/N_2/CO_2/CO$ at 4 bar total feed pressure and 30 ^oC. Data points represent experimental values and lines are modeling results.

These results indicate competitive sorption between H_2 and CO_2 for the sorption sites present in the matrix, which get saturated at a certain pressure, thereby leading to a decrease in solubility at higher penetrant pressures. At a given concentration (vol %) of the feed mixture, as the feed pressure is increased , more sorption of carbon dioxide in the Langmuir sites occurs because of carbon dioxide's larger affinity constant and solubility in polyimide Matrimid membrane. As a consequence

hydrogen molecules are prevented to diffuse and therefore the effect of competitive sorption between carbon dioxide and hydrogen is increased.

It can also be mentioned that when a pure H_2 permeation experiment was performed after an experiment with CO_2, the time needed to reach a steady state H_2 permeability value was much larger than the usual 30 min established in the procedure. It can be assumed that H_2 permeability was affected even by trace levels of the CO_2 present in the installation tubes or even in the membrane as sorbed specie.

H_2 / CO mixtures

Figure II - 14 shows that H_2 permeability is not influenced by the presence of CO in the feed gas mixture, and therefore there is no evidence of competitive transport phenomena between these two species. Also, the permeability of CO is equal to the pure gas permeability reported in Table II - 3.

Ternary and quaternary mixtures

Hydrogen permeation data for $H_2/CO_2/N_2$ ternary mixtures is shown in Figure II - 16. The arrows indicate the concentration of each component in the mixture.

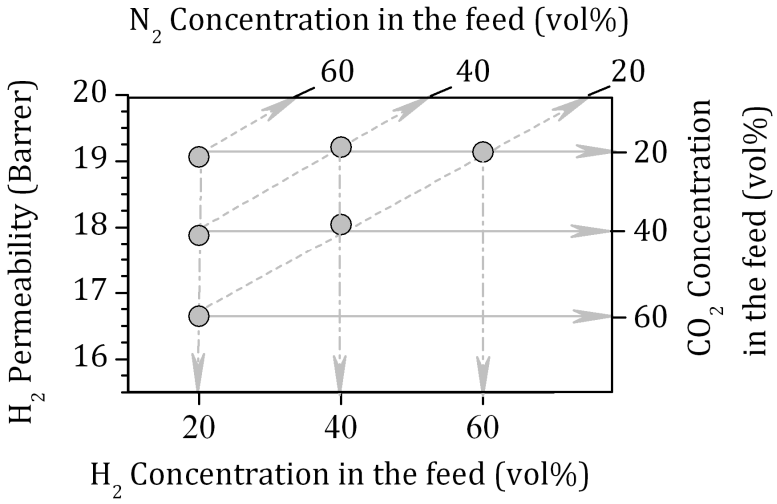

Figure II – 16. H_2 permeability variation in H_2, N_2 and CO_2 ternary mixtures, at 30 ^oC and 4 bar

At a constant concentration of CO_2 the H_2 permeability coefficient is constant even if the concentration of N_2 changes substantially; therefore it is clear that hydrogen transport is affected only by the amount of CO_2. The supplementary presence of N_2 does not affect the transport of H_2.

In the case of the quaternary gas mixtures, the mixture labeled M1 in Table II – 2, represents a synthetic mixture similar to the dry post-combustion gas stream obtained in the production of carbon black. The next three mixtures (M2, M3 and M4) had a constant concentration of CO_2, an increasing concentration of H_2 and a constant and equal to unity ratio N_2/CO. The last quaternary mixture studied (M5) had a slightly higher partial pressure of CO_2.

The results in terms of H_2 permeability are plotted all together in Figure II – 15 where three points differentiate. The upper left pint is the value of the H_2 permeability coefficient of the mixture M1. The next one in decreasing order is actually a cumulus of three points corresponding to the H_2 permeability coefficient of the mixtures M2, M2 and M3 were the constant concentration of CO_2 determined a lower but constant permeability value for H_2 regardless the concentrations of N_2 and CO. This makes clear once more that hydrogen transport is affected only by the amount of CO_2. The supplementary presence of either N_2 or CO does not affect the transport of H_2. The lowest H_2 permeability value belongs to mixture M5 with a higher concentration of CO_2.

The Arrhenius specific parameters for permeation with the quaternary mixture M1 were calculated, obtaining slightly different values to those obtained with pure gases. These values are summarized in Table II - 4.

Analysis of CO_2 permeation

In all mixtures (binary H_2/CO_2 at 4 and 6 bar total pressure, CO_2/N_2, ternary H_2/CO_2/N_2 and quaternary H_2/N_2/CO_2/CO mixtures) the transport rate of CO_2 is slightly lower than for the pure gas but it presents a similar behavior of decreasing permeability with increasing CO_2 fugacity (Figure II - 17). Also, CO_2 permeability data are equal for all mixtures at the same values of CO_2 partial pressure, indicating that the CO_2 transport rate is almost unaffected by the nature of the other components. Therefore, the competitive sorption between H_2 and CO_2 influences considerably more the transport rate of H_2 than the transport rate of CO_2.

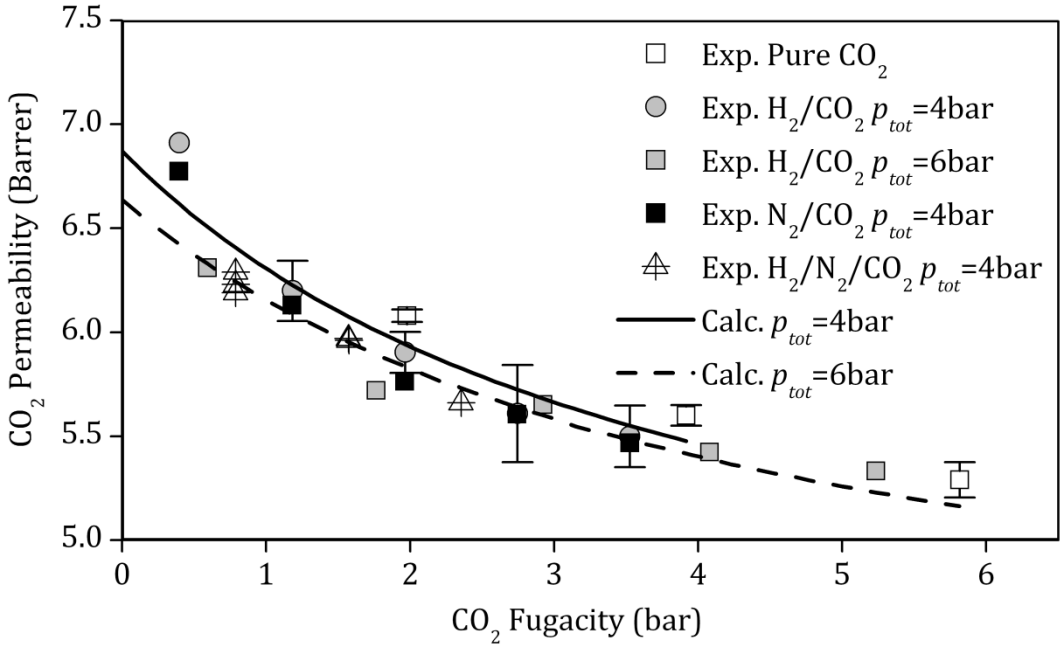

Figure II – 17. CO_2 Permeation variation with CO_2 fugacity for mixtures: H_2/CO_2 at 4 and 6 bar, CO_2/N_2 and $H_2/CO_2/N_2$ at 4 bar total feed pressure and 30 ^oC. Data points represent experimental values and lines are modeling results.

2.4.3. Mixed gas selectivity

As a result of the lower H_2 permeability in mixtures with CO_2, the real selectivity for the H_2/CO_2 gas pair, calculated from the permeability data obtained in mixed gas experiments, results in an average value of 2.93 (Figure II - 18). The latter value is significantly lower than the selectivity calculated from pure gas permeability data, which resulted in an average value of 4.2. In Figure II – 18 the ideal selectivity is calculated from gas permeability values obtained with pure H_2 and respectively CO_2 at 2, 4 and 6 bar total feed pressure; meanwhile the mixed gas selectivity is calculated from feed and permeate gas concentration values according to Equation I – 9 (Chapter I).

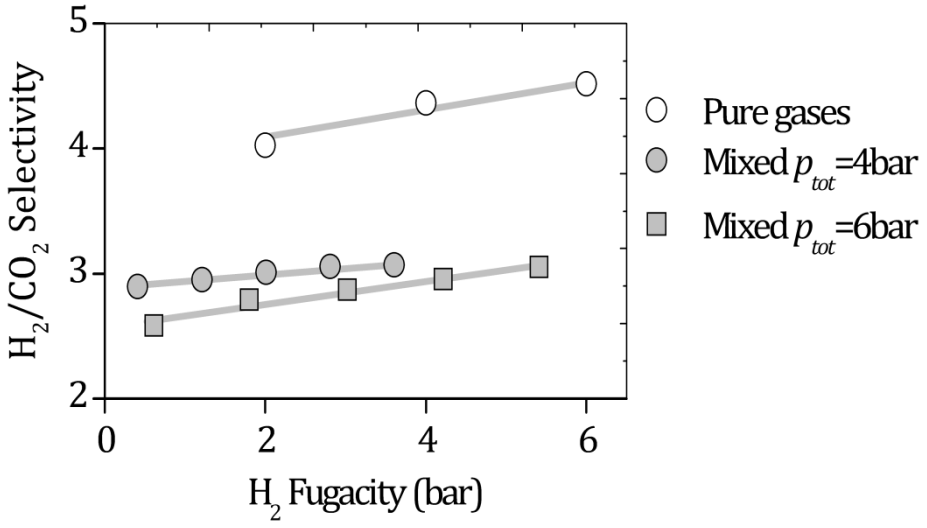

Figure II – 18. H_2/CO_2 selectivity variation with H_2 fugacity in the feed for pure and mixed (H_2/CO_2) feed gas

Similarly depression in H_2 permeability in mixtures with CO_2 was reported in surface modified 6FDA-durene polyimide membranes where the H_2/CO_2 selectivity decreased from an ideal value of 101 to a value of 42 [32]. The same phenomenon occurs in the reverse selective membranes that exhibit favorable interactions with CO_2 and permeate preferentially CO_2 to H_2. These membranes exhibit a CO_2/H_2 selectivity higher than 1. One example is the work of Chen et al. [33] that reveals a drastic increase in CO_2/H_2 selectivity in mixed gas test compared to the selectivity obtained from pure gas permeability coefficients for membranes made of copolymers between poly(ethylene oxide) and a polyimide.

2.4.4. Mathematical modelling

The adequacy of the dual sorption-partial immobilization model for the prediction of H_2 and CO_2 permeation through Matrimid® 5218 membrane was tested. Experimental permeability data, corresponding to pure, binary, ternary and quaternary mixtures, were fitted to Equation II - 13 by a non-linear multiparametric regression procedure using the Aspen Custom Modeler (AspenTech) software tool. Pure gas dual-mode solubility parameters were taken from the literature [34, 35], for CO_2 and N_2 and are listed in Table II – 6. Up to our knowledge there are no published data of dual-sorption model parameters for H_2 and CO in Matrimid polymer, although some authors have studied the sorption of H_2 in other glassy polymers [27, 36].

Table II – 6. Available literature data for the dual – sorption model parameters for N_2 and CO_2 in Matrimid dense films [34]

Model parameter	Gas	
	N_2	CO_2
b (1/bar)	0.086	0.39
k_D (cm^3(STP) cm^{-3} bar^{-1})	0.119	1.44
C'_H(cm^3(STP) cm^{-3})	3.94	25.5
$K=C'_H \cdot b/k_D$	2.86	6.5

To facilitate calculation, a new set of parameters was defined as follows,

$$A_1 = k_D D_D \qquad \text{(II - 17)}$$

$$A_2 = k_D FKD_D = D_H c'_H b \qquad \text{(II - 18)}$$

By substitution of Equations (II - 17) and (II - 18) into Equation (II - 13), two new equations are obtained as follows:

$$P_{H2} = A_{1H2} + \frac{A_{2H2}}{1 + b_{H2} f_{H2} + b_{N2} f_{CO2} + b_{CO2} f_{CO2} + b_{CO} f_{CO}} \qquad \text{(II - 19)}$$

$$P_{CO2} = A_{1CO2} + \frac{A_{2CO2}}{1 + b_{H2} f_{H2} + b_{N2} f_{CO2} + b_{CO2} f_{CO2} + b_{CO} f_{CO}} \qquad \text{(II - 20)}$$

The resulting model is composed of two equations with six independent parameters: A_{1H2}, A_{1CO2}, A_{2H2}, A_{2CO2}, b_{H2}, b_{CO}. The regression solution was unique due to the vast domain of experimental data used. The estimated values of the parameters are given in Table II - 7.

As expected, the CO2 Langmuir's population moving fraction F = 0.07 was lower than 1 [37]. In the case of H2 permeation, due to the lack of sorption parameters in Matrimid polymer, the results obtained are expressed as a function of the grouped parameters A_1 and A_2 and the affinity parameter b. The estimated value of the latter, b_{H2} = 0.05 bar^{-1}, is close to the one reported by El-Azzami and Grulke [27] of 0.09 bar^{-1} in a natural glassy polymer, Chitosan, at 20 ^oC. On the other hand, the value of the Langmuir solubility parameter for carbon monoxide obtained by fitting the experimental results is b_{CO} = 0.05 bar^{-1}.

Table II – 7. Dual-mode sorption, partial immobilization model estimated parameters for H_2 and CO_2 permeation in Matrimid 5218 membrane

Model parameter	Gas	
	H_2	CO_2
$A_1 = k_D D_D$ (Barrer)	7.23	4.20
$A_2 = k_D FKD_D = D_H c'_H b$ (Barrer)	19.51	3.22
b (1/bar)	0.05	known value
D_D (cm²/s)	-	$1.62 \cdot 10^{-8}$
D_H (cm²/s)	-	$2.45 \cdot 10^{-9}$
K	-	11.6
F	-	0.07

Figure II - 19 shows the parity graph of the experimental and simulated permeability coefficients of H_2 and CO_2. There is a satisfactory agreement between predicted results and experimental data with correlation coefficient (R) higher than 0.95 and mean squared relative error (MSRE) lower than 0.01.

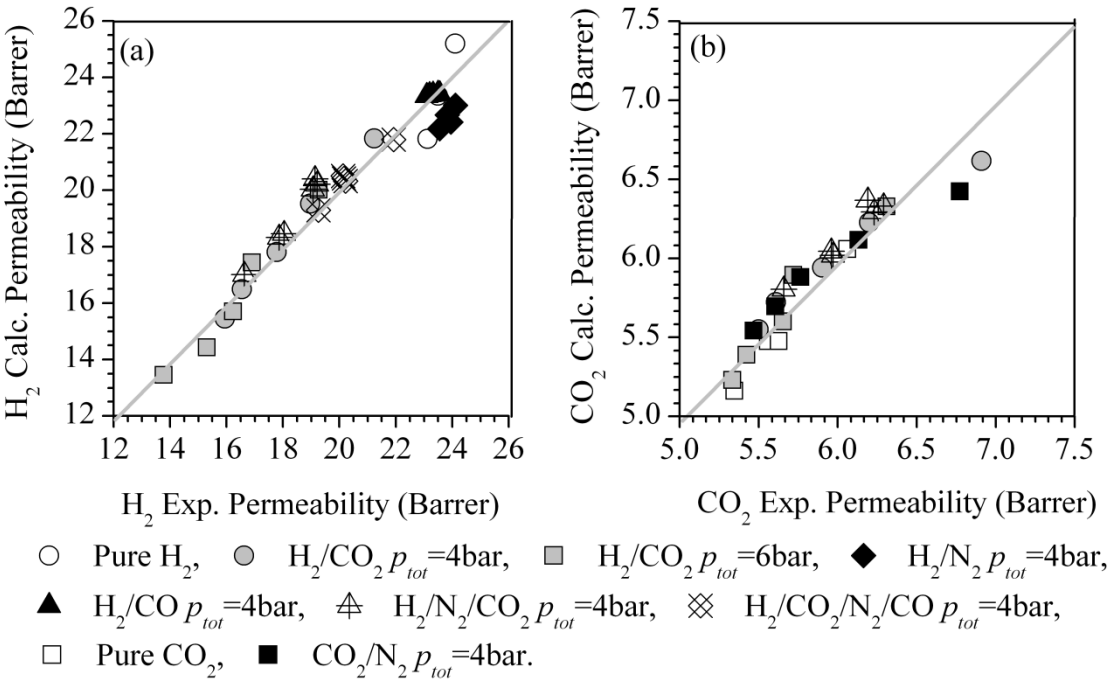

Figure II – 19. Parity graphs of the predicted H_2 (a) and CO_2 (b) gas permeability data by the dual sorption-partial immobilization model with the experimental results

2.5. CONCLUSIONS

The mixed gas permeation through a Matrimid homogeneous thick film has been investigated over the full range of concentrations for the separation of H_2 from N_2, CO and CO_2. Also, the influence of temperature and pressure on gas permeation was examined.

For pure gases, the permeability coefficients decreased in the following order of average values (Barrer): P_{H2} = 23.6 > P_{CO2} = 5.7 > P_{CO} = 0.43 > P_{N2} = 0.17, which is also the order of increasing kinetic diameters of the gas molecules.

As temperature increased all four gas permeabilities increased. The ideal selectivity α_{H_2/CO_2} increases with temperature, while the selectivity α_{H_2/N_2} and $\alpha_{H_2/CO}$ decreases with temperature. The same behavior with temperature was observed for a quaternary gas mixture.

For the highly permeable H_2 gas the concentration polarization phenomenon was put in evidence for H_2/N_2 mixtures at feed concentrations lower than 10 vol % H_2. In pure gas, at a feed pressure of 6 bar and a temperature of 30 ^oC, the hydrogen permeability was 23.1 Barrer, and the ideal H_2/CO_2 selectivity was 4.4.

In mixed gas experiments, for binary 10/90 (vol %) H_2/CO_2 mixtures, competitive sorption between H_2 and CO_2 led to significant decays both in H_2 permeability, which was reduced to 13.8·Barrer and in the selectivity α_{H_2/CO_2} that decreased to 2.7. For CO_2, transport rate was unaffected by the presence of hydrogen, nitrogen and carbon monoxide.

H_2 and CO_2 permeation behavior from pure, binary, ternary and quaternary mixtures ($H_2/N_2/CO/CO_2$) through planar Matrimid membrane was satisfactorily described by the "dual-mode sorption, partial immobilization" model. The model sorption parameters for H_2 and for CO were unknown and obtained from the fitting of the experimental data to the proposed model.

These results provide useful knowledge related to the intrinsic material properties, considering gas mixtures of industrial interest and essential when other membrane configurations like hollow fibers, mixed matrix membranes or polymer blends are proposed.

References

1. S. Matteucci, Y. Yampolskii, B.D. Freeman, I. Pinnau, Transport of Gases and Vapors in Glassy and Rubbery Polymers, in: Materials Science of Membranes for Gas and Vapor Separation, John Wiley & Sons, Ltd, New York, 2006, pp. 1-47.

2. R.M. Barrer, J.A. Barrie, J. Slater, Sorption and diffusion in ethyl cellulose. Part III. Comparison between ethyl cellulose and rubber, J. Polym. Sci. 27 (1958) 177.

3. A.S. Michaels, W.R. Vieth, J.A. Barrie, Solution of gases in polyethylene terephthalate, J. Appl. Phys. 34 (1963) 1-12.

4. K. Toi, G. Morel, D.R. Paul, Gas sorption and transport in poly(phenylene oxide) and comparisions with other glassy polymers., J. Appl. Polym. Sci. 27 (1982) 2997-3005.

5. W.J. Koros, A.H. Chan, D.R. Paul, Sorption and transport of various gases in polycarbonate, J. Membr. Sci. 2 (1977) 165-190.

6. R.W. Baker, Membrane Technology and Applications, 2nd edition ed., John Wiley and Sons, New York, 2004.

7. J.D. Wind, Improving polyimide membrane resistance to carbon dioxide plasticization in natural gas separations, Ph.D. dissertation, The University of Texas at Austin (2002).

8. W.J. Koros, D.R. Paul, A.A. Rocha, Carbon dioxide sorption and transport in polycarbonate, J. Polym. Sci. , Polym. Phys. 14 (1976) 687-702.

9. E.S. Sanders, W.J. Koros, H.B. Hopfenberg, V.T. Stannett, Pure and mixed gas sorption of carbon dioxide and ethylene in poly(methyl methacrylate), J. Membr. Sci. 18 (1984) 53-74.

10. T. Oishi, J.M. Prausnitz, Estimation of solvent activities in polymer solutions using a group-contribution method, Ind. Eng. Chem. , Process Des. Dev. 17 (1978) 333-339.

11. R.M. Conforti, T.A. Barbari, P. Vimalchand, M.D. Donohue, A lattice-based activity coefficient model for gas sorption in glassy polymers, Macromolecules 24 (1991) 3388-3394.

12. R.G. Wissinger, M.E. Paulaitis, Molecular thermodynamic model for sorption and swelling in glassy polymer-CO2 systems at elevated pressures, Ind. Eng. Chem. Res. 30 (1991) 842-851.

13. M. Minelli, S. Campagnoli, M.G. De Angelis, F. Doghieri, G.C. Sarti, Predictive model for the solubility of fluid mixtures in glassy polymers, Macromolecules 44 (2011) 4852-4862.

14. M.C. Ferrari, M. Galizia, M.G. De Angelis, G.S. Sarti, Vapor Sorption and Diffusion in Mixed Matrices Based on Teflon AF 2400, in: Y. Yampolskii, B. Freeman (Eds.), Membrane Gas Separation, Wiley, Chichester, 2010, pp. 125.

15. F. Doghieri, G.C. Sarti, Predicting the low pressure solubility of gases and vapors in glassy polymers by the NELF model, J. Membr. Sci. 147 (1998) 73-86.

16. R.H. Lacombe, I.C. Sanchez, Statistical thermodynamics of fluid mixtures, J. Phys. Chem. 80 (1976) 2568-2580.

17. I.C. Sanchez, R.H. Lacombe, Statistical thermodynamics of polymer solutions, Macromolecules 11 (1978) 1145-1156.

18. I.C. Sanchez, R.H. Lacombe, An elementary molecular theory of classical fluids. Pure fluids, J. Phys. Chem. 80 (1976) 2352-2362.

19. I.C. Sanchez, R.H. Lacombe, Elementary equation of state for polymer liquids., J. Polym. Sci. Part B Polym. Lett. 15 (1977) 71-75.

20. U. S. Enviromental protection agency, Hazard Summary -1,1,2,2-Tetrachloroetane, http://www.epa.gov/ttn/atw/hlthef/tetrachl.html (2007).

21. M. Koretsky, Engineering and Chemical Thermodynamics, John Wiley & Sons, New Jersey, 2003.

22. Y. Zhang, I.H. Musselman, J.P. Ferraris, K.J. Balkus Jr., Gas permeability properties of Matrimid® membranes containing the metal-organic framework Cu-BPY-HFS, J. Membr. Sci. 313 (2008) 170-181.

23. S.S. Hosseini, M.M. Teoh, T.-S. Chung, Hydrogen separation and purification in membranes of miscible polymer blends with interpenetration networks, Polymer 49 (2008) 1594-1603.

24. H.-W. Rösler, Membrantechnolgie in der Prozessindustrie - Polymere Membranwerkstoffe, Chem. Ing. Tech. 77 (2005) 485-503.

25. H.-Y. Zhao, Y.-M. Cao, X.-L. Ding, M.-Q. Zhou, Q. Yuan, Effects of cross-linkers with different molecular weights in cross-linked Matrimid 5218 and test temperature on gas transport properties, J. Membr. Sci. 323 (2008) 176-184.

26. S. Shishatskiy, C. Nistor, M. Popa, S.P. Nunes, K.V. Peinemann, Polyimide asymmetric membranes for hydrogen separation: Influence of formation conditions on gas transport properties, Adv. Eng. Mater. 8 (2006) 390-397.

27. L.A. El-Azzami, E.A. Grulke, Dual mode model for mixed gas permeation of CO2, H2, and N2 through a dry chitosan membrane, J. Polym. Sci. Part B 45 (2007) 2620-2631.

28. K. Tanaka, H. Kita, K. Okamoto, A. Nakamura, Y. Kusuki, Gas permeability and permselectivity in polyimides based on 3,3',4,4'-biphenyltetracarboxylic dianhydride, J. Membr. Sci. 47 (1989) 203-215.

29. J. Marchese, E. Garis, M. Anson, N.A. Ochoa, C. Pagliero, Gas sorption, permeation and separation of ABS copolymer membrane, J. Membr. Sci. 221 (2003) 185-197.

30. K. Simons, K. Nijmeijer, J.G. Sala, H. van der Werf, N.E. Benes, T.J. Dingemans, M. Wessling, CO2 sorption and transport behavior of ODPA-based polyetherimide polymer films, Polymer 51 (2010) 3907-3917.

31. A. Bos, I.G.M. Pünt, M. Wessling, H. Strathmann, CO2-induced plasticization phenomena in glassy polymers, J. Membr. Sci. 155 (1999) 67-78.

32. T.-S. Chung, L. Shao, P.S. Tin, Surface modification of polyimide membranes by diamines for H2 and CO2 separation, Macromol. Rapid Comm. 27 (2006) 998-1003.

33. H. Chen, Y. Xiao, T.-S. Chung, Synthesis and characterization of poly (ethylene oxide) containing copolyimides for hydrogen purification, Polymer 51 (2010) 4077-4086.

34. T.T. Moore, W.J. Koros, Gas sorption in polymers, molecular sieves, and mixed matrix membranes, J. Appl. Polym. Sci. 104 (2007) 4053-4059.

35. C.A. Scholes, W.X. Tao, G.W. Stevens, S.E. Kentish, Sorption of methane, nitrogen, carbon dioxide, and water in matrimid 5218, J. Appl. Polym. Sci. 117 (2010) 2284-2289.

36. S. Zhou, S.A. Stern, The solubility of hydrogen in glassy poly(vinyl acetate) at elevated pressures, J. Membr. Sci. 50 (1990) 19-29.

37. C.L. Aitken, W.J. Koros, D.R. Paul, Gas transport properties of biphenol polysulfones, Macromolecules 25 (1992) 3651-3658.

Chapter III

HYDROGEN MIXED GAS SEPARATION STUDY USING ASYMETRIC HOLLOW FIBER MEMBRANES

ABSTRACT

The characterization of mixed gas permeation through hollow fiber membranes is essential for the industrial application of gas separation technology.

In chapter II specific phenomena that occur in the permeation of H_2-containing gas mixtures through planar dense Matrimid membranes and determine a different transport behavior with respect to pure gas were reported. Phenomena like concentration polarization and competitive transport were thoroughly studied and modeled. In this chapter the same application is assessed using asymmetric hollow fibers membranes because large-scale gas separation applications demand highly productive membranes with high membrane surface/volume ratios and membranes with hollow fiber geometry have a distinct advantage over flat sheet membranes as they possess a much thinner dense skin layer and thus they are much more productive.

This chapter is focused on the characterization of H_2-containing gas mixtures permeation through asymmetric hollow fiber membranes using binary (H_2/N_2, H_2/CO, H_2/CO_2) and quaternary ($H_2/N_2/CO/CO_2$) gas mixtures at a constant temperature of 30 ^oC and pressures up to 10 bar. Also, the effect of temperature over mixed gas permeation was studied using a $H_2/N_2/CO/CO_2$ quaternary mixture similar to the flue gases obtained in carbon black manufacturing.

First, in order to compare gas separation behavior of hollow fiber with dense films, asymmetric hollow fibers fabricated from the same polymeric material as the dense films (Matrimid), were used. Then, as means of further increasing gas selectivity towards H_2 and suppressing CO_2 plasticization new asymmetric hollow fiber membranes were fabricated from polymer blends of Matrimid and polybenzimidazole (PBI). Fibers with good morphology and without defects were obtained only from the pure Matrimid. Regrettably, polymer blending lead to fibers with poor mechanical properties. Also, the comparative permeation performance between Matrimid and a much more permeable material PPO was done using commercial PPO asymmetric hollow fibers modules obtained from Parker Filtration and Separation B.V.

Using a Matrimid based hollow fiber membrane, the ideal selectivity values obtained for H_2/N_2, H_2/CO and H_2/CO_2 gas pairs were of 74.4, 42.6 and 5 respectively with a H_2 permeance of 67 GPU at 2.3 bar feed pressure. For mixtures that contain H_2 and CO_2 the performance was better than that of dense films since a lower depression in the permeability of H_2 was observed. Phenomena related to the complex morphology of the asymmetric hollow fibers like substructure resistance, induced accelerated plasticization with CO_2 and competitive sorption effects between H_2/CO_2 are presented. Therefore, it is clear that use of thick film data to design or select

membrane materials only gives a rough approximation of the performance that might be realized in practice.

In contrast with Matrimid hollow fiber membranes the use PPO hollow fiber membranes gives considerably higher gas permeability with a value of 2152 GPU for pure H_2 at the expense of lower gas selectivities with values for H_2/N_2, H_2/CO and H_2/CO_2 gas pairs of 30, 22 and 3 respectively. Thus the H_2 concentration in the permeate of a PPO hollow fiber module was of only 40 vol % meanwhile in the Matrimid hollow fiber module was more than double (87 - 89 vol %).

3.1. PREPARATION OF ASYMMERTIC HOLLOW FIBER MEMBRANES - BACKGROUND

The fabrication of hollow fibers membranes is based on a dry/wet spinning method when a phase inversion process takes place.

The concept of phase inversion covers a range of different techniques such as solvent evaporation, precipitation by controlled evaporation, thermal precipitation, precipitation from the vapor phase and immersion precipitation [1]. In all cases the starting point is a thermodynamically stable solution which is subject to demixing (phase separation). A membrane is made by casting a polymer solution on a support and then bringing the solution to phase separation by means of solvent outflow and/or nonsolvent inflow [2, 3]. This can be done by temperature changes or changes in composition.

The phase separation process by immersion precipitation allows the formation of defect-free, high-flux membranes [1, 4] that have an asymmetric structure with a thin, selective skin on a much thicker but highly porous supporting layer. The thin selective layer is formed during the short “healing” period or “dry” step (i.e., free standing evaporation) prior to the immersion in the non-solvent bath where phase separation occurs to the rest of the membrane. These membranes developed within the Loeb-Sourirajan process allowed the industrial breakthrough in 1960’s of synthetic membrane processes such as reverse osmosis and ultrafiltration and in 1979 the breakthrough of gas separation process for hydrogen recovery.

The phase diagram of a typical membrane forming system by the dry/wet phase inversion technique is schematically shown in Figure III – 1 [5]. The system has three components: a polymer, a solvent and a nonsolvent, which is miscible with the solvent but not with the polymer. The corners of the triangle represent pure components, the sides represent binary mixtures of the two components connected and the interior of the triangle represents a ternary mixture of the three components. The binodal boundary divides the phase diagram into a single-phase region, where the three components are miscible in all compositions, and a two-phase region, where

the system separates into two phases. The tie lines connect points on the binodal that are in equilibrium. A composition within this two-phase region always lies on a tie line and it splits into two phases represented by the two intersections between the tie lines and the binodal. Thus one end point of the tie line is rich in polymer and the other end point is poor in polymer. At the end of phase separation, the polymer-rich phase forms the membrane matrix, whereas the polymer-lean phase forms the membrane pores. The spinodal boundary further divides the two-phase region into a metastable region and an unstable region. Within the metastable region the phase separation proceeds via a nucleation and growth of one of the phases and results in cellular structures. Within the unstable region the phase transition is characterized by a fast and uniform separation of the two phases that leads to interconnected, bicontinuous structures.

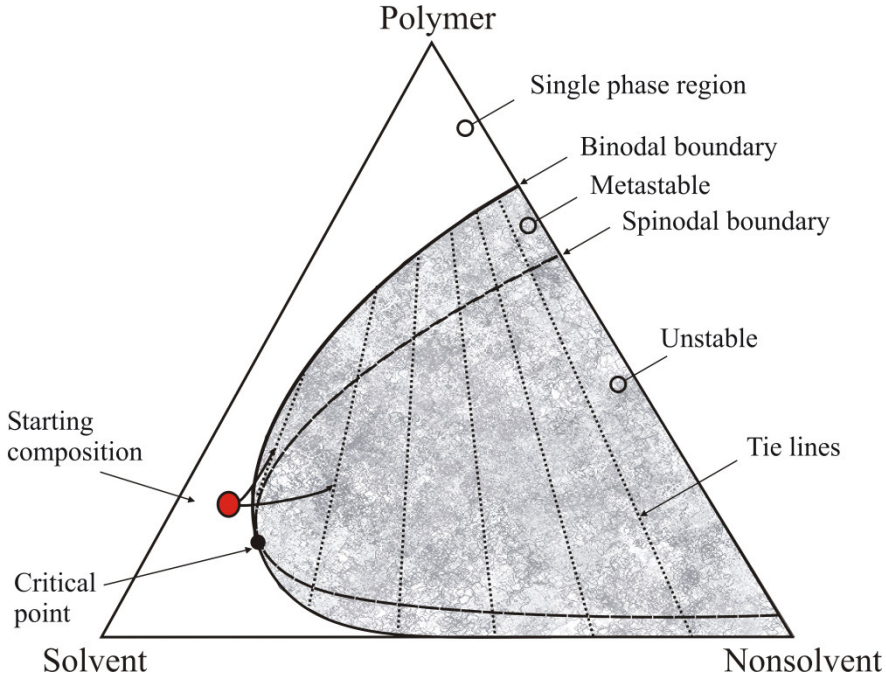

Figure III – 1. Scheme of the three component phase diagram indicating a starting solution formed of three components: polymer, solvent and nonsolvent [3].

Application of such a dry/wet process in hollow fiber geometry is more complicated than with simple flat sheets. All mass transfer associated with the “dry” step in fiber spinning must occur during the nascent fiber’s residence time in the air gap (see Experimental methodology section), which is extremely shorter than with flat sheets. Therefore the formation conditions must be set to values that allow a rapid formation of a defect free outer skin layer during the nascent fiber’s residence time in the air gap:

(I) First it must be decided if a non – solvent will be used within the dope solution. The use of a non-solvent approaches the dope solution composition closer to the binodal boundary allowing a rapid phase separation (see Figure III – 1). EtOH is usually chosen as non-solvent instead of water because water is such a strong non-solvent that practical titration of the spin dope close to the binodal becomes difficult.

(II) Then, the dope formulation is based on experimentally estimations of the binodals for the multi-component (solvent, non-solvent, and polymer) system on the basis of cloud point measurements. Figure III – 2 shows literature binodal results for the ternary NMP, EtOH, Matrimid system.

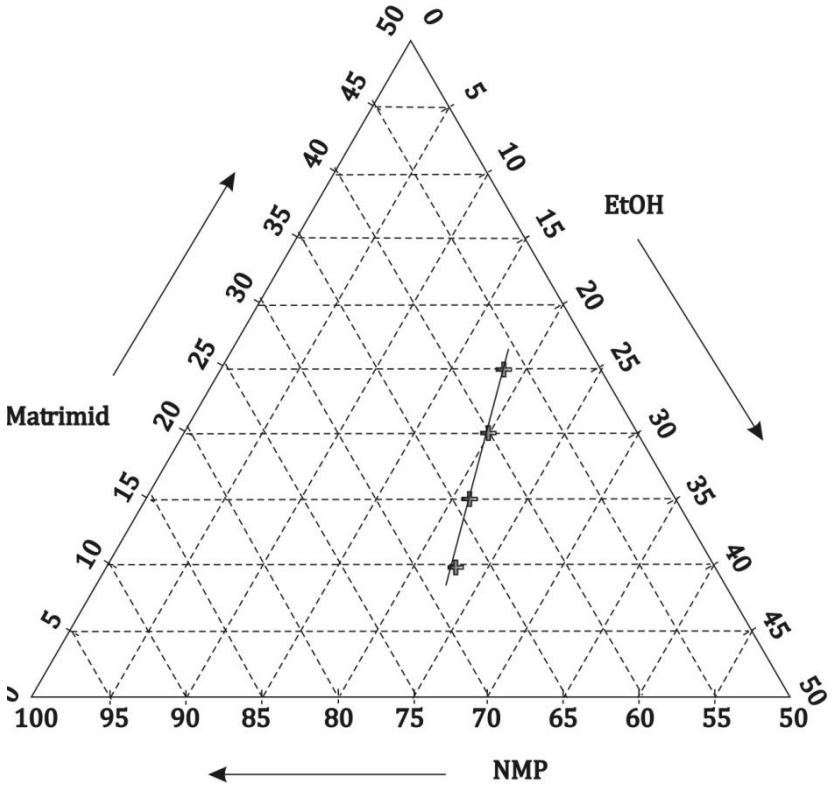

Figure III – 2. Binodals for the ternary NMP, EtOH and Matrimid system at 23°C [6]

(III) In order to obtain a good morphology of the functional layer, from the various possible formulations found close to the binodal line, the optimum corresponds to polymer concentrations a few lower than the "critical polymer concentration" (c. p. c.). C. p. c. is defined as the polymer concentration point from where the dope solution viscosity increases exponentially with the polymer concentration and it is calculated from the intersection of the tangent lines to the two domains of the viscosity trend curve as shown in Figure III – 3 where real literature data for various polymer/solvent systems of interest in this work are reported.

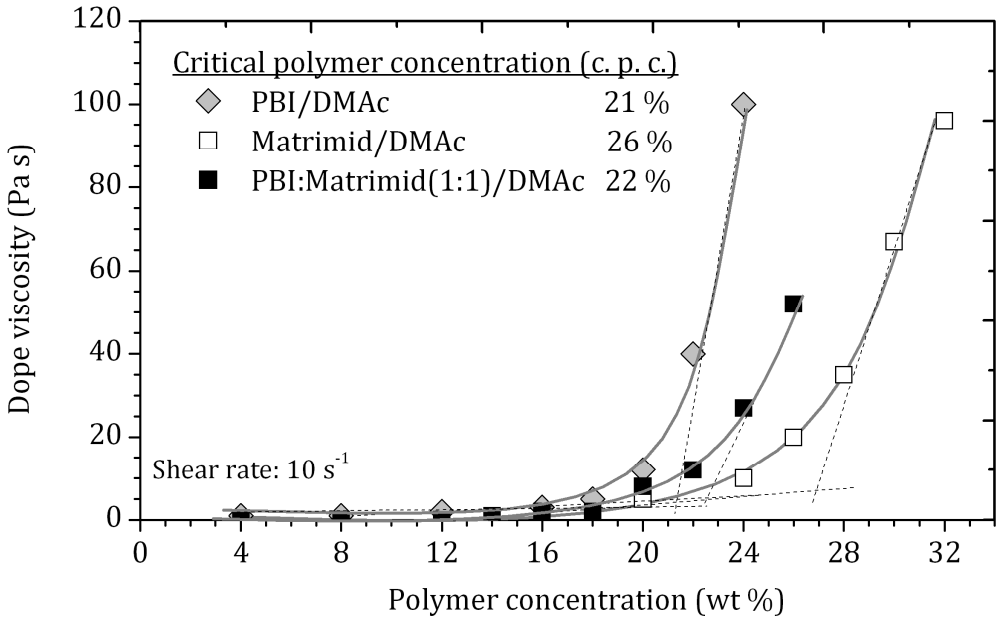

Figure III – 3. The trend of changes in dope viscosity as a function of polymer concentration in the solvent [7].

(IV) A higher temperature of the dope than the air gap temperature allows a rapid evaporation of the solvent when the dope solution enters the air gap. As the nascent fiber cools down the viscosity increases giving a mechanically stable nascent fiber. The viscosity variation with temperature of all dope solutions used in this work (see Experimental and methodology section) is shown in Figure III – 4.

(V) In order to obtain a defect-free top layer, a volatile solvent can be added in small concentration to the dope solution.

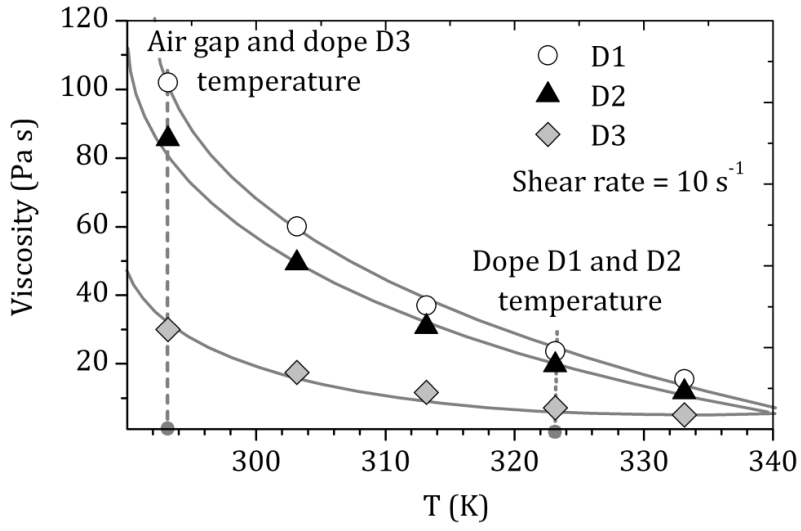

Figure III – 4. Dope solution viscosity variation with temperature

3.2. EXPERIMENTAL METHODODOLOGY

3.2.1. Materials

The commercial polymer Matrimid 9725 (polyimide of 3,3´, 4,4´-benzophenone tetracarboxylic dianhydride and diamino-phenylidane) was kindly provided by Huntsman Advanced Polymers. Matrimid 9725 is a micropulverized version of Matrimid 5218. Polybenzimidazole (PBI) polymer was obtained from PBI Performance Products, Inc. The 1-methyl-2-pirrolidone (NMP) solvent and ethanol (EtOH) as non-solvent (absolute grade, 99.9% purity) were used as received for the preparation of the polymer solutions. Solvent exchange fluids included EtOH (technical grade, 96-98% purity), hexane and tap water. LiCl salt was used for the stability (in order to avoid gelation) of the dope formed by polymer blending of Matrimid with PBI. Gases were purchased from Air Liquide (Spain) with a purity of at least 99.95 %. PPO hollow fibers modules were provided by Parker Filtration and Separation B. V.

3.2.2. Fabrication of asymmetric hollow fiber membranes by the dry/wet spinning process

The operation conditions applied for the fabrication of the asymmetric hollow fiber membranes are listed in Table III – 1. The pure Matrimid based hollow fibers were labeled D1 and three different fibers were obtained (D1-M1, D1-M2, D1-M3) by varying the gap height. The two Matrimid - PBI polymer blend based fibers were labeled D2 and D3.

For the pure Matrimid hollow fibers the operation conditions are based on optimized procedures reported in the literature [6, 8-10].

In the case of the formulation of Matrimid/PBI dopes (D2 and D3), NMP was preferred as solvent instead DMAc that was used in literature [7] because is a less hazardous solvent. Therefore, the critical polymer concentration had to be determined for the dope D2 that is based on two components: polymer blend and solvent. The viscosity of polymer solution samples of increasing concentration was measured with a Haake Viscotester 550 (see Figure III - 4). The resulting c. p. c. value of 26.4 wt% is somewhat higher than the reported value of 22% in DMAc (see Figure III - 3).

Also, a new and optimized formulation for the Matrimid – PBI dope - D3 was proposed by using a non solvent (EtOH) as additional component. In order to determine the formulation of the dope - D3, EtOH was added in 3 cm^3 quantities to a

30 wt % binary mixture (polymer blend and NMP) until demixing occurred at 23.5 wt % polymer and 21.7 wt % EtOH. The optimum formulation of the dope D3 is close to the demixing concentration but a much higher polymer concentration was preferred due to a higher necessary viscosity for spinning. As shown in Figure III – 5 at 50 ^{o}C the viscosity if the dope D3 is still much lower than the viscosities of the dopes D1 and D2 and therefore a lower temperature of 25 ^{o}C were preferred for spinning. Regrettably, the experimentally determination of the binodal for the multi-component system (polymer blend, NMP, EtOH) was not carried out.

Table III – 1. Formation Conditions for the asymmetric hollow fiber membranes

Dope composition (wt %)		D1	D2	D3
Matrimid:PBI		(1:0) 26.2	(1:1) 26.4	(1:1) 27.6
NMP		58.9	72.2	62.3
EtOH		14.9	0	8.3
Additives (LiCl)		0	1.4	1.4
Bore composition (wt %)				
NMP		96	80	80
H_2O		4	20	20
Spinning conditions				
Tube in orifice spinneret (mm)	OD	0.5	0.5	0.5
	ID	0.2	0.2	0.2
Dope temperature (^{o}C)		50	50	25
Dope flow rate ($cm^3\ h^{-1}$)		122.4	114	504
Bore flow rate ($cm^3\ h^{-1}$)		360	360	180
Air gap height (cm)	D1 - M1	12	10	4
	D1 - M2	6		
	D1 - M3	3		
Room temperature (^{o}C)		22	21.3	21.8
Room humidity %		32	34	33
Quench Temperature – water (^{o}C)		20	20	20
Take-up rate (m min^{-1})		13.4	8.4	9
Sequential dehydration procedure				
(1) Water baths		continuous flow 24 h		
(2) MeOH baths		3 (20 min each)		
(3) Hexane baths		3 (20 min each)		
(4) Ambient dry				

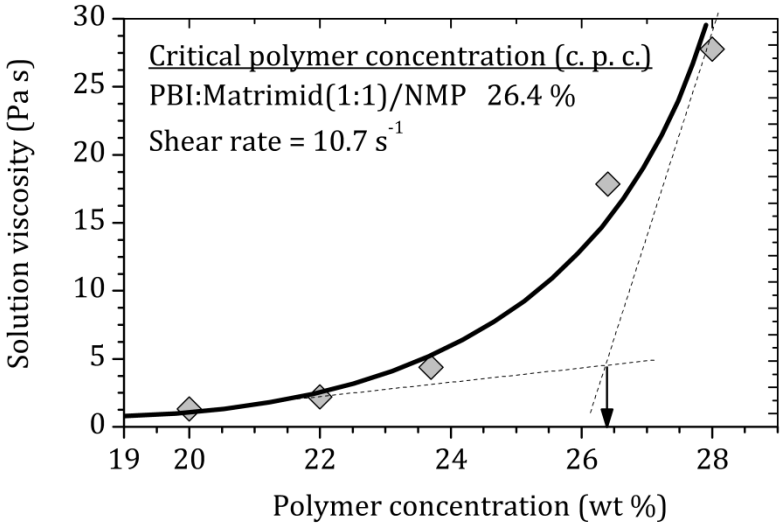

Figure III – 5. The trend of changes in solution viscosity as a function of polymer concentration in the solvent.

For the fabrication of all fibers a similar procedure was applied using a spinning equipment located at the Membrane Technology Group, University of Twente (see Figure III – 6 and Figure III - 7). The polymer powder was dried in a vacuum oven at 100°C for at least 12 h prior to use. The dope solution was prepared at 50°C in a Pyrex® vessel with mechanical stirring (Heidolph RZR 2041) and a coiled condenser to prevent ethanol loss. After mixing for at least 8 hours the dope solution was filtered with a 15 μm sintered metallic filter (Bekipor STAL3 Bekaert) and poured in a sealed spinning dope tank where it was left to degas at the specified dope temperature for 24 h before spinning. The bore solution and the water quench bath were also left to degas 24 h before spinning. Polymer solution and bore fluid were simultaneously pumped through a tube-in-orifice spinneret using gear pumps. Figure III – 8 shows the spinneret assembly with several detailed views from the upper and lower part and a vertical cross – section with dimensions. A triple - orifice spinneret was used as a dual – spinneret by closing the external channel.

The extruded fibers passed first through an air gap before entering in the coagulation bath filled with tap water at room temperature. The nascent fiber was oriented by a guiding wheel and pulled by a third and forth wheel, that had the same pulling speed, into a collecting wheel with the perimeter of 1 m from where they were cut and rinsed for 24 h in a water bath with continuous renewal of tap water. Next, the solvent exchange procedure using methanol and hexane listed in Table III – 1 and III - 2 was applied.

The solvent exchange process was found to play a critical role in the resulting membrane morphology and permeation performance [6]. After spinning, the porous

substructures of the hollow fiber membranes are filled with water. Drying such water – wet membranes can cause significant changes in porous structure due to the enormous capillary forces that are present during water removing. The solvent exchange procedure used in this work replaces water with more volatile fluids of lower surface tension before drying.

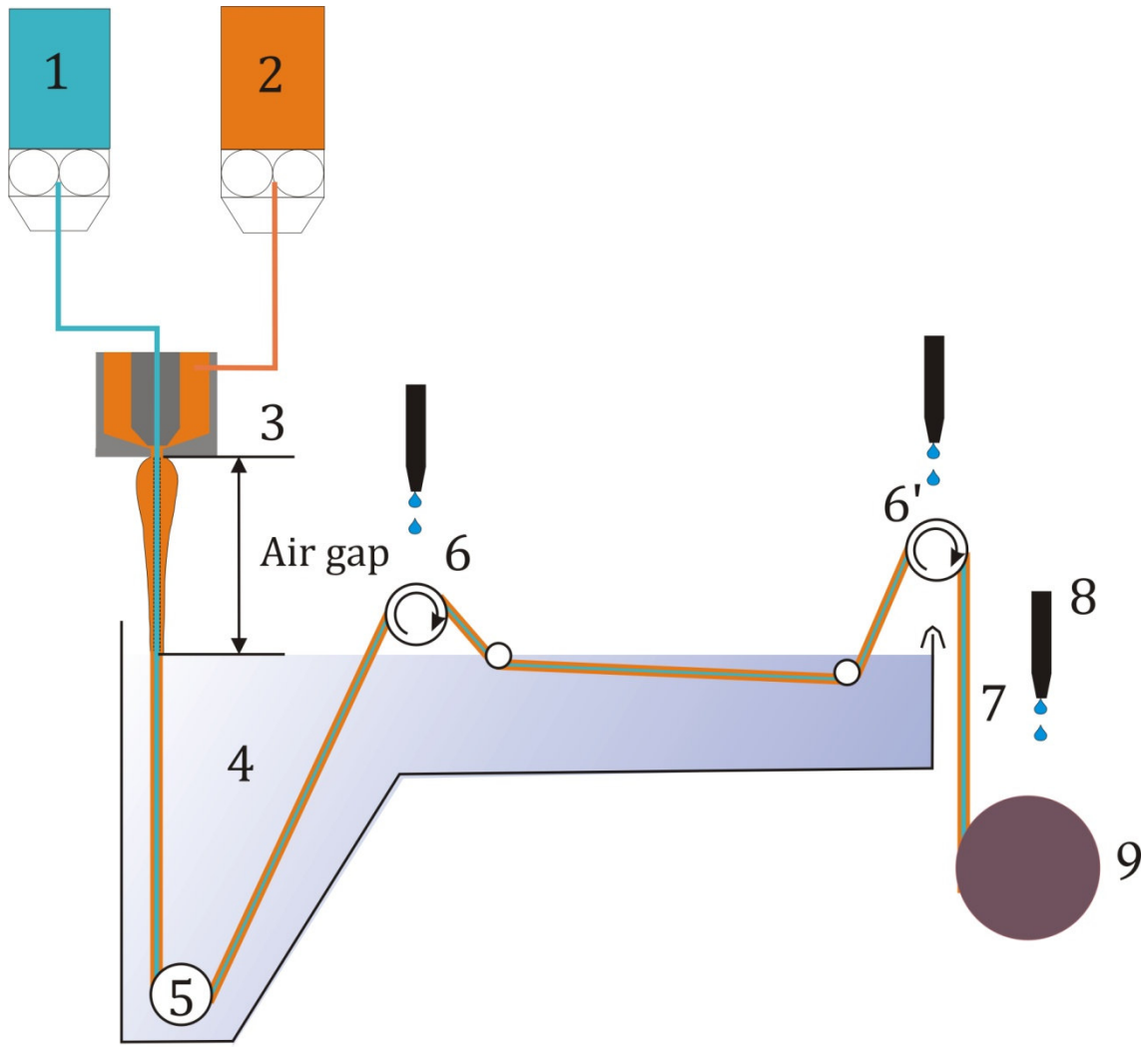

Figure III – 6. Hollow fiber spinning set – up: (1) spinning dope tank; (2) bore liquid vessel; (3) spinneret; (4) coagulation bath; (5) fiber guiding wheel; (6, 6') pulling wheels; (7) spinning line; (8) water spray; (9) fiber collecting wheel.

Figure III – 7. Image of the spinning line used for the fabrication of the asymmetric hollow fiber membranes (University of Twente).

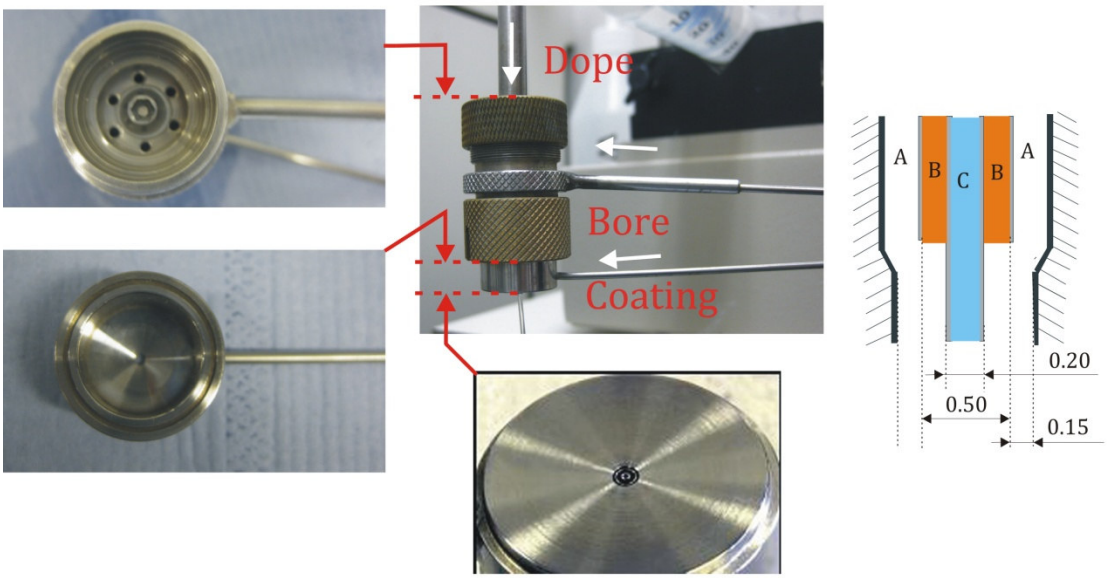

Figure III – 8. The triple - orifice spinneret used for the fabrication of the asymmetric hollow fiber membranes (A: outer channel – closed, B: dope channel, C: bore channel).

3.2.3. Permeation set-up

Membrane permeation properties were determined using an experimental set-up and procedure described in the Chapter II of this thesis. The planar membrane module was replaced with a hollow fiber membrane module. The Matrimid hollow fiber module was built by insertion of 1 fiber of ~10 cm length within a tubular stainless steel container in a counter-flow configuration as shown in Figure III – 9 and Figure III - 10. An epoxidic resin was used for sealing. The resulting membrane area was of 1.3 cm^2.

The PPO hollow fiber module was used as received and was composed of 5 fibers 15 cm length with an outer fiber diameter of 0.53 µm. The resulting membrane area was of 12.5 cm^2

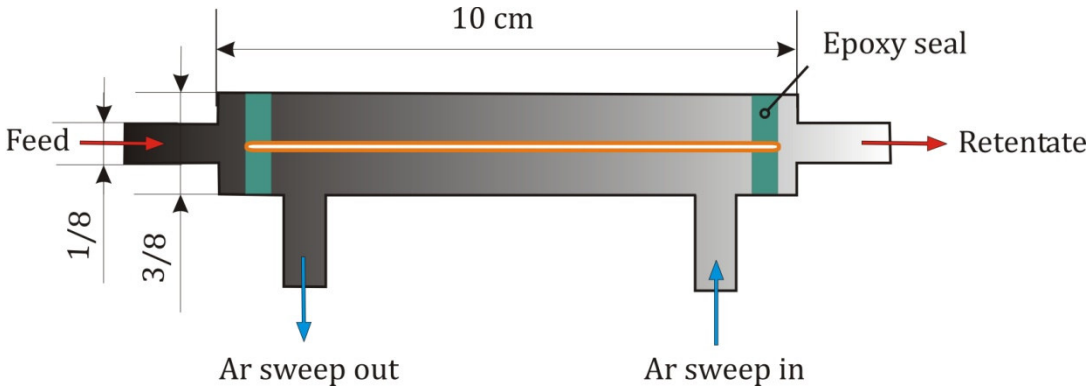

Figure III - 9. Hollow fiber module configuration

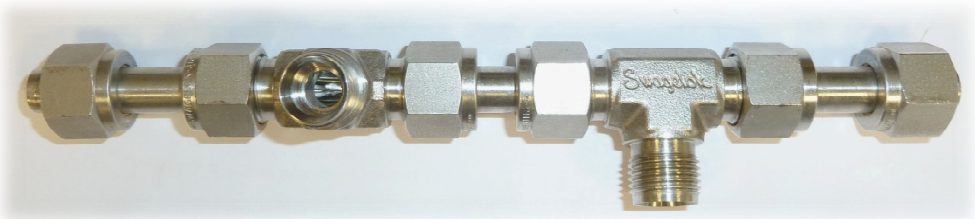

Figure III – 10. Hollow fiber module image

The Matrimid hollow fiber module was pressurized with the feed gas mixture at the bore side and an argon sweep gas was passed through the fiber shell to remove and transport the permeate to a gas chromatograph (Agilent Micro GC 3000). Details on the analytical method are given in the Appendix II of this thesis. The feed flow was in counter-current with the argon sweep gas flow. A sweep gas was used due to the very low permeate flow rate that is obtained when a hollow fiber module is built from only one fiber with low permeability. This configuration allowed the removal of side effects like concentration polarization and thus ideal hydrodynamic conditions were achieved.

In the case of the PPO hollow fiber module, because of the high gas permeability and a much higher membrane area, there was no need for the use of a sweep gas in the permate. Therefore, when we worked with pure gases the permeate and retentate gas streams were composed of pure gases and thus the gas chromatograph was not used. The permeance coefficient was calculated from known values of pressure and flow rate. When working with gas mixtures, the permate and retentate were analyzed with the recalibrated gas chromatograph with multiple gas mixtures of increasing gas concentration up to values of 90 vol %. The same analytical method was used.

The feed gas pressure was measured at both the inlet and outlet ports of the membrane module. At the inlet port of the membrane module a pressure gauge (Swagelok PGI-40M-BC9-LANX) was inserted and at the outlet port, the pressure was indicated by a back pressure regulator (Brooks 5866), which controls the pressure in the feed side of the membrane.

For the calculation of the gas permeability through the membrane the logarithmical mean between the pressures at the entrance and exit of the module (feed and retentate stream pressures) was used as total feed pressure at each phase.

3.2.4. Experimental procedure and operation conditions

Matrimid hollow fiber

In the gas separation experiments well aged fibers were used since the impact of physical aging over the permeation properties of Matrimid hollow fiber asymmetric membranes has been revealed to determine a decrease in the permeation of N_2 in time even after 250 days of storage prior to permeation experiments [9].

Before studying pure and mixed gas permeation, the occurrence of the concentration polarization phenomenon was studied in order to be avoided. This phenomenon was studied using the fibers labeled D1 - M3 by varying the feed flow

rate for pure H_2 and for binary mixtures H_2/N_2 = 50/50 (vol ratio) from 10 to 200 cm^3 (STP) min^{-1} at total pressures of 2, 4 and 6 bar and at a constant temperature of 30°C. Then, pure and mixed gas permeation studies were carried-out at feed pressures ranging from 2 to 10 bar with H_2, CO_2, CO and N_2 using the Matrimid® hollow fibers membranes D1 – M1, at a constant temperature of 30 °C.

Permeation experiments with mixed gases were performed with binary mixtures (H_2/CO_2, H_2/N_2 and H_2/CO) and with a quaternary mixture ($H_2/CO_2/N_2$/CO) at compositions listed in Table III - 2 using the Matrimid® hollow fiber membrane M1 and M3 developed as described in section 3.2.2.

Also, the influence of temperature over the permeance of mixed gases was analyzed for the quaternary H_2/CO_2/ N_2/CO mixture of 16.3/5.3/60.7/17.8 (vol %), temperatures ranging from 30 to 130 °C at a pressure of 4 bar using the hollow fiber D1 – M1.

Table III - 2. Mixed gas compositions used for gas permeation experiments

Gas mixture	Compositions (vol %)
H_2/CO_2	20/80, 40/60, 60/40, 80/20
H_2/N_2	20/80, 50/50, 80/20
H_2/CO	20/80, 50/50, 80/20
$H_2/CO_2/N_2$/CO	1616.3/5.3/60.7/17.8

PPO hollow fiber

Permeation experiments using PPO hollow fibers with pure gases were performed at pressure gradients within the range from 0.4 to 0.8 bar for H_2, 0.4 to 1.2 bar for CO_2 and 1 to 5 bar for CO and N_2 at a constant temperature of 30°C. When working at feed pressures higher than 1.8 bar for H_2 and 2.2 bar for CO_2, due to the high gas permeation flow of the 5 fiber module, the permeate flow rate was higher than the maximum capacity of the mass flow meter installed at the permeate side (10 cm^3 (STP) min^{-1}) and therefore we could not further measure the gas permeance.

Permeation experiments with mixed gases were performed with a quaternary mixture $H_2/CO_2/N_2$/CO = 16.3/5.3/60.7/17.8 vol % in the pressure gradient range from 1 to 4.9 bar at a constant temperature of 30 °C.

3.3. RESULTS AND DISCUSSION

3.3.1 Morphological and structural characterization

Pure Matrimid hollow fibers

The morphological and structural characteristics of the asymmetric hollow fibers were investigated using SEM analysis. Figure III – 11 shows SEM images of the three pure Matrimid hollow fibers fabricated in this work. The Matrimid hollow fiber membranes displayed satisfactory cross-sectional circularity and concentricity with constant wall thickness. The values of the outer and inner diameters of the fibers were evaluated from an average of at least 4 cross-sectional SEM images taken from samples cuts at different length of the same fiber (Table III - 3).

Table III - 3. Structural dimensions of Matrimid® asymmetric hollow fiber membranes

Membrane	OD (μm)	ID (μm)	Skin layer thickness, δ (nm)			
			H_2	CO_2	N_2	CO
D1 - M1	500±10	291±31	358	540	239	275
D1 - M2	427±4.5	249±1	not measured			
D1 - M3	381±13	143±13	143	160	17	46

The outer diameter of the fibers seems to increase as the air gap height decreases. The dimensions of the fiber D1 - M1 are practically equal to the dimensions of the spinneret. The effect of air gap height on the macroscopic dimensions of a hollow fiber is complex, the outer diameter can increase or decrease as the air gap height increases [11]. All hollow fiber have a typical asymmetric structure; a dense thin top layer at the outside supported by a spongy porous substructure with isolated finger like macrovoids found at the internal wall. The macrovoids are more predominant for fiber D1 - M1, less for fiber D1 - M2 and inexistent for fiber D1 - M3. The presence of macrovoids is not detrimental as it does not influence the separation performance but only decrease the mechanical resistance of the membrane. For industrial high-pressure gas separation processes however, macrovoids should not be present in support structure.

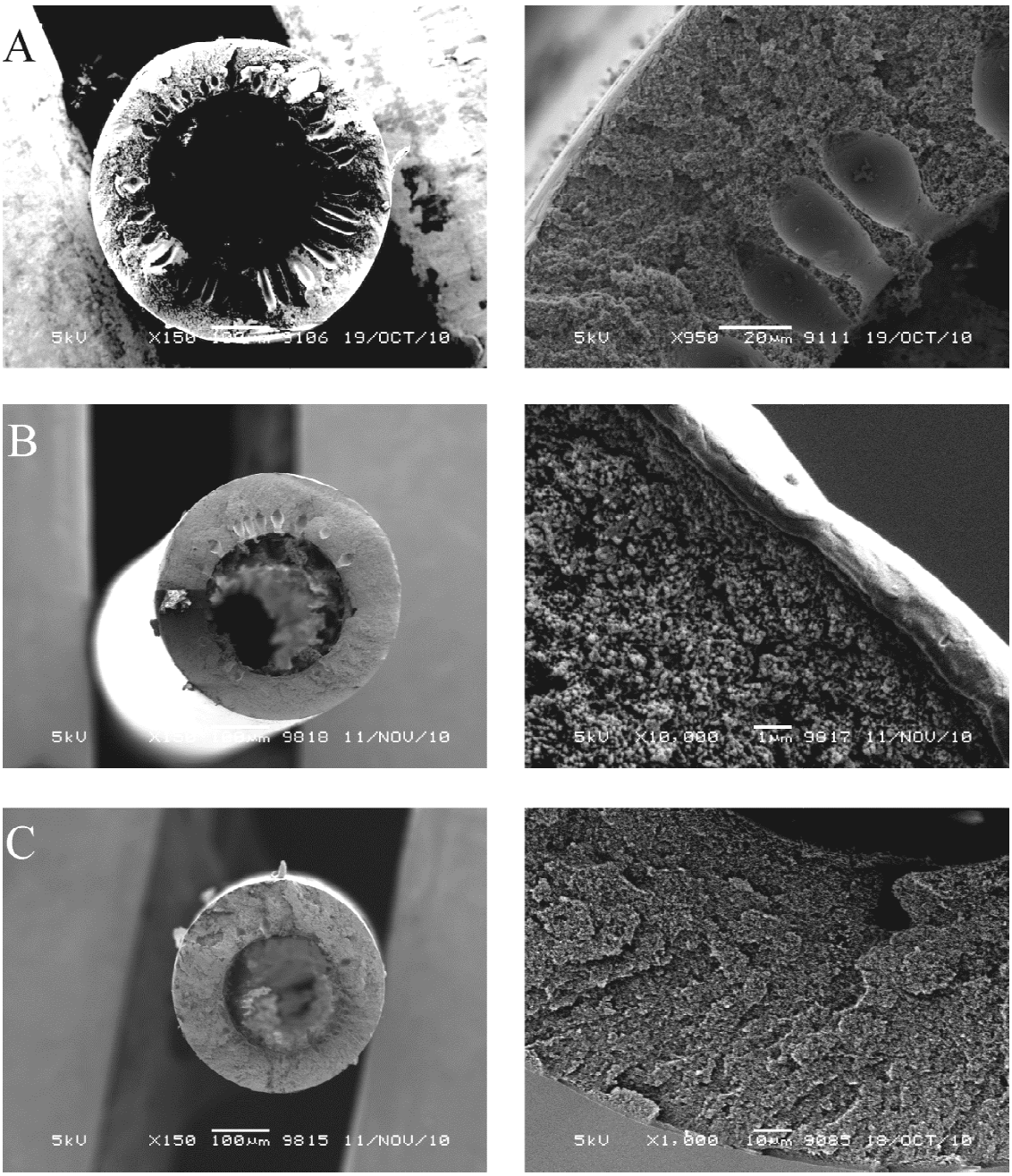

Figure III - 11. SEM images of Matrimid® hollow fibers, left - cross section; right - detail of the dense skin layer: (A) fiber D1 - M1; (B) fiber D1 – M2 and (C) fiber D1 - M3.

As shown in Table III – 3, the thickness of the external dense skin layer *(l)* decreases when the air gap height decreases with values calculated from pure gas permeation data obtained at a feed pressure of 2 bar using Eq. (III - 1) for each gas:

$$\delta\ (nm) = \frac{Permeability\ (Barrer)}{Permeance\ (GPU)} \cdot 10^3 \qquad (\text{III} - 1)$$

where the permeability (Barrer) represents the intrinsic permeation property of the polymeric material that is obtained from pure gas permeation experiments with a dense Matrimid® film of known thickness, and the permeance (GPU) is the transport flux per unit transmembrane driving force through a hollow fiber.

The pure gas permeability of the Matrimid dense film and the hollow fiber permeance used for the calculation of the dense layer thickness in the asymmetric hollow fibers developed in this study are listed in Table III -4. The fiber dimensions and pure gas permeability results obtained in this work are comparable with published literature data (Table III – 4).

Table III - 4. Pure gas permeation data for Matrimid® asymmetric hollow fibers at 30°C.

Mem. type	P (bar)	Permeance (GPU)				Ideal selectivity			
		H_2	CO_2	N_2	CO	H_2/N_2	H_2/CO_2	H_2/CO	CO_2/N_2
Hollow fiber D1 - M1	2.3	66.7±0.3	13.4±0.7	0.91±0.01	1.6±0.03	74.4	5.0	42.6	14.72
	4.1	65.8±0.8	14.4±0.6	0.94	1.6±0.04	71.0	4.5	40.4	15.3
	6.1	66.9±0.1	15.9±0.1	0.93	1.7±0.03	72.3	4.2	40.0	17.1
	8.0	64.1	16.8	0.92	1.6	69.7	3.8	39.3	18.3
	10.0	65.5	19.1	0.93	1.7	70.4	3.4	38.5	20.5
Hollow fiber D1 - M3	2.2	159±5.7	40±3.6	9.1±0.5	9.1	17.5	4.0	17.4	3.2
	4.1	164.2±9.2	41±2.7	10.0±0.2	9.5	16.4	4.0	17.3	3.5
	6.1	169.6±6.9	43±4.3	10.3±0.1	10.1	16.5	3.9	16.7	3.7
Matrimid dense film[a]	2	23.9 (Barrer)	7.3 (Barrer)	0.2 (Barrer)	0.4 (Barrer)	110.9	3.3	54.8	36.5
Knudsen selectivity						3.7	4.7	3.8	0.8

[a]: average values from the literature [12-17], 1 GPU = 1 x 10^6 cm^3(STP) cm^{-2} s^{-1} $cmHg^{-1}$

According to Koros and co-workers [18], the thickness of the dense polymer layer in an asymmetric hollow fiber structure used for gas separation should have around 100 nm. However, as shown in Table III- 5 in general, the majority of studies achieved higher thickness values, showing the difficulty in obtaining such a thin layer thickness without surface defects. Among the published results, the hollow fiber fabricated by Favvas et al. [19] with an asymmetric layer thickness of 72.8 nm had low gas selectivity and were considered defective.

Table III – 5. Literature data for gas permeance and fiber dimensions of Matrimid based asymmetric hollow fiber membranes.

Fiber dimensions			Gas permeability (GPU)							P	T	Ref.
OD (μm)	Δ_{Wall} (μm)	*l* (nm)	He	H_2	CO	CO_2	CH_4	O_2	N_2	(bar)	(^oC)	
500	100	72.8	330	342	26	85	31	34	23		40	[19]
620	140	289				9	0.5	4.6	0.7	8.3	25	[20]
280	145	150						4.5	0.6	10	25	[9, 18]
700	200	150						6.36	1.49	4		[21]
860	680	145				11[a]	0.2[a]			15	20	[8]
								9.2	1.4	10	20	
520	120	350				8.5[a]	0.2[a]			10	35	[10]
								2.8	0.4	4	35	
-	-	500				14.7		0.3		9	30	[22]
800	140	351		39		5.6	1.9			10	35	[b][7]

[a] binary mixtures CO_2/CH_4 = 20/80 (vol %), [b] dual layer asymmetric hollow fiber (Polysulphone - inner layer, Matrimid/PBI=1/1 wt% blend – outer layer)

The results (Table III – 3) from the calculation of the asymmetric layer thickness are quite different depending on the tested gas. In the literature [6, 23] the thickness of the dense layer is usually calculated with one gas, usually O_2. The effect of film thickness on the gas permeation characteristics of glassy polymer membranes was thoroughly studied in literature and it was demonstrated that the use of the intrinsic dense film permeability data to estimate skin thickness from flux observations on asymmetric or composite membrane structures is a very approximate method [24].

Another method consists of fitting permeability versus permeance data for a number of different pure gases in the same plot and to obtain the thickness from the

slope [26] (see Figure III - 12). In our case the latter procedure gives an average value of 354 nm for fiber D1 - M1 when pure gas (H_2, CO_2, CO and N_2) permeability versus permeance data obtained in the feed pressure range between 2 to 10 bar are plotted together (Figure III – 12). This result is close to the thickness calculated from permeability/permeance data using pure H_2, since the slope value is actually determined by the gas with the highest permeance.

The dependence in the value of the dense layer thickness on the tested gas indicates a complex morphology of the external asymmetric skin that is discussed later in section 3.3.2.

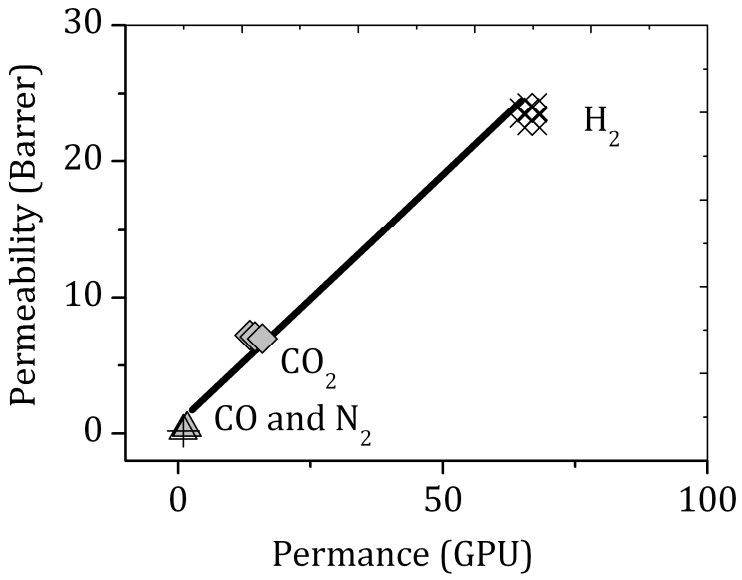

Figure III – 12. Permeability versus permeance plot for the determination of the Matrimid hollow fiber asymmetric layer thickness

Matrimid – PBI blend hollow fibers

Figure III – 13 shows SEM images of the two hollow fibers obtained from the Matrimid – PBI polymer blend. The fiber D2 is hollow with satisfactory cross-sectional circularity and concentricity and with constant wall thickness, but does not have a porous structure, it seems that it has a dense morphology over the entire wall. For the formulation of the fiber D3 dope, EtOH non – solvent was added as means of approaching decomposition and thus achieving a porous morphology. As shown in Figure III – 13 (B) this procedure was somewhat successful, a spongy like structure morphology was obtained with a low pore size, but the inner diameter of the fiber D2 is too small. Also, a lack of mechanical stability was observed for both fibers. Dense films from Matrimid/PBI=1/1 (wt%) polymer blend were also prepared following strictly the same recipe developed in literature [15]. The resulted dense films presented a good morphology but they also had a lack of mechanical stability. The films were so brittle that it broke when transmembrane pressure of 2 bar was applied. The recipe needs further improvement and the use of a dual – layer hollow fiber spinning process must be contemplated [7].

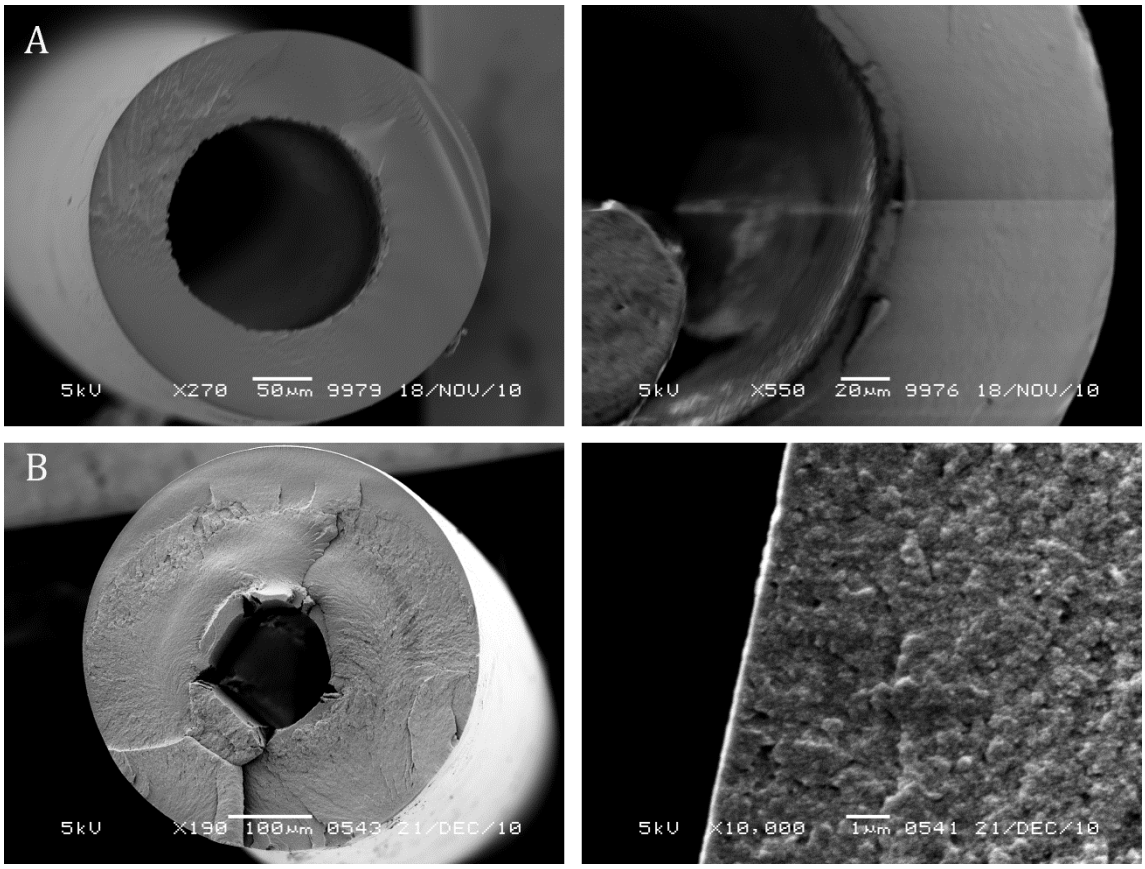

Figure III - 13. SEM images of Matrimid:PBI=1:1 hollow fibers, left - cross section; right - detail of the shell: (A) fiber D2 cm; (B) fiber D3.

3.3.2 Gas permeation through asymmetric Matrimid hollow fibers

Concentration polarization phenomena

The occurrence of concentration polarization phenomena was not found at the feed side of the membrane in the case of the permeation of pure H_2 whose permeance values remained constant with the feed flow rate. In contrast the concentration polarization phenomenon was found for H_2/N_2 mixtures at feed flow rates lower than 50 cm^3 min^{-1} as depicted by Figure III – 14. Therefore, for further gas permeation experiments the feed flow rate and the sweep gas flow rate were kept constant at 100 cm^3 (STP) min^{-1} and at 10 cm^3 (STP) min^{-1} respectively.

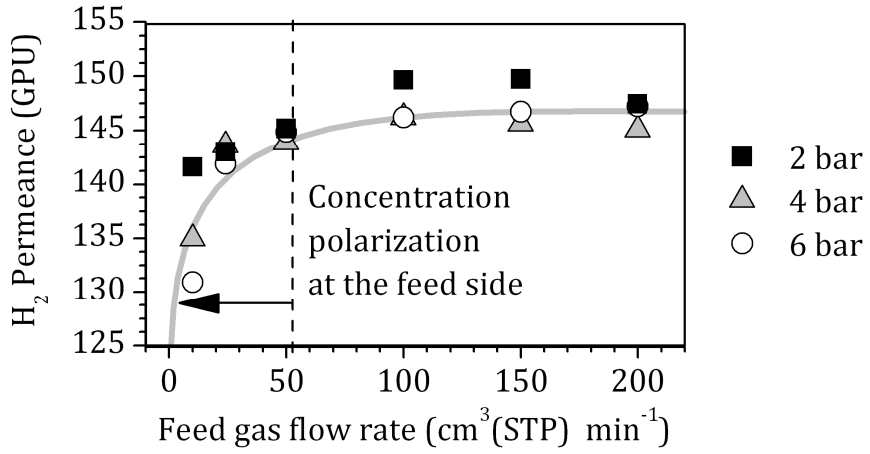

Figure III – 14. The effect of feed gas flow rate on H_2 permeance at 30 °C and feed pressures of 2, 4 and 6 bar for mixtures H2/N2 = 50/5 (vol ratio), using membrane D1 - M3.

Pure gas permeation

Pure gas permeance and ideal selectivity data are listed in Table III - 4. All data represent an average from several runs. The permeance of all gases is higher for membrane D1 - M3 than for membrane D1 - M1. In the case of membrane D1 - M3, the different gas pair values of ideal selectivity are low (15.7% of the intrinsic selectivity of a dense film for H_2/N_2 gas pair) and approaching the Knudsen selectivity showing that this hollow fiber possesses important surface defects. In literature, asymmetric hollow fiber membranes with a gas selectivity of only 55% of a dense film values where considered to be "moderately defective membranes" meanwhile those with a gas selectivity equal with the Knudsen selectivity where considered to be "severely

defective membranes" [18]. To recover the intrinsic selectivity of the material, usually a post-treatment by applying a PDMS coating is applied. This method is not attractive at commercial scale and therefore we preferred to further use in our study the defect free fiber D1 – M1.

It can be observed that the developed Matrimid® hollow fiber D1 - M1 possesses gas permeance and ideal selectivity values similar to published data for commercial hollow fiber membrane used for H_2 separation and recovery, with selectivity values of 80 and 50 for H_2/N_2 and H_2/CO respectively [4, 27]. As it can be calculated from the values reported in Table III – 4, the ideal selectivity values of the hollow fiber membrane D1 - M1 for the gas pairs H_2/N_2 and H_2/CO are of 67 % and 78 % of a dense Matrimid® film. In contrast, at 2 bar the selectivity of H_2/CO_2 gas pair is of 150 % of dense film. These contrary results show again the complexity of the asymmetric layer morphology.

Between the skin layer and the porous substrate a transition layer (substructure) can exist. This transition layer might have small enough pores to determine gases to flow in a Knudsen regime and to contribute substantially to the overall membrane resistance, as previously has been reported by Koros et al. [28, 29]. The gas transport through porous membranes in the Knudsen regime is slow and comparable to the one governed by solution-diffusion mechanism in dense membranes and it takes place when the pore radius is lower than 0.05 times the mean free path (λ) of the gas molecules [30]. λ increases in the following order: CO_2 < N_2 < CO < H_2 with noticeable higher values for H_2. At 1 bar and 303.15 K the λ values for CO_2, N_2, CO and H_2 are listed in Table III – 6 and are calculated using Equation III - 2 [30]

$$\lambda = \frac{R \cdot T}{N_A \cdot 2^{0.5} \pi \cdot d^2 \cdot p} \qquad (\text{III} - 2)$$

where R is the general constant of gases (8.31 J mol^{-1} K^{-1}), T is the temperature (K), N_A is the Avogadro's number (6.023 x 10^{23}), d (m) is the molar average collision diameter with values taken from Hirschfelder [31] and p (Pa) is the pressure. The resulting λ values have the unit in meter. Table III – 6 also, lists the d values of the gases of interest in our work.

The much higher λ value for H_2 than for the N_2, CO and CO_2 determines a pore radius range in which the transport of H_2 is in Knudsen regime meanwhile the transport of CO, N_2 and CO_2 is faster (slip flow for pore radius between 0.05 λ and 50 λ or viscous flow for pore radius higher than 50 λ). At 1 bar this range is between 3.43 nm (= $0.05\lambda_{CO}$) and 5.55 nm (= $0.05\ \lambda_{H2}$). A higher contribution of Knudsen flow to the transport of H_2 than to the transport of CO and N_2 could determine a higher

overall resistance to the transport of H_2 and therefore the lower H_2/CO and H_2/N_2 selectivity values experienced for hollow fibers than those obtained for dense films.

Table III – 6. The values of the molar average collision diameter, *d*, and gas mean free path, λ.

Gas	*d* (nm)	λ (nm)*
H_2	0.292	111
CO_2	0.390	62
N_2	0.375	67
CO	0.371	69

*λ values were calculated at 1 bar and 303.15 K

If only Knudsen transport resistance is assumed for the substructure then also the H_2/CO_2 selectivity should be lower for hollow fibers than for dense membranes, but quite on the contrary this value is higher and therefore the overall membrane resistance is higher for CO_2 than for H_2. For the transport of the more condensable CO_2, a contribution of surface flow through porous media could be assumed [30]. In surface flow mechanism a film of densely packed condensed molecules is formed at the pore wall interface and moves at a steady state velocity along the surface. Surface diffusion is a process that influences and occurs in parallel with Knudsen diffusion. The liquid film formed on the pore wall – gas interface decreases the effective pore diameter and thus the contribution to the overall transport of Knudsen regime is increased.

In order to evaluate the contribution of the substructure to the overall resistance a simple resistance model where skin and substructure resistance are considered to be connected in series can be considered as depicted by Figure III – 15 [29, 30, 32].

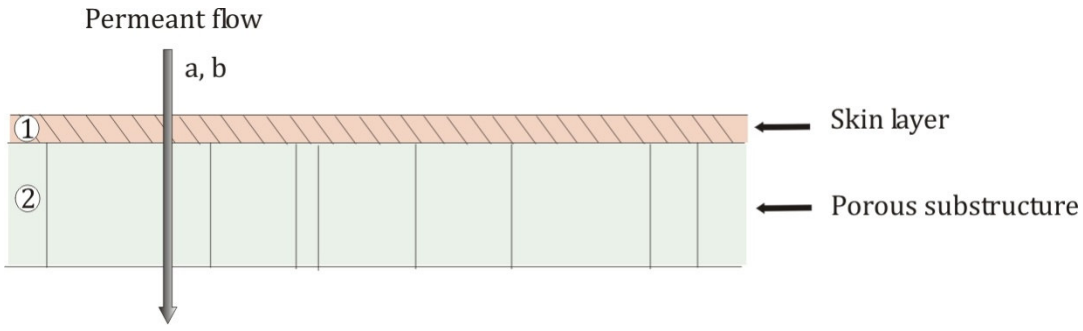

Figure III – 15. Resistances connected in series in composite membranes.

In this case the following equations apply [29, 30, 32].

$$(R_{tot})_a = (R_1)_a + (R_2)_a \qquad (\text{III} - 3)$$

$$(R_{tot})_b = (R_{skin})_b + (R_{sub})_b \qquad (\text{III} - 4)$$

where R_{tot} is the total resistance to gas transport (reciprocal of the permeance), R_{skin} and R_{sub} refer to the skin layer and the substructure and subscripts *a* and *b* refer to two different gases. The skin layer resistance is given by the intrinsic value of the resistance of a dense film. Therefore, the ratio of the resistances for permeants *a* and *b*, that is the asymmetric layer selectivity, $(\alpha_{skin})_{a/b}$, is equal to the ratio of permeability of *a* to *b* of a dense film, that is the dense film selectivity, $(\alpha_{dense\ film})_{a/b}$:

$$(\alpha_{skin})_{a/b} = \frac{(R_{skin})_b}{(R_{skin})_a} = \frac{(P_{skin})_a}{(P_{skin})_b} = \frac{(P_{dense\ film})_a}{(P_{dense\ film})_b} = (\alpha_{dense\ film})_{a/b} \qquad (\text{III} - 5)$$

The ratio of the overall resistance for permeants *a* and *b*, of the hollow fibers is:

$$\alpha_{a/b} = \frac{(R_{tot})_b}{(R_{tot})_a} \qquad (\text{III} - 6)$$

Substituting Eq. III – 4 and III – 5 into Eq. III – 6, gives:

$$\alpha_{a/b} = \frac{(\alpha_{skin})_{a/b}(R_{skin})_a + (\alpha_{sub})_{a/b}(R_{sub})_a}{(R_{sub})_a + (R_{skin})_a} \qquad (\text{III} - 7)$$

The rearrangement of Eq III – 7 gives:

$$\alpha_{a/b} = \frac{(\alpha_{skin})_{a/b} + (\alpha_{sub})_{a/b}[(R_{sub})_a/(R_{skin})_a]}{1 + [(R_{sub})_a/(R_{skin})_a]} \qquad (\text{III} - 8)$$

If Knudsen selectivity is assumed for the microporous substructure selectivity, then using the intrinsic dense Matrimid® selectivity values for H_2/N_2 and CO_2/N_2 gas pairs ($(\alpha_{skin})_{H_2/N_2}$ and $(\alpha_{skin})_{CO_2/N_2}$) the ratio of substructure resistance to skin layer resistance can be calculated at different transmembrane pressures. The results in terms of relative contribution of substrate resistance to the overall membrane resistance for the hollow fiber membrane D1 - M1 are listed in Table III – 7 and are calculated from the values reported in Table III - 4.

Table III – 7. The relative contribution of substrate resistance to the overall membrane resistance for the hollow fiber membranes D1 - M1 towards the permeation of pure H_2 and CO_2

Pressure (bar)	R_{sub}/R_{tot} (%)	
	H_2	CO_2
2.3	34	61
4.1	37	59
6.1	36	54
8	38	51
10	38	45

From the values reported in Table III – 7 it can be noticed that an important contribution to the overall transport resistance through the hollow fiber membrane is given by the substructure, with values as high as 61 % for CO_2 at 2.3 bar and 303.15 K. In the case of H_2, the pressure does not have a significant effect over the substructure resistance. This indicates that the transport of H_2 through the porous substructure is driven only by a Knudsen mechanism since the Knudsen coefficient is constant with pressure. Although for the calculation of the R_{sub}/R_{tot} (%) values for CO_2 only Knudsen flow was assumed, the variation with pressure of this fraction indicates a contribution of the surface flow to the transport of CO_2. Assuming a Henry's law for the gas adsoption on the pore wall, the amount of gas adsorbed in the polymer material increases with pressure and therefore the contribution of the substructure resistance to the total resistance increases.

In the case of fiber D1 - M1, another remarkable aspect is that, in the pressure range studied, from 2 to 10 bar, H_2, CO and N_2 pure gas permeance data (see Table III - 4) remained almost constant with pressure. In contrast, the permeance of CO_2 strongly rose, reaching an increase of 42% from 2 to 10 bar. This tendency in the permeation of condensable gases like CO_2 is already very well documented in the literature for asymmetric hollow fibers, thin and thick planar membranes and it is attributed to plasticization phenomena [33, 34]. In the literature it has been reported that in dense Matrimid thick films (thickness around 30 μm) the permeability of CO_2 first decreases with pressure until it reaches a minimum at 15 bar at 35 ^oC [35] and at 12 bar at 22 ^oC [36] from which it begins to increase.

The decrease in gas permeability is related to the decrease in gas solubility coefficient with pressure since the polymer sorption sites found in the polymer matrix become saturated with gas molecules at increasing values of pressure. At the

plasticization pressure, the polymeric chain packing is disrupted by the penetrant molecules due to the increase in the segmental mobility that expands both the frequency and the average size of transient gaps that enable diffusion, thereby increasing the permeability. It was reported in literature that in Matrimid® thin films (thickness below 5.2 μm) [37] or for even thinner films as those obtained in asymmetric hollow fibers, the minimum may even disappear and the permeability increases immediately from low feed pressures. The accelerated plasticization is assumed to occur because of the steep swelling induces stress gradients related to the thinner membrane / film thickness [38].

Comparative results for the variation with pressure of CO_2 permeance in Matrimid® hollow fibers were previously reported in other studies [39]. In our work, the different trend in the transport rate of H_2 and CO_2 determines a decrease in the H_2/CO_2 ideal selectivity with pressure from a value of 5.0 at 2 bar to 3.4 at 10 bar as shown in Table III - 4.

Mixed gas permeation

Figure III - 16 shows the permeation results for H_2 transport from binary H_2/CO_2 feed mixtures plotted against the fugacity of H_2 (Fig. III - 16.a) and plotted against the fugacity of CO_2 (Fig III- 16.b) at different total feed pressures for the hollow fiber D1 – M1.

In comparison with pure gas permeation results, the permeance of H_2 in mixtures is lower and, for a constant gas composition, it decreases at increasing total feed pressure, i.e., when the fugacity of both H_2 and CO_2 increases. This phenomenon is related to the competitive sorption between H_2 and CO_2 for the sorption sites which are associated to the excess (non-equilibrium) free volume fraction of the polymer [40]. Working with a gas mixture the availability of the sorption sites for one component is lowered due to the presence of the other component and thus its transport rate is also lowered when it is compared with pure gas transport rate. While H_2 is a relatively inert and fast permeating gas whose transport rate is diffusion based, CO_2 is a more condensable gas and possesses higher solubility in membranes. Therefore the polymer sorption sites are preferentially occupied with CO_2 than with H_2 leading in both hollow fiber and flat membranes to a higher decay in the permeability of H_2 than in the permeability of CO_2, for H_2/CO_2 gas mixtures with respect to pure gases.

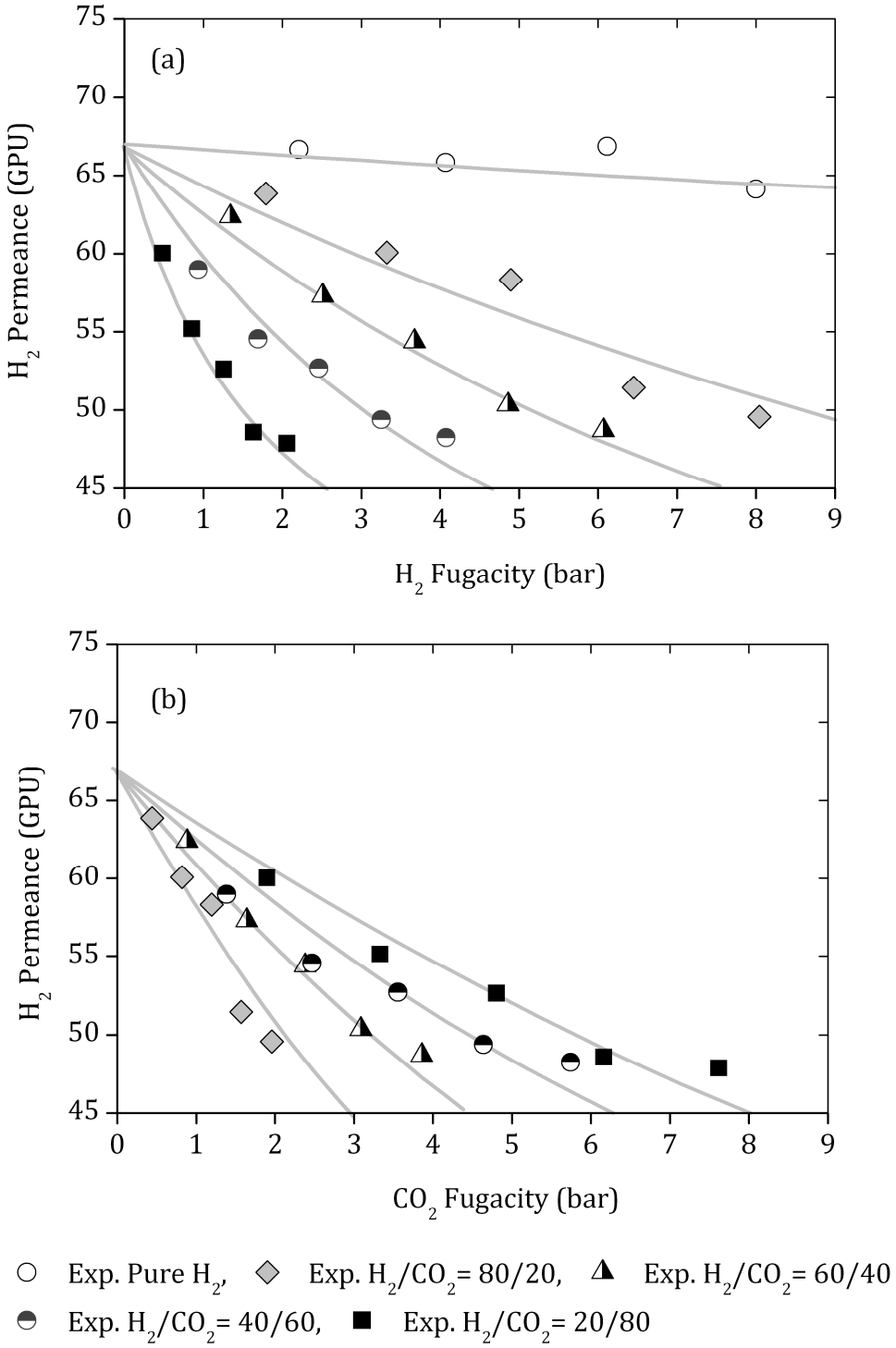

Figure III - 16. H_2 permeance variation as function of the fugacity of H_2 (a) and of CO_2 (b) for H_2/CO_2 mixtures and pure H_2 in asymmetric Matrimid® hollow fiber membranes D1 – M1. The lines are drawn to guide the eye.

In flat membranes (see Chapter II – 2.4.2, Figure II - 15) the mixed gas permeation of H_2 was dependant of only the fugacity of CO_2; i.e., equal values for the H_2 mixed gas permeability data were obtained for H_2/CO_2 mixtures when the fugacity of CO_2 was kept constant and the fugacity of H_2 was increased. In contrast in hollow fiber membranes this behavior is not repeatable and lower H_2 permeance values were obtained at higher fugacity of H_2 for the same fugacity of CO_2 (see Fig. III - 16.b.). The explanation of such behavior will be discussed later on after analyzing the CO_2 permeation data.

Figure III - 17 shows the permeation results for CO_2 transport in binary H_2/CO_2 mixtures plotted against the fugacity of CO_2 for different feed composition in the range H_2/CO_2 = 20/80 to H_2/CO_2 = 80/20. The maximum operating pressure was 10 bar and therefore the maximum attainable fugacity of CO_2 in the mixture H_2/CO_2 = 80/20 was of 2 bar.

The permeance of CO_2 decreased with its fugacity for the H_2/CO_2 mixture of 80/20 (vol %), remained practically constant for the mixture H_2/CO_2 = 60/40 (vol %) and for the rest of the mixtures (with CO_2 concentration > 40%) the CO_2 permeance increases as the concentration of CO_2 in the mixtures increased, reaching values close to pure CO_2 permeance data. This tendency corresponds to a balance between two contrary effects that affect CO_2 transport through a thin Matrimid layer: competitive sorption and plasticization phenomenon for H_2/CO_2 mixtures in hollow fibers. While plasticization increases the permeation of CO_2 with pressure, competitive sorption between H_2 and CO_2 determine a decrease in the permeation of CO_2. As shown in the Chapter II, section 2.4.2, using thick planar Matrimid films plasticization was not found and the permeability of CO_2 obtained with H_2/CO_2 mixtures was slightly lower than pure gas permeability and presented a similar behavior of decreasing permeability with increasing CO_2 fugacity [17] (also, see Figure II – 17 from Chapter II). In Matrimid hollow fibers, at high concentration of H_2 in the H_2/CO_2 mixture, competitive sorption prevails and the permeance of CO_2 decreases with its fugacity. As the concentration of CO_2 increases, plasticization counteracts competitive sorption and equality between the two phenomena is reached when the permeance of CO_2 remains constant with its fugacity. At high concentration of CO_2 in the H_2/CO_2 mixture plasticization dominates the transport rate of CO_2 and the permeance of CO_2 increases with its fugacity. Similar results were reported in literature for CO_2/CH_4 mixtures in Matrimid asymmetric hollow fiber membranes. In some studies [10, 37, 38] plasticization was dominant at high CO_2 feed gas concentrations (80 vol % CO_2) while competitive sorption effects were dominant at low CO_2 feed gas concentrations (20 vol %). In another study [9] working with a 10/90 (vol %) CO_2/CH_4 feed mixture competitive sorption was also dominant and the permeance of CO_2 decreased with CO_2 partial pressure.

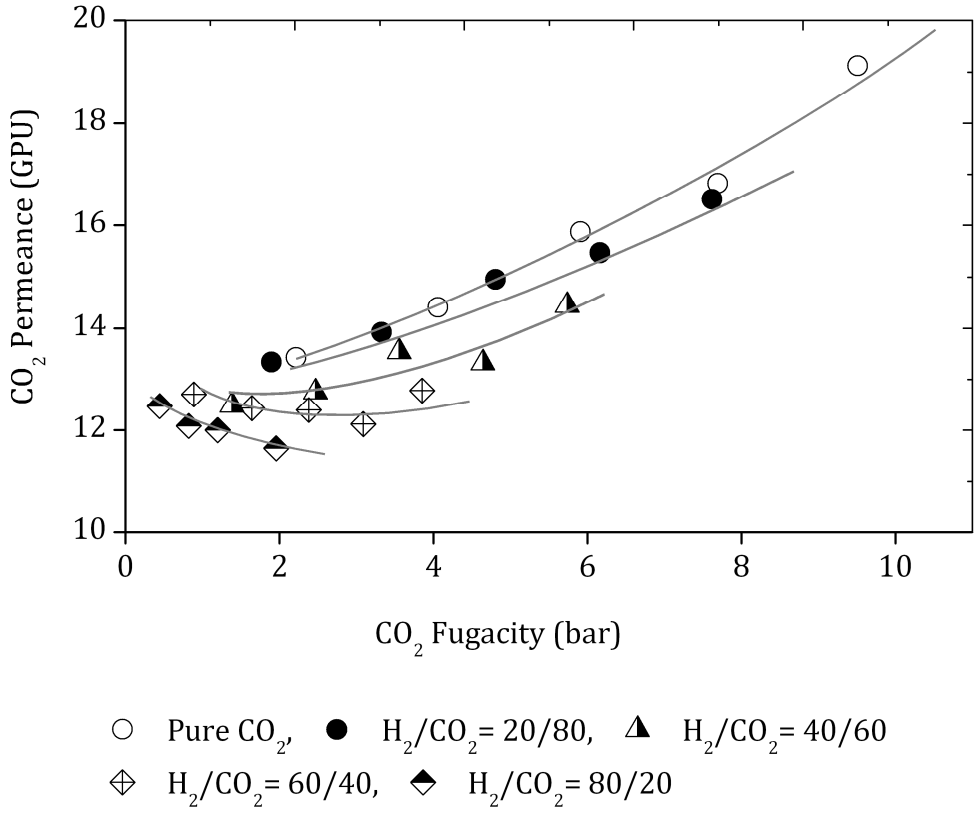

Figure III - 17. CO_2 permeance variation with its fugacity for H_2/CO_2 mixtures and pure CO_2 in asymmetric Matrimid® hollow fiber membrane D1 - M1. The lines are drawn to guide the eye.

Plasticization of the membrane by CO_2 can also affect the transport rate of H_2. Figure III - 18 shows the ratio between H_2 permeance and respectively permeability values obtained working with pure gas and binary H_2/CO_2 feed mixtures for asymmetric hollow fibers and dense films. The effect of using thin asymmetric layers in hollow fiber (fiber D1 - M1) structure versus planar thick Matrimid films is also resembled.

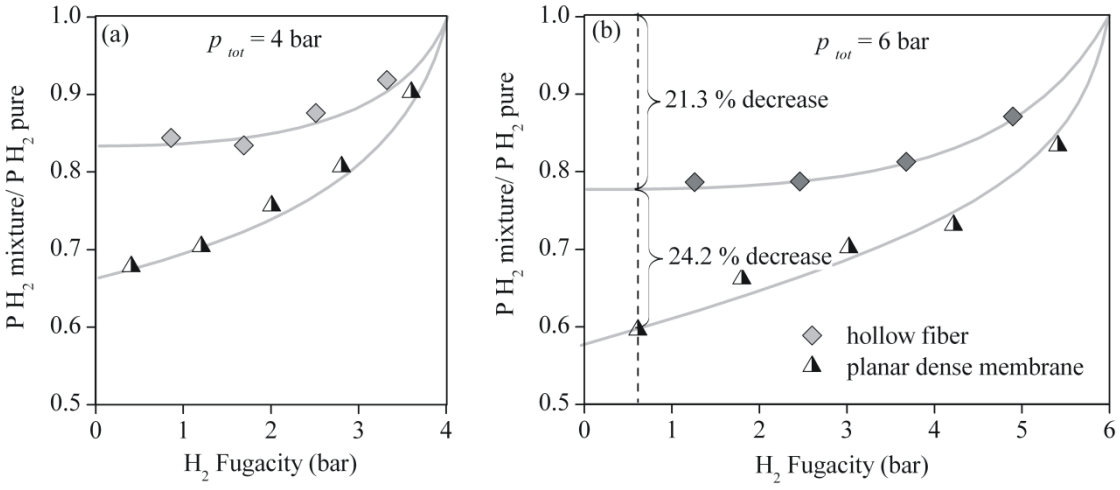

Figure III - 18. Hollow fiber M1 vs. planar dense membrane comparative study for the depression in the permeation of H_2 for H_2/CO_2 mixtures in respect to pure gas, at total feed pressure of 4 bar (a) and 6 bar (b).

The pure and mixed gas H_2 permeability values for planar films were reported in Chapter II, section 2.4.2 of this thesis. At a total feed pressure of 6 bar the decay in the permeation values of H_2 in respect to pure gas values is higher for Matrimid films than for hollow fibers: in Matrimid planar films the decay was of 45% meanwhile the decay in the hollow fibers the decay was of only 21%. Under the used operating conditions, in dense Matrimid films the CO_2 plasticization phenomena was not found, and only the competitive sorption phenomena was present, thus we can conclude that the CO_2 plasticization phenomena found in the permeation of H_2/CO_2 mixtures trough Matrimid® hollow fibers determines higher permeation values for H_2. This is better explained in terms of so called "transport plasticization" that can occurs in the presence of highly sorbing penetrants, which are capable of swelling the polymer matrix to introduce additional free volume that enable higher values for penetrant diffusion [41]. As shown in Figure III - 16, for mixtures with a higher concentration in H_2 and the same concentration in CO_2 the plasticization with CO_2 is lower, competitive sorption phenomenon dominates and thus the decay in the permeation of H_2 with respect to pure gas is higher.

Hollow fiber mixed gas selectivity values, calculated as described in Chapter I, section 1.3.1 – Eq. I – 9, have been plotted in Figure III - 19 for H_2/CO_2 mixtures.

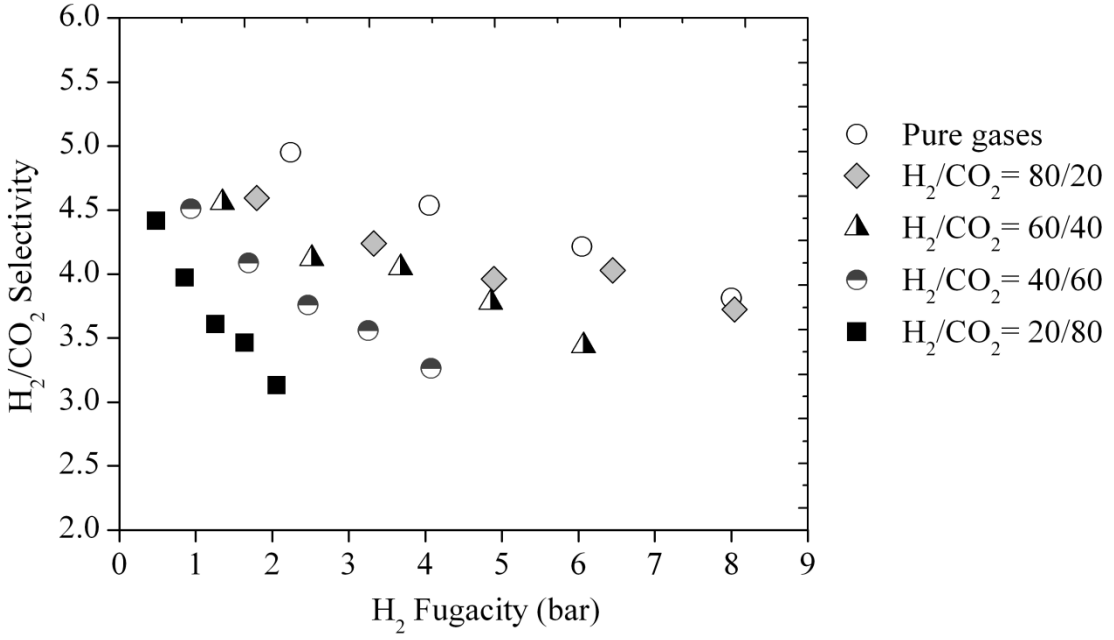

Figure III - 19. H_2/CO_2 selectivity variation with the fugacity of H_2 for binary H_2/CO_2 mixtures in asymmetric Matrimid® hollow fiber membranes.

The lower permeation of H_2 in binary H_2/CO_2 mixtures determines a considerably lower selectivity for the H_2/CO_2 gas pair than the ideal selectivity. The mixed gas selectivity strongly varies with gas composition and pressure with values of α = 3.1 for the 20/80 H_2/CO_2 mixture at a total pressure of 10 bar and H_2 fugacity of 2 bar compared to 4.6 for the 80/20 H_2/CO_2 mixture at total pressure of 2 bar. The selectivity values are lower for mixtures than for pure gases but are higher than the average mixed gas selectivity obtained with planar membranes with a value of 2.7. Two factors might contribute to determine this difference: a lower depression in the transport rate of H_2 in H_2/CO_2 mixtures for hollow fiber than for dense films and a higher substructure resistance towards the transport of CO_2.

In the case of the mixtures of H_2 with relatively more inert gases: N_2 and CO the permeance values for H_2 are close to pure gas values and are slightly lower when the copartner for H_2 was CO (Figure III - 20). This demonstrates that between H_2 and N_2 or CO only slight competitive sorption effects are found, which are relatively stronger for H_2/CO mixtures than for H_2/N_2 mixtures. Contrary to other report [27], there is no plasticization phenomena present in H_2/CO mixtures or for pure CO whose permeance is constant within the pressure range 1 - 10 bar (see Table III - 4). These results are consistent with published literature data for pure H_2 and CO and for H_2/CO mixtures in another polyimide membrane [42].

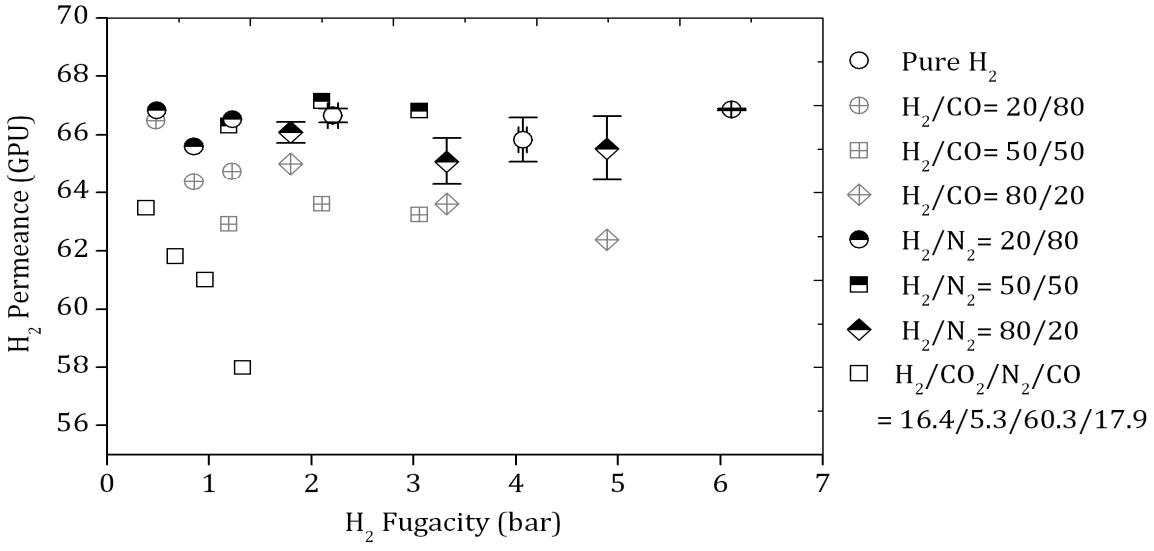

Figure III - 20. H_2 permeance variation with its fugacity for pure H_2, binary H_2/N_2, H_2/CO and quaternary $H_2/CO_2/N_2/CO$ gas mixtures and in asymmetric Matrimid® hollow fiber membrane D1 - M1.

Figure III - 20 also shows H_2 permeance values for the quaternary $H_2/CO_2/N_2/CO$ mixture. With respect to pure gas permeability a small percentage of CO_2 (5.36 vol %) as it is found in the tail gas from carbon black manufacturing determines a 12 % decrease in the permeance values for H_2 working at a total feed pressure of 8 bar.

The concentration of H_2 in the permeate stream leaving the hollow fiber membrane module was between 87 and 89 vol % calculated if Ar sweep gas is not taken into account. We assume that under industrial operating conditions the concentration of H_2 in the permeate stream is expected to be somehow lower, since our experimental values were obtained close to ideal operation conditions: counter currently plug flow and very low stage cut.

Temperature effect over mixed gas experiments

The influence of temperature over the permeance of mixed gases was analyzed for the quaternary $H_2/CO_2/N_2/CO$ mixture of 16.3/5.3/60.7/17.8 (vol %) at temperatures ranging from 30 to 130 ^oC and a pressure of 4 bar and a constant feed and sweep gas flow rate of 100 cm^3 (STP) min^{-1} and of 10 cm^3 (STP) min^{-1} respectively. This mixture represents a synthetic mixture similar to the dry post combustion gas stream obtained in the production of carbon black. As temperature increased all four gas permeabilities increased. Arrhenius plots are represented in Figure III - 21 showing an Arrhenius - type dependence with temperature for temperatures up to 110 ^oC. At temperatures higher than 110 ^oC the permeance of all gases had lower values than the corresponding to the Arrhenius type dependence. Matrimid hollow fiber membranes were reported to maintain stable permeation properties at temperatures up to 150 ^oC [43]. In the case of the hollow fibers obtained in this work, at T > 110 ^oC, we assume that the decay in permeance can be attributed to structural modifications in the morphology of the membrane. The reorientation of the polymeric chains in order to attain equilibrium is faster and a possible densification can occur under the pressure working conditions. The specific Arrhenius parameters (the permeation activation energy, E_{ap} and P_0) for permeance of H_2, CO_2, N_2 and CO in the synthetic mixture were calculated (Table III - 8). The E_{ap} values for H_2 and CO_2 are similar to those obtained in planar dense membranes (see Table II - 4). On the other hand the E_{ap} values obtained for N_2 and CO are lower than in planar dense membranes, giving the following order in the increase of the E_{ap}: $CO_2 < N_2 < CO < H_2$.

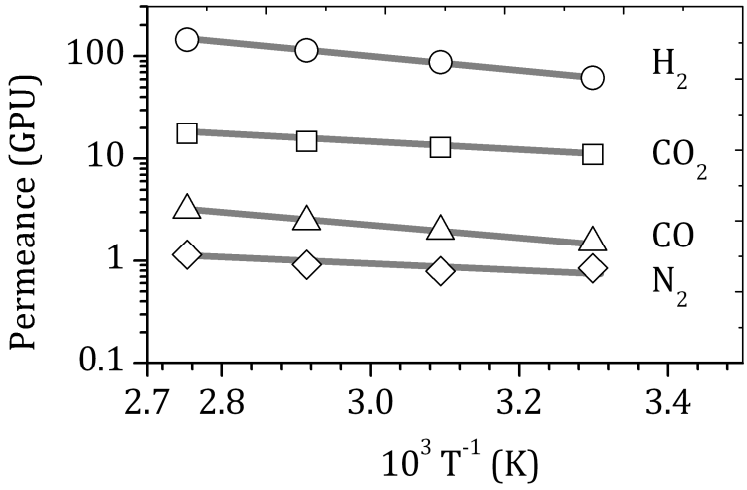

Figure III- 21. The permeance of mixed $H_2/CO_2/CO/N_2$ = 16.3/5.3/60.7/17.8 (vol %) as a function of temperature at 4 bar feed pressure.

Table III – 8. Arrhenius parameters for CO_2, N_2, H_2 and CO permeation through a Matrimid hollow fiber membrane for quaternary $H_2/CO_2/N_2/CO$ mixture of 16.3/5.3/60.7/17.8 (vol %)

Arrhenius parameters	Gas			
	N_2	H_2	CO_2	CO
P_0 (GPU)	3.21	11623	187.8	122.4
E_{aP} (kJ mol^{-1})	9.3	12.8	7.2	11.1

Figure III – 22 shows the effects of temperature on the mixed gas selectivity for H_2/CO_2, H_2/N_2, H_2/CO and CO/N_2 separations through the Matrimid hollow fiber membrane. The mixed gas selectivity $\alpha_{H2/CO2}$ increases with temperature from a value of 5.33 at 30 °C to 7.0 at 110 °C. The selectivity of the other gas pairs is almost constant with temperature with an average value of 109 for $\alpha_{H2/N2}$, 40 for $\alpha_{H2/CO}$and with a slight increase from a value of 1.8 at 30 °C to 2.8 at 30 °C for $\alpha_{CO/N2}$

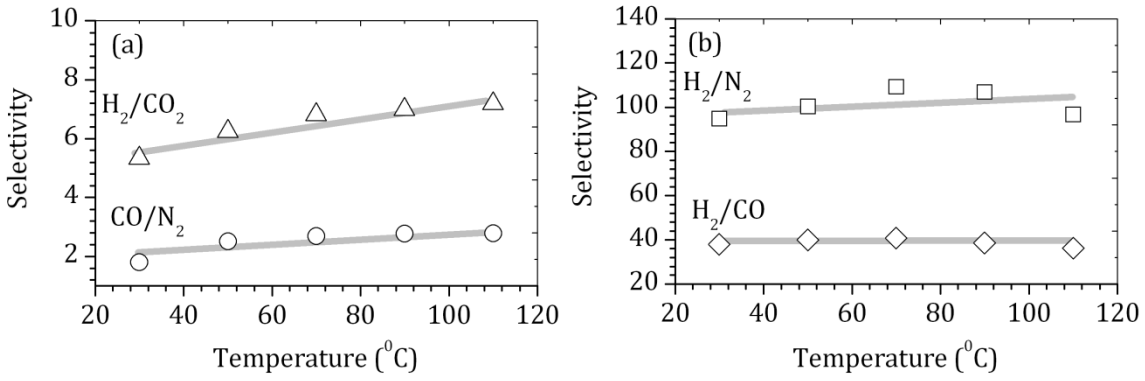

Figure III – 22. Mixed gas selectivity variation with the temperature for (a) H_2/CO_2, N_2/CO and (b) H_2/N_2, H_2/CO gas pairs at 4 bar feed pressure for a quaternary $H_2/CO_2/N_2/CO$ mixture of 16.3/5.3/60.7/17.8 (vol %), through Matrimid hollow fiber membranes.

3.3.3. Gas permeation through asymmetric PPO hollow fibers

The use of asymmetric hollow fibers based on PPO material is generally for the easy task separation of O_2 from N_2. Therefore the use of the highly permeable PPO is advantageous for achieving high gas productivity. In this work it was decided to perform a comparative study between hollow fiber membranes made of materials with contrasting gas permeation properties (Matrimid and PPO). However we found experimental difficulties related with the analysis of PPO hollow fibers. A more thoughtful research is needed and the few results obtained are herein given.

Table III – 9 lists the permeance and ideal selectivity values for the pure gas permeation through the PPO asymmetric hollow fiber module obtained at a pressure gradient of 1 bar and 30 ^{o}C. All data represent an average from several duplicates. The different gas pair values of ideal selectivity are similar to published data for PPO dense films. Literature published data for the gas permeability coefficient through PPO membranes is found in a wide range of values. It was shown that the casting solvent has an important influence over the gas permeability through PPO planar films [44]. However, the fabrications conditions of the commercial PPO asymmetric hollow fibers used in this work are proprietary and not known.

The thickness of the external dense skin *(δ)* was calculated fitting permeability versus permeance data for H_2, CO_2, CO and N_2 pure gases (see Figure III - 23) and an average value of 39.5 nm was obtained in the feed pressure range between 2 to 10 bar. This result is similar to the asymmetric layer thickness of approximately 35 - 40 nm as referenced by the provider (Parker Filtration).

Table III - 9. Pure gas permeation data for PPO asymmetric hollow fibers and dense films.

Mem. type	Permeance (GPU) or Permeability (Barrer)				Ideal selectivity			
	H_2	CO_2	N_2	CO	H_2/N_2	H_2/CO_2	H_2/CO	CO_2/N_2
Hollow fiber	2152±147	968.9±42	70.8±0.6	98.41	30	3	22	13.7
PPO dense film[a]	80 - 110	43 - 66	2.7-4.4	4.2	24	1.6	19	19

[a]: values from literature [25, 45, 46]

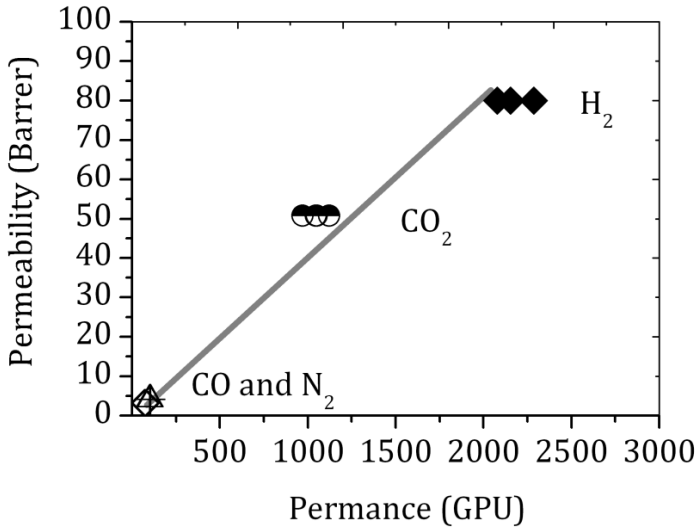

Figure III – 23. Permeability versus permeance plot for the determination of the PPO hollow fiber asymmetric layer thickness

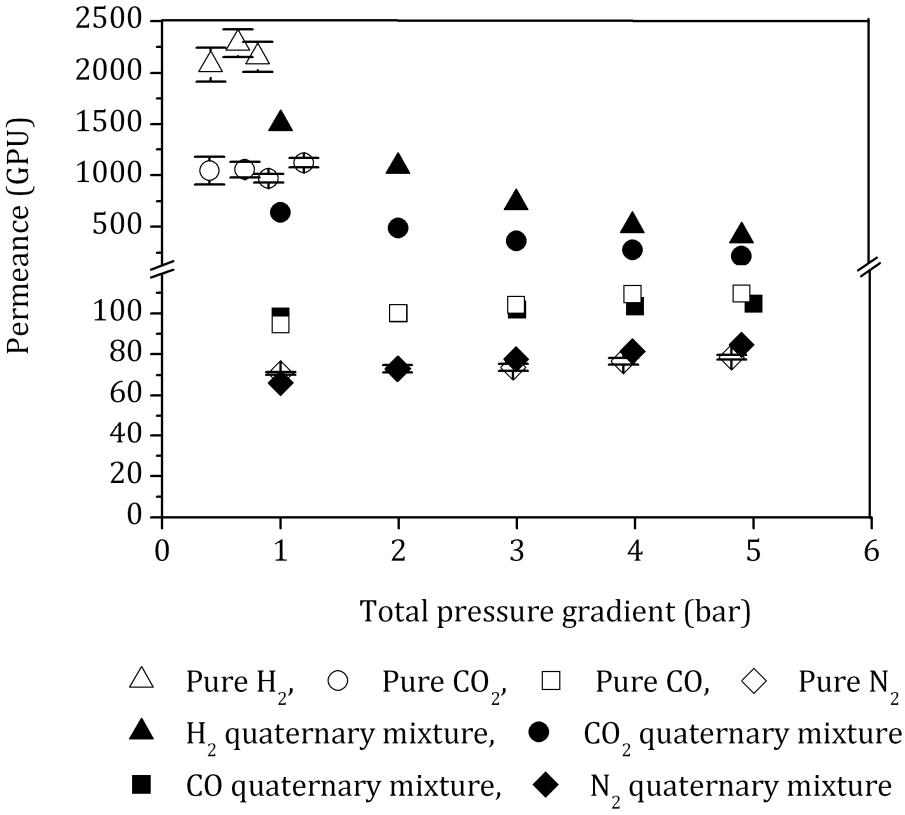

Figure III – 24. Pure and mixed gas permeance variation with the pressure gradient for the asymmetric PPO hollow fiber membranes.

Figure III – 24 shows that in the narrow pressure range studied pure gas permeance data remained constant with pressure for all components. In contrast to Matrimid asymmetric hollow fiber membranes, CO_2 plasticization phenomenon was not found in the PPO membranes. In literature, when mixed gas permeation (CO_2/CH_4) was analyzed for asymmetric hollow fiber membranes based on several polymers (cellulose acetate, Matrimid, PPO) and polymer blends (polyethersulfone/Matrimid, polyimide P84/Matrimid, Matrimid), PPO membranes appeared to be less susceptible to plasticization, but gave low mixed gas CO_2/CH_4 selectivities [10].

When analyzing the mixed gas permeation data, it is noticed that the mixed gas permeance of H_2 and CO_2 is considerably lower than for pure gases and it has decreasing values as the total pressure gradient increases. On the other hand, the mixed gas permeance of CO and of N_2 is similar to pure gas permeance. We assume that the pure gas permeance data for H_2 and CO_2 has significant experimental error due to the experimental difficulties encountered in the measurement of the transmembrane pressure. On the other hand, when we worked with the quaternary gas mixture that has a high concentration of low permeating N_2 we were able to increase the feed gas pressure to considerably higher values and thus we could precisely know and control the operation conditions. Considering also that the mixed and pure gas permeance coefficients for N_2 and CO are similar, we assume that the mixed gas permeation data has a low experimental error. Therefore it can be concluded that the decrease in the permeance coefficient for H_2 and CO_2 for the quaternary gas mixture is again determined by competitive sorption effects.

The concentration of H_2 in the permeate stream leaving the hollow fiber membrane module was of only 40 vol % meanwhile for the Matrimid hollow fiber module was of 89 vol%. At the same time, the mixed gas solubility coefficient for the various gas pairs of interest are significant lower in the PPO membranes than in the Matrimid membranes. The H_2/N_2 and H_2/CO mixed gas selectivity varied from 20 to 5 and 15 to 5 respectively in the pressure range studied for the quaternary gas mixture $H_2/CO_2/N_2/CO$ = 1616.3/5.3/60.7/17.8. The H_2/CO_2 mixed gas selectivity was constant with a value of 2.

3.4. CONCLUSIONS

Distinct gas separation performance was found for Matrimid asymmetric hollow fibers with respect to planar membranes fabricated from the same polyimide.

First, in the case of pure gas permeation, a higher membrane substructure resistance for CO_2 than for H_2 followed by N_2 and CO determines a higher H_2/CO_2 and lower H_2/N_2 and H_2/CO ideal separation factors with respect to planar membranes. As in planar dense membrane, the permeance of H_2, N_2 and CO remained almost constant with pressure (up to 10 bar) with average values of 65.8 GPU for H_2, 0.93 GPU for N_2 and 1.63 GPU for CO. In contrast, the permeance of CO_2 strongly increased with pressure, with values of 13.4 GPU at 2 bar and 19.1 GPU at 10 bar, showing a contrary behavior to planar membranes. This is related to an CO_2 induced accelerated plasticization in the asymmetric hollow fiber membrane due to a much thinner dense skin layer compared to the usual thickness of an planar dense membrane (0.1 ~ 0.5 μm compared to 30 μm).

In the case of the permeation of gas mixtures, as in planar membranes, competitive sorption effects determine a decrease in the permeation of H_2 with respect to pure gas. For H_2/CO_2 binary mixtures this depression is higher than for H_2/N_2 or H_2/CO mixtures for which is almost null. Due to plasticization induced higher transport rate of H_2, in H_2/CO_2 mixtures, the decay in the permeation of H_2 is not as high as in planar membranes. A maximum decay in the permeation of H_2 of 21 % was reached at H_2 fugacity below 1 bar at 6 bar total feed pressure, meanwhile in the planar membrane the decay was of 46 % in the same conditions.

These results determine a strong variation of the mixed gas H_2/CO_2 selectivity with the composition and pressure with values ranging from 4.6 to 3.1. These values are higher than in planar membranes, the minimum of 3 reached for the composition H_2/CO_2 = 20/80 at 10 bar total pressure of 3.1 approaches the average value of 2.9 obtained in planar membrane.

In contrast with Matrimid hollow fiber membranes the use PPO hollow fiber membranes gives considerably higher gas permeability at the expense of lower gas selectivities. Thus, when a feed gas mixture with a similar composition to the post combustion dry flue gas coming from carbon black manufacturing was used (H2/CO2/N2/CO = 16.3/5.3/60.7/17.8 vol %), the H_2 concentration in the permeate of a PPO hollow fiber module was of only 40 vol % meanwhile the Matrimid hollow fiber module was more than double (87 - 89 vol %).

It makes clear that use of thick film data to design or select membrane materials only gives a rough approximation of the performance that might be realized in practice. Our results suggest that for H_2 mixtures that contain CO_2 the hollow fiber membrane performance is better than of planar membranes.

References

1. M. Mulder, Basic Principles of Membrane Technology, Kluwer Academic Publishers, Dordrecht, 1996.

2. D.M. Koenhen, M.H.V. Mulder, C.A. Smolders, Phase separation phenomena during the formation of asymmetric membranes., J. Appl. Polym. Sci. 21 (1977) 199-215.

3. J.G. Wijmans, J. Kant, M.H.V. Mulder, C.A. Smolders, Phase separation phenomena in solutions of polysulfone in mixtures of a solvent and a nonsolvent: relationship with membrane formation, Polymer 26 (1985) 1539-1545.

4. R.W. Baker, Membrane Technology and Applications, 2nd edition ed., John Wiley and Sons, New York, 2004.

5. P.Z. Çulfaz, Microstructured hollow fibers and microsieves: Fabrication, characterisation and filtration applications, PhD dissertation, University of Twente (2010).

6. D.T. Clausi, W.J. Koros, Formation of defect-free polyimide hollow fiber membranes for gas separations, J. Membr. Sci. 167 (2000) 79-89.

7. S.S. Hosseini, N. Peng, T.S. Chung, Gas separation membranes developed through integration of polymer blending and dual-layer hollow fiber spinning process for hydrogen and natural gas enrichments, J. Membr. Sci. 349 (2010) 156-166.

8. G. Dong, H. Li, V. Chen, Factors affect defect-free Matrimid® hollow fiber gas separation performance in natural gas purification, J. Membr. Sci. 353 (2010) 17-27.

9. J.S. Lee, W. Madden, W.J. Koros, Antiplasticization and plasticization of Matrimid® asymmetric hollow fiber membranes-Part A. Experimental, J. Membr. Sci. 350 (2010) 232-241.

10. T. Visser, N. Masetto, M. Wessling, Materials dependence of mixed gas plasticization behavior in asymmetric membranes, J. Membr. Sci. 306 (2007) 16-28.

11. S.A. McKelvey, D.T. Clausi, W.J. Koros, A guide to establishing hollow fiber macroscopic properties for membrane applications, J. Membr. Sci. 124 (1997) 223-232.

12. H.-Y. Zhao, Y.-M. Cao, X.-L. Ding, M.-Q. Zhou, Q. Yuan, Effects of cross-linkers with different molecular weights in cross-linked Matrimid 5218 and test temperature on gas transport properties, J. Membr. Sci. 323 (2008) 176-184.

13. S. Shishatskiy, C. Nistor, M. Popa, S.P. Nunes, K.V. Peinemann, Polyimide asymmetric membranes for hydrogen separation: Influence of formation conditions on gas transport properties, Adv. Eng. Mat. 8 (2006) 390-397.

14. H.-W. Rösler, Membrantechnolgie in der Prozessindustrie - Polymere Membranwerkstoffe, Chem. Ing. Tech. 77 (2005) 485-503.

15. S.S. Hosseini, M.M. Teoh, T.S. Chung, Hydrogen separation and purification in membranes of miscible polymer blends with interpenetration networks, Polymer 49 (2008) 1594-1603.

16. Y. Zhang, I.H. Musselman, J.P. Ferraris, K.J. Balkus Jr., Gas permeability properties of Matrimid® membranes containing the metal-organic framework Cu-BPY-HFS, J. Membr. Sci. 313 (2008) 170-181.

17. O.C. David, D. Gorri, A. Urtiaga, I. Ortiz, Mixed gas separation study for the hydrogen recovery from H2/CO/N2/CO2 post combustion mixtures using a Matrimid membrane, J. Membr. Sci. 378 (2011) 359-368.

18. S.B. Carruthers, G.L. Ramos, W.J. Koros, Morphology of integral-skin layers in hollow-fiber gas-separation membranes, J. Appl. Polym. Sci. 90 (2003) 399-411.

19. E.P. Favvas, G.C. Kapantaidakis, J.W. Nolan, A.C. Mitropoulos, N.K. Kanellopoulos, Preparation, characterization and gas permeation properties of carbon hollow fiber membranes based on Matrimid® 5218 precursor, J. Mater. Process. Technol. 186 (2007) 102-110.

20. L. Jiang, T.-S. Chung, D.F. Li, C. Cao, S. Kulprathipanja, Fabrication of Matrimid/polyethersulfone dual-layer hollow fiber membranes for gas separation, J. Membr. Sci. 240 (2004) 91-103.

21. X. Ding, Y. Cao, H. Zhao, L. Wang, Q. Yuan, Fabrication of high performance Matrimid/polysulfone dual-layer hollow fiber membranes for O2/N2 separation, J. Membr. Sci. 323 (2008) 352-361.

22. S. Sridhar, R.S. Veerapur, M.B. Patil, K.B. Gudasi, T.M. Aminabhavi, Matrimid polyimide membranes for the separation of carbon dioxide from methane, J. Appl. Polym. Sci. 106 (2007) 1585-1594.

23. S.B. Carruthers, G.L. Ramos, W.J. Koros, Morphology of integral-skin layers in hollow-fiber gas-separation membranes, J. Appl. Polym. Sci. 90 (2003) 399-411.

24. Y. Huang, D.R. Paul, Effect of film thickness on the gas-permeation characteristics of glassy polymer membranes, Ind. Eng. Chem. Res. 46 (2007) 2342-2347.

25. V. Abetz, T. Brinkmann, M. Dijkstra, K. Ebert, D. Fritsch, K. Ohlrogge, D. Paul, K.-. Peinemann, S.P. Nunes, N. Scharnagl, M. Schossig, Developments in membrane research: From material via process design to industrial application, Adv. Eng. Mat. 8 (2006) 328-358.

26. J.C. Jansen, M. Macchione, E. Drioli, On the unusual solvent retention and the effect on the gas transport in perfluorinated Hyflon AD® membranes, J. Membr. Sci. 287 (2007) 132-137.

27. M. Peer, S.M. Kamali, M. Mahdeyarfar, T. Mohammadi, Separation of hydrogen from carbon monoxide using a hollow fiber polyimide membrane: Experimental and simulation, Chem. Eng. Technol. 30 (2007) 1418-1425.

28. D.T. Clausi, S.A. McKelvey, W.J. Koros, Characterization of substructure resistance in asymmetric gas separation membranes, J. Membr. Sci. 160 (1999) 51-64.

29. I. Pinnau, W.J. Koros, Relationship between substructure resistance and gas separation properties of defect-free integrally skinned asymmetric membranes, Ind. Eng. Chem. Res. 30 (1991) 1837-1840.

30. T. Matsuura, Synthetic Membranes and Membrane Separation Processes, 1st ed., CRC Press, Inc., Florida, 1993.

31. J.O. Hirschfelder, C.F. Curtiss, R.B. Bird, The Molecular Theory of Gases and Liquids, John Wiley & Sons, Inc., New York, 1954.

32. J.M.S. Henis, M.K. Tripodi, Composite hollow fiber membranes for gas separation: The resistance model approach, J. Membr. Sci. 8 (1981) 233-246.

33. S. Matteucci, Y. Yampolskii, B.D. Freeman, I. Pinnau, Transport of Gases and Vapors in Glassy and Rubbery Polymers, in: Materials Science of Membranes for Gas and Vapor Separation, John Wiley & Sons, Ltd, 2006, pp. 1-47.

34. K. Simons, K. Nijmeijer, J.G. Sala, H. van der Werf, N.E. Benes, T.J. Dingemans, M. Wessling, CO2 sorption and transport behavior of ODPA-based polyetherimide polymer films, Polymer 51 (2010) 3907-3917.

35. A. Bos, I.G.M. Pünt, M. Wessling, H. Strathmann, Plasticization-resistant glassy polyimide membranes for CO2/CO4 separations, Sep. Purific. Technol. 14 (1998) 27-39.

36. A. Bos, I.G.M. Pünt, M. Wessling, H. Strathmann, CO2-induced plasticization phenomena in glassy polymers, J. Membr. Sci. 155 (1999) 67-78.

37. M. Wessling, M. Lidon Lopez, H. Strathmann, Accelerated plasticization of thin-film composite membranes used in gas separation, Sep. Purific. Technol. 24 (2001) 223-233.

38. T. Visser, M. Wessling, Auto and mutual plasticization in single and mixed gas C3 transport through Matrimid-based hollow fiber membranes, J. Membr. Sci. 312 (2008) 84-96.

39. T. Visser, G.H. Koops, M. Wessling, On the subtle balance between competitive sorption and plasticization effects in asymmetric hollow fiber gas separation membranes, J. Membr. Sci. 252 (2005) 265-277.

40. W.J. Koros, R.T. Chern, V. Stannett, H.B. Hopfenberg, Model for permeation of mixed gases and vapors in glassy polymers., J. Polymer Sci. Part A-2, Polymer physics 19 (1981) 1513-1530.

41. J.S. Lee, W. Madden, W.J. Koros, Antiplasticization and plasticization of Matrimid® asymmetric hollow fiber membranes. Part B. Modeling, J. Membr. Sci. 350 (2010) 242-251.

42. K. Haraya, K. Obata, N. Itoh, Y. Shndo, T. Hakuta, H. Yoshitome, Gas permeation and separation by an asymmetric polyimide hollow fiber membrane, J. Membr. Sci. 41 (1989) 23-35.

43. W.J. Koros, D.G. Woods, Elevated temperature application of polymer hollow-fiber membranes, J. Membr. Sci. 181 (2001) 157-166.

44. D.M. Sterescu, D.F. Stamatialis, E. Mendes, J. Kruse, K. Rätzke, F. Faupel, M. Wessling, Boltom-modified poly(2,6-dimethyl-1,4-phenylene oxide) gas separation membranes, Macromolecules 40 (2007) 5400-5410.

45. D.M. Sterescu, D.F. Stamatialis, E. Mendes, M. Wübbenhorst, M. Wessling, Fullerene-modified poly(2,6-dimethyl-1,4-phenylene oxide) gas separation membranes: Why binding is better than dispersing, Macromolecules 39 (2006) 9234-9242.

46. A. Alentiev, E. Drioli, M. Gokzhaev, G. Golemme, O. Ilinich, A. Lapkin, V. Volkov, Y. Yampolskii, Gas permeation properties of phenylene oxide polymers, J. Membr. Sci. 138 (1998) 99-107.

Chapter IV

ON THE IMPROVED ABSORPTION OF CARBON MONOXIDE IN THE IONIC LIQUID 1-HEXYL-3-METHYLIMIDAZOLIUM CHLOROCUPRATE

ABSTRACT

This chapter is focused on the design of a liquid phase system to be used in facilitated transport-supported ionic liquid membranes (SILMs) for the recovery of carbon monoxide from gaseous streams based on the ability of CO molecules to form π complexation bonds with Cu^{+} ion. As liquid phase we propose the use of the ionic liquid 1-hexyl-3-methyl-imidazolium chlorocuprate prepared by the direct mixture of copper(I) chloride (CuCl) with 1-hexyl-3-methylimidazolium chloride ([hmim][Cl]).

A comprehensive look at the reaction mechanism and the equilibrium parameters obtained from the experimental characterization of the physical and chemical solubility of carbon monoxide in pure [hmim][Cl], and in mixtures CuCl/[hmim][Cl] is presented.

The gas equilibrium solubility experimental work was carried out in the CuCl/[hmim][Cl] molar ratio range from 0 to 0.75, temperature from 273.15 K to 303.15 K and pressures up to 20 bar.

The values of the Henry's law constant for the physical solubility of CO in [hmim][Cl] changed from 15.3 x 10^{-3} mol kg^{-1} bar^{-1} to 2.7 x 10^{-3} mol kg^{-1} bar^{-1} as the temperature increased from 273.15 to 293.15 K.

The chemical solubility of CO in the reactive ionic liquid media increased with the increase of the concentration of CuCl, with the increase of pressure and with temperature decreasing. In the operation range of variables the maximum absorption of CO was of 2.26 mol kg^{-1} that was reached working at 20 bar, at CuCl/[hmim][Cl] molar ratio of 0.75 and 273.15 K. These results are higher than reported values obtained using the COSORB solution (a $CuAlCl_4tol_2$ complex in toluene) that is industrially used [1], although the operation conditions are not equal. In the latter case, 1.3 mol l^{-1} CO was absorbed at CO pressures of 1 bar and a of 1.7 mol l^{-1} initial complex concentration.

An equilibrium model that quantitatively describes the occurring reactions and phenomena was proposed and the equilibrium reaction parameters where determined. The calculated enthalpy of complexation presents a negative value of -13.4 kJ mol^{-1} and a reaction equilibrium constant, *Keq* with values between 8.5 and 16 Kg mol^{-1} in the temperature range from 30 ^{o}C to 0 ^{o}C was found.

4.1. THE SELECTION OF CARRIER/SOLVENT SYSTEM

The facilitated transport of carbon monoxide by a metallic salt was already studied in literature with water-based systems [2-4] and organic-based systems [5-8]. In Chapter I, Table I – 7 of this thesis, a brief overview was made and the following extra remarks can be added.

Water based systems:

The solubility of CuCl in water is of only 1.1 x 10^{-3} M [4]. It can be increased by forming cationic complexes with ammonia, amines and other basic ligands (alkanol amines or pyridine). This basic ligands also acts as stabilizing agents for Cu(I) against disproportion (Eq. IV – 1) since in aqueous systems, the cupric state of copper is more stable than the cuprous state [9]. The competitive equilibrium in such systems may be described by the following reactions:

$$2Cu(I) \overset{K1}{\leftrightarrow} Cu^0 + Cu(II) \qquad (\text{IV} - 1)$$

$$Cu(II) + aL \overset{K2}{\leftrightarrow} Cu(II)L_a \qquad (\text{IV} - 2)$$

$$Cu(I) + bL \overset{K3}{\leftrightarrow} Cu(I)L_a \qquad (\text{IV} - 3)$$

$$4Cu(I) + 4H^+ + O_2 \overset{K4}{\leftrightarrow} 4Cu(II) + 2H_2O \qquad (\text{IV} - 4)$$

where *L* can be any type of ligand (a solvent, an anion, or a stabilizing agent)

Copper(II) effectively coordinates ligands classified as hard bases, such as water, in reaction (IV - 2). This consumes cupric ions and drives reaction (IV - 1) to further disproportionation of cuprous ions. To prevent depletion of Cu(I) by this mechanism, reaction (IV - 3) must compete with reaction (IV - 2). This can be accomplished via introduction of a stabilizing ligand to retain Cu(I) in the monovalent state. For example, at 25 °C the ratio between the equilibrium constant of the forward and backward reaction, *K1* = 10^6 in pure water; in aqueous ammonia solution, *K1* = 10^{-2} [10]. On the other hand, adding a complexing stabilizing ligand decreases cuprous ion activity. A lower activity indicates decreased interactions with carbon monoxide. Another disadvantage of water based systems is that

cuprous solutions are oxidized to the inactive cupric state when exposed to air (Eq. IV – 4)

Cuprous salts also dissolve readily in acidified solutions of various electrolytes with the formation of anionic complexes in the form $CuCl_x^{1-x}$, where x is determined by the ratio of the salt concentrations. The solubility of CuCl in aqueous solutions of KCl and HCl is in the range of 0.02 -0.2 M at 1.0 M KCl and 0.1 M HCl [11]. The use of chloride ions as stabilizing ligands for the cuprous ion has several advantages. The chloride electrolytes have a negligible vapor pressure, minimizing the loss of solution components, they are less readily oxidized by oxygen and the disproportionation reaction is retarded.

Noble et al. reported that facilitation factors as high as 20 were obtained in the transport of carbon monoxide when acidified solutions of CuCl were used as liquid media for supported liquid membranes [2]. The facilitation factor increased with an increase of total carrier concentration and a decrease in feed gas concentration. A parasitic binding mechanism was proposed:

$$CuCl_x^{1-x} + CO \rightleftarrows COCuCl_x^{1-x} \qquad (\text{IV} - 5)$$

$$CuCl_x^{1-x} + COCuCl_x^{1-x} \rightleftarrows CO(CuCl_x^{1-x})_2 \qquad (\text{IV} - 6)$$

Organic based systems:

Nonaqueous copper solutions exhibit minimal disproportionation of cuprous ions and do not require addition of a stabilizing ligand [9]. This is because the solvent often acts as a weakly complexing stabilizer. However, an inert (oxidizer-free) atmosphere must be maintained and moisture must be excluded to prevent disproportionation. Nearly all cuprous salts are quite soluble in coordinating solvents such as alkyl thiocyanates, alkyl sulfides, amines, and nitriles. Solubility in aromatics is generally low. However, cuprous aluminum tetrachloride ($CuAlCl_4$) and cuprous tetrafluoroborate ($CuBF_4$) form stable complexes with aromatics, leading to high solubility. Cuprous trifluoroacetate ($CuCF_3COO$) dissolves in aromatics due to its low crystal energy [10].

The facilitated transport of carbon monoxide with Cu(I) dissolved in DMSO using N-methylimidazole as ligand gave ideal separation factors CO/N_2 of 36.9 [7].

Ligand-Cu(I) complexes based on various pyridylalkylamine compounds in THF as solvent have been proposed [12] with a structure example shown in the Figure IV - 1. High equilibrium constant with values ranging from 660-56000 M were found.

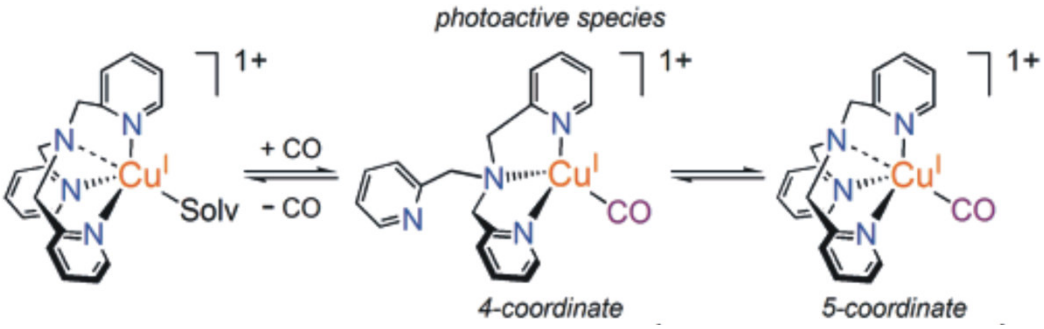

Figure IV – 1. The reaction scheme pyridylalkylamine Cu(I) based complexes with carbon monoxide.

On the principle of improving the utility of metal ions as carriers via the formation of complex ions, other metal ions have also been used. Complex ions derived from macrocycles or other polydentate are attractive for studying the facilitated transport since they are relatively stable [13].

The reversible binding of CO with several Fe(II) tetraimine complexes in benzonitrile was studied by Sharma et al. and Koval et al. [5, 6], and it was shown that the nitrile solvent ligands could be replaced by other ligands such as CO as illustrated in Figure IV – 1. The stability of this complex towards oxidation in benzonitrile suggested the possibility of constructing of a membrane system for the separation of CO from O_2. Low facilitation factors of maximum 2.8 were found for the Fe(Me_2Ph_2TIM) complex carrier and it was determined that the limiting factor is the solubility of the carrier.

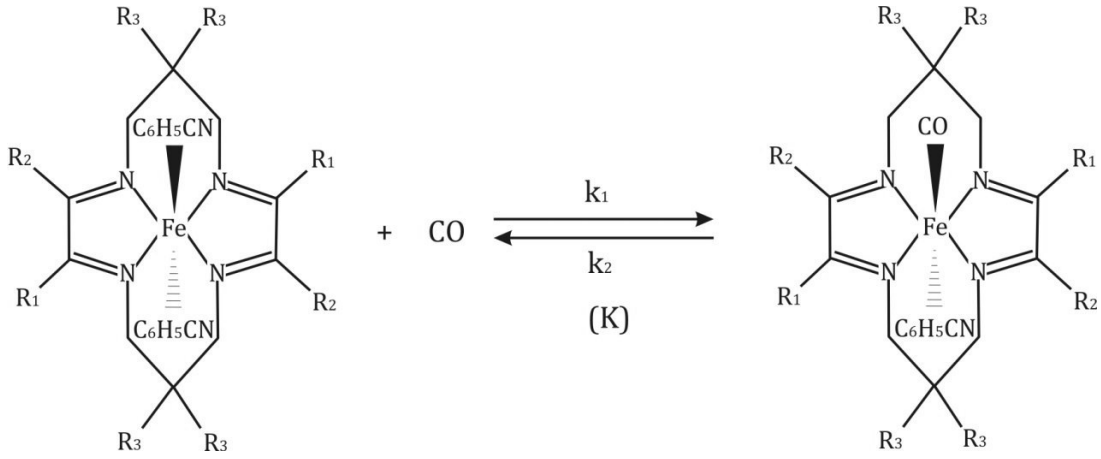

Figure IV – 2. Structural drawing depicting the reversible 1:1 complexation reaction of Fe(II) macrocyclic complex ions with carbon monoxide, $R_1=R_2=CH_3$, $R_3=H$ for Fe(TIM), $R_1=R_2=R_3=CH_3$ for Fe(Me_4TIM) and $R_1=CH_3$, $R_2=C_6H_5$, $R_3=H$ for Fe (Me_2Ph_2TIM) and $R_1=R_2=R_3=C_6H_5$ for Fe(Ph_4TIM).

The separation of carbon monoxide from gas mixtures using palladium based complexes with 1,1,2- trichloroethane (TCE) as solvent has also been proposed in a continuous bench-scale apparatus consisting of absorber and stripper columns [8] (see Figure IV - 3). The binding of CO become stronger in turn as I is replaced by Br, Cl, or NCO. Only the Pd based complexes with Cl and Br had a satisfactory solubility of 0.15 and 0.035 M respectively.

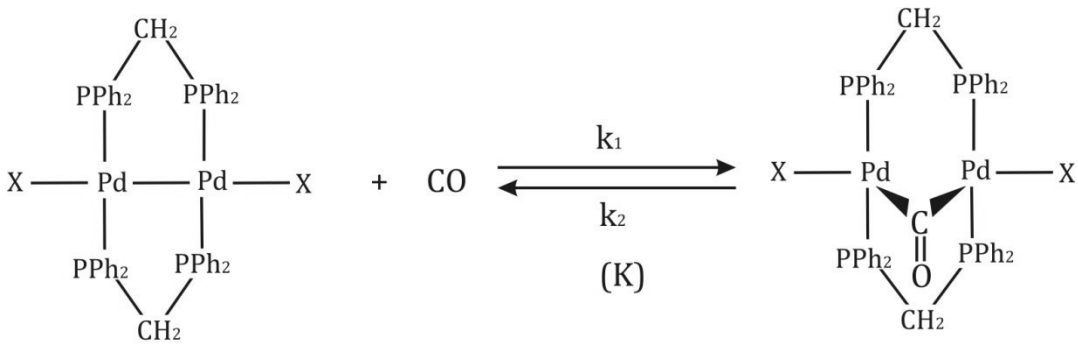

Figure IV – 3. Structural drawing depicting the reversible 1:1 complexation reaction of Pd(0) macrocyclic complex with carbon monoxide

Mass transfer, rather than reaction, was indicated as the controlling rate process. The kinetics were fast and high reaction equilibrium constant were obtained (35000 M^{-1}) for Br based complex.

As described in Chapter I, section 1.3.1. of this thesis, the key issue in developing a supported liquid membrane separation process based on reversible complexation is the ability of a carrier to bind selectively to the permeant with appropriate equilibrium (K_{eq}) and rate constants. The complexation reaction should be strong enough in order be selective, but should also be reversible in order for the permeating species to be released at the permeate side of the membrane. From the values reported in table I – 7 it can be concluded that the magnitude of K_{eq} for copper (I) based systems is within the recommended range by Noble et al [6] (2 x 10^2 M^{-1} and 2 x 10^4 M^{-1}) and therefore copper (I) can be considered as the optimum carrier in membrane facilitated transport.

Once the optimum metal carrier was identified, a solvent must be chosen also. We decided to use an ionic liquid as solvent as means to obtain stable SILMs due to their negligible vapor pressure and their high viscosity which could avoid solvent loss due to evaporation and also, slow down the displacement of the liquids from the micropores under pressure.

Possible ionic liquids/carrier agent systems are summarized in Table IV – 1. These systems are based on the supposition that the use as solvent of an imidazolium - based ionic liquid with the identical anion as the anion of the copper based salt will provide a successful solubilization for the copper (I) salt.

For instance it is known that the mixture of CuCl with [Rmim][Cl] leads to a so called Lewis acid-based ionic liquid [14] where the metal halide CuCl acts as Lewis acid. Depending on the relative proportions of CuCl and [Rmim][Cl] several anionic species are present at equilibrium [15-18] as reported in Table IV - 2. Consequently [Rmim][Cl] based ionic liquids are able to solubilize high amounts of CuCl.

Therefore, at this early research stage of the chemical absorption of carbon monoxide in ionic liquid media we decided to start with CuCl/[Hmim][Cl] based systems. The drawback of these types of ionic liquids is their water sensitivity; they absorb water from the atmosphere leading to their decomposition by hydrolysis [14]. Also HCl can be formed, giving them a highly corrosive character. Furthermore, Cu (I) can disproportionate to Cu(II) and Cu^0. To avoid these phenomena, the samples should be stored in vacuum sealed vials or be quickly used after preparation. However these absorption media are by far more stable than aqueous medium.

Table IV – 1. Possible ionic liquids/carrier agent systems to be used as liquid phase in SILMs

Ionic liquid	Carrier agent
1-hexyl-3-methylimidazolium chloride, [Hmim][Cl] 1-octyl-3-methylimidazolium chloride, [Omim][Cl] 1-decyl-3-methylimidazolium chloride, [Dmim][Cl]	Copper (I) chloride
1-hexyl-3-methylimidazolium bromide, [Hmim][Br] 1-octyl-3-methylimidazolium bromide, [Omim][Br] 1-decyl-3-methylimidazolium bromide, [Dmim][Br]	Copper (I) bromide
1-hexyl-3-methylimidazolium iodide, [Hmim][I]	Copper (I) iodide
1-octyl-3-methylimidazolium trifluoromethanesulfonate, [Omim] [OTf] 1-hexyl-3-methylimidazolium trifluoromethanesulfonate, [Hmim][OTf] 1-decyl-3-methylimidazolium trifluoromethanesulfonate, [Dmim][OTf]	Copper(I) trifluoromethanesulfonate toluene or benzene complex: $[CuOTf]_2 \cdot C_6H_6$ or $[CuOTf]_2 \cdot C_7H_9$
1-hexyl-3-methylimidazolium acetate, [Hmim][Ac]	Copper (I) acetate
1-butyl-3-methylimidazolium trifluoroacetate, [Bmim][TfAc]	Copper (I) trifluoroacetate

Table IV - 2. Anionic species presented in equilibrium at various molar ratios of CuCl and [Rmim][Cl] [15-18]

Molar ratio CuCl/[Rmim][Cl]	Environment	Reactions	Predominant anionic specie
[0/1→1/1]	Basic (chlorine rich)	$CuCl^- + Cl^- \rightleftarrows CuCl_2^-$	$CuCl_3^{2-}$
		$CuCl_2^- + nCl^- \rightleftarrows CuCl_{2+n}^{(1+n)-}$ (n = 1, 2)	
1/1	Neutral	$CuCl^- + Cl^- \rightleftarrows CuCl_2^-$	$CuCl_2^-$
		$2\,CuCl_2^- \rightleftarrows Cu_2Cl_3^- + Cl^-$	
[1/1→2/1]	Acidic (chlorine poor)	$CuCl_2^- + y\,CuCl^- \rightleftarrows Cu_{1+y}Cl_{2+y}^-$	$Cu_2Cl_3^-$
		(y = 1, etc.)	$Cu_3Cl_4^-$

To conclude, this chapter studies the reactive absorption of CO in a copper (I) based ionic liquid formed by the mixture of [hmim][Cl] and CuCl salt. The equilibrium parameters, namely the equilibrium constant, K_{eq}, and the enthalpy of reaction, ΔH_r, were evaluated. In addition new data for the physical solubility of CO in [hmim][Cl] are also reported.

4.2. EQUILIBRIUM MODELING

In order to describe the absorption process, an equilibrium model able to explain quantitatively the occurring reactions and phenomena is required. First we considered that all the copper (I) introduced in the reaction medium was active for the π-complexation reaction and that the strength of the π-bound formed between CO and the different copper based anionic species present at equilibrium (see Table IV - 2) was equal. Additionally, $CuCl_3^{2-}$ is the most abundant copper chloride species in the molar ratio of CuCl/[hmim][Cl] lower than 1 used in this work, according to [15-18] (see Table IV – 2). Figure IV – 4 shows a schematic depiction of the physical followed by the chemical solubility of CO in the ionic liquid media considered as absorption mechanism as previously found for propylene reactive absorption in Ag^+/BmimBF$_4$ based systems [19].

The equilibrium reaction is shown in Equation IV - 7 for the case of a 1:1 copper (I):carbon monoxide complex.

$$CO + CuCl_3^{2-} \rightleftharpoons Cu(CO)Cl_3^{2-} \qquad \text{(IV–7)}$$

The equilibrium constant is defined as follows,

$$K_{eq} = \frac{[Cu(CO)Cl_3^{2-}]}{[CO]\cdot[CuCl_3^{2-}]} \qquad \text{(IV–8)}$$

where $[Cu(CO)Cl_3^{2-}]$ is the equilibrium concentration of the complex, $[CO]$ is the equilibrium concentration of physically absorbed carbon monoxide into the ionic liquid and $[CuCl_3^{2-}]$ is the equilibrium concentration of copper (I) chloride anionic specie.

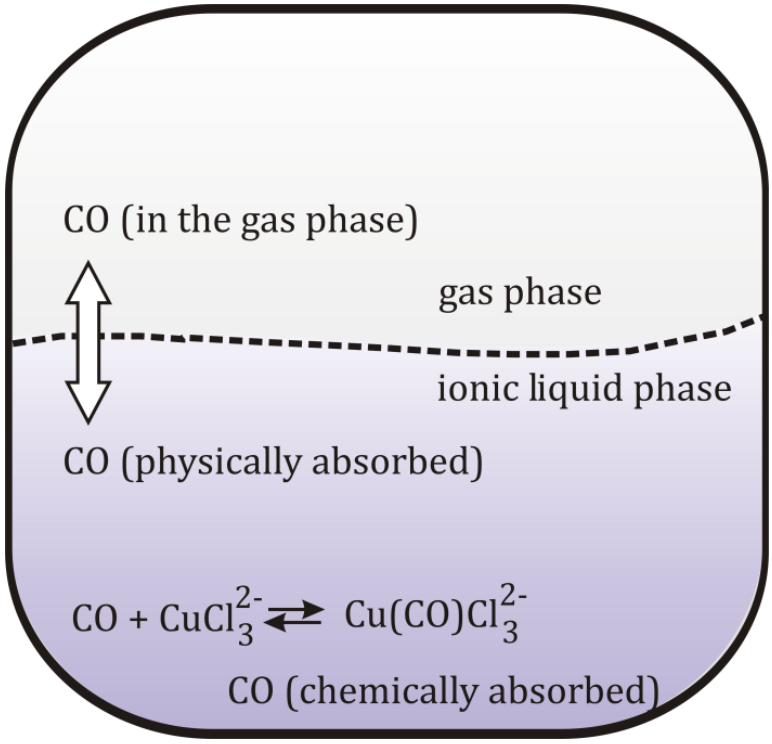

Figure IV – 4. Schematic depiction of physical followed by chemical solubility of CO in ionic liquid media

The concentration of physically dissolved carbon monoxide is given by the Henry's law,

$$[CO] = k_H p_{CO} \qquad \text{(IV–9)}$$

where k_H is the Henry's constant (mol kg^{-1} bar^{-1}) and p_{CO} is the partial pressure of carbon monoxide that is equal to the total pressure in the system when working with pure gases.

The following mass balance equations can be applied, where the equilibrium concentration of the total absorbed CO, $[CO]_T$, is obtained from the sum between the physically and chemically absorbed gas, Equation (IV - 10), and the concentration of copper (I) chloride anionic specie at equilibrium is given by the difference between the initial concentration, $[CuCl_3^{2-}]_0$, and the equilibrium concentration of the complex specie, Equation (IV – 11).

$$[CO]_T = k_H p_{CO} + [Cu(CO)Cl_3^{2-}] \quad \text{(IV–10)}$$

$$[CuCl_3^{2-}] = [CuCl_3^{2-}]_0 - [Cu(CO)Cl_3^{2-}] \quad \text{(IV–11)}$$

The equilibrium constant for the 1:1 reaction can be calculated by substitution of the mass balance equations (Eqs. IV - 10 and IV - 11) into Eq. (IV - 8), and subsequent rearrangement to a linear form, Eq. (IV - 12). The use of a linear expression allows an easy calculation for the K_{eq} by plotting multiple values obtained from the same absorption experiment (as described in the experimental methodology section) of $[CO]_T - k_H p_{CO}$ against $k_H p_{CO}(k_H p_{CO} + [CuCl_3^{2-}]_T - COT$ and obtaining K_{eq} value from the slope.

$$[CO]_T = K_{eq} k_H p_{CO}(k_H p_{CO} + [CuCl_3^{2-}]_0 - [CO]_T) + k_H p_{CO} \quad \text{(IV–12)}$$

The equilibrium constant of the complexation reaction is a function of temperature that can be described by means of the van't Hoff equation (Eq. IV - 13):

$$\frac{d \ln K_{eq}}{d(1/T)} = -\frac{\Delta H_r}{R} \quad \text{(IV–13)}$$

where T is the temperature (K), ΔH_r is the enthalpy of reaction (kJ mol^{-1}) and R is the gas constant (kJ mol^{-1} K^{-1}).

4.3. EXPERIMENTAL PROCEDURE

4.3.1. Preparation of the copper (I) based ionic liquid

The ionic liquid 1-hexyl-3-methyl-imidazolium chlorocuprate used in this study was prepared by mixing under vacuum for 1 h at 353.15 K specific amounts of 1-hexyl-3-methylimidazolium chloride ([hmim][Cl]) and CuCl in the autoclave of the absorption set - up, prior to the absorption experiments. This procedure is similar to the one used by Huang et al. [17]. In that work they used heptane as a copartner of the mixture. Heptane had the purpose of acting as a "blanket" against hydrolysis [14] and thus avoiding working in a dry box. We assume that simply working under vacuum avoids hydrolysis.

Our preparation procedure serves also to degas and remove trace amounts of volatile impurities and thus no further purification step is needed prior to the absorption experiments. Purified copper (I) chloride (>99%) was purchased from Sigma Aldrich and was used without further purification. 1-hexyl-3-methyl-imidazolium chloride was purchased from Iolitec with a purity of 99%. The main impurities are water (0.795%) and 1-methylimidazole (<1%) as stated in the certificate of analysis.

4.3.2. Absorption set-up and measuring procedure

The experimental method is based on the isochoric saturation technique in which a known quantity of the gaseous solute is put in contact with a known quantity of degassed solvent at a constant temperature inside a reactor with known volume. When thermodynamic equilibrium is attained, the pressure above the liquid solution remains constant and is directly related to the solubility of the gas in the liquid medium [20].

The apparatus and measurement procedure are basically identical to those described in a previous publication by our research group [19]. The apparatus is shown in Figure IV – 5. The equipment consisted of a stainless steel vessel (upper chamber) used to transfer a known amount of gas into a stainless steel autoclave (lower chamber, Autoclave Engineering) for gas–liquid contacting. The volume of the lower chamber (V_{low}) was of 66.3 cm^3 and the volume of the upper chamber (V_{upp}) was of 133.7 cm^3. The temperature of the system is controlled by computer

controlled electric heating. The temperature was monitored with a type K thermocouple (Assy) placed inside the lower chamber and automatically maintained within 0.1 K of the setpoint. The pressure in the upper chamber is measured by a digital pressure gauge (Omega Engineering DPG1000B-30V100G with an accuracy of ±0.017 bar), and the autoclave pressure was measured with a pressure transducer (Hirsschmann12B-GDM0-25 bar with an accuracy of ±0.001 bar).

The feed line was of pure carbon monoxide or nitrogen (Air Liquide, 99.97% purity) and it was connected to the upper chamber of the set-up. The stirring speed was 2500 rpm.

The absorption of CO in pure [hmim][Cl] and mixtures of [hmim][Cl] with CuCl was carried-out at pressures lower than 8 bar. After performing this first set of experiments the experimental set-up was adapted to stand higher pressures and some specific experiments were done at pressures up to 20 bar. This was done by changing the original digital pressure gauge with a new one (Keller 303010.0005, Leo 2/-1-30bar/81021, with an accuracy of 0.1% at full scale) capable to withstand higher pressures. All the other components of the set-up were left unchanged.

In order to begin the absorption experiments, a volume of 15 ml of the ionic liquid media was prepared into the autoclave. Air was removed from both the upper and the lower chambers by a vacuum pump. The valve separating the two chambers was closed. Then, a gas sample was injected into the upper chamber to a desired initial pressure. The valve separating the two chambers was opened and the absorption process began. The stirrer was turn on and the ionic liquid was constantly stirred throughout the experiment. The system pressure changed with time due to the system approaching equilibrium, the pressure readings were recorded in 5 min intervals. The equilibrium was reached when the pressure remained unchanged for at least 10 minutes. The final pressure difference was used to determine the number of moles of gas absorbed. A mass balance was used to relate the initial moles of gas in the upper chamber with moles of gas in the total volume at any given time during the experiment. For one experiment multiple experimental points were obtained by repeating the procedure described several times at increasing initial pressures up to a final pressure which was tried to be the same for all experiments.

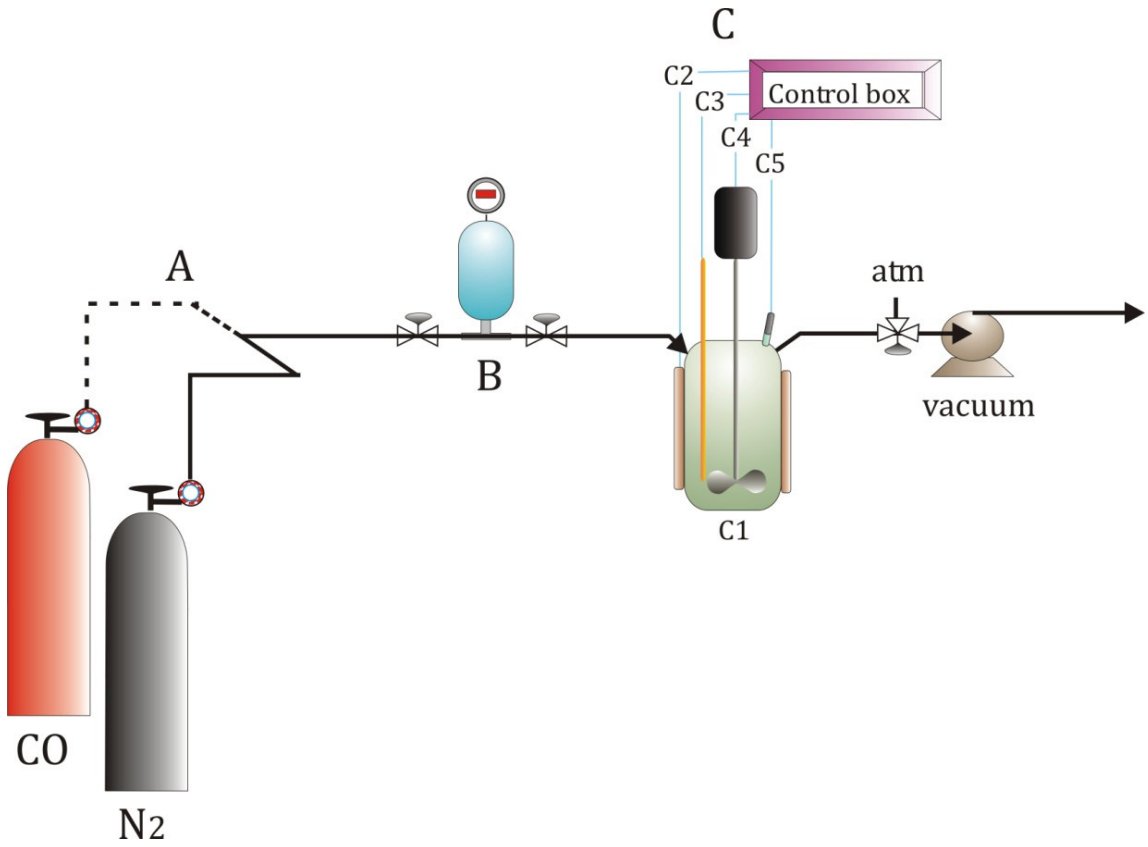

Figure IV – 5. The experimental set – up for the study of gas solubility in liquids: (A) feed line; (B) upper chamber steel vessel with digital pressure gauge; (C1) lower chamber vessel (C2) heating jacket; (C3) thermocouple; (C4) magnetic stirrer and (C5) pressure transducer.

When the reaction medium was to be reused in a new absorption experiment a desorption step was needed to get the regeneration of the mixture. The desorption was done by means of increasing the temperature up to 333.15 K and under complete vacuum conditions. The complete regeneration of the reaction medium was checked by consecutive repetition of a similar absorption run. In order to assure the correct preparation of the ionic liquid we repeated absorption experiments with different solutions of the same concentration. The results were replicable and the weighted standard deviation is shown in the figures as error bars.

4.3.3. Experimental measurements and operation conditions

The solubility of CO and N_2 was measured in pure [hmim][Cl], and the solubility of N_2 was also measured in CuCl/[hmim][Cl] reactive medium (molar ratio of 0.5) at temperatures of 273.15, 283.15 and 293.15 K in the pressure range up to 20 bar.

The absorption of CO in mixtures of [hmim][Cl] with CuCl was studied at temperatures from 273.15 K to 303.15 K, molar ratios CuCl/[hmim][Cl] from 0.13 to 0.75 and at pressures of up to 8 bar. Then, the saturation of reaction media was verified at pressures up to 20 bar at a temperature of 273.15 K and for a molar ratio CuCl/[hmim][Cl] of 0.75.

The viscosity of various samples of pure [hmim][Cl] and its mixtures with CuCl at molar ratio $n_{CuCl}/n_{[hmim][Cl]}$= 0.5 and 0.75 was measured in the temperature range from 268.15 to 303.15 K using a Fungilab Alpha Series viscometer.

4.4. RESULTS AND DISCUSSION

4.4.1. The physical solubility of CO and N2 in pure [hmim][Cl] and in the reactive CuCl/[hmim][Cl] medium

Figure IV – 6 shows the experimental results for the physical absorption of N_2 and CO in the ionic liquid medium. The solubility of both gases increased linearly with the system pressure and decreased with the system temperature.

In pure [hmim][Cl] the solubility parameters of CO and N_2 present similar values at the three temperatures under study, the slight differences are within the experimental error range.

The physical solubility of CO in the reactive CuCl/[hmim][Cl] medium cannot be measured directly. Therefore, it was estimated by analogy with the physical solubility of N_2 in the reactive CuCl/[hmim][Cl] medium. This estimation is based on a comparative study between the physical solubilities of N_2 and CO in the non-reactive [hmim][Cl] medium: N_2 has a molecular weight and size similar to CO. This approach has already been used in the literature by Hogendoorn et al. [1] to estimate the physical solubility of CO in reactive mixtures. A similar analogy is commonly used between N_2O and CO_2 [21-24]. Due to the very low gas solubility we were unable to measure the physical solubility of CO and N_2 at temperatures higher than 303.15 K.

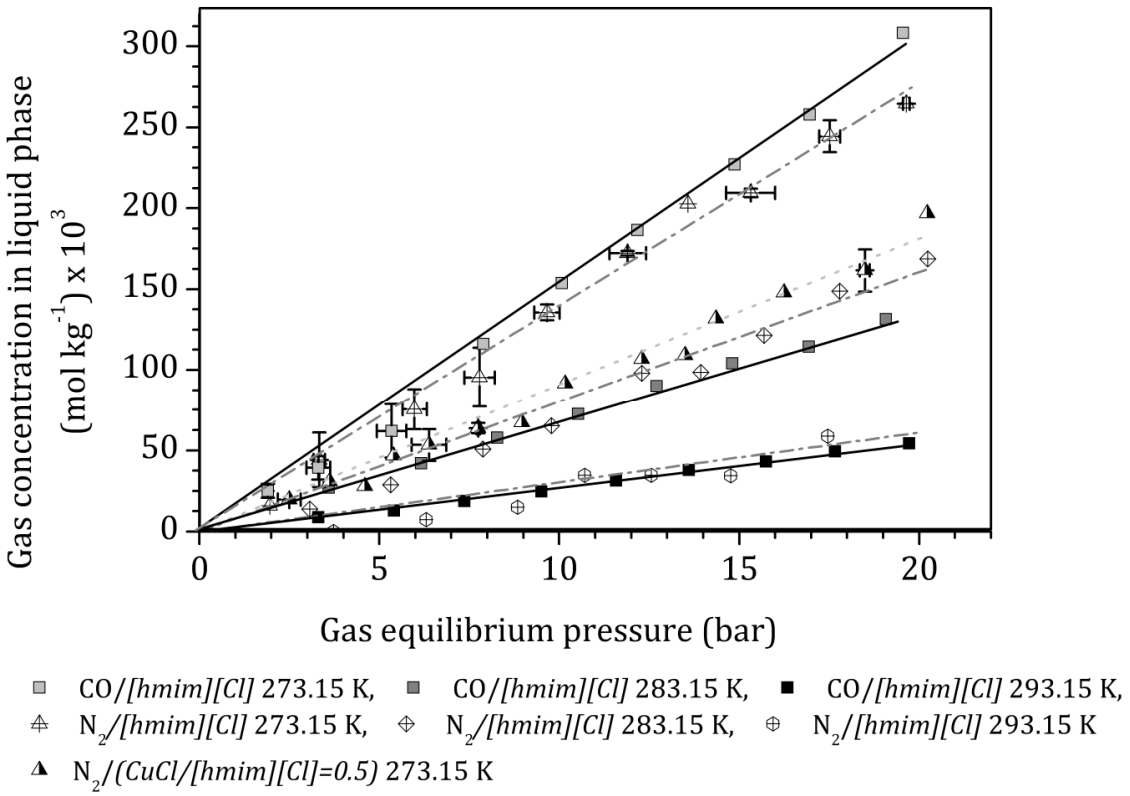

Figure IV – 6. Physical solubility of CO and N_2 in HmimCl and of N_2 in [Hmim][Cl]/CuCl = 0.5 molar ratio.

Table IV – 3. CO and N_2 solubility results in ionic liquid medium

Gas	Ionic liquid medium	T (K)	k_H x 10^3 (mol kg^{-1} bar^{-1})	ΔH_{sol} (kJ mol^{-1})	R^2
CO	*[hmim][Cl]*	273.15	15.3	-57.3	0.992
		283.15	6.8		0.996
		293.15	2.7		0.996
N_2	*[hmim][Cl]*	273.15	13.8	-56.6	0.990
		283.15	7.0		0.963
		293.15	2.9		0.849
N_2	$n_{CuCl}/n_{[hmim][Cl]}$ = 0.5	273.15	8.9	- 21.4	0.979
		283.15	5.4		0.986
		293.15	4.7		0.946

The resulting values of the Henry's constants (k_H) were obtained by fitting the experimental data to a straight line according to Eq. 3 (including 0,0 point) using a least squares regression method (see Table IV - 3).

The resulting values of the k_H for CO physical absorption in [hmim][Cl] are between 15.3 and 2.7 x 10^{-3} mol kg^{-1} bar^{-1} and seem coherent with literature data listed in Table IV - 4 for other imidazolium based ionic liquids.

Studies of the solubility of CO in [bmim][PF_6] by different research groups and different experimental techniques report data with a deviation higher that 100%. CO is a gas with a considerably lower solubility than CO_2 [25] and has been reported as undetectable by other authors when a gravimetric microbalance was used [26]. The resulting ideal separation factor obtained in the present work for carbon monoxide to nitrogen around 1 is within the range from 0.5 to 2.9 reported by J. Blath et al. in other ionic liquids [27].

When measuring the physical solubility of N_2 in the reactive medium formed by a mixture of CuCl/[hmim][Cl] of 0.5 molar ratio at 273.15 K, the data revealed that N_2 absorption is lower than in pure [hmim][Cl], $k_{H,N_2/(CuCl/[hmim][Cl])=0.5}$ = 8.9 x 10^{-3} mol kg^{-1} bar^{-1} in comparison with $k_{H,N_2/[hmim][Cl]}$=13.8 x 10^{-3} mol kg^{-1} bar^{-1}. Thus we can predict that the physical solubility of CO in the reactive medium is similar to the solubility of N_2.

The temperature dependence of the Henry's law constant was studied using a van't Hoff-type equation [34].

$$k_H(T) = k_{H_0} e^{-\frac{\Delta H_{sol}}{RT}} \qquad \text{(IV–14)}$$

Figure IV - 7 shows the values of the Henry's constant for CO and N_2 absorption in pure [hmim][Cl] and for N_2 in the mixture CuCl/[hmim][Cl] = 0.5 molar ratio plotted against temperature. The k_H experimental values in pure [hmim][Cl] are overlapped for CO and N_2.

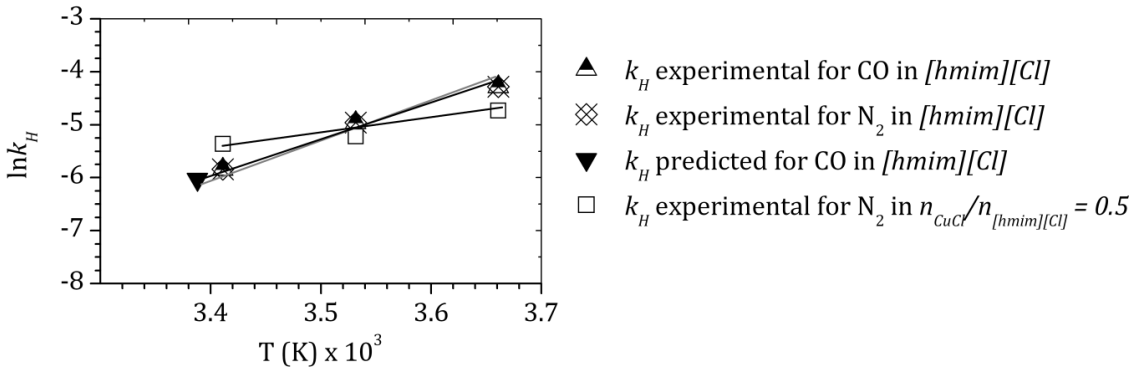

Figure IV - 7. CO and N_2 Henry's constant as function of temperature in [hmim][Cl] ionic liquid and in chlorocuprate based ionic liquid at a molar ratio CuCl/[hmimCl][Cl] of 0.5.

Table IV – 4. Literature data for the solubility of CO in ionic liquids

RTIL (abbrev.)										Experimental technique	Ref.
[bmim] [PF_6]	T	293.2	313.8	334.5	354.35	374.15				Bubble point	[28]
	$k_H x10^3$	1.81	1.79	1.82	1.79	1.79					
	T	283.16	293.2	303.38	303.41	313.33	323.25	333.57		Isochoric saturation	[29]
	$k_H x10^3$	0.40	0.39	0.39	0.39	0.38	0.37	0.36			
	T	295								NMR spectroscopy	[30]
	$k_H x10^3$	1.1									
[bmim] [CH_3SO_4]	T	293.15		333.15		373.15	413.15			Bubble point	[31]
	$k_H x10^3$	1.07		1.13		1.19	1.27				
[bmim] [Tf_2N]	T	303.2	313.11		323	333				Isochoric saturation	[32]
	$k_H x10^3$	5.27	5.23		4.71	4.22					
[bmim] [BF_4]	T	283.18	293.16	303.39	313.27	313.28	323.2	333.09	343	Isochoric saturation	[20]
	$k_H x10^3$	3.11	3.10	3.07	3.07	3.10	3.03	3.04	3.01		
[hmim] [Tf_2N]	T			333						Isochoric saturation	[27]
	$k_H x10^3$			4.44							
	T	293.3		333.2		373.25	413.15			Bubble point	[33]
	$k_H x10^3$	3.13		2.98		2.88	2.91				
[hmim] [Cl]	T	273.15	283.15	293.15						Isochoric saturation	This work
	$k_H x10^3$	15.3	6.8	2.7							

As means of validation of our experimental data, apart from the experimental results, we also included the predicted value of the Henry's constant at 295.15 K for CO in [hmim][Cl]. This was based on the use of a simple correlation between the Henry's constant and the molar volume of an ionic liquid developed by Camper et al [35]. In the case of CO the simulation fits satisfactorily well to the experimental data.

The standard solvation enthalpy for gas-to-liquid transfer (ΔH_{sol}) obtained from the fitting of the experimental data to Eq. (IV - 8) is of -57.3 kJ mol^{-1} for CO and of -56.6 kJ mol^{-1} for N_2.

In all the reported cases in the literature (see Table IV - 4) the solubility of CO in ionic liquids shows a very low variation with temperature. It usually decreases as temperature increases and the resulting values of the solvation enthalpy are negative and close to zero.

The solvation enthalpy is related to the molecular interactions in the solution and can give clues regarding to the molecular mechanism of solvation. Probably the higher magnitudes of solvation enthalpies found in our study can be related to a different molecular mechanism of solvation. It was reported that the solubility of CO is dependant on the nature of the ionic liquid [30].

The forces and interactions that govern the dissolution and solubility of different components in ionic liquids also control the melting points of ionic liquids. In general, increases in anion size give rise to reductions in the melting points of salts through reduction of the Coulombic attraction contribution to the lattice energy of the crystal and increasing covalency of the ions. In addition, large ions permit charge delocalization, reducing the overall charge density further on [14].

For example, with increasing radius of the anion, from Cl^- to $[PF_6]^-$ to $[Tf_2N]^-$, the melting points of the 1-ethyl-3-methylimidazolium-based ionic liquids decrease from 334.1 K to 307.1 K to 240.1 K [36]. In addition, [hmim][Cl] is significantly more viscous than second generation ionic liquids that incorporate large anionic groups. Thus, the solubility of solutes in [hmim][Cl] can be slightly different as well.

4.4.2. The total solubility of CO in the reactive CuCl/[hmim][Cl] medium

The influence of CuCl concentration and temperature over the total solubility (chemical and physical) of CO in the reactive medium formed by the mixture of CuCl and [hmim][Cl] is shown in Figure IV – 8.

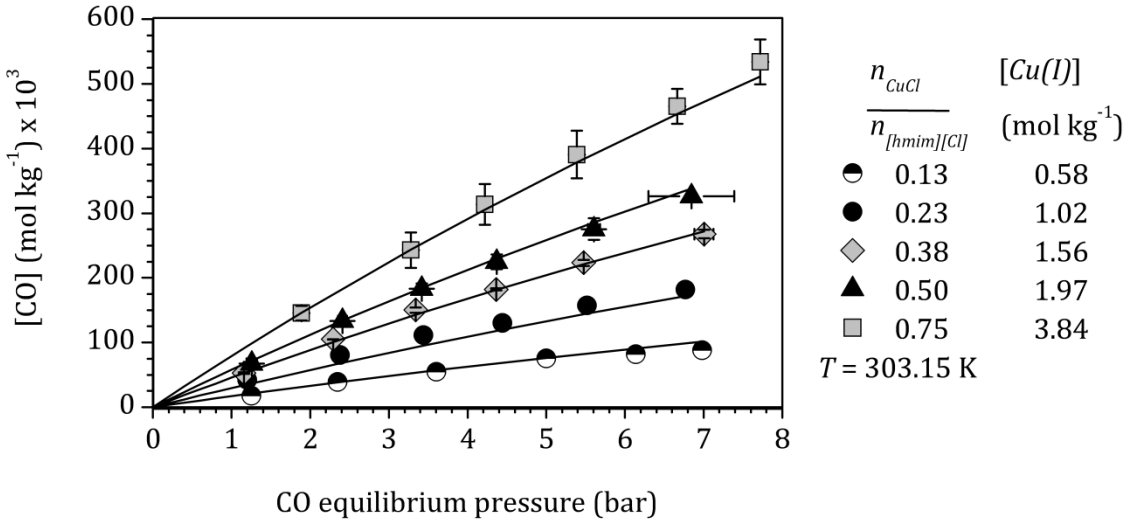

Figure IV - 8. Carbon monoxide solubility in copper(I)-based ionic liquid at various molar ratios CuCl/[hmim][Cl] and constant temperature of 303.15 K. Experimental data and simulated results (lines).

It is observed that at higher concentrations of CuCl, the solubility of CO increases significantly. For operation pressures lower than 8 bar, the physical solubility is negligible in comparison with the total solubility and therefore the total solubility represents actually the chemical one.

The maximum solubility obtained was of 534 x 10^{-3} mol kg^{-1} at a molar ratio CuCl/[hmim][Cl] of 0.75, 7.7 bar CO pressure and 303.15 K.

The solid lines represent the simulated data provided by the equilibrium model together with the fitting parameters that where obtained as it will be described later on.

The total solubility of CO in the chlorocuprate-based ionic liquid media is expected to increase as the concentration of CuCl in [hmim][Cl] increases. At the same time, the viscosity of the mixture is function of the CuCl content. In literature it was reported that the viscosity of CuCl/[emim][Cl] based ionic liquid mixtures presents a minimum at a molar ratio of 1 from which it begins to increase [18]. Therefore we did not further increased the concentration of CuCl and for molar ratios CuCl/[hmim][Cl] from 0.13 to 0.75, CuCl was soluble in [hmim][Cl].

The viscosity of various samples of pure [hmim][Cl] and its mixtures with CuCl was measured at different temperatures. From Figure IV - 9 it is observed that the viscosity strongly decreases as the amount of added salt increases. At the highest

molar ratio CuCl/[hmim][Cl] the viscosity decreased by two orders of magnitude with respect to the pure ionic liquid. While the pure ionic liquid is transparent and highly viscous at room temperature the copper (I)-based ionic liquid has a brown yellow colour. The room temperature ionic liquids based on the mixtures of various metal chloride and alkyl-imidazolium chloride are eutectic mixtures [14] and have in general lower melting points, lower viscosity, higher density and higher specific conductivity than the pure alkyl-imidazolium chloride. These differences have been attributed in the literature to charge delocalization of [hmim] and $CuCl_x^{-x+1}$ (x = 2, 3) [29].

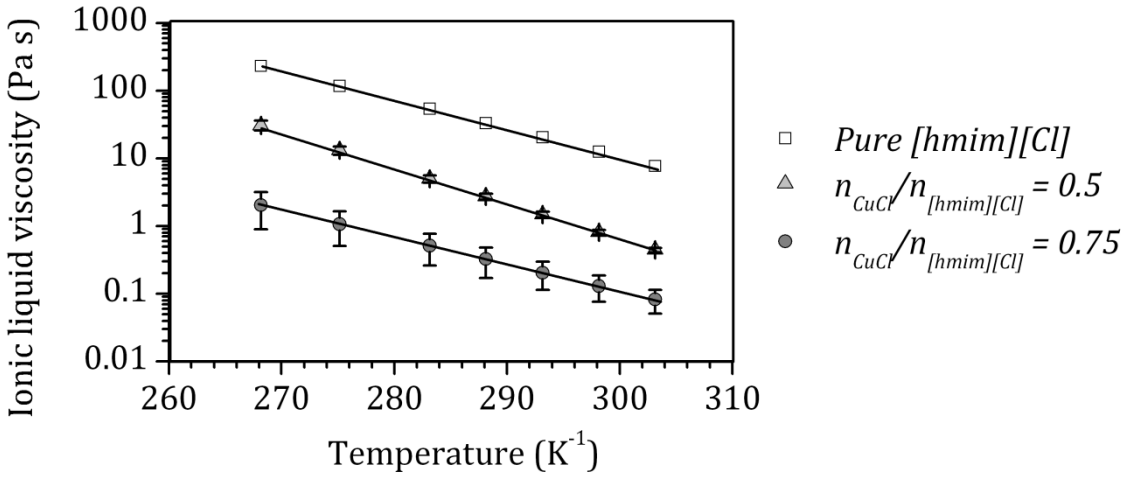

Figure IV - 9. Viscosity of pure [hmim][Cl] and its mixtures with CuCl at various molar ratios.

These differences in viscosity imply improved mass transfer coefficients for copper (I)-based ionic liquid medium in comparison with the ionic liquid alone which are important aspects involved in the design of absorption equipment.

In Figure IV – 10 the influence of temperature on the total solubility of CO is shown at a constant molar ratio between CuCl/[hmim][Cl] of 0.5.

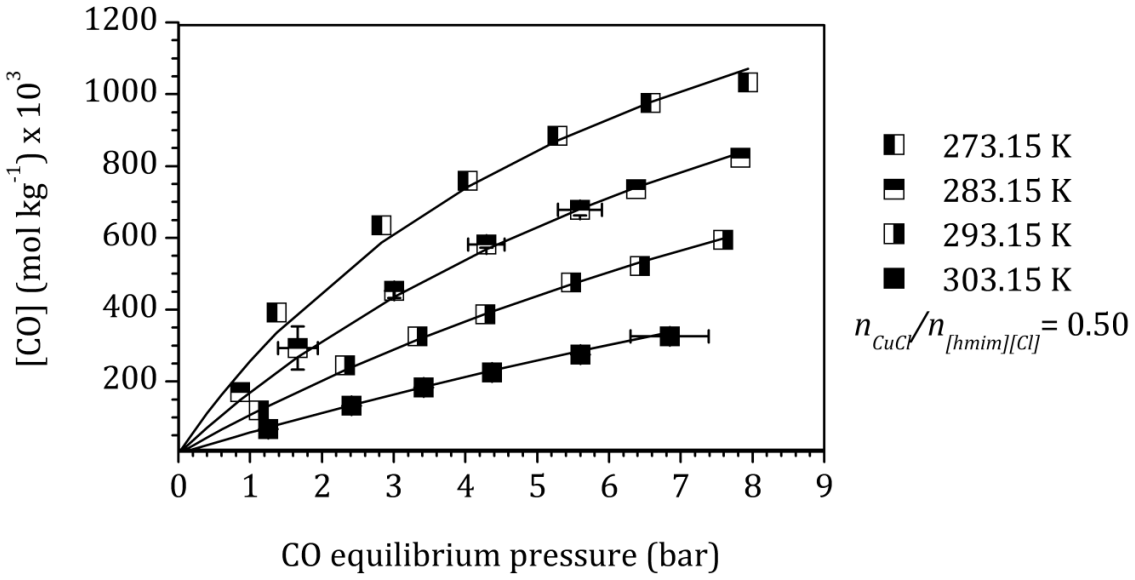

Figure IV - 10. Carbon monoxide solubility in copper(I) based ionic liquid at constant molar ratio CuCl/[hmim][Cl] = 0.5 and various temperatures. Experimental data and simulated results (lines).

It is observed that the temperature presents a strong influence over the solubility of CO which is considerably higher at lower temperatures; therefore it is concluded that the complexation reaction is exothermic.

Here also, the total solubility is practically equal to the chemical solubility. For instance at 293.15 K the total carbon monoxide solubility in the copper (I) based ionic liquid is 32 times the physical solubility when compared with the values obtained at a pressure of 7.4 bar.

It can be also observed that even for the highest solubility of CO of 1032 x 10^{-3} mol kg^{-1}, the molar ratio between the total absorbed carbon monoxide (i.e. at the final experimental system pressure) and the initial concentration of copper (I) chloride (n_{CO}/n_{CuCl}) has the value of 0.52, as shown in table 5, far lower than unity. This indicates that if all the copper (I) added to the solution was active for complexation and a 1:1 stoichiometry is considered, the saturation of the reaction medium was not reached, and therefore there are still copper (I) species which have not reacted.

In the experimental range of variables used in this work, the ideal separation factor (α) between CO and N_2 obtained from the ratio of the pure gases solubilities in the reactive medium reached high values that were between 24 and 6. In the calculation of the values of the ideal separation factor $\alpha_{CO/N2}$ we used the solubility

of N_2 obtained in the reactive medium at CuCl/[hmim][Cl] molar ratio of 0.5 (data listed in Table IV - 2) and the chemical solubility data for CO obtained from the mixtures CuCl/[hmim][Cl] with a molar ratio from 0.13 to 0.75, temperatures from 273.15 to 303.15 K and pressures below 8 bar. Similar to the chemical solubility for CO, the CO/N_2 ideal separation factor increases as the pressure increases, as the concentration of CuCl increases and as the temperature decreases. The maximum value of 24 was obtained at 2.5 bar equilibrium pressure, 273.15 K and 0.5 molar ratio CuCl/[hmim][Cl].

The ratio between the total number of moles of absorbed CO and the initial number of moles of CuCl, n_{CO}/n_{CuCl}, are listed in Table IV – 4. The total number of absorbed CO is calculated from the final equilibrium pressure of the last experimental point. It is shown that for pressures below 8 bar and at constant temperature of 303.15 K, this ratio presents almost no variation with the concentrations of CuCl in [hmim][Cl] leading to an average value of 0.167. Much CuCl remains available for the complexation reaction and, thus at these operation conditions the saturation of the reaction medium is far from being reached. When temperature decreases the ratio n_{CO}/n_{CuCl} increases up to a value of 0.52 that is reached at 273.15 K.

In comparison with a study of Huang et al [17] these values are significantly higher in all cases. These authors studied the absorption of thiophene in [bmim][Cl]/CuCl ionic liquids and based on their reported experimental conditions and results we have been able to calculate a value of 7.49×10^{-3} for $n_{thiophene}/n_{CuCl}$ molar ratio.

Table IV – 4. The CO saturation study of the complexating agent

Temperature (K)	$n_{CuCl}/n_{[hmim][Cl]}$	Final pressure (bar)	n_{CO}/n_{CuCl}	K_{eq} (mol^{-1} Kg)
273.15	0.50	7.94	0.523	16.00
281.15	0.50	7.83	0.417	13.43
293.15	0.50	7.59	0.303	12.05
	0.75	7.72	0.145	
	0.50	6.85	0.167	
303.15	0.38	7.01	0.169	8.49
	0.23	6.77	0.175	
	0.13	6.98	0.151	

In an attempt to verify the saturation of the reaction medium an additional experiment was performed at pressure up to 20 bar, at the lowest temperature studied of 273.15 K and for a molar ratio CuCl/[hmim][Cl] of 0.75. As shown in Figure IV - 11 at higher pressures the physical solubility begins to present values that cannot be ignored and therefore the chemical solubility was calculated as the difference between the total solubility and the physical one.

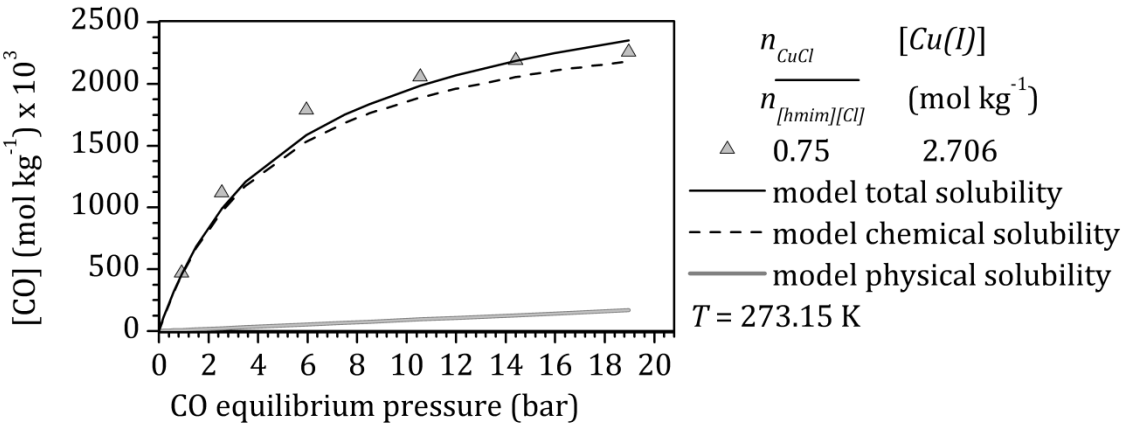

Figure IV - 11. Saturation of the copper (I) based reaction media at pressure up to 20 bar and 273.15 K.

The physical solubility of CO in the reaction medium was considered to be analogous to the solubility of N_2 in the chlorocuprate ionic liquid. It can be observed that the major part of the chemical complexation reaction took part at pressures below 10 bar. Beyond this point, the final slope of the equilibrium curve remains constant but still higher than the slope of the physical solubility, therefore the chemical complexation is still active. The final ratio between the absorbed number of moles of carbon monoxide and the initial number of moles of copper (I) was of 0.9, a value close to 1 that corresponds to the maximum saturation described by a 1:1 stoichiometric ratio.

The equilibrium constant defined in Eq. (IV - 8) was calculated from the slope of the linear regression line obtained from the fitting of the experimental data to Eq. (IV - 12) as shown in Figure 12. In all cases, the physical solubility of CO was considered to be analogous to the solubility of N_2 in the reactive medium. As shown in Table IV - 4 the equilibrium constant of the complexation reaction is dependant on temperature, increases as the temperature decreases, and has values comprised between 16.0 kg mol^{-1} and 8.49 kg mol^{-1} in the temperature range from 273.15 K to 303.15 K.

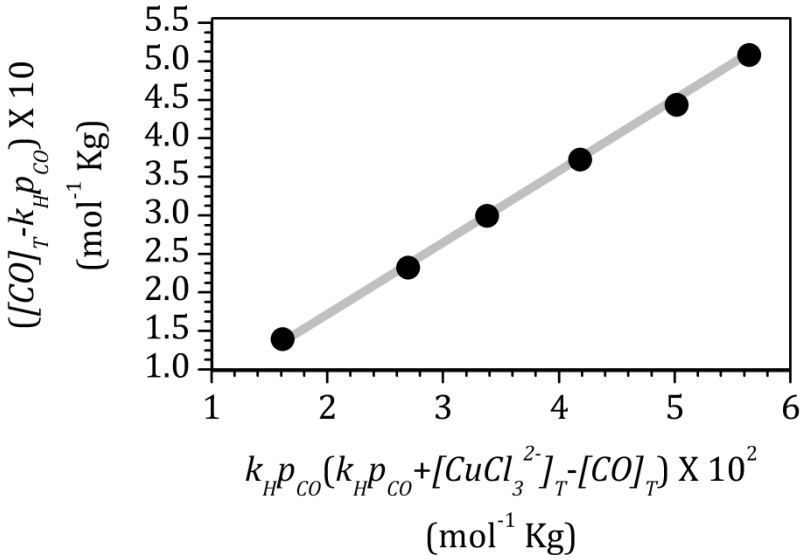

Figure 12. Fitting to Eq. (IV - 12) of the experimental data obtained at 303.15 K and a molar ratio $n_{CuCl}/n_{[hmim][Cl]}$ = 0.75.

Applying the van't Hoff relation expressed in Eq. (IV - 13) with 298.15 K as reference temperature the resulting enthalpy of complexation has a negative value of ΔH_r = -13.4 kJ mol^{-1}. This indicates that the complex formation between CO and copper (I) chloride anionic species present in the ionic liquid 1-hexyl-3-methylimidazolium-chlorocuprate media is an exothermic process.

The goodness of the data fitting is presented in the parity graph shown in Figure IV - 13. Predicted concentration values, $[CO]_{sim}$, are plotted versus experimental data, $[CO]_{exp}$, for results obtained at pressures lower than 8 bar and from 273.15 K to 303.15 K. All the results of $[CO]_{sim}$ fall within the interval Cexp ±10% Cexp, proving that the proposed model offers a satisfactory description of the reactive absorption equilibrium.

After the absorption experiments no precipitates or cloudiness was observed, and the mixtures stored in sealed vials were stable in time long after the experiments were carried out.

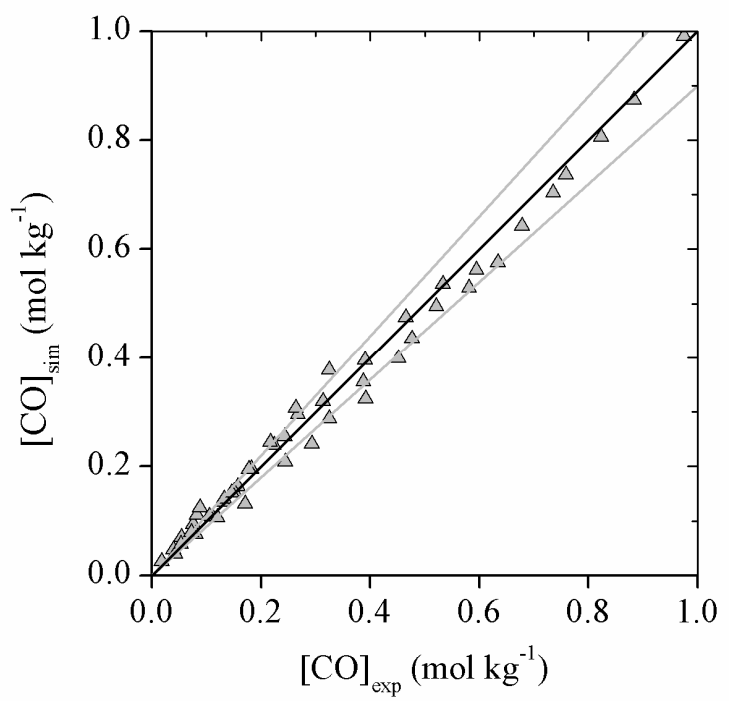

Figure IV - 13. Parity graph between experimental and simulated results of CO adsorption. Data obtained at various temperatures and CuCl/[hmim][Cl] molar ratios are included.

4.4.3. Desorption study

The future development of facilitated transport membranes for the separation of carbon monoxide depends on the reversibility of the π - complexation reaction at the low pressure side of the membrane. Considering that there is no temperature gradient across a liquid membrane we conducted a desorption study based on applying only vacuum. The complete regeneration of the reaction medium was checked by consecutive repetition of an absorption run after a desorption step consisting of complete vacuum conditions without increasing temperature as previously done. The experimental results for two absorption runs applied for a new mixture of molar ratio CuCl/[Hmim][Cl] of 0.5 at 303.15 K (Figure IV – 15) are similar and therefore we can conclude that the desorption is complete under vacuum conditions and that this liquid medium can be applied for liquid membranes formulation.

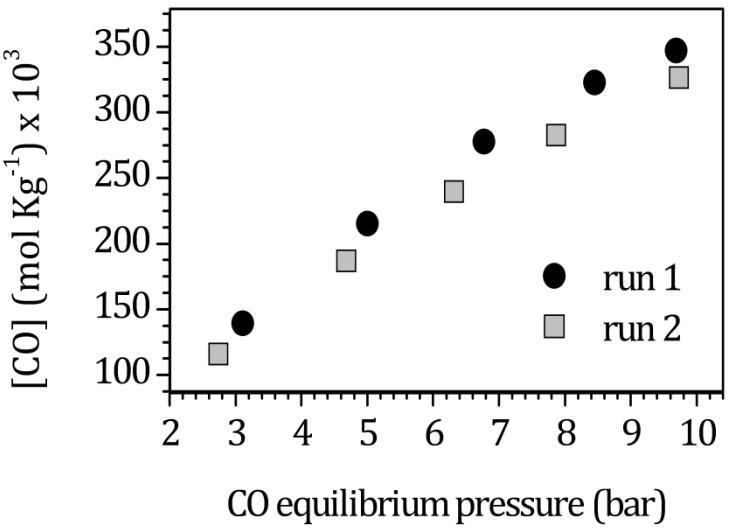

Figure IV – 15. Consecutive absorption runs for the mixture CuCl/[Hmim][Cl]=0.5 molar ratio and 303.15 K with an intermediate desorption step of only vacuum.

In this study we report the thermodynamic equilibrium for the solubility of CO in the reactive system which is enhanced at lower temperatures, as the absorption process is exothermic. In a further step the kinetics of the system will be studied, thus allowing us to determine the optimal conditions to develop the process, which should be a trade-off between this two effects.

4.5. CONCLUSIONS

In this chapter, the absorption of carbon monoxide via copper (I) complexation has been successfully carried out in the ionic liquid 1-hexyl-3-methyl-imidazolium chlorocuprate prepared by the direct mixture of copper(I) chloride (CuCl) with 1-hexyl-3-methylimidazolium chloride ([hmim][Cl]).

First, it was observed that the solubilities of both carbon monoxide and nitrogen in the pure [hmim][Cl] were very similar, with values of the Henry's constant in the range 15.3 x 10^{-3} mol kg^{-1} bar^{-1} to 2.7 x 10^{-3} mol kg^{-1} bar^{-1} as the temperature increased from 273.15 to 293.15 K.

After addition of CuCl to [hmim][Cl], the carbon monoxide absorption capacity of the ionic liquid was improved by a large factor, while nitrogen solubility was maintained in the low values previously observed for the pure [hmim][Cl]. Thus it was concluded that the CuCl/[hmim][Cl] mixture enhances the carbon monoxide absorption via the chemical π - complexation of CO with copper (I) species formed in the reactive ionic liquid. This conclusion is also supported by the increasing capacity for CO absorption at higher contents of CuCl in the reactive ionic liquid media.

The equilibrium solubility study showed that the reaction takes place in the whole pressure range studied; the major part of the complexation reaction took place at pressures up to 10 bar and was almost complete at pressures of 20 bar showing the importance of this operation variable.

The solubility of carbon monoxide in the absorbing liquid decreased at higher temperatures due to the fact that the π - complexation reaction is exothermic. The calculated enthalpy of complexation presents a negative value of -13.4 kJ mol^{-1} and a reaction equilibrium constant, K_{eq} with values between 8.5 and 16 Kg mol^{-1} in the temperature range from 30 ^{o}C to 0 ^{o}C was found.

The highest value of the ideal separation factor for carbon monoxide to nitrogen was 24, in the experimental range studied.

The two ionic liquid media used in this work were highly hygroscopic. When absorbing water from the environment, HCl was formed and thus the ionic liquid media was highly corrosive. In this case, enameled vessels should be used. Moreover Cu (I) specie is unstable when water is found within the highly hygroscopic ionic liquid and gives a disproportionation reaction to Cu(II) and metallic copper that do not react with CO. Therefore, considering on the one hand the difficulty of operating in a water free environment in a supported liquid membrane formulation and on the other hand that the equilibrium constant found

in this work was lower than the recommended one for facilitated transport through supported liquid membranes, it is proposed to look for a different carrier/ionic liquid solvent system. The a mixture between [Bmim][OTf] and the complex $[CuOTf]_2 \cdot C_6H_6$ has been identified as a candidate. This choice is based on: (i) the principle of using a Cu(I) salt as CO complexing agent and an ionic liquid that have the same anion; (ii) the use of a less hygroscopic and not corrosive ionic liquid and (iii) the use of a Cu(I) salt found in a complex form similar to the Cu(I) complex used in the COSORB process ($CuAlCl_4 toluene_2$).

References

1. J.A. Hogendoorn, W.P.M. van Swaaij, G.F. Versteeg, The absorption of carbon monoxide in COSORB solutions: absorption rate and capacity, Chem. Eng. J. Biochem. Eng. J. 59 (1995) 243-252.

2. A. Dindi, R.D. Noble, J. Yu, C.A. Koval, Experimental and modeling studies of a parasitic binding mechanism in facilitated membrane transport, J. Membr. Sci. 66 (1992) 55-68.

3. D.R. Smith, J.A. Quinn, Facilitated transport of carbon monoxide through cupprous chloride solutions., AIChE J. 26 (1980) 112-120.

4. G.S. Patil, S. Baruah, N.N. Dutta, Facilitated transport of carbon monoxide: A review, Gas Sep. Purif. 5 (1991) 2-8.

5. C.S. Sharma, P.K. Goswami, N.N. Dutta, Studies on facilitated transport of carbon monoxide using a novel iron(II) complex, Sep. Sci. Technol. 28 (1993) 1789-1797.

6. C.A. Koval, R.D. Noble, J.D. Way, B. Louie, Z.E. Reyes, B.R. Bateman, G.M. Horn, D.L. Reed, Selective transport of gaseous CO through liquid membranes using an iron(II) macrocyclic complex, Inorg. Chem. 24 (1985) 1147-1152.

7. M. Junidi, O. Munchise, K. Osama, New carrier systems for separation of carbon monoxide, Mitsubishi Kasei R&D Review 6, (1) (1992) 96-101.

8. S.E. Lyke, M.A. Lliga, R.M. Ozanich, D.A. Nelson, B.R. James, C.-. Lee, Separation of syngas components using a dissolved palladium complex, Ind. Eng. Chem. Prod. Res. Dev. 25 (1986) 517-521.

9. G.C. Blytas, Separation of unsaturates by complexing with nonaqueous solutions of cuprous salts, in: N.N. Li, J.M. Calo (Eds.), Separation and Purification Technology, Marcel Dekker, New York, 1992.

10. D.J. Safarik, R.B. Eldridge, Olefin/paraffin separations by reactive absorption: a review, Ind. Eng. Chem. Res. 37 (1998) 2571-2581.

11. N.N. Dutta, G.S. Patil, Developments in CO separation, Gas Sep. Purif. 9 (1995) 277-283.

12. H.C. Fry, H.R. Lucas, A.A.N. Sarjeant, K.D. Karlin, G.J. Meyer, Carbon monoxide coordination and reversible photodissociation in copper(I) pyridylalkylamine compounds, Inorg. Chem. 47 (2008) 241-256.

13. R.D. Noble, C.A. Koval, Review of facilitated transport membranes, in: Y. Yampolskii, I. Pinnau, B.D. Freeman (Eds.), Materials Science of Membranes, Wiley, West Sussex, England, 2006, pp. 411.

14. J.H. Davis Jr., C.M. Gordon, C. Hilgers, P. Wasserscheid, Synthesis and purification of ionic liquids, in: P. Wasserscheid, T. Welton (Eds.), Ionic Liquids in Synthesis, 2002, pp. 12-14.

15. S.A. Bolkan, J.T. Yoke, Room temperature fused salts based on copper(I) chloride-1-methyl-3-ethylimidazolium chloride mixtures. 1. Physical properties, J. Chem. Eng. Data 31 (1986) 194-197.

16. R. Luä, H. Tangbo, Z. Cao, Ab Initio calculation of room temperature ionic liquid 1-ethyl-3-methyl-Imidazolium chlorocuprate (I), J. Nat. Gas Chem. 16 (2007) 70-77.

17. C. Huang, B. Chen, J. Zhang, Z. Liu, Y. Li, Desulfurization of gasoline by extraction with new ionic liquids, Energy Fuels 18 (2004) 1862-1864.

18. J. Zhang, C.-. Huang, B.-. Chen, Y.-. Li, C.-. Qiao, Extractive desulfurization from gasoline by [BMIM] [Cu2Cl3], J. Fuel. Chem. Technol. 33 (2005) 431-434.

19. A. Ortiz, A. Ruiz, D. Gorri, I. Ortiz, Room temperature ionic liquid with silver salt as efficient reaction media for propylene/propane separation: Absorption equilibrium, Separation and Purification Technology 63 (2008) 311-318.

20. J. Jacquemin, M.F. Costa Gomes, P. Husson, V. Majer, Solubility of carbon dioxide, ethane, methane, oxygen, nitrogen, hydrogen, argon, and carbon monoxide in 1-butyl-3-methylimidazolium tetrafluoroborate between temperatures 283 K and 343 K and at pressures close to atmospheric, J. Chem. Thermodyn. 38 (2006) 490-502.

21. F. Bougie, M.C. Iliuta, CO2 absorption into mixed aqueous solutions of 2-amino-2-hydroxymethyl-1, 3-propanediol and piperazine, Ind. Eng. Chem. Res. 49 (2010) 1150-1159.

22. S.S. Laddha, J.M. Diaz, P.V. Danckwerts, The N2O analogy: The solubilities of CO2 and N2O in aqueous solutions of organic compounds, Chem. Eng. Sci. 36 (1981) 228-229.

23. G.F. Versteeg, W.P.M. Van Swaaij, Solubility and diffusivity of acid gases (CO2, N2O) in aqueous alkanolamine solutions, J. Chem. Eng. Data 33 (1988) 29-34.

24. J. Xiao, C.-H. Li, M.-. Li, Kinetics of absorption of carbon dioxide into aqueous solutions of 2-amino-2-methyl-1-propanol + monoethanolamine, Chem. Eng. Sci. 55 (2000) 161-175.

25. M.B. Shiflett, A.D. Shiflett, A. Yokozeki, Separation of tetrafluoroethylene and carbon dioxide using ionic liquids, Sep. Purif. Technol. 79 (2011) 357-364.

26. J.L. Anthony, E.J. Maginn, J.F. Brennecke, Solubilities and thermodynamic properties of gases in the ionic liquid 1-n-butyl-3-methylimidazolium hexafluorophosphate, J. Phys. Chem. B 106 (2002) 7315-7320.

27. J. Blath, M. Christ, N. Deubler, T. Hirth, T. Schiestel, Gas solubilities in room temperature ionic liquids - Correlation between RTiL-molar mass and Henry's law constant, Chem. Eng. J. 172 (2011) 167-176.

28. J. Kumełan, A.P.-S. Kamps, D. Tuma, G. Maurer, Solubility of CO in the ionic liquid [bmim][PF6], Fluid Phase Equilib. 228-229 (2005) 207-211.

29. J. Jacquemin, P. Husson, V. Majer, M.F.C. Gomes, Low-pressure solubilities and thermodynamics of solvation of eight gases in 1-butyl-3-methylimidazolium hexafluorophosphate, Fluid Phase Equilib. 240 (2006) 87-95.

30. C.A. Ohlin, P.J. Dyson, G. Laurenczy, Carbon monoxide solubility in ionic liquids: Determination, prediction and relevance to hydroformylation, Chem. Comun. 10 (2004) 1070-1071.

31. J. Kumełan, A. P.-S. Kamps, D. Tuma, G. Maurer, Solubility of the single gases H2 and CO in the ionic liquid [bmim][CH3SO4], Fluid Phase Equilib. 260 (2007) 3-8.

32. Q. Gan, Y. Zou, D. Rooney, P. Nancarrow, J. Thompson, L. Liang, M. Lewis, Theoretical and experimental correlations of gas dissolution, diffusion, and thermodynamic properties in determination of gas permeability and selectivity in supported ionic liquid membranes, Adv. Colloid Interface Sci. 164 (2011) 45-55.

33. J. Kumelan, Á.P.-S. Kamps, D. Tuma, G. Maurer, Solubility of the single gases carbon monoxide and oxygen in the ionic liquid [hmim][Tf2N], J. Chem. Eng. Data 54 (2009) 966-971.

34. K.C. Hansen, Z. Zhou, C.L. Yaws, T.M. Aminabhavi, Determination of Henry's law constants of organics in dilute aqueous solutions, J. Chem. Eng. Data 38 (1993) 546-550.

35. D. Camper, J. Bara, C. Koval, R. Noble, Bulk-fluid solubility and membrane feasibility of Rmim-based room-temperature ionic liquids, Ind. Eng. Chem. Res. 45 (2006) 6279-6283.

36. H.L. Ngo, K. LeCompte, L. Hargens, A.B. McEwen, Thermal properties of imidazolium ionic liquids, Thermochim. Acta 357-358 (2000) 97-102.

Chapter V

OVERALL CONCLUSIONS AND PROSPECTS FOR THE FUTURE
(CONCLUSIONES GLOBALES Y PERSPECTIVAS PARA EL FUTURO)

(I) The separation and recovery of H_2 using H_2 permeable polymers

The membrane-based separation and recovery of hydrogen from process gas mixtures using H_2 permeable polymers seems feasible for obtaining a H_2 rich product stream. Therefore, considering that the product can be used in several industrial applications with specified moderate to high purity requirements like: hydrodesulfuration (90% purity), hydrocracking (70-80% purity) and as fuel gas (54-60% purity) the selection of the polymeric material with appropriate permeability and selectivity coefficients is essential in the first stage. The gas mixture studied in this work is the tail gas stream obtained in the production of carbon black, and it contains mostly N_2 (60 vol%) and CO (18 vol %), both of them with low permeability through polymeric membranes, together with the highly permeable H_2 (16 vol %), CO_2 (5 vol%) and others (1 vol%). Therefore, a H_2 permeable commercial polyimide, 5(6)-amino-1-(4'aminophenyl)-1,3,-trimethylindane (Matrimid® 5218), characterized by a high selectivity towards H_2 and a reasonable gas permeability was selected as optimum polymeric material for membrane fabrication.

Pure and mixed gas permeation was studied in both planar dense films and asymmetric hollow fibers made of Matrimid and it was demonstrated that gas permeation properties of the polymer varied significantly with the gas composition and membrane morphology. The use of planar films allowed analyzing the intrinsic material behavior towards the transport of pure and mixed gases meanwhile the use of thinner and more permeable asymmetric hollow fibers allowed determining the performance that might be expected in practice.

In the case of the permeation of gas mixtures, in both planar and asymmetric hollow fiber membranes, competitive sorption effects determined a decrease in the permeation of H_2 with respect to pure gas properties. A strong dependency of the hydrogen permeability on CO_2 concentration was observed even at low concentrations of CO_2, thus for H_2/CO_2 binary mixtures this depression is considerably higher than for H_2/N_2 or H_2/CO mixtures where is almost null. The H_2 and CO_2 permeation behavior from pure, binary, ternary and quaternary mixtures ($H_2/N_2/CO/CO_2$) through planar Matrimid membrane was satisfactorily described by the “dual-mode sorption, partial immobilization” model and the unknown model sorption parameters for H_2 and for CO were obtained from the fitting of the experimental data to the proposed model.

Distinct gas separation performance was found for Matrimid asymmetric hollow fibers with respect to planar membranes fabricated from the same polyimide. Due to the thin selective layer of the asymmetric hollow fiber membrane, the accelerated plasticization of the polymer matrix occurred in the presence of CO_2,

a phenomena that determined a strong increase with pressure in the permeance coefficient of CO_2. In thick dense films the plasticization with CO_2 was not found and the permeability coefficient of CO_2 had a contrary trend and it decreased with pressure. When working with H_2/CO_2 mixtures the plasticization with CO_2 of the asymmetric hollow fiber membrane induced a higher transport rate of H_2. Therefore the decay in the permeation of H_2 in H_2/CO_2 mixtures was not as high in hollow fibers as in planar membranes. A maximum decay in the permeation of H_2 of 21.3 % was reached using hollow fibers at H_2 fugacity below 1 bar and a total feed pressure of 6 bar, meanwhile in the planar membrane the decay was of 45.5 % in the same conditions.

Therefore, it makes clear that use of thick film data to design or select membrane materials only gives a rough approximation of the performance that might be realized in practice. Our results suggest that for H_2 mixtures that contain CO_2 the hollow fiber membrane performance is better than the one obtained with planar membranes.

The pure and mixed gas permeation was analised using also a commercial asymmetric hollow fiber made of a much more permeable and more resistant to plasticization polymer, polyphenylenoxide (PPO). In contrast with Matrimid hollow fiber membranes the use PPO hollow fiber membranes gives considerably higher gas permeability at the expense of much lower gas selectivities. Thus, when a feed gas mixture with a similar composition to the post combustion dry flue gas generated in the carbon black manufacturing was used ($H_2/CO_2/N_2/CO$ = 16.3/5.3/60.7/17.8 vol %), the H_2 concentration in the permeate of a PPO hollow fiber module was of only 40 vol % meanwhile the Matrimid hollow fiber module was more than double (87 - 89 vol %).

(II) The separation and recovery of CO by means of chemical complexation

The selective removal by a membrane technology of CO from a mixture that majorly consists of N_2 is difficult using polymeric membranes since the permeation (diffusivity and solubility) properties of these two gases are similar. Then it was determined that a viable approach could be the use of a reactive supported liquid membrane system where the selective removal of CO can be obtained by facilitated transport with a proper carrier. Two essential properties were considered for the selection of the proper carrier agent/liquid solvent system: (i) a copper (I) salt was selected as carrier due to the π-complexation properties of Cu(I) with carbon monoxide and (ii) a room temperature ionic liquid (RTIL) was selected as solvent

due to its negligible volatility that is needed in order to avoid solvent evaporation and membrane instability.

The absorption of carbon monoxide via copper (I) complexation was successfully carried out in the ionic liquid 1-hexyl-3-methyl-imidazolium chlorocuprate prepared by the direct mixture of copper (I) chloride (CuCl) with 1-hexyl-3-methylimidazolium chloride ([hmim][Cl]). The equilibrium solubility study showed that the reaction takes place in the whole pressure range studied (0-20 bar); the major part of the complexation reaction took place at pressures up to 10 bar and it was almost completed at pressures of 20 bar showing the importance of this operation variable.

The solubility of carbon monoxide in the absorbing liquid decreased at higher temperatures due to the fact that the π - complexation reaction is exothermic. The calculated enthalpy of complexation presents a negative value of -13.4 kJ mol^{-1} and a reaction equilibrium constant, K_{eq} with values between 8.5 and 16 Kg mol^{-1} in the temperature range from 30 ^{o}C to 0 ^{o}C was found.

The highest value of the ideal solubility selectivity for carbon monoxide to nitrogen was 24, in the experimental range studied.

(III) General prospects for further research and industrial implantation

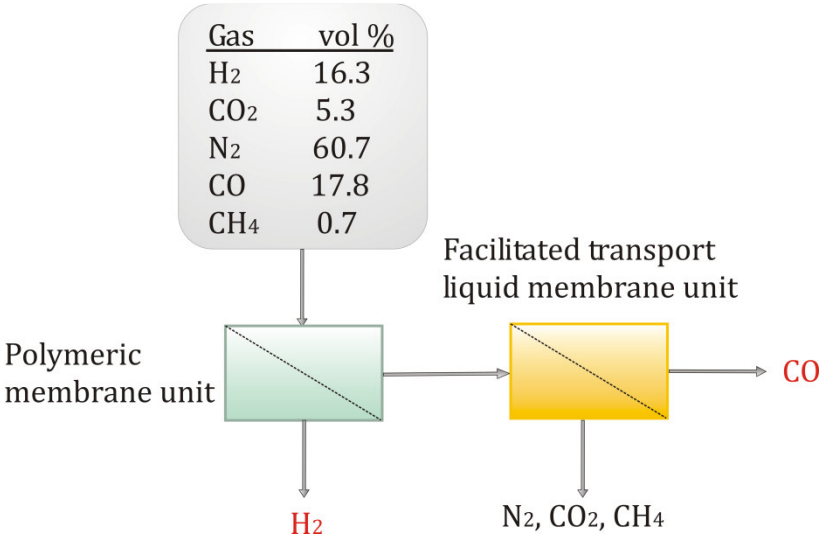

Figure V - 1. Schematic representation of a cascade gas separation proposal

The separation and valorization of industrial flue gases with complex composition such as the tail gas generated in the manufacturing of carbon black will be best carried out using a cascade gas separation unit as shown in Figure V -1. The first step includes the separation and recovery of H_2 using H_2 permeable polymers and the second step consists in the separation and recovery of CO by means of chemical complexation using facilitated transport liquid membranes. This proposal will give two product gas streams enriched in H_2 and CO respectively.

In order to reach the industrial implantation of this technology more fundamental research over the facilitated transport of CO using an ionic liquid membrane system is needed. We demonstrated that the π - complexation reaction of CO with a Cu (I) based ionic liquid is successful. Now the experimental determination of the appropriateness of the use of this ionic liquid medium in facilitated transport liquid membrane systems must be carried out. Also, the ionic liquid medium used in this work had the drawback of being corrosive. For further research the system [Bmim][OTf]/ $[CuOTf]_2 \cdot C_6H_6$ is proposed since [Bmim][OTf], that is also a hydrophilic ionic liquid like [Hmim][Cl], is less water sensible. Other possible systems are listed in Table IV -1 (Chapter IV).

(I) La separación y recuperación de H_2 mediante polímeros permeables hacia el H_2

La separación y recuperación de H_2 de corrientes de gases residuales provenientes de procesos de industriales con contenidos moderados de este gas, mediante la tecnología de membranas parece factible para obtener como producto una corriente gaseosa enriquecida en H_2. Teniendo en cuenta que este producto podría usarse en varias aplicaciones industriales con requerimientos de pureza específicos como la hidrodesulfuración (90 % pureza), el hidrocraqueo (70-80 % pureza) o como gas combustible (54-60% pureza), en una primera etapa es imprescindible una selección del material polimérico con propiedades óptimas de permeabilidad y selectividad hacia el transporte de hidrógeno. La mezcla gaseosa estudiada en este trabajo es el gas de cola obtenido en el proceso de fabricación de negro de carbono y está compuesta principalmente por N_2 (60 vol%) y CO (18 vol %), ambos gases con una permeabilidad baja a través de membranas poliméricas, junto con el altamente permeable H_2 (16 vol %) además de CO_2 (5 vol %) y otros gases (1 vol%). Teniendo en cuenta estas condiciones, para la fabricación de las membranas se eligió como material óptimo una poliimida comercial, 5(6)-amino-1-(4'aminofenil)-1,3,-trimetilindano (comercialmente conocida como Matrimid® 5218), caracterizada por una selectividad alta hacia el H_2 y con propiedades de permeabilidad moderadas.

La permeación de gases puros y mezclas de gases se estudió en dos configuraciones de membrana: (i) planas densas y (ii) en fibras huecas asimétricas, ambas fabricadas del mismo material, Matrimid, y se demostró que las propiedades de permeación del material polimérico varían considerablemente con la composición de las mezclas de gases y con la morfología de las membranas. El empleo de películas planas permitió el análisis de las propiedades intrínsecas de transporte de gases puros y mezclas de gases del material polimérico mientras que el uso de las membranas con una configuración de fibra hueca asimétrica permitió determinar el rendimiento que podría alcanzarse en la implementación práctica de la tecnología.

En el caso de la permeación de mezclas de gases, tanto en membranas densas planas como en membranas asimétricas de fibra hueca, los efectos de adsorción competitiva determinan una disminución en la permeación de H_2 en comparación con el gas puro. Para mezclas binarias H_2/CO_2 se observo una dependencia considerable en la permeabilidad de H_2 con la concentración de CO_2, incluso a bajas concentraciones de CO_2, determinando una disminución mayor en la permeabilidad de H_2 para mezclas H_2/CO_2 que para mezclas H_2/N_2 o H_2/CO donde es despreciable. Las características de permeabilidad de H_2 y CO_2 tanto para gases puros como en mezclas binarias, ternarias y cuaternarias se describió satisfactoriamente

empleando el modelo matemático *"dual-mode sorption, partial immobilization"* y los parámetros de trasporte para el H_2 y el CO se obtuvieron ajustando los datos experimentales con el modelo propuesto.

Al emplear membranas asimétricas de fibra hueca de Matrimid en comparación con una membrana densa fabricada del mismo material se han encontrado distintas propiedades de separación de gases. Debido a que la capa selectiva es mucho más fina en la fibra hueca asimétrica, en comparación con la película plana, se produjo una plastificación acelerada de la matriz polimérica inducida por el CO_2 que determinó un aumento considerable del coeficiente de permeabilidad del CO_2 puro con la presión. En membranas planas densas con un espesor mucho mayor el fenómeno de plastificación no tuvo lugar y el coeficiente de permeabilidad de CO_2 tuvo un comportamiento contrario, disminuyendo con la presión. Al trabajar con mezclas H_2/CO_2 la plastificación con CO_2 de la fibra hueca asimétrica provocó un aumento en la velocidad de transporte del H_2 que compensa en parte el efecto contrario debido a la adsorción competitiva. Como consecuencia, en mezclas binarias H_2/CO_2 la caída en la permeación del H_2 no es tan importante en fibras huecas asimétricas como en películas densas. Una caída máxima de 21.3 % se obtuvo a fugacidades de H_2 menores de 1 bar y a una presión total en la alimentación de 6 bar mientras tanto en películas planas la disminución fue de máximo 45.5 % en las mismas condiciones.

Resulta evidente que el uso de datos de permeación obtenidos con películas densas gruesas da solo una aproximación a los rendimientos que se pueden obtener en la práctica. Nuestros resultados sugieren que para mezclas de H_2 que contienen CO_2 el rendimiento de las membranas asimétricas de fibra hueca es mayor que el de las membranas planas densas.

La permeación de gases puros y mezclas de gases se analizó también con una fibra asimétrica comercial fabricada de un polímero mucho más permeable y más resistente hacia la plastificación, el polifenilenoxido (PPO). En contraste con las membranas de fibra hueca de Matrimid, al usar fibras huecas de PPO resulta una permeabilidad considerablemente mayor, pero con selectividades mucho menores. Por consiguiente, cuando se analizó el comportamiento para una mezcla sintética de gases con una composición similar con la de los gases residuales de la industria del negro de carbono ($H_2/CO_2/N_2/CO$ = 16.3/5.3/60.7/17.8 vol %), la concentración en H_2 obtenida en el permeado de un modulo de fibras huecas de PPO fue de solo un 40 vol % mientras que en el caso del modulo de fibra hueca de Matrimid se alcanzo una concentración muy superior (87 - 89 vol %).

(II) **La separación y recuperación del CO mediante complejación química.**

La separación selectiva del CO basada en la tecnología de membranas a partir de una mezcla que contiene N_2 es difícil de llevar a cabo empleando membranas poliméricas debido a que las propiedades de permeación (solubilidad y difusividad) de ambos gases son similares. Se determinó que un planteamiento viable puede ser el uso de un sistema de membranas liquidas soportadas donde la separación selectiva del CO se basa en un mecanismo de transporte facilitado de CO basado en una reacción con un agente transportador apropiado. Para elegir el mejor sistema agente transportador/disolvente líquido se consideraron dos propiedades esenciales: (i) se seleccionó una sal de cobre debido a las propiedades de complejación – π del Cu(I) con el CO y (ii) como disolvente se eligió un líquido iónico a temperatura ambiente (RTIL) debido a que los RTIL poseen una presión de vapor despreciable, propiedad necesaria para evitar pérdidas de disolvente por evaporación y problemas de inestabilidad de la membrana.

La absorción del monóxido de carbono mediante la complejación con cobre (I) se llevó a cabo exitosamente en el líquido iónico 1-Hexil-3-metilimidazolio clorocuprato preparado mediante la mezcla directa del líquido iónico puro 1-Hexil-3-metilimidazolio cloruro con cloruro de cobre (I). El estudio de los equilibrios de solubilidad indicó que la reacción de complejación tiene lugar en el todo rango de presión estudiado; la mayor parte de la reacción tuvo lugar a presiones por debajo de los 10 bar y se completó casi totalmente a 20 bar, demostrando la importancia de esta variable de operación.

La solubilidad del CO en el líquido iónico disminuye al aumentar la temperatura debido a que la reacción de complejación - π es exotérmica. La entalpía de reacción calculada tiene un valor negativo de -13.4 kJ mol^{-1}. Se encontraron valores para la constante de equilibrio, K_{eq}, entre 8.5 y 16 Kg mol^{-1} en el rango de temperaturas entre 30 ^{o}C y 0 ^{o}C.

En el rango experimental estudiado el mayor valor alcanzado de coeficiente de selectividad ideal CO/N_2 ha sido de 24 calculado en base a la solubilidad de ambos gases.

(III) Perspectivas generales para la investigación futura y para la implantación industrial

La separación y valorización de corrientes industriales de gases con composición compleja, tales como los generados en la producción del negro de

carbono se puede realizar en una unidad de separación de gases en etapas, como se presenta en la Figura V - 1. La primera etapa incluye la separación y recuperación de H_2 mediante el uso de membranas poliméricas selectivas hacia el H_2 y la segunda etapa consiste en la separación y recuperación de CO mediante la complejación química en una unidad de membranas líquidas con transporte facilitado.

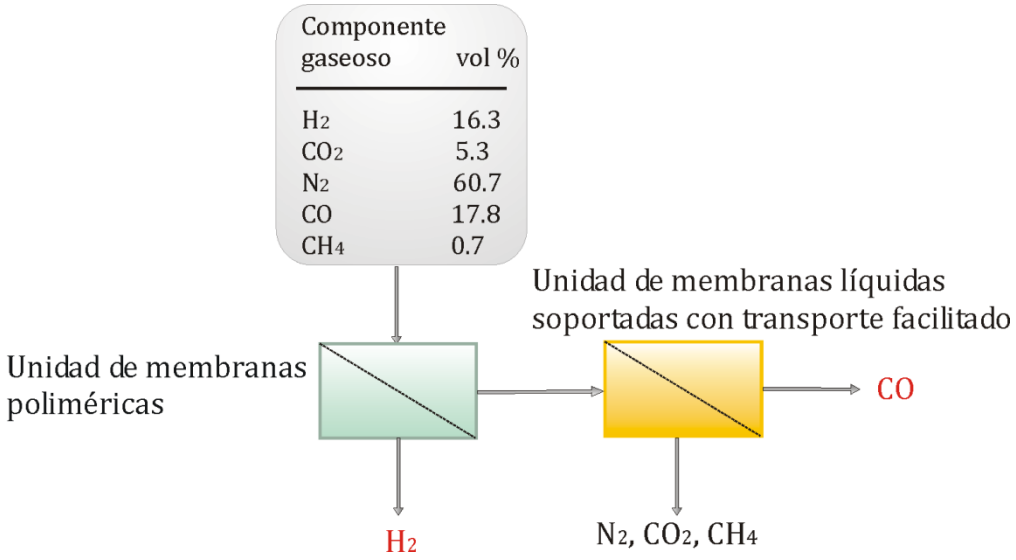

Figure V - 1. Representación esquematica de la propuesta de separación en etapas

Para conseguir la implantación industrial de esta tecnología es necesaria más investigación fundamental sobre el transporte facilitado de CO en sistemas de membranas líquidas soportadas que usan líquidos iónicos como fase líquida. Se demostró que la complexación – π del CO en un líquido iónico que contiene iones cuprosos es exitosa. Ahora, es necesaria la determinación experimental de la viabilidad del uso de este medio líquido para el transporte facilitado de CO en una membrana líquida soportada. Teniendo en cuenta de que este medio líquido puede resultar corrosivo se propone como alternativa el sistema [Bmim][OTf]/ $[CuOTf]_2{\cdot}C_6H_6$ puesto que el líquido iónico [Bmim][OTf], aunque sigue siendo hidrófilo al igual que [Hmim][Cl], es menos sensible al agua y no es corrosivo. Otros sistemas posibles se presentaron en la Tabla IV – 1 (Capítulo IV).

Appendix I

MATRIMID® POLYMER DATA SHEET

HUNTSMAN

Enriching lives through innovation

Advanced Materials

Matrimid® 5218# / Matrimid® 9725#

Soluble polyimide

DATA SHEET

Matrimid® 5218 / Matrimid® 9725 is a soluble thermoplastic polyimide. It is fully imidized during manufacturing, eliminating the need for high temperature processing. Matrimid® 5218 / Matrimid® 9725 is soluble in a variety of common solvents. Evaporation of the solvents leaves a strong, durable, tough coating.

Matrimid® 9725 is a micropulverized version of Matrimid® 5218.

CHEMICAL DESCRIPTION

Matrimid® 5218 / Matrimid® 9725 is a thermoplastic polyimide based on a proprietary diamine, 5(6)-amino-1-(4' aminophenyl)-1,3,-trimethylindane

CHEMICAL STRUCTURE

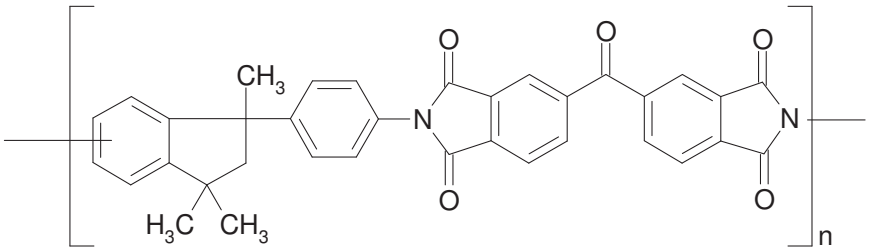

PROPERTIES

- Fully imidized polymer
- Does not require high temperatures for processing
- Soluble in a variety of common solvents : NEP , NMP , γBL , THF
- Excellent adhesion on various substrates such as metals, engineering plastics, glass
- Durable and tough films
- Excellent chemical resistance
- Very good thermal properties (Tg DMA > 300°C)
- Compatible with epoxies and other chemistries
- 100% solid powder

APPLICATIONS

- Temperature resistant adhesives
- Toughening of adhesives and composites martrices when high temperature resistance is a key
- Temperature resistance coatings

In addition to the brand name product denomination may show different appendices, which allows us to differentiate between our production sites: e.g. BD = Germany, US = United States, IN = India, CI = China, etc. These appendices are in use on packaging, transport and invoicing documents. Generally the same specifications apply for all versions. Please address any additional need for clarification to the appropriate Huntsman contact.

KEY DATA

Specified key data

Aspect (visual)	**Yellow powder**
Inherent viscosity(1)	**0.62 - 0.68 dl/g**
Volatile content(2)	**0 - 1.5%**
For Matrimid 9725	
Typical particle size range <106µ	**70 - 100%**

(1) 0.5 in NM Pat 25 °C

(2) 2 mg sample heated to 260 °C for 45 minutes

Specified key data are individually checked throughout and guaranteed.

SPECIAL FEATURES

Matrimid® 5218 / Matrimid® 9725 is a soluble thermoplastic polyimide. There is no polyamic acid precursor in the product that would require a high temperature cure to convert to the imide form. This lack of amic acid groups allows relatively simple processing compared to conventional polyamic acid precursor polyimides. For example, when solutions of Matrimid® 5218 / Matrimid® 9725 are used for coating applications, the substrate need only be heated to a temperature and for a time sufficient to thoroughly remove the solvent. When the solvent has been removed, a strong, durable polymide coating remains. By contrast, the more common polyamic acid precursor polyimides must be heated to high temperatures for long periods to convert the polyimide structure. This "curing" process evolves a water by-product and makes it very difficult to form pinhole-free coatings or void-free parts from those materials. No water is evolved in using Matrimid® 5218 because no curing (imidization) occurs during processing.

Matrimid® 5218 / Matrimid® 9725 has very unusual and desirable properties. Its high thermal stability and high glass transition temperature make Matrimid® 5218 / Matrimid® 9725 suitable for adhesive applications as well as matrix resin for composite applications. Figure 1 shows the change in modulus versus temperature of a neat resin molding based on Matrimid® 5218 (Dynamic Mechanical Analysis). Table 1 illustrates the adhesive properties of Matrimid® 5218 with a variety of substrates.

Matrimid® 5218 is soluble in many organic solvents and possesses excellent chemical resistance to water, steam, brine, acids, caustic and non-polar organic solvents, unlike other polyimides. As a soluble thermoplastic, Matrimid® 5218 / Matrimid® 9725 retains its solubility in certain polar organic solvents after processing, unless it has been thermally or chemically crosslinked before exposure to these solvents.

Matrimid® 5218 / Matrimid® 9725 is soluble in the following solvents. In general, 20 percent solutions are possible with these solvents.

Methylene chloride
Ethylene chloride
Chloroform
Tetrachloroethane
Tetrahydrofurane (THF)
Dioxane
Acetophenone
Cyclohexanone
m-Cresol
γ-Butyrolactone
Dimethylformamide (DMF)
Dimethylacetamide (DMAC)
N-methylpyrrolidone (NMP)

SPECIAL FEATURES (CONTINUED)

Table 1
Adhesive Properties

Substrate	Adhesion
Aluminum[3], mirror finish	Excellent
Aluminum, Alodine treated	Excellent
Steel, hot or cold rolled	Excellent
Stainless steel	Excellent
Brass	Excellent
Titanium	Excellent
Copper, untreated	Good
Copper, etched with $(NH_4)_2S_2O_8$	Excellent
Glass, untreated	Poor
Glass, aminosilane treated	Excellent
Ryton® PPS (Phillips) untreated	Poor
Ryton PPS (Phillips) acid etched	Excellent
Kapton® (Du Pont) untreated	Poor
Kapton (Du Pont) acid etched	Excellent

(3) To obtain excellent adhesion to some aluminum surfaces a surfactant, such as 3M's Fluorad® FC 430, must be added to the polyimide varnish.

Figure1
Dynamic Mechanical Analysis of Matrimid 5218

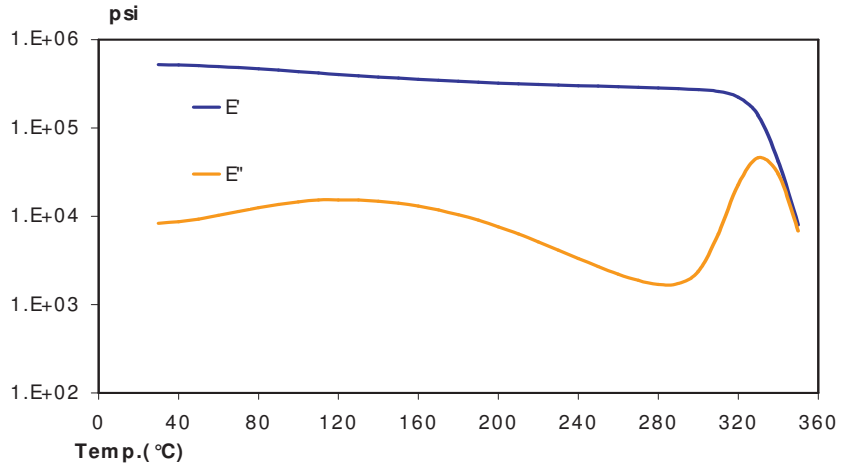

MECHANICAL PROPERTIES

Matrimid® 5218 Film

Machine-made film cast from a methylene chloride/Matrimid® 5218 solution.

Final drying temperature	240 °C by infrared heating rollers
Film thickness	1 mil unoriented
Tensile strength, ksi	
at break	12.4
at yield	12.6
Elongation, %	
at break	48.6
at yield	6.9
Tensile modulus, ksi	420
Density, g/cm^3	1.2
Refractive index	1.614
Coefficient of linear expansion in/in/°C	2.8×10^{-5}
Moisture absorption at 51% R.H. (equilibrium), %	0.87

MATRIMID® 5218/ GRAPHITE PREPREG

Formulation

Dissolve Matrimid® 5218 in γ-Butyrolactone solvent (20 percent solids). Use Hercules Magnamite AS4-12K graphite fibers to prepare unidirectional prepreg.

B-stage prepreg in an air circulating oven with temperature starting at 25°C, increasing to 204°C. Keep the prepreg at 204°C for 45 - 60 minutes. The prepreg should then have the solvent retention necessary for flow during composite fabrication.

A composite panel was prepared in the following manner:

Press mold:	260 - 316 °C @ 100 psi
Cool down:	to room temp. @ 100 psi
Dwell time:	30 min @ 316 °C
Post cure: (free standing)	16 hrs. @ 316 °C

Mechanical Properties @ 25°C

Fiber content, %	65
Short beam shear strength, psi	11.000
Fracture toughness G_{IC} $in\text{-}lb/in^2$	4
Tg (DMA), °C	
Dry	280
Wet	265

Thermal Properties

Temp. (°C)	Time (Wks)	Weight Loss (%)	
		Neat Resin	Composite Molding
232	1	0	0.25
	4	0.12	0.73
	10	0.40	1.33
316	1	0.33	0.61
	4	0.70	1.41
	6	1.22	2.09

PACKAGING & STORAGE	Matrimid® 5218 & Matrimid® 9725 should be stored at room temperature in original container protected from direct sunlight in a dry, cool and well ventilated area , away from food, drink and incompatible materials. Keep container tighly closed and sealed until ready for use . Containers that have been opened must be carefully resealed and kept upright to prevent leakage . Don't store in unlabelled containers. Use appropriate containment to avoid environmental contamination .
HANDLING PRECAUTIONS	Mandatory and recommended industrial hygiene procedures should be followed whenever our products are being handled and processed. For additional information please consult the corresponding product safety data sheets and the brochure "Hygienic precautions for handling plastics products".

Huntsman Advanced Materials
(Switzerland) GmbH
Klybeckstrasse 200
4057 Basel
Switzerland

Tel: +41 (0)61 299 11 11
Fax: +41 (0)61 299 11 12

www.huntsman.com/advanced_materials
Email: advanced_materials@huntsman.com

ISO 9001
DNV
REGISTERED

Appendix II

CHROMATOGRAPHIC METHODS

Configuration of the gas chromatograph

3000 GC Configuration	Column A	Column B
Injector Type	Backflush	Timed
Carrier Gas	Argon	Helium
Column Type	Molecular Sieve	Plot U
Detector Type	TCD	TCD
Separating species	H_2, N_2, CO	CO_2

Chromatographic method for the analysis of H_2 and CO_2

3000 GC Setpoints	Column A	Column B
Sample Inlet Temperature (°C)	100 [ON]	Same as A
Injector Temperature (°C)	100 [ON]	70 [ON]
Column Temperature (°C)	100 [ON]	65 [ON]
Sampling Time (s)	10 [ON]	10 [ON]
Inject Time (ms)	10	30
Run Time (s)	150	150
Post Run Time (s)	10	10
Pressure Equilibration Time (s)	10	10
Column Pressure (psi)	30.00 [ON]	18.00 [ON]
Post Run Pressure (psi)	30.00 [ON]	18.00 [ON]
Detector Filament	Enabled	Enabled
Detector Sensitivity	Standard	Standard
Detector Data Rate (Hz)	50	50
Baseline Offset (mV)	0	0
Backflush Time (s)	9.5	n/a

Chromatographic method for the analysis of N_2 and CO

3000 GC Setpoints	Column A	Column B
Sample Inlet Temperature (°C)	100 [ON]	Same as A
Injector Temperature (°C)	100 [ON]	70 [ON]
Column Temperature (°C)	100 [ON]	65 [ON]
Sampling Time (s)	10 [ON]	10 [ON]
Inject Time (ms)	200	30
Run Time (s)	150	150
Post Run Time (s)	10	10
Pressure Equilibration Time (s)	10	10
Column Pressure (psi)	30.00 [ON]	18.00 [ON]
Post Run Pressure (psi)	30.00 [ON]	18.00 [ON]
Detector Filament	Enabled	Enabled
Detector Sensitivity	Standard	Standard
Detector Data Rate (Hz)	50	50
Baseline Offset (mV)	0	0
Backflush Time (s)	9.5	n/a

Appendix III

PERMEATION TEST CELL SCALE DRAWINGS

Upper and lower part of the permeation cell.

Cross section and upper view.

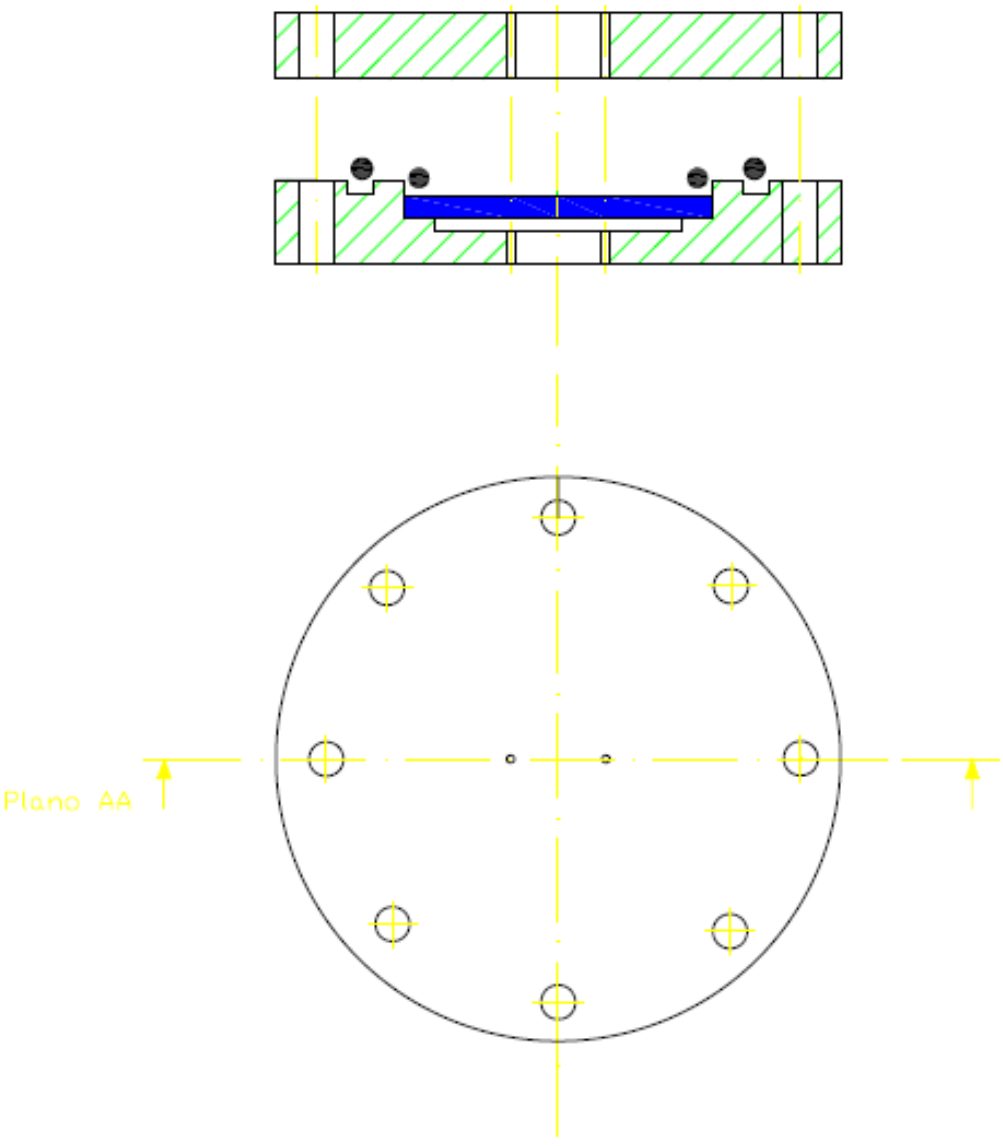

Upper part of the permeation cell.

Dimensions in mm

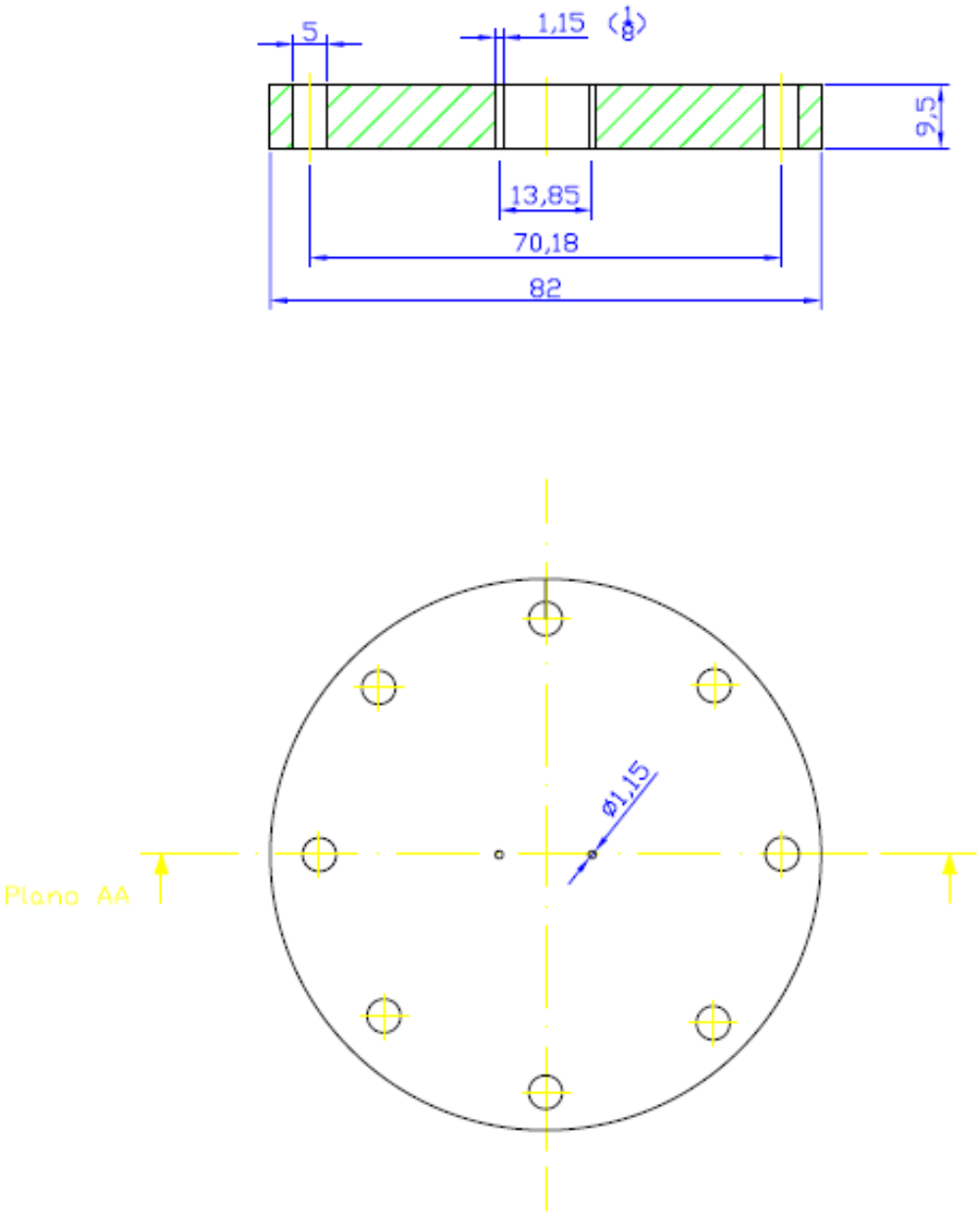

Lower part of the permeation cell

Dimensions in mm

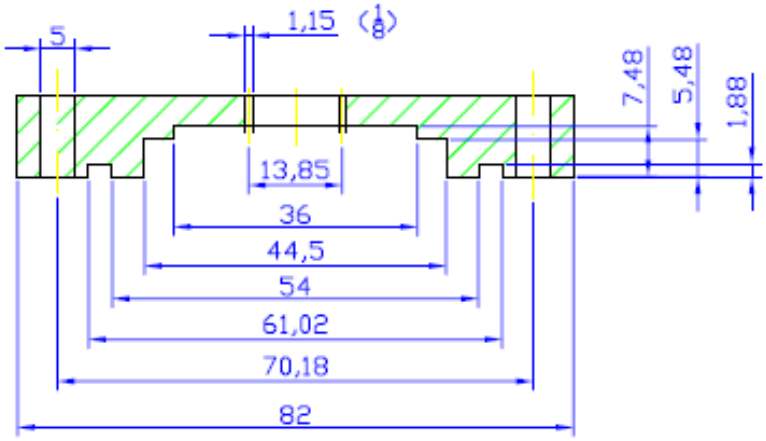

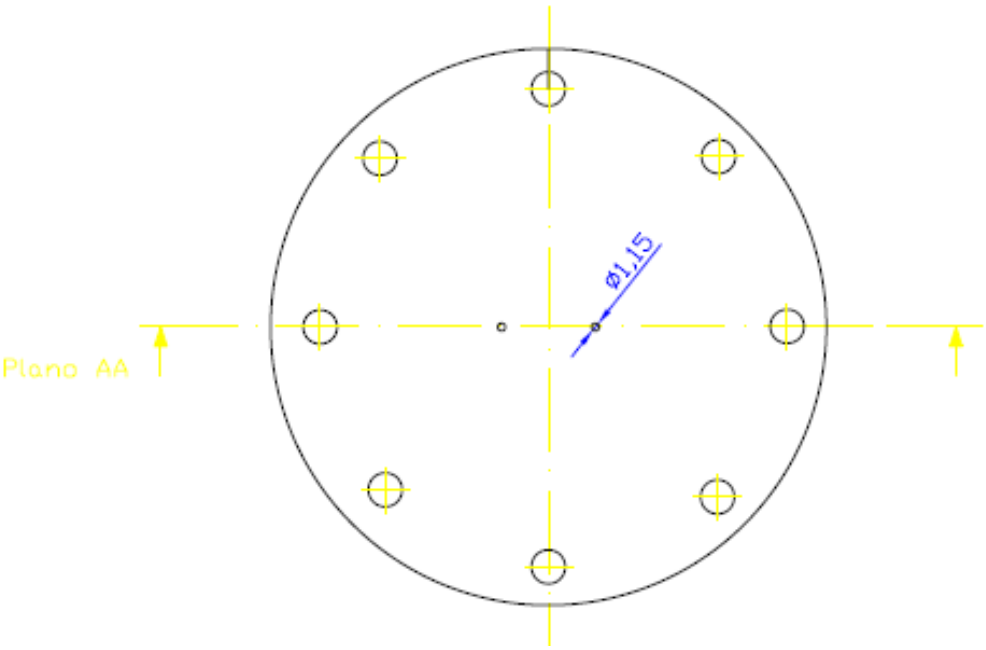

Publications in relation with this PhD thesis

1. Articles

"Dual-sorption model for H_2/CO_2 permeation in glassy polymeric Matrimid membrane" O.C. David, D. Gorri, I. Ortiz, A.M. Urtiaga. **Desalination and Water Treatment** 27 (1-3), pp. 31-36 (2011).

"Mixed gas separation study for the hydrogen recovery from $H_2/CO/N_2/CO_2$ post combustion mixtures using a Matrimid membrane" O.C. David, D. Gorri, A. Urtiaga, I. Ortiz. **Journal of Membrane Science**, 378, pp. 359-368 (2011).

"*On the improved absorption of Carbon Monxide in the ionic liquid 1-hexyl-3-methylimidazolium chlorocuprate*" O.C. David, Zarca G., D. Gorri, A. Urtiaga, I. Ortiz. **Separation & Purification Technology**, doi: 10.1016/j.seppur. 2012.02.015 (2012).

"Hydrogen separation from multicomponent gas mixtures containing CO, N_2 and CO_2 using Matrimid asymmetric hollow fiber membranes" O.C. David, D. Gorri, K. Nijmeijer, A. Urtiaga, I. Ortiz**. Journal of Membrane Science***,* submitted, April 2012.

2. Congress contributions

"Carbon black tail-gas separation using a Matrimid® polymeric membrane" A. Urtiaga, O. C. David, D. Gorri, I. Ortiz. ***8TH World Congress of Chemical Engineering*** August, 27, 2009, Montréal, Quebec, Canada. Oral presentation.

"Carbon black tail-gas separation using a Matrimid® polymeric membrane" O. David, D. Gorri, I. Ortiz and A. Urtiaga. **NYM 2009, Network Young Membrane 2009 Conference.** September 3, 4, 2009, Montpellier, France. Oral presentation.

"Carbon black tail-gas separation using a Matrimid® polymeric membrane" O. David, D. Gorri, I. Ortiz and A. Urtiaga. **EUROMEMBRANE 2009 Conference.** September 6-10, 2009, Montpellier, France. Poster session.

"Dual-sorption model for mixed- gas CO_2 permeation in Matrimid membrane" O. David, A. Urtiaga, D. Gorri, I. Ortiz CITEM 2010, **VIIth Ibero-American Conference on Membrane Science and Technology.** April 11-14, 2010, Sintra, Portugal. Poster session.

"*Carbon monoxide recovery by means of facilitated transport in RTIL supported liquid membranes."* O. C. David, G. Zarca, D. Gorri, I. Ortiz, A. Urtiaga. **ILSEPT 2011, 1st International Conference on Ionic Liquids in Separation and Purification Technology.** September, 4-7, 2011, Sitges, Spain. Oral presentation.

"*Hydrogen recovery from carbon black flue gases by means of membrane technology - a comparative study* " O. C. David, D. Gorri, A. Urtiaga, I. Ortiz. **ECCE / ECAB 2011, 8th European Congress of Chemical Engineering** September 25-29, 2011, Berlin, Germany. Oral presentation.

"*Selective CO/H_2 separation by reactive absorption of carbon monoxide with ionic liquid containing cuprous chloride*" O. C. David, G. Zarca, A. Urtiaga, I. Ortiz. **12TH Mediterranean Congress of Chemical Engineering.** November 15-18, 2011, Barcelona, Spain. Poster session.

Oana Cristina David

About the author

Oana Cristina David was born in 19th of January 1984 in Reghin, a small town found in the Transilvania Depression, Romania. In 2002 she graduated in the "Petru Maior" High School with a biology/chemistry profile and latter in 2007 she completed the Chemical Engineering degree at the Polytechnic University of Bucharest, Faculty of Applied Chemistry and Materials Science with a specialization in Polymer Science and Engineering.

Her research activity started in the period of her university education when she collaborated in several research projects in the fields of chemical thermodynamics and polymer science, under the supervision of Prof. Dr. Ing. Viorel Feroiu and Prof. Dr. Ing. Mircea Teodorescu, respectively. During this period she performed the diploma thesis in the Department of Chemical Engineering and Inorganic Chemistry of the University of Cantabria (UC) in Spain, under the frame of the Erasmus academic mobility program of the EU. The research dealt with the application of membrane distillation technology to the recovery of aroma compounds and was supervised by Prof. Ane Urtiaga and Dra. Nazely Diban.

In September 2007 she became a researcher in the Advanced Separation Research Group of the UC and started the PhD in Chemical and Process Engineering of the University of Cantabria, a program that is awarded with the Quality Mention of the Ministry of Education (Spain). Her work was focused to the research and development of polymeric membranes and room temperature ionic liquids (RTIL) to the energy valorization of mixed gas streams generated in the process industry, under the supervision of Prof. Ane Urtiaga and Prof. Daniel Gorri. In 2008 she received a FPU predoctoral fellowship financed by the Ministry of Education (Spain). Within the PhD program, in 2009 she completed a MSc in Chemical Engineering: Sustainable Production and Consumption. The doctorate was completed by an internship period in the Membrane Science & Technology Group, University of Twente, The Netherlands under the supervision of Dr. Kitty Nijmeijer.

Currently, Oana David is the author of 5 scientific articles published in international journals in the field of Membrane Science and Technology.

Notes

Notes

Notes

Notes